Evolution of Alteration and Mineralization at the Red Chris Cu-Au Porphyry Deposit East Zone, Northwestern British Columbia, Canada

by

Jessica Rose Norris

B.Sc., Hons., The University of Alberta, 2006

A THESIS SUBMITTED IN PARTIAL FULFILLMENT OF THE

REQUIREMENTS FOR THE DEGREE OF

MASTER OF SCIENCE

in

The Faculty of Graduate Studies

(Geological Sciences)

THE UNIVERSITY OF BRITISH COLUMBIA

(Vancouver)

April, 2012

Abstract

Located in northwestern British Columbia within the Stikine terrane, the Red Chris Cu-Au porphyry deposit is hosted in the Late Triassic Red Stock (~203.8 Ma). The Red Stock is a quartz monzodiorite to monzonite intrusion hosted in the broadly contemporaneous volcanic rocks of the Stuhini Group. Red Chris has features that are characteristic of calc-alkalic and alkalic porphyry deposits and shares many similarities with the Ridgeway deposit of the Cadia district in New South Wales, Australia. A combined measured and indicated resource of 936 million tonnes at 0.374 % Cu, 0.385 g/t Au, and 1.224 g/t Ag has been outlined from the Main and East zones.

Copper and gold are associated with bornite, chalcopyrite and lesser pyrite, hosted in quartz veins and stockworks as disseminations and fracture-controlled veinlets. High-grade mineralization is directly associated with high quartz vein density. Copper-iron sulphide minerals are laterally zoned, with a bornite > chalcopyrite core, grading outward to a chalcopyrite > pyrite shell and outward and upward to a pyrite > chalcopyrite halo. Five major groups of veins are recognized, of which the oldest two sets contain much of the copper and gold.

Stable isotopic analysis indicates the presence of magmatic and mixed magmatic-meteoric hydrothermal fluids. Evidence from sulphur isotopes demonstrates a high temperature oxidized magmatic fluid was responsible for transporting and depositing much of the copper and gold. A vertical and lateral zonation in sulphur isotopes exists, whereby deep regions exhibit δ^{34}S values between -1.9 to -0.9 ‰ and transition to near-surface regions in the pyrite halo that exhibit δ^{34}S values between +0.9 to +1.9 ‰. Isotopic analysis of oxygen and deuterium of hydrothermal alteration minerals provide evidence for a magmatic fluid (secondary biotite and muscovite) and a mixed magmatic-meteoric fluid (illite and kaolinite). Low temperature clay alteration (illite-kaolinite; intermediate argillic assemblage) significantly overprinted high temperature alteration (K-silicate, phyllic) in the upper levels of the system and gradually diminished intensity with depth. Carbonate veins and alteration also characterize the shallow levels and isotopic analysis of carbon and oxygen suggest a magmatic source with the possibility of minor mixing with an external meteoric fluid.

Table of Contents

List of Tables

List of Figures

List of Abbreviations

BC = British Columbia

CDT = Canyon Diablo Troilite

CL = Cathodoluminescence

CODES = Center for Excellence in Ore Deposits

FWHM = Full-width Half-maximum

IP = Induced Polarization

LGR = Los Gatos Research

MDRU = Mineral Deposit Research Unit

NAD = North American Datum

NI = National Instrument

NTS = National Topographic System

PCIGR = Pacific Center for Isotopic and Geochemical Research

PDB = Peedee Belemnite

QFIR = Queen's Facility for Isotopic Research

SCC = Sericite-Clay-Chlorite

SMOW = Standard Mean Ocean Water

SWIR = Short-wave Infrared

TSG = The Spectral Geologist

UBC = University of British Columbia

UTM = Universal Transverse Mercator

VPDB = Vienna Peedee Belemnite

VSMOW = Vienne Standard Mean Ocean Water

XRD = X-Ray Diffraction

Mineral Abbreviations

Anh = Anhydrite

Ank = Ankerite

Bn = Bornite

Carb = Carbonate

Chl = Chlorite

Cp = Chalcopyrite

Cv = Covelite

Dol = Dolomite

En = Enargite

Ep = Epidote

Gn = Galena

Gyp = Gypsum

Hbl = Hornblende

Hm = Hematite

Ill = Illite

Kaol = Kaolinite

K-fsp = K-feldspar

Mo = Molybdenite

Mt = Magnetite

Musc = Muscovite

Plag = Plagioclase

Py = Pyrite

Qtz = Quartz

Sph = Sphalerite

SpHm = Specular Hematite

Tm = Tourmaline

Tn = Tennantite

Acknowledgements

To my family

1   Introduction and Rationale for Study

The Canadian Cordillera is well endowed with porphyry copper deposits and prospects of both alkalic and calc-alkalic types. Their distinction and classification is primarily based on associated intrusive rock composition and some differences in the characteristics of the mineralized areas. However, the alteration assemblages and character of the different porphyry Cu deposit types are similar. The distinction that all porphyry deposits represent either an alkalic or calc-alkalic deposit is somewhat dogmatic, and to the exclusion of a porphyry deposit that exhibits characteristics of each type.

Established models of porphyry deposits outline temporal and spatial relationships between different alteration events. This includes a general sequence in which not all of the following alteration stages may form: sodic-calcic, calc-potassic, potassic, propylitic, chlorite-sericite, sericitic/phyllic, and various forms of argillic alteration. In most cases mineralization is hosted within high-temperature alteration zones that are bounded and capped by sericitic/phyllic alteration and lower temperature argillic alteration higher in the system. High level, low-temperature zones of argillic alteration are recognized at porphyry deposits, although not co-spatial to ore and are commonly not fully preserved as they are easily weathered and eroded. Sericitic/phyllic alteration may be preserved in the upper parts of porphyry Cu deposits or as pervasive halos around and above a system. In many deposits sericitic/phyllic alteration hosts a portion of the ore. Lack of preservation and distance to ore foster a biased attitude towards recognizing and describing late-stage, low-temperature alteration events. Additionally, the terminology used to describe late-stage, low-temperature argillic alteration at porphyry deposits is inconsistent.

The Red Chris Cu-Au porphyry deposit in northwestern British Columbia (Figure 1.1) has characteristics of alkalic and calc-alkalic deposits, and represents a transition between these two classes of porphyry Cu deposits. Many features of Red Chris are similar to porphyry deposits of the Cadia District in New South Wales, Australia, namely Ridgeway, which also exhibits characteristics of a transitional alkalic to calc-alkalic deposit type (see below). The Dinkidi Cu-Au porphyry deposit of the Didipio Region, Northern Luzon, Philippines is another example of an alkalic porphyry with features common to calc-alkalic deposits (Wolfe and Cooke, 2011). Red Chris furthermore and unlike many porphyry Cu-Au deposits in British Columbia has high-grade

ore (> 1% Cu and 1 g/t Au) to depth in two of the four mineralized centers. But in contrast to most porphyry Cu-Au systems in British Columbia, the Red Chris deposit is characterized by pervasive clay alteration and carbonate veins and alteration preserved in the shallow parts of the system. This thesis characterizes the East zone deposit, where the higher Cu and Au grades are currently known, focusing on the evolution of the hydrothermal system, and examines the origin of the pervasive low temperature clay alteration that characterize the system.
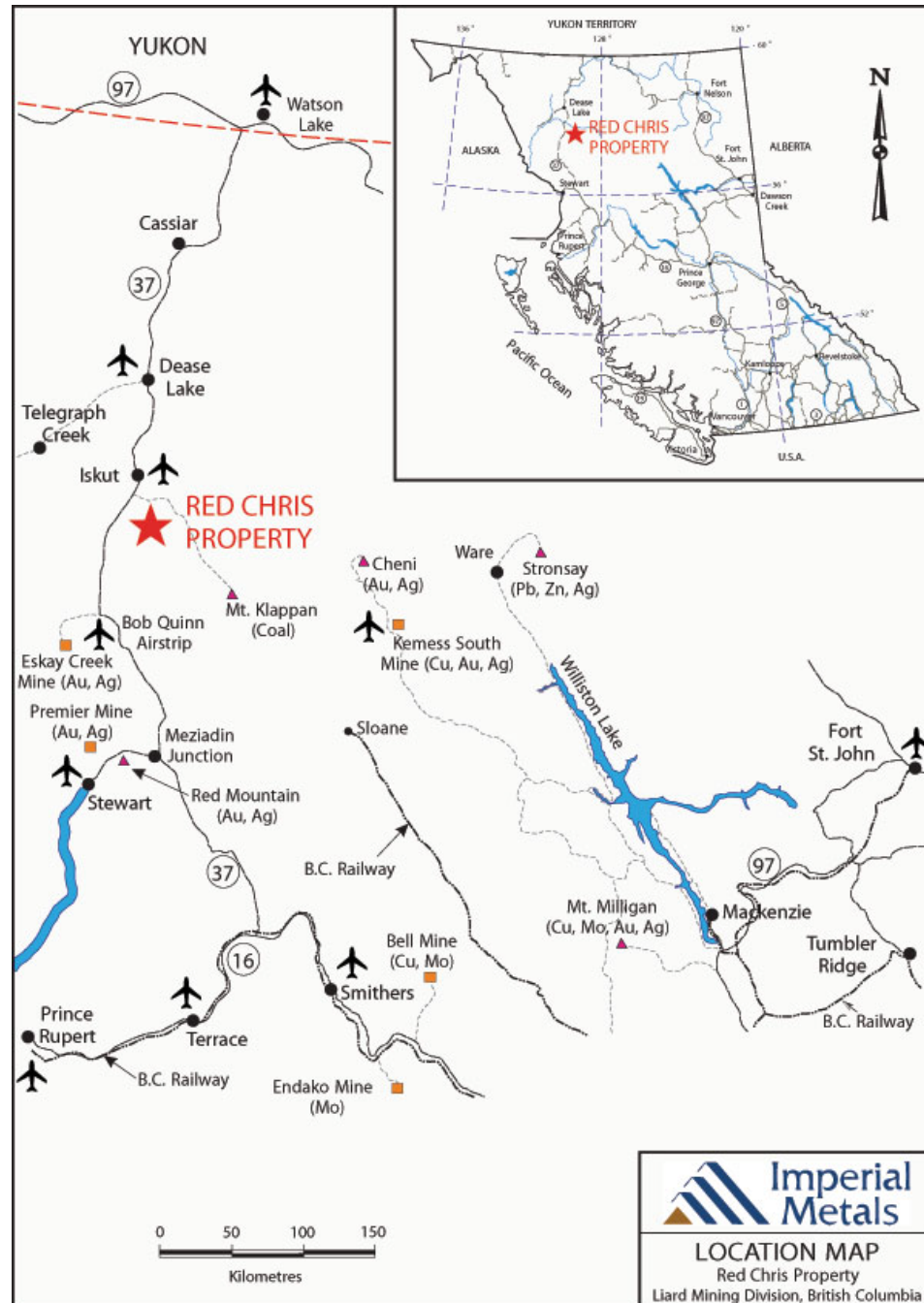
Figure 1.1 Location of the Red Chris Cu-Au porphyry deposit, northwestern British Columbia, Canada and select mines and mineral deposits.

1.1 Alkalic and Calc-alkalic Porphyry Deposits

Much of the characterization of the alteration and mineralization features at porphyry deposits has been well-established by studies of Lowell and Guilbert (1970), Gustafson and Hunt (1975), Beane and Titley (1981), among many others. Investigations into the alkalic suite of deposits (Barr et al., 1976) and characteristic alteration (Lang et al., 1994, 1995a, 1995b; Wilson et al., 2003, 2007; and Cooke et al., 2007) note the features of the alkalic type deposits in British Columbia and Australia. Recent advancements and discussions on the porphyry copper model have been described by Sillitoe (2000), Seedorff et al. (2005), Holliday and Cooke (2007), and Sillitoe (2010).

Porphyry deposits have a wide range of features and characteristics that are used to classify them into different types. The most commonly used classification is on the basis of the intrusive host rock chemistry, which divides porphyry deposits into alkalic and calc-alkalic types. Intrusions associated with alkalic deposits have a high K/Na ratio and a high alkali/silica ratio whereas intrusions associated with calc-alkalic deposits have a low K/Na ratio and a low alkali/silica ratio. Alkalic porphyry deposits generally form as clusters whereby mineralization is centered on narrow (< 200 m diameter) pipes or dyke swarms, or hosted in larger intrusive complexes (Holliday and Cooke, 2007), whereas calc-alkalic deposits can range from clusters of mineralized centers to ones that have lateral dimensions on the kilometer scale.

Copper, gold, and molybdenum are the major economically important elements associated with porphyry deposits with additional deposits hosting appreciable amounts of tungsten, tin, as well as trace metals such a rhenium (Seedorff et al., 2005). The average grade of these deposits is enriched by 100 to 1000 times the concentration compared to unmineralized intrusions of a similar composition. The size (tonnage) of porphyry deposits ranges over 4 orders of magnitude and typically vary in the order of Cu > Mo ~ Au > Sn > W (Seedorff et al., 2005). The major difference in metal budget between alkalic and calc-alkalic deposits is that the latter may contain significant amounts of molybdenum, whereas alkalic porphyry deposits do not. In both deposit types, copper-iron sulphides commonly form in veins and/or hydrothermal breccias and as lesser disseminations (Holliday and Cooke, 2007). Metal within the mineralized intrusive complex and the adjacent wallrock is typically zoned.

Zones of hydrothermal alteration assemblages can vary between calc-alkalic and alkalic porphyry deposits. In high-grade cores of calc-alkalic deposits, well developed zones of potassic alteration (secondary biotite, K-feldspar, magnetite ± anhydrite), phyllic alteration (quartz, sericite, pyrite), and advanced argillic alteration (quartz, alunite, kaolinite ± pyrophyllite) are typically present (Holliday and Cooke, 2007). Within alkalic deposits, potassic alteration is common and may also include calc-potassic alteration (orthoclase ± biotite ± garnet ± actinolite ± epidote) in the core of the deposit. Phyllic alteration is typically poorly developed or absent in alkalic deposits (Holliday and Cooke, 2007). Additionally, alkalic deposits typically lack significant volumes of advanced argillic alteration.

Common to most porphyry deposit types, propylitic (chlorite, epidote, albite, carbonate, and pyrite) alteration forms as halos to the core of porphyry deposits and can extend for several kilometers outboard of the mineralized center. Where present, sodic-calcic (albite/oligoclase, actinolite, magnetite) alteration may form at alkalic and calc-alkalic porphyry deposit types, in deep parts of porphyry systems (Dilles and Einaudi, 1992). Intermediate argillic (sericite, illite, chlorite, calcite, smectite) alteration is a widespread but under recognized pale green overprint on K-silicate alteration in the upper parts of porphyry stocks (Sillitoe, 2000). Further, where porphyry deposits come into contact with carbonate wallrocks calc-silicate (skarn) alteration assemblages (garnet, pyroxene, epidote, calcite, chlorite, sulphides, quartz, and anhydrite) can form.

1.2 Red Chris

The Red Chris deposit has several characteristics which are not common among most of the porphyry deposits in the Canadian Cordillera. Attempts to classify Red Chris as an alkalic porphyry have not been conclusive as the deposit features characteristics of both calc-alkalic and alkalic porphyry deposits. Host rock composition, and presence of a cluster of small Cu-Au mineralized intrusions lend to Red Chris being classified as an alkalic deposit. Style of mineralization and certain alteration assemblages are consistent with calc-alkalic porphyry deposits. The bulk of the alteration mineralogy in the shallow portions of the system is clay (illite-kaolinite) and carbonate, a lower temperature assemblage than sericite (muscovite) alteration which is commonly reported at shallow levels of porphyry systems. There is a significant amount of carbonate at Red Chris, as a pervasive overprint and as late stage veins, and infill material of earlier veins and breccia cement. Understanding these characteristics and

the larger-scale processes that gave rise to them will place Red Chris in context with other porphyry deposits in British Columbia.

1.2.1   **Introduction**

The Red Chris deposit is in northwestern BC (Figure 1.1), approximately 80 km south of the town of Dease Lake and 12 km east of the Stewart-Cassiar Highway (Highway 37). Red Chris is accessed by a 23 km gravel road. The deposit is situated at latitude 57°42' N and longitude 129°47' W, in NTS area 104H/12W.

The Red Chris deposit consists of several mineralized zones: the Main, East, Far West and Gully zones (Figure 1.2). Currently only the Main and East zones host measured and indicated resources. The Main zone has a larger areal extent than the East zone, and their centers are ~600 m apart. Both Main and East zones are vertical to sub-vertical, apparent pipe-like orebodies that are bounded to the south by the general east-northeasterly-trending faults in the region (Collins et al., 2004). Recent drilling includes deep drillholes in the Gully zone as well as the recently discovered East Ridge zone, which occurs East of the planned pit (Figure 1.2).
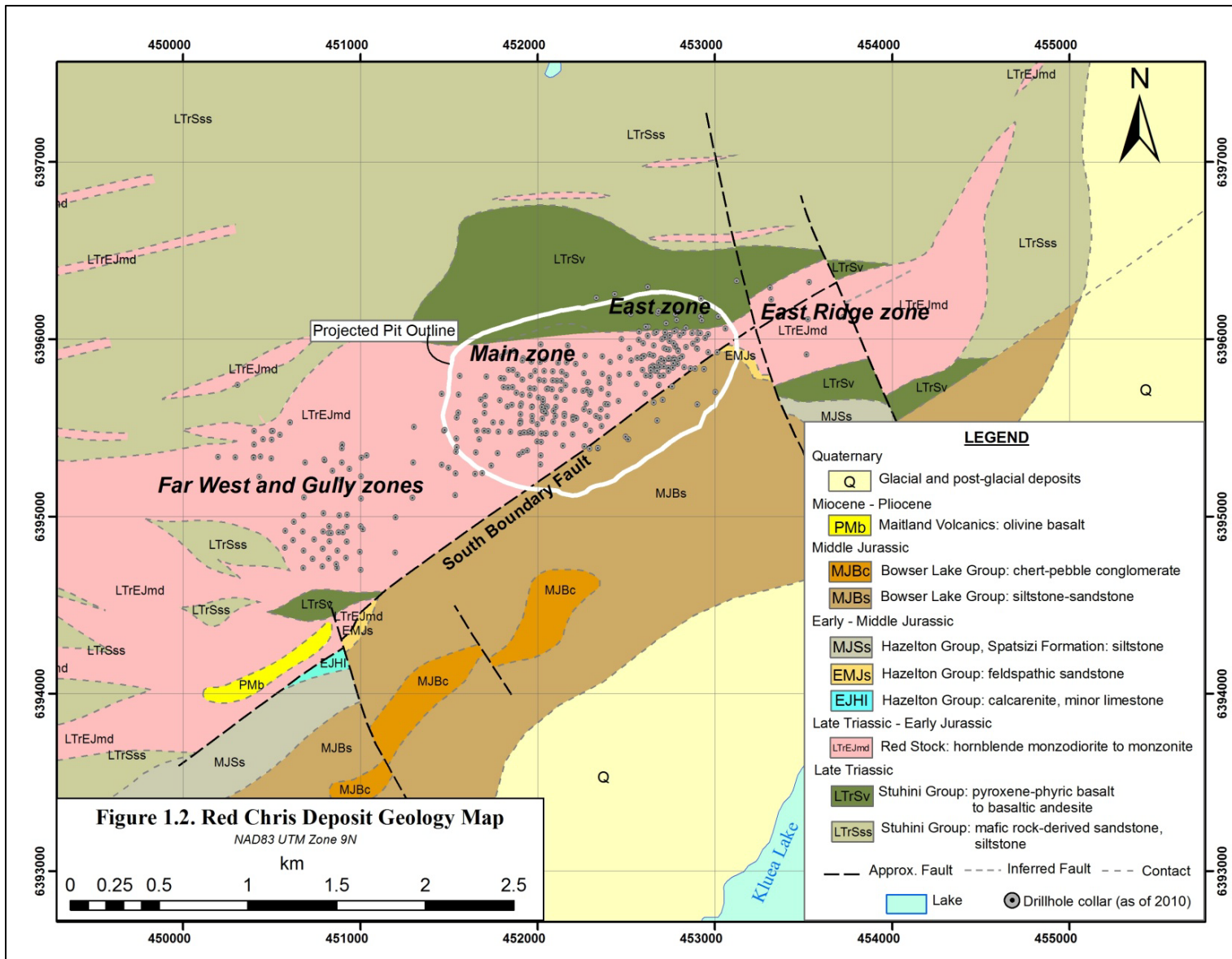
Figure 1.2 Geology map of Red Chris with mineralized centers of the Far West, Gully, Main, East, and East Ridge zones.

1.2.2   **Exploration History and Discovery of High-Grade to Depth**

Initial exploration efforts at Red Chris began in 1956 where Conwest Exploration Ltd prospected the area and staked the first claims over several large gossans. Percussion drilling, trenching and diamond drilling continued on the property by several different exploration companies throughout the 1970's. From 1981 to 1994, there was no exploration of the property. In 1994 and 1995, American Bullion Minerals initiated an exploration effort of soil geochemistry, ground geophysics, and diamond drilling totaling over 55,000 m. There was a stoppage in drilling between 1996 and 2003 until bcMetals completed the first feasibility study at Red Chris in 2004 which resulted in a resource calculation of 276 million tonnes at 0.35 % Cu and 0.27 g/t Au (Collins et al., 2004).

Imperial Metals acquired bcMetals in 2007 and began exploring the deeper parts of the Main and East zones. These deep drilholes resulted in the discovery of high grade mineralization at depth. An intersection of 1.01 % Cu, 1.26 g/t Au and 3.92 g/t Ag over 1024.1 m in drillhole RC07-335 (Imperial Metals Corporation, 2007) indicated a vertical extent of mineralization previously unknown at Red Chris. The deep mineralization has significant implications for further exploration and mine planning. Throughout 2009 and 2010 Imperial Metals drilled deep holes to delineate the extent of mineralization across the deposit. Additional high grade intersections were encountered, including 152 m of 4.12 % Cu, 8.83 g/t Au and 10.46 g/t Ag at a depth of 540 m in drillhole RC09-350 (Gillstrom and Robertson, 2010). In 2011, exploration included deep drillholes in the Gully zone whereby several mineralized zones were intersected, including 0.31 % Cu and 0.29 g/t Au over 807.5 m in drillhole RC11-477 starting at 172.5 m depth (Gillstrom et al., 2012). Additionally, in late 2011, drilling commenced at the East Ridge zone whereby drillhole RC11-565 intersected 79.0 m of mineralization grading 0.39 % Cu and 0.21 g/t Au at a depth of 713.9 m (Imperial Metals Corporation, 2012). On a broader scale, results from these deep drillholes indicate significant potential for high Au and Cu grades in BC's alkalic porphyry systems.

Based on the deep drilling programme, Imperial Metals Corporation updated the resource and calculated an estimated reserve for the contained metals at the Main and East zones of Red Chris. In early 2012, a resource estimate of 936 million tonnes (measured and indicated) at 0.374 % Cu, 0.385 g/t Au, and 1.224 g/t Ag (at 0.3 % Cu-equivalent cut-off, with inferred resources of

871 million tonnes at 0.315 % Cu, 0.349 g/t Au, and 1.138 g/t Ag) was released (Gillstrom et al., 2012). Giroux and Bellamy (2004) reported inferred resources at the Far West and Gully zones containing 76.8 million tonnes of 0.17 % Cu and 0.33 g/t Au (at 0.1 % Cu-equivalent cut-off) and 230.3 million tonnes of 0.2 2% Cu and 0.20 g/t Au (at 0.1 % Cu-equivalent cut-off) respectively.

1.2.3 **Alkalic and Calc-alkalic Associations**

Red Chris has characteristics of alkalic and calc-alkalic porphyry deposits. Whereas Ash et al. (1995) defined Red Chris as a 'copper-gold porphyry deposit' others describe Red Chris as an alkalic deposit with the calc-alkalic features being caused by secondary processes (Schink, 1977; Newell and Peatfield, 1995). Red Chris is representative of an alkalic and calc-alkalic porphyry deposit and provides a unique opportunity to gain insight into features that characterize a transitional deposit type.

Several features at Red Chris are consistent with an alkalic porphyry deposit. Although not conclusive, the host rocks range from quartz monzodiorite to monzonite as it is uncertain how much of the K-feldspar is a product of alteration versus igneous crystallization. Additionally, the chemistry of least altered host rocks suggest a high-K calc-alkalic to alkalic composition with high alkali/silica ratios (B. Riedell, 2011 personal communication). The stock is relatively small and the lateral extent of the mineralization is limited (Ash, 1995). Red Chris is a cluster of deposits, with several mineralized zones. Potassic and propylitic alteration are common at Red Chris with propylitic alteration restricted to outboard of the East zone. Additionally, phyllic alteration is only poorly developed. Red Chris is gold-rich with abundant copper and minor to rare molybdenum, which is also common in alkalic porphyry deposits.

The Red Chris deposit has a few features which are characteristic of a calc-alkalic porphyry deposit model. Mineralization is hosted in quartz-sulphide vein stockworks, which is a major feature of calc-alkalic deposits. Minor amounts of sphalerite, galena, and molybdenite are present, which is also characteristic of calc-alkalic porphyry deposits (Ash et al., 1995). The alteration pattern and more specifically intense intermediate argillic (clay) alteration at Red Chris are considered to be more typical of a calc-alkalic deposit (Baker et al., 1997).

Overall, many of the features of Red Chris are consistent with an alkalic porphyry deposit however there are some major features representative of the calc-alkalic model. The major features associated with the host rock intrusions (composition, chemistry, and size), associated metals and poorly developed phyllic alteration zone, and carbonate alteration are consistent with an alkalic porphyry deposit. However the style of mineralization and superposition of a low temperature and late stage intermediate argillic alteration are are more commonly described in calc-alkalic porphyry deposits. The alkalic to calc-alkalic nature of the Red Chris deposit is not fully understood and it is likely that Red Chris is a transitional porphyry deposit that represents an intermediary deposit between the two end-member classification models.

1.2.4 Low Temperature Clay Alteration Overprint

Lateral and vertical zonation patterns around porphyry deposits are important in mineral exploration as they can help vector towards ore. At Red Chris, alteration is widespread and intense across the East zone. Intermediate argillic (illite-kaolinite) clay alteration at Red Chris dominates much of the current alteration mineralogy at shallow levels of the deposit. Overall, the shallow level of the system is dominated by illite, with kaolinite and relict muscovite generally occurring in near-surface zones and gradually diminishes with depth. The illite-kaolinite alteration is different from the phyllic alteration assemblage of Lowell and Guilbert (1970), which consists of quartz-sericite-pyrite, whereby sericite is used as a textural term to describe a fine-grained white mica (muscovite). Pervasive illite-kaolinite alteration reflects a lower temperature assemblage than a phyllic/sericitic assemblage that contains muscovite.

1.2.5 Carbonate Veins and Alteration

The presence of moderate amounts of carbonate in veins as well as weak and locally pervasive carbonate alteration distinguish Red Chris (Baker et al., 1997). The moderate, pervasive carbonate alteration occurs throughout the East zone and is dominant in the upper 300 to 400 m, commonly replacing the groundmass and lesser phenocrysts. Much of the carbonate veins occur late in the paragenetic sequence and cross-cut nearly all other vein types observed. This carbonate alteration appears to be associated with the illite overprint and also gradually diminishes with depth. Zones of carbonate breccias are present across the East zone whereby carbonate cements angular clasts of variably altered intrusive rocks. The carbonate has a ferroan dolomite to ankerite composition (Baker et al., 1997) in addition to rare siderite.

Carbonate veins and alteration may occur throughout the paragenesis of alkalic porphyry deposits (Wolfe and Cooke, 2011), whereas in calc-alkalic deposits, carbonate alteration is restricted to the outer propylitic halo. Carbonate alteration and veins have been reported at several alkalic porphyry deposits in British Columbia, including Mt. Milligan (Jago et al., In Press), Mount Polley (Pass et al., In Press), and Galore Creek (Micko et al., In Press), and as late-stage veins and alteration within alkalic porphyry deposits in New South Wales, Australia (Cooke et al., 2007). At Red Chris, there may be a relationship between carbonate in veins and mineralization, as quartz-sulphide veins are observed to have carbonate occurring interstitial to the sulphide minerals. The source of the carbonate may be hydrothermal, meteoric or as the result of a regional influx of carbonate associated to an event unrelated to the formation of Red Chris. The amount of carbonate observed at Red Chris is not common to other alkalic porphyry deposits, particularly those in the Canadian Cordillera of British Columbia and makes for an interesting feature to be studied.

1.2.6   **Similarities with the Cadia District**

Alkalic porphyry copper deposits are common in British Columbia however other districts around the world are also host to numerous alkalic deposits, namely the Cadia District of New South Wales, Australia. Ordovician to Early Silurian porphyry copper deposits of the Cadia district span a 7 km northwest trending corridor of alteration and mineralization within the Lachlan fold belt of the Macquarie Arc (Wilson et al., 2003 and Cooke et al., 2007). The Cadia district is comprised of four mineralized centers: Ridgeway, Cadia Quarry, Cadia Hill and Cadia East, which share striking similarities to features of Red Chris (Cooke et al., 2007). The Ridgeway Au-Cu porphyry deposit perhaps is the most similar to Red Chris, as it also likely represents a transitional alkalic to calc-alkalic porphyry deposit (Wilson et al., 2003). Major similarities between Ridgeway deposit and Red Chris are related to the composition of the host intrusions, Au-rich character, sulphide zonation, quartz-stockwork hosted mineralization and to a lesser extent, calc-potassic and potassic alteration assemblages related to ore (Table 1.1, after Wilson et al., 2003). Additionally, Ridgeway lacks a pervasive phyllic alteration assemblage, whereby strong phyllic alteration envelopes are only developed around late-stage brittle faults (Wilson et al., 2003) and only recently has a spatially restricted phyllic alteration zone also been recognized at Red Chris.

Table 1.1 Comparison of Major Features of the Ridgeway and Red Chris Porphyry Deposits

	Ridgeway, Australia	Red Chris, Canada
Host Intrusion	Monzodiorite – quartz monzonite	Monzonite - quartz monzodiorite
Sulphide Zonation	Bornite → Chalcopyrite → Pyrite	Bornite → Chalcopyrite → Pyrite
Quartz Stockwork	Yes	Yes
High Quartz Vein Density to High Grade	Strong Correlation	Strong Correlation
Ore-related Alteration	Actinolite-biotite-magnetite-quartz	Orthoclase-biotite-magnetite-quartz
Abundant Magnetite	Yes	Yes, often altered to hematite

(modified after Wilson et al., 2003)

1.3   Thesis Objectives and Outline of Thesis

A major goal of this thesis is to place Red Chris into context with respect to porphyry systems as a whole, as well as with respect to porphyry systems of the Canadian Cordillera. As Red Chris represents a transitional alkalic/calc-alkalic porphyry deposit, another objective is to investigate what features characterize such a deposit. This thesis also strives to understand the nature and evolution of the hydrothermal system that operated during the formation of the deposit. Finally, the study identifies potential chemical vectors that could be used in exploration targeting for similar deposits in the region.

Chapter 2 outlines the tectonic setting and major terranes that host porphyry deposits in the Canadian Cordillera. Additionally, the different classifications and styles of porphyry deposits of the Canadian Cordillera are discussed. The chapter also outlines the regional geology around the Red Chris deposit as well as the deposit-scale structures. Finally, the chapter compares three porphyry deposits of northern Stikinia with Red Chris: GJ, Schaft Creek, and Galore Creek; all of which are hosted in the same host volcanic rocks and are known to form around the same time (Late Triassic).

Chapter 3 of this thesis outlines the field methods by which this study was conducted and compiles a thorough description of the rock types, alteration assemblages, veins, hypogene sulphide mineralogy and paragenesis of the deposit. These descriptions are placed into context

within the understanding of porphyry deposits to determine how Red Chris fits into the overall porphyry copper model.

Chapter 4 examines the nature and evolution of the hydrothermal system during the formation of Red Chris by the analysis of stable isotopes from sulphide, hydrosilicate, and carbonate minerals. Sulphur isotopes are used to estimate temperature and oxidation state of the initial high-temperature magmatic fluid. Oxygen and deuterium analysis of hydrothermal alteration minerals investigate the source of fluids for different alteration types. Carbon and oxygen isotopes investigate the source of carbonate veins throughout the deposit. Overall, a model is created that outlines the general evolution of the deposit as different alteration types are formed by different fluids as the temperature of the system decreased. This chapter describes the sources and formation of fluids responsible for the characteristic and pervasive low temperature clay and carbonate alteration in the upper parts of the deposit.

Finally, Chapter 5 summarizes the major conclusions of the study and provides implications for exploration targeting by outlining possible vectors toward mineralization. Further, recommendations for future work are outlined to provide the scientific community with avenues of future research to be undertaken, if desired.

1.4   Support for Project

This project was co-funded by Imperial Metals Corporation and Geoscience BC with direct supervision and support by the Mineral Deposit Research Unit (MDRU) at the University of British Columbia (UBC), Canada. Logistical support, including accommodation and support in the field was provided by Imperial Metals Corporation at the Red Chris camp. The MDRU was also instrumental in designing and organizing the project. Two papers have been published by Geoscience BC in the 2009 and 2010 Summary of Activities volumes (Norris et al., 2010 and Norris et al., 2011) that outline observations and conclusions after each of the two field seasons.

All of the core-logging and sampling was conducted by the author (Jessica Norris) in the field. Additional laboratory analysis at UBC including shortwave infrared spectroscopy (SWIR) by the TerraSpec, X-Ray diffraction (XRD), clay separation, sulphide grain separation and carbon and oxygen isotopic analysis by the Los Gatos Research (LGR) high -CO_2 concentration

isotopic analyzer was also carried out by the author. Petrogeochemical analysis on least altered rocks at Red Chris were sampled and results provided by Brock Riedell.

Additional stable isotopic studies were conducted by external sources. Carbon and oxygen isotopic analysis was conducted by the Pacific Center for Isotopic and Geochemical Research (PCIGR) at UBC. Sulphur isotopic analysis was carried out at the Queen's Facility for Isotope Research (QFIR) at Queen's University in Kingston, Ontario, Canada. Oxygen and deuterium isotopic analysis was conducted at the Stable Isotope Laboratory of GNS Science in Gracefield, New Zealand.

Overall, all observations and interpretations were made by the author under the guidance of the project supervisors, geologists and contractors of Imperial Metals Corporation, and externally involved geologists. Additionally, analytical techniques and geological discussions with colleagues at the MDRU were instrumental in the overall success of this study.

2 Tectonic and Geological Settings of Porphyry Deposits of the Canadian Cordillera

The Canadian Cordillera is diverse in both geologic and metallogenic character and is divided into five morphogeological belts. Each of these belts is underlain by one or more tectonic terranes, which are crustal scale packages of rocks with internally coherent stratigraphy and differing tectonic history from adjacent rocks that cannot be explained by facies changes (Coney, 1980). Thus, each morphogeological belt represents different physiographic attributes that relate from a combination of lithological, structural, and tectonic features (Gabrielse et al., 1991a). Certain terranes preferentially host particular types of mineral deposits that reflect different processes and conditions in place at the time of their formation.

The Intermontane Belt of the Canadian Cordillera is well endowed with porphyry style mineralization. Major porphyry deposits of the Intermontane Belt within British Columbia occur within the accreted terranes of Quesnellia and Stikinia which formed over two separate periods; in pre and post terrane accretionary time. British Columbia contains many major porphyry deposits of both the alkalic and calc-alkalic types. Northern Stikinia hosts several notable porphyry deposits including Red Chris, Galore Creek, Schaft Creek and GJ. These deposits are of similar age and occur in the same volcanic host however represent a suite of deposits with a range of metals, mineralization and alteration styles and overall general porphyry type.

2.1 The Canadian Cordillera and Intermontane Superterrane

2.1.1 Morphogeological Belts of the Canadian Cordillera

The Canadian Cordillera is composed of linear, physiographic regions that are characterized by common surface features reflecting their underlying geologic components and erosional history, known as morphogeological belts. These belts are, from east to west from the ancient North American continental margin, the Foreland Belt, the Omineca, Intermontane, Coast, and Insular Belts (Monger et al., 1991; Figure 2.1). Descriptions of the rocks underlying the different belts are taken from Gabrielse et al. (1991a). The Foreland Belt is composed of imbricated and folded miogeoclinal strata and clastic wedge assemblages that were deposited on and adjacent to the western edge of the stable North American craton. The eastern boundary of the Foreland Belt is marked by the limit of deformation between the strata of the foothills and mountain systems on the west and the undeformed, flat-lying strata of the Interior Plains on the east. The Omineca Belt is underlain by granitic and metamorphic rocks whereby accretion, subsequent crustal thickening and intrusions caused significant uplift of the region. The

14

Intermontane Belt is topographically low in comparison to the adjacent Omineca and Coast Belts. The Intermontane Belt spans much of central British Columbia along a broad northwest trending belt. Rocks of volcanic island arc and oceanic arc affinity underlie the Intermontane Belt and are overlapped by sedimentary rocks derived from bordering uplifted sedimentary basins. The Coast Belt is a high relief region that forms the Coast and Cascade Mountains which are largely comprised of batholiths and metamorphic rocks of the Coast Plutonic Complex. The Insular Belt is composed of mafic to felsic volcanic and clastic and carbonate rocks (Monger and Price, 2002). The distinct morphogeological belts are a reflection of the rocks and terranes that underlie them and represent complex tectonic activity that occurred throughout the protracted formation of the Canadian Cordillera.
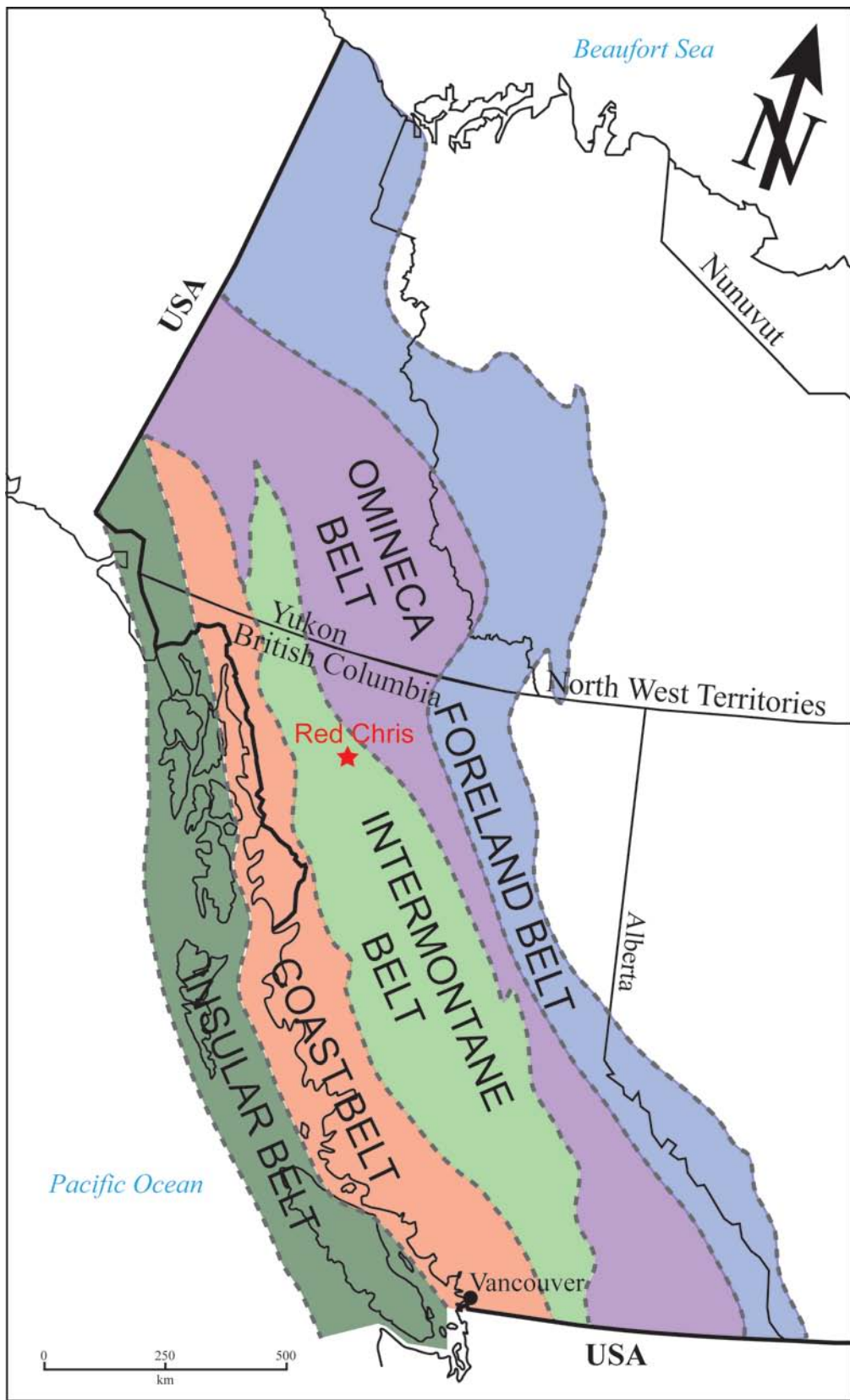
Figure 2.1 Morphogeological belts of the Canadian Cordillera (after Gabrielse et al., 1991a).

2.1.2 The Intermontane Superterrane

The major tectonic element of the Intermontane Belt is the Intermontane Superterrane, an amalgamation of distinct terranes prior to accretion to the North American continent in the Jurassic period. The Intermontane Superterrane consists of several Devonian through Jurassic volcanic-island arc and oceanic-arc assemblages of the Quesnellia, Stikinia, and Cache Creek terranes (Monger and Price, 2002; Nelson and Colpron, 2007 Figure 2.2). Volcanic arc and associated plutonic rocks underwent significant deformation during terrane amalgamation and subsequent accretion. The Stikine and Skeena Arches are two broad regions of uplift in north and central British Columbia formed by contraction during terrane amalgamation and accretion (Gabrielse et al., 1991a). Middle and Late Cretaceous uplift of rocks underlying the Omineca and Coast Belts provided source regions for much of the widespread clastic sedimentary deposits overlapping Quesnellia, Stikinia and Cache Creek (Yorath, 1991) including the Bowser and Skeena-Sustut basins (Gabrielse et al., 1991a). Additionally, the Nechako basin is another sedimentary basin south of the Skeena Arch, however the term 'Nechako basin' is often used inconsistently in literature, referring to different regions and contains a wide range of rock types such that Riddell (2011) suggests that the term be discontinued. Flat lying, widespread Tertiary volcanic rocks overlie Jurassic to Cretaceous strata and older rocks (Yorath, 1991). Much of the Canadian Cordillera was glaciated in Quaternary time.
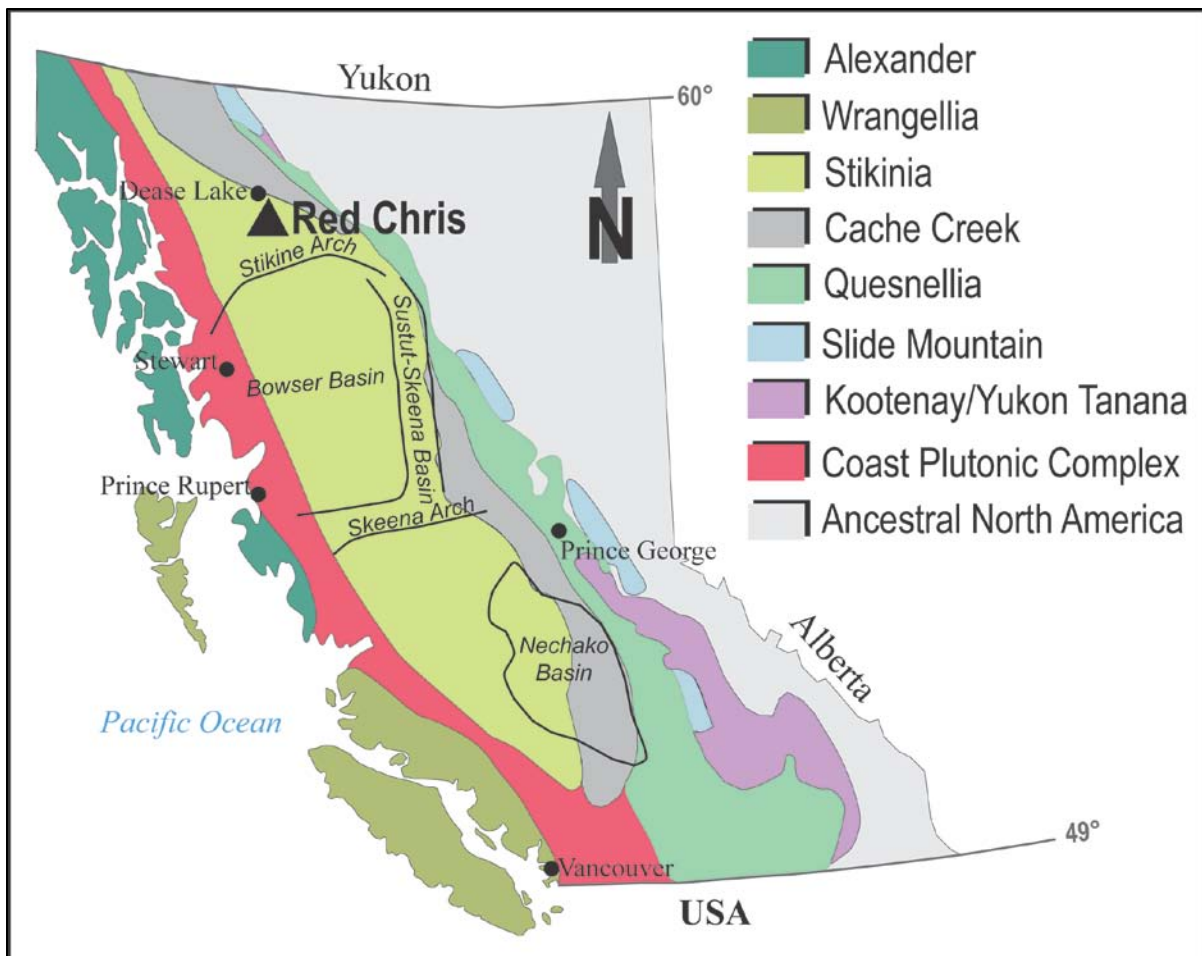
Figure 2.2 Major terranes and tectonic elements of British Columbia including major arches and sedimentary basins of Stikinia. Arches and basins from Gabrielse et al., 1991a.

Quesnellia and Stikinia have been considered to be a single continuous, elongated arc prior to amalgamation and accretion onto the North American continental margin (Nelson and Mihalynuk, 1993). Quesnellia and Stikinia are dominated by Late Triassic to Early Jurassic volcanic island-arc terranes, are built on Permian limestones with *McCloud* type faunas (Nelson and Mihalynuk, 1993), have similar compositions and stratigraphy with significant volumes of augite-phyric basalt, and host similar porphyry copper deposits. The Cache Creek terrane, which currently separates Quesnellia and Stikinia across much of the length of the Intermontane Superterrane, is composed of oceanic plateaus with distinct exotic *Tethyan* fusilinind faunas (Monger and Ross, 1971). Oceanic plateaus of the Cache Creek terrane could have impinged upon this elongated Quesnellia-Stikinia island arc in the latest Permian to Middle Triassic, causing an anti-clockwise rotation of the northern Stikinia portion around the plateaus, eventually enclosing the Cache Creek between the two island arcs sometime in the Middle Jurassic (Nelson and Mihalynuk, 1993; Figure 2.3).

18
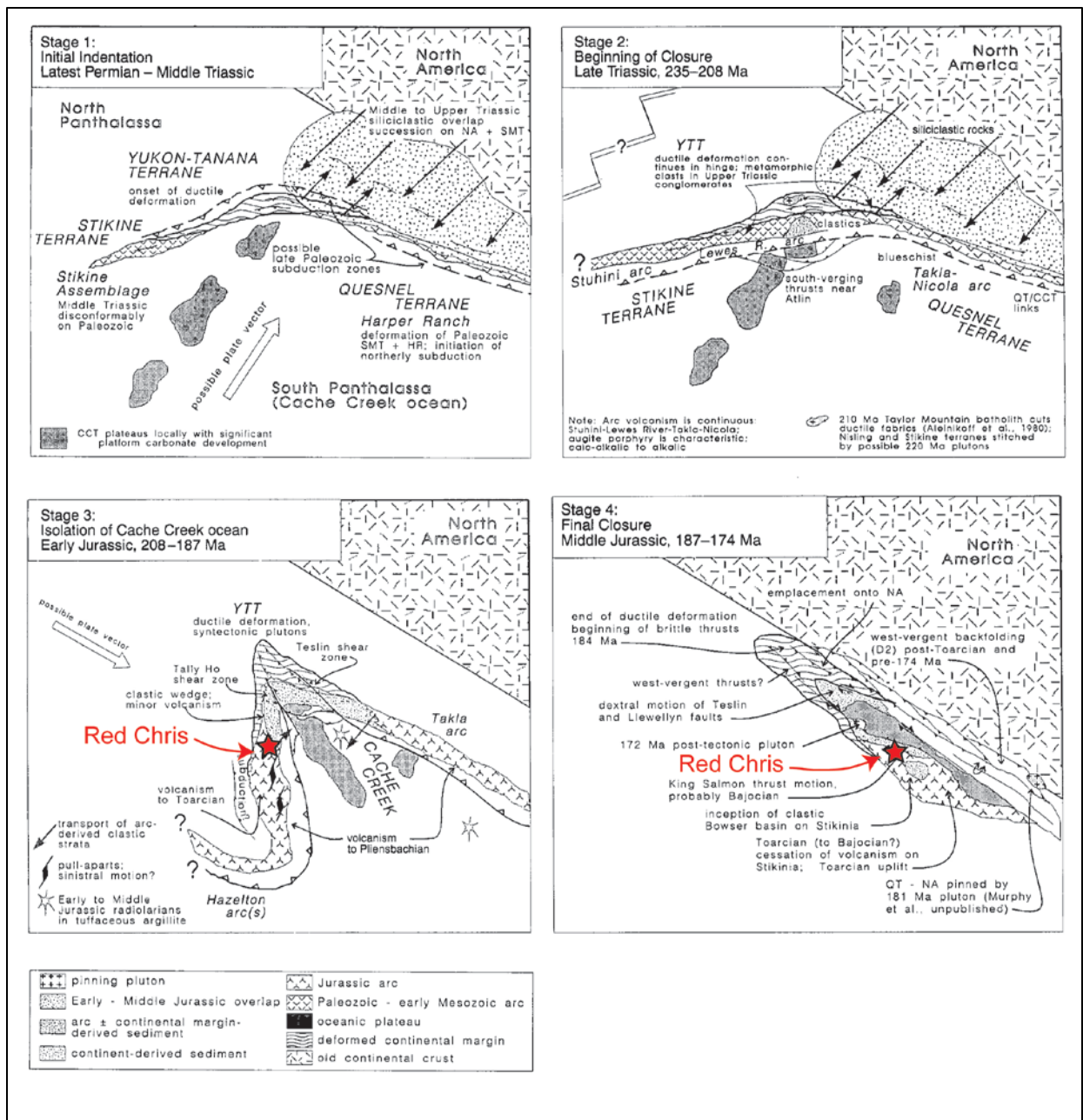
Figure 2.3 Staged evolution of the Cache Creek enclosure whereby the elongated Quesneillia-Stikinia island arc enclosed oceanic plateaus of Cache Creek by counter-clockwise rotation of Stikinia through latest Permian to Middle Jurassic time (from Nelson and Mihalynuk, 1993). Formation of Red Chris in northern Stikinia during Stage 3 (~204 Ma). NA = North American miogeocline, CCT = Cache Creek terrane, SMT = Slide Mountain terrane, HR = Harper Ranch Group, YTT = Yukon-Tanana terrane, QT = Quesnellia terrane

2.1.3 **Quesnellia**

Quesnellia spans from the southern border of British Columbia to the middle of the province where it then narrows to a discontinuous sliver north of Prince George (Monger et al., 1991; Figure 2.2). Quesnellia structurally overlies the Slide Mountain, Cassiar and Kootenay terranes to the east, and on the west is bounded by steep dipping faults and is in structural contact

19

with the Cache Creek Terrane and Stikinia (Dawson et al., 1991). Quesnellia is composed of Upper Paleozoic and Mesozoic volcanic and sedimentary rocks and associated plutons (Monger et al., 1991; Dawson et al., 1991; Figure 2.4).
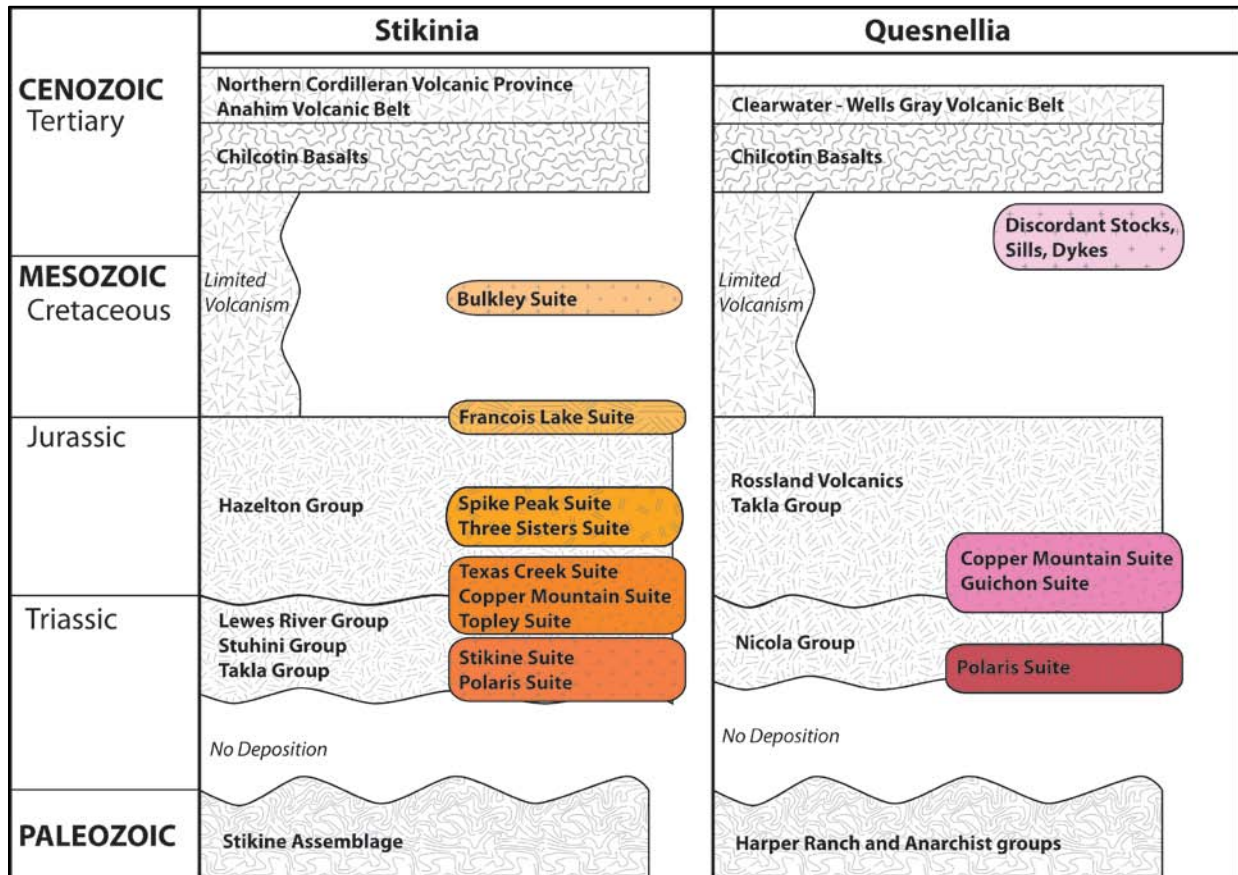
Figure 2.4 Generalized stratigraphic columns of major volcanic and plutonic suites of Stikinia and Quesnellia. Formation of Red Chris is associated with the Copper Mountain Suite of northern Stikinia.

2.1.3.1   Volcanic Rocks of Quesnellia

The oldest volcanic units in Quesnellia belong to Upper Paleozoic sequences of the Harper Ranch and Anarchist groups, which contain abundant clastic detritus, including volcanic sandstone and minor andesite, basalt flows and pyroclastic rocks (Souther, 1991). The Harper Ranch Group, in its type area in southern Quesnellia is comprised of two major sequences, Late Devonian to Late Mississippian successions of volcaniclastic rocks, siliciclastic rocks, and limestone, which are unconformably overlain by Permian limestone (Beatty et al., 2006). The Harper Ranch and Anarchist groups are unconformably overlain by the island arc volcanic and sedimentary strata of the Upper Triassic Nicola Group, a unit characteristic of Quesnellia (Dawson et al., 1991, Souther, 1991; Monger et al., 1991). Mafic lavas of the Nicola Group are widespread in southern Quesnellia and can be divided into three distinct petrological and

geochemical types (Mortimer, 1987). The first type is strongly augite-porphyritic alkaline lavas representative of a high-potassium to shoshonitic rock series. The second type is augite- and plagioclase-porphyritic subalkaline lavas representative of a low-potassium, calc-alkaline series. The third type is volumetrically subordinate to the other types and is composed of tholeiitic to transitional lavas.

After a hiatus between latest Triassic to Early Jurassic, volcanic activity resumed in Jurassic time with the eruption of the Rossland Group volcanic rocks in southern Quesnellia and the Takla Group in central and northern British Columbia (Souther, 1991, Monger et al., 1991). The Rossland Group in its type area in southeastern British Columbia consists of Jurassic volcanic rocks and conglomerate intercalated with marine shale and siltstone (Souther, 1991; Beatty et al., 2006). Lavas associated with the Rossland Group are typically augite porphyry basalt, similar to the underlying Nicola Group (Souther, 1991).

Volcanism in the Cretaceous and Tertiary was concentrated along the western margin of the Intermontane Superterrane (Souther, 1991). Notable volcanic activity in Neogene includes the Chilcotin back-arc basalt lavas, a 36 500 km^2 plateau in south-central British Columbia that extends through the Intermontane Superterrane from southern British Columbia to the Bowser Basin (Souther, 1991; Andrews and Russell, 2007). Late Cenozoic volcanic activity in the Clearwater-Wells Gray area includes alkali olivine basalt flows that lie east of the Chilcotin Group basalts and define the eastern margin of the Anahim Volcanic Belt (Hickson and Souther, 1984; Souther, 1991).

2.1.3.2 Plutonic Rocks of Quesnellia

Plutonic activity within Quesnellia is concentrated in the Mesozoic with lesser activity occurring in early Tertiary time. Most of the plutons emplaced in the Late Triassic are restricted to small, Alaskan-type ultramafic bodies of the Polaris Ultramafic Suite that occur in northern Quesnellia near the north and east margins of the Hogem Batholith (Woodsworth et al., 1991). Dominantly Late Triassic calc-alkaline batholiths and alkaline bodies of the Guichon and Copper Mountain intrusive suites show both spatial and temporal affinities with Upper Triassic Nicola Group volcanic rocks (Woodsworth et al., 1991, Monger et al., 1991). The latest Triassic Guichon Suite forms numerous large and generally calc-alkaline plutons as one of the characteristic units of Quesnellia. This includes the Guichon Creek, Hogem and Pitman

batholiths, which are generally elongated, hornblende rich, granodioritic plutons (Woodsworth et al., 1991). The Guichon Creek Batholith, dated by U-Pb analysis on zircon to be 210 ± 3 Ma (Mortimer, 1990) is the most studied pluton in the Canadian Cordillera and it is host to porphyry Cu-Mo deposits including Highland Valley. Other Early Jurassic plutons of southern Quesnellia include the Pannask and Wildhorse batholiths in addition to several other smaller plutons.

The Copper Mountain Suite, also characteristic of Quesnellia, consists of numerous, small alkaline intrusive bodies that form in a roughly linear, northwest-trending belt extending from the southern border of British Columbia to the Stikine Arch (Woodsworth et al., 1991). These dominantly Late Triassic, small, equant stocks are typically only a few square kilometers in diameter and are commonly syenite, monzonite, and monzodiorite in composition with local diorite, monzogranite and clinopyroxenite (Woodsworth et al., 1991). The largest pluton of the Copper Mountain Suite in north-central Quesnellia is the Duckling Creek Syenite Complex, spatially related to the Hogem Batholith and hosts the Lorraine Cu-Au porphyry deposit, dated as 178.8 to 176.5 Ma, Early Jurassic (Bath et al., In Press). The Duckling Creek Syenite Complex is composed of two distinct intrusive phases, a feldspathic pyroxenite, mela-syenite and monzonite phase, and a leucosyenite and K-feldspar megacrystic porphyry phase (Nixon and Peatfield, 2003). In southern Quesnellia, Late Triassic intrusions of the Copper Mountain Suite host many alkalic Cu-Au ± Ag-rich porphyry deposits, including Copper Mountain, dated as 202.7 ± 4.4 Ma by U-Pb analysis of zircon (Mortensen et al., 1995). The Afton-Ajax Cu-Au porphyry deposit is associated with the Iron Mask Batholith (Copper Mountain Suite) and dated around 205 Ma by U-Pb analysis of zircon (Mortensen et al., 1995). Abundant Early Tertiary plutons occur in Quesnellia as small, high-level discordant stocks, sills and dykes, many of which are spatially and genetically related to volcanic rocks in the region (Woodsworth et al., 1991).

2.1.4 **Stikinia**

Stikinia is the largest terrane in the Canadian Cordillera, spanning from southern Yukon to south-central British Columbia (Gabrielse et al., 1991a; Figure 2.2). Stikinia is in fault contact with the Cache Creek Terrane to the east and its relationship with the Alexander and Wrangellia terranes to the west is obscured by Cretaceous and Tertiary plutonism and metamorphism of the Coast Plutonic Complex (Monger et al., 1991). Stikinia is comprised of a well-stratified sequence of Lower Devonian to Middle Jurassic volcanic and sedimentary strata along with

several plutonic suites that are largely coeval with the arc-related volcanic rocks (Dawson et al., 1991; Monger et al., 1991; Figure 2.4).

2.1.4.1 Volcanic Rocks of Stikinia

The Paleozoic Stikine assemblage represents the structurally and stratigraphically lowest rock unit in northern Stikinia (Logan et al., 2000). Rocks of the Stikine assemblage typically occur around the periphery of, and likely beneath the Bowser Basin, as tholeiitic to calc-alkaline, mafic and bimodal flows and volcaniclastic rocks interbedded with carbonate, shale, volcanic sandstone and minor chert (Souther, 1991; Logan et al., 2000). Unconformably overlying the Stikine assemblage are the Upper Triassic volcanic assemblages of the Lewes River, Stuhini, and Takla groups (Souther, 1991; Logan et al., 2000). The Lewes River and Stuhini groups are best developed in north and north-central Stikinia, and the Takla Group occurs on the eastern margin of Stikinia (Souther, 1991, Monger et al., 1991). These volcanic rocks resemble the eastern part of the Nicola Group in Quesnellia (Monger et al., 1991). The Lewes River Group is comprised of basalt and andesite flows, breccias and tuff which are associated with coarse conglomerate and greywacke (Souther, 1991). The Stuhini Group contains andesites and basaltic andesites with augite ± feldspar phenocrysts as well as bladed feldspar porphyries (Souther, 1991). The Takla Group covers more than 30 000 km^2 in Stikinia and is well exposed in the McConnell Creek map area, the type area for the group (Dostal et al., 1999). The Takla Group is comprised of basaltic to andesitic flows and pyroclastic rocks, volcanogenic sandstones and argillites deposited under subaerial to submarine conditions (Church, 1975; Souther, 1991; Dostal et al., 1999). In the Forrest Creek – Mess Creek area, the mainly submarine volcanic rocks of the Stuhini Group are unconformably overlain by the Jurassic, mainly subaerial volcanic and sedimentary rocks of the Hazelton Group (Logan et al., 2000). The Hazelton Group contains three major sequences, a lower unit of intermediate flows and volcaniclastic rocks, a middle felsic volcanic unit and an upper unit of sedimentary and submarine bimodal volcanic rocks (Logan et al., 2000).

In Stikinia, limited volcanism occurred during the Cretaceous Period. As in Quesnellia, the Neogene Chilcotin Group basalts cover much of central and southern Stikinia. Neogene volcanism also includes the Anahim Volcanic Belt in south-central Stikinia and the northern Cordilleran volcanic province in northern Stikinia (Edwards and Russell, 2000). Within the northern Cordilleran volcanic province, the most voluminous volcanic deposits are broad plateaus of coalesced, basaltic shield volcanoes (Edwards and Russell, 2000). In northern

Stikinia, these include the Level Mountain, Mount Edziza, Heart Peaks and Maitland volcanic complexes.

2.1.4.2 Plutonic Rocks of Stikinia

Plutonic activity in Stikinia was concentrated in Late Triassic through Early Jurassic time with lesser activity throughout the Mesozoic and Cenozoic. In the Late Triassic, two plutonic suites developed within Stikinia, the Polaris and Stikine suites, forming between 228 to 221 Ma (Logan et al., 2000). The Polaris Ultramafic Suite, a belt of numerous, small, Alaskan-type ultramafic to mafic intrusions forms an arcuate belt around the eastern and northern margin of the Bowser Basin (Woodsworth et al., 1991). The Stikine Suite intrudes Stikinia along the Stikine Arch on the north and western margin of the Bowser Basin and is comprised of tholeiitic to calc-alkaline granitoids (Woodsworth et al., 1991), including the Hickman Pluton which hosts the Cu-Mo ± Au Schaft Creek deposit (Logan et al., 2000; Scott et al., 2008).

Three major suites intruded Stikinia in Late Triassic to Early Jurassic time, the Topley, Copper Mountain and Texas Creek suites. The Topley Suite, occurring along the Skeena Arch contains calc-alkaline stocks and batholiths of massive to weakly foliated biotite and hornblende bearing granite to quartz diorite (Woodsworth, et al., 1991) and has been dated between 218 and 193 Ma (U-Pb on zircon and Ar/Ar on hornblende and biotite; MacIntyre et al., 2001.) The Copper Mountain Intrusive Suite comprises a series of small, alkaline bodies that intruded Stikinia along the eastern margin of the Coast Plutonic Complex (Woodsworth et al., 1991; Logan et al., 2000). Intrusions of the Copper Mountain Suite compositionally vary from monzodiorite to monzonite to syenite, are between 210 and 195 Ma age, and host copper and gold mineralization in deposits such as Galore Creek (Logan et al., 2000) and Red Chris. The Texas Creek Suite is centered near Stewart, and defines a northwest trending belt in northwestern British Columbia, roughly parallel with the international border with Alaska (Logan et al., 2000). Plutons consist of calc-alkaline, hornblende granodiorite and quartz monzonite to alkaline, K-feldspar megacrystic monzogranite (Kerr, 1948; Anderson, 1993; Woodsworth et al., 1991) and are considered to be Early Jurassic in age, between 195 and 189 Ma (Brown et al., 1996; Logan et al., 2000). Local mesothermal and epithermal base and precious metal vein deposits are associated with the Texas Creek Suite.

Early to Middle Jurassic plutonic activity includes intrusions of the Three Sisters and Spike Peak suites. Intrusions of the Three Sisters Suite occur along the Stikine Arch, north of the Bowser Basin in the western part of the Iskut River and Telegraph Creek areas (Woodsworth et al., 1991; Anderson, 1993; Brown et al., 1996). The suite comprises large, north and east trending calc-alkaline quartz monzonite to granite plutons, 179 to 176 Ma age (Brown et al., 1996; Logan et al., 2000). The Yehiniko Pluton is a major intrusion of the Three Sisters Suite and has cooling ages around 172 ± 6 Ma (K-Ar on biotite; Holbek, 1988). Plutons of the Spike Peak Suite (MacIntyre et al., 2001) are recognized as pink to red quartz monzonite and hornblende diorite intrusions in regions between Babine and Takla Lakes. These intrusions are lithologically similar to the Topley Suite but are compositionally distinct and younger, dated between 178.6 ± 0.3 Ma (U-Pb on zircon) and 166.0 ± 0.2 Ma (Ar/Ar on hornblende; MacIntyre et al., 2001).

Late Jurassic to Early Cretaceous plutons of the Francois Lake Suite intrude along the eastern portion of the Skeena Arch in central British Columbia (Woodsworth et al., 1991). Most intrusions are northwesterly elongate batholiths and biotite granite to quartz monzonite with conspicuous K-feldspar megacrysts represents the dominant lithology (Woodsworth et al., 1991). Intrusions of the Francois Lake Suite are mostly 145 to 135 Ma (K-Ar on biotite) with some reporting older ages (White et al., 1970).

Late Cretaceous plutons intrude across central British Columbia as small, high-level discordant stocks, dykes and sills, concentrated along the Skeena Arch are known as the Bulkley Suite (Woodworth et al., 1991). Most of the intrusions are granodiorite and quartz diorite and many of the smaller bodies host Cu-Mo porphyry mineralization. Widespread plutonic activity in the Canadian Cordillera was finished by Middle Eocene (Woodsworth et al., 1991).

2.2 Porphyry Deposits of the Canadian Cordillera

Throughout the Canadian Cordillera, porphyry deposits broadly formed during two distinct time periods, and can be classified as pre-accretionary, syn-accretionary or post-accretionary deposits (MacMillan et al., 1995). Pre- and syn-accretionary porphyry deposits formed in the Early Mesozoic, while the post-accretionary deposits formed in the Late Mesozoic to Cenozoic (McMillan et al., 1995). Pre- and syn-accretionary deposits are further subdivided into calc-

alkalic and alkalic porphyry deposits on the basis of the composition of their host rocks and deposit styles. The post-accretionary deposits are dominantly calc-alkalic.

Pre-accretionary porphyry deposits mostly formed in island arcs that formed outboard from the continent prior to their accretion to the western margin of the ancient North American craton. These deposits formed between Late Triassic and Middle Jurassic time and are genetically linked to subduction-related tectonics and arc formation (McMillan et al., 1995). Pre-accretionary porphyry deposits formed in Quesnellia, Stikinia, and Wrangellia and occur locally in Cache Creek (Table 2.1). Pre-accretionary deposits hosted in Quesnellia formed mostly between 210 and 200 Ma (McMillan et al., 1995; Mortensen et al., 1995) and include Brenda, the Highland Valley District, Afton-Ajax, Mount Polley, and Copper Mountain. Pre-accretionary porphyry deposits in Stikinia are concentrated in northern British Columbia and formed between 220 and 196 Ma (McMillan et al., 1995; Mortensen et al., 1995), and include Kemess, Kerr, Schaft Creek, Sulphurets, Galore Creek, Red Bluff and Red Chris. Syn-accretionary deposits formed during the accretion of the terranes to the continent in the middle Jurassic and include the Mt. Milligan and Lorraine deposits of Quesnellia, emplaced between 190 and 176 Ma (Mortensen et al., 1995, Jago et al., In Press). Post-accretionary porphyry deposits formed in terranes that previously amalgamated and accreted to the North American margin. These deposits are Late Cretaceous to Eocene in age and are hosted in a wide range of older country rocks (McMillan et al., 1995).

Table 2.1 Pre- and Syn-Accretionary Porphyry Deposits of the Intermontane Superterrane

Deposit	Metals	Host Intrusive	Terrane	Age of Mineralization
Pre-Accretionary Deposits				
Brenda	Cu-Mo	Calc-alkaline	Quesnellia	~210 Ma
Highland Valley	Cu-Mo	Calc-alkaline	Quesnellia	~210 Ma
Kemess	Cu-Au ± Mo	Calc-alkaline	Stikinia	~202 Ma
Kerr	Cu-Au	Calc-alkaline	Stikinia	~197 Ma
Schaft Creek	Cu-Mo ± Au	Calc-alkaline	Stikinia	~220 Ma
Sulphurets	Cu-Au-Mo	Calc-alkaline	Stikinia	~196 Ma
Afton-Ajax	Cu-Au	Alkaline (silica saturated)	Quesnellia	~205 Ma
Mount Polley	Cu-Au	Alkaline (silica undersaturated)	Quesnellia	~202 Ma
Copper Mountain	Cu-Au	Alkaline (silica saturated)	Quesnellia	~204 Ma
Galore Creek	Cu-Au	Alkaline (silica undersaturated)	Stikinia	~210 Ma
Red Chris	Cu-Au	Alkaline (silica saturated) /Calc-alkaline?	Stikinia	~204 Ma
Red Bluff	Cu-Au	Alkaline (silica saturated) /Calc-alkaline?	Stikinia	~210 Ma
Gibraltar	Cu-Mo	Calc-alkaline	Cache Creek	~217 Ma
Syn-Accretionary Deposits				
Lorraine	Cu-Au	Alkaline (silica saturated/ undersaturated)	Quesnellia	~178 Ma
Mount Milligan	Cu-Au	Alkaline (silica saturated)	Quesnellia	~183 Ma

 (After McMillan et al., 1995, Mortensen et al., 1995, and Bath et al., In Press)

2.2.1   **Pre-Accretionary Calc-alkalic Porphyry Deposits of the Canadian Cordillera**

Pre-accretionary calc-alkalic porphyry deposits contain copper, molybdenum and locally gold within two distinct regions of the Intermontane Belt (Figure 2.5). In the southern Quesnellia and the southern Cache Creek terranes, the calc-alkalic deposits are rich in copper and molybdenum (Cu-Mo) and include Brenda, Gibraltar and Highland Valley. These deposits formed between ~217-210 Ma (McMillan et al., 1995). The second region hosting pre-accretionary calc-alkalic porphyry deposits is northern Stikinia and contains copper, gold and molybdenum-rich deposits (Cu-Au-Mo). Major deposits include Kerr, Schaft Creek, Sulphurets and both the North and South zones of the Kemess deposit. These Cu-Au-Mo deposits formed over a wider range in time than their southern Quesnellia, Cu-Mo counterparts, between ~220-196 Ma (McMillan et al., 1995).
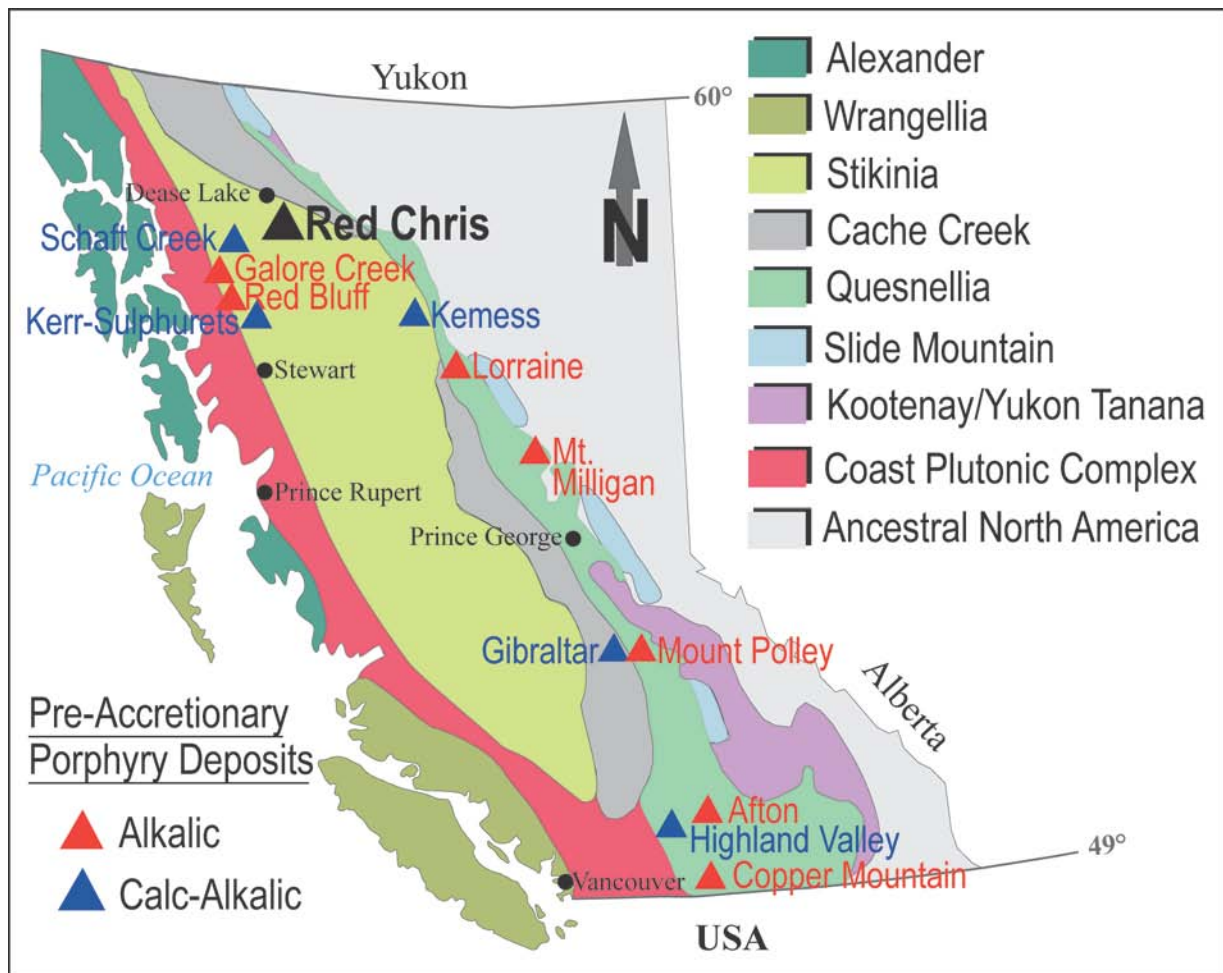
Figure 2.5 Major terranes, tectonic elements and select pre-accretionary porphyry deposits of British Columbia.

2.2.2 Pre-Accretionary Alkalic Deposits of the Canadian Cordillera

Alkalic porphyry deposits are entirely pre-accretionary, strictly copper- and gold-rich (Cu-Au), occur in two major areas of the Intermontane Belt, south to central Quesnellia and northern Stikinia, and are classified as either silica-saturated or silica-undersaturated deposits (Lang et al., 1995b).

Silica-undersaturated porphyry deposits are related to Late Triassic alkaline intrusions in Quesnellia and Stikinia with distinctive chemical, mineralogical and textural features (Lueck and Russell, 1994). The host intrusions are commonly syenite, and lesser pyroxenite composed of aegerine-augite, K-feldspar, biotite, melanite, titanite and apatite with local hornblende, magnetite, plagioclase and vishnevite-cancrinite (Lueck and Russell, 1994). Diagnostic features of silica-undersaturated intrusions include the presence of accessory melanite (Ti-bearing andradite garnet), zoned plutons, commonly with a pyroxenite border and a central syenite core,

28

and a prominent mineral fabric of planar crystal alignment (Lueck and Russell, 1994). Porphyry deposits associated with silica-undersaturated intrusions occur in middle Quesnellia (Mount Polley) and in northern Stikinia (Galore Creek; Lang et al., 1995b). Lorraine, in northern Quesnellia has alteration and mineralization characteristics of silica-undersaturated as well as silica-saturated intrusions (Lang et al., 1994, 1995b).

Silica-saturated porphyry deposits are related to intrusions that have fewer distinguishing features than silica-undersaturated intrusions. These Early Mesozoic intrusions are predominantly in Quesnellia and were emplaced into alkalic, augite-phyric, mafic to intermediate mafic rocks of the Nicola or Takla Groups (Lang et al., 1995b). The intrusions range from batholiths to dyke swarms and comprise equigranular to porphyritic diorite to monzonite (Lang et al., 1995b). The typical igneous mineral assemblage includes augite, biotite, magnetite, plagioclase, K-feldspar and apatite with less common hornblende and titanite with trace to minor quartz (Lang et al, 1995b). Each mineral, except for quartz, occurs as a phenocryst phase. Neither textural nor compositional zonation is observed in silica-saturated plutons, with the exception of Copper Mountain (Lang et al., 1995b). Quesnellia hosts the silica-saturated alkalic porphyry deposits of Mt. Milligan, Copper Mountain and deposits associated with the Iron Mask Batholith (Afton, Ajax, Pothook, and Crescent) and Lorraine (Lang et al., 1995b). Red Chris and Red Bluff are associated with monzonite to quartz monzodiorite and quartz diorite to monzodiorite, respectively (Baker et al., 1997; Rhys, 1995). Red Chris and Red Bluff have not formally been classified as silica-saturated deposits however their host intrusions have similar features and are best classified as silica-saturated alkalic stocks of northern Stikinia.

2.3   Regional Geology and Structure of Red Chris

Early Carboniferous to Late Tertiary rocks compose the northern Stikinia stratigraphy around Red Chris (Figure 2.6). The oldest rocks are the Paleozoic Stikine assemblage which is overlain by the voluminous and widespread Triassic to Middle Jurassic volcanic-arc successions of the Stuhini and Hazleton Groups (Evenchick and Thorkelson, 2005). In the early Middle Jurassic, Stikinia amalgamated with Cache Creek and Quesnellia and accreted to the ancient North American margin to the west. This closure of the Cache Creek Ocean between Stikinia and Quesnellia resulted in the obduction of the Cache Creek terrane onto Stikinia (Evenchick and Thorkelson, 2005). In the Middle Jurassic in a dominantly amagmatic environment, a large clastic marine basin was deposited onto Stikinia between the Skeena and Stikine Arches, termed

the Bowser Basin. The Bowser Lake Group represents a basin filling succession derived from the northeast and east due to erosion of the Cache Creek Terrane. Chert clasts within the Bowser Basin provide a provenance link between Stikinia and Cache Creek Terrane (Evenchick and Thorkelson, 2005). Several suites of subvolcanic intrusions were emplaced into the Paleozoic Stikine assemblage and volcanic rocks of the Stuhini and Hazelton Groups prior to accretion. A small volume of these intrusions are Paleozoic, however the majority are Triassic to early Middle Jurassic in age (Evenchick and Thorkelson, 2005).

Figure 2.6 Regional geological map around Red Chris as mapped and compiled by C. Rees. Legend on following page.

LEGEND

STRATIFIED ROCKS

QUATERNARY — Q: Glacial and post-glacial sediments

PLIOCENE — PMb: Olivine basalt *(Maitland Volcanics)*

MIDDLE JURASSIC — MJBs: Sandstone, siltstone, conglomerate *(Bowser Lake Group)*

EARLY to MIDDLE JURASSIC — EMJH: Siltstone, sandstone, minor limestone *(Hazelton Group)*

LATE TRIASSIC to EARLY JURASSIC — LTrEJabxs: Andesitic volcanics, volcaniclastics

LTrEJvbxs: Basaltic to andesitic volcanics, volcaniclastics, sediments

LATE TRIASSIC — LTrSl: Limestone

LTrSss: Sandstone, siltstone *(Stuhini Group)*

LTrSv: Basaltic-andesitic volcanics, volcaniclastics *(Stuhini Group)*

LATE PALEOZOIC — PZv: Mafic volcanics, greenstone *(Stikine assemblage)*

EMc: Limestone, dolostone *(Stikine assemblage)*

EMsv: Metavolcanics, metasediments *(Stikine assemblage)*

INTRUSIVE ROCKS

JURASSIC-TERTIARY — JTi: Leucogranite, quartz monzonite

EARLY JURASSIC — EJg: Alkali granite

LATE TRIASSIC - EARLY JURASSIC — LTrJEmd: Equigranular diorite, monzodiorite *(Ealue Stock)*

LTrEJmd: Porphyritic diorite, monzodiorite, monzonite *(Red Stock)*

LTrEJd: Diorite

LATE TRIASSIC — LTri: Monzodiorite

EARLY MISSISSIPPIAN — EMgd: Granodiorite, diorite

—— River/Stream   — — — Approx. Fault   — — — Inferred Fault   - - - - Contact

Property Boundary   Lake   Mountain

Legend for Figure 2.6.

32

2.3.1 **Stratified Rocks**

2.3.1.1 Late Paleozoic Stikine Assemblage

The oldest rocks are small outcrops of the Late Paleozoic Stikine assemblage as described by Read and Psutka (1990) and Ash et al. (1997a) as cleaved and deformed greenstone, limestone, other variably metamorphosed sedimentary rocks and mafic to felsic plutonic rocks. Rocks of the Stikine assemblage near Red Chris occur mostly north of Ealue Lake. Mafic volcanic rocks and tuff (unit **PZv** on Figure 2.6) occur along a border between the metavolcanic rocks and metasedimentary rocks (unit **EMsv** on Figure 2.6) of the Stikine assemblage with a unit of Triassic to Jurassic andesitic volcaniclastic rocks to the west. A small unit of grey to white bedded limestone (unit **EMc** on Figure 2.6) is also associated with the metavolcanic rocks and metasedimentary rocks (Evenchick and Thorkelson, 2005). Stikine assemblage strata are distinguished from younger rocks by the presence of a penetrative cleavage and greenschist-facies metamorphism (Evenchick and Thorkelson, 2005).

2.3.1.2 Late Triassic Stuhini Group Volcanic and Sedimentary Rocks

The Late Triassic volcanic and sedimentary rocks of the Stuhini Group underlie much of the area between Ealue and Kluea Lakes and are the first unit of volcanic rocks to be built upon the Paleozoic basement of Stikinia. The volcanic rocks (unit **LTrSv** on Figure 2.6), basaltic-andesite volcanic and volcaniclastic rocks consist of greenish-grey, aphyric to porphyritic mafic lava flows (Evenchick and Thorkelson, 2005). Augite phenocrysts dominate and are associated with plagioclase, serpentinized olivine and lesser biotite phenocrysts. The augite basalt flows are locally intercalated with pyroclastic rocks of intermediate composition, and in places have lapilli of hornblende feldspar porphyry (Schink, 1977). The mafic-derived sedimentary rocks of the Stuhini Group (unit **LTrSss** on Figure 2.6) include shale, siltstone, sandstone and conglomerate. The Stuhini Group volcanic and sedimentary rocks were deposited in a mainly submarine setting (Evenchick and Thorkelson, 2005). The mafic lava flows contain serpentinized olivine and rarely contain iddingsitized olivine and reddish flow margins.

2.3.1.3 Triassic-Jurassic Conglomerate

Conglomerate that is not clearly related to either the Stuhini Group or the Hazelton Group are mapped as a Triassic to Jurassic unit of andesitic volcaniclastic rocks and conglomerate (units **LTrEJabxs** and **LTrEJvbxs** on Figure 2.6). These rocks were not mapped as separate, distinct units by Read and Psutka (1990) and Gabrielse and Tipper (1984) and were assigned as

part of the Stuhini or Hazelton Groups. A substantial portion of the map area north of Ealue Lake is underlain by the conglomeratic unit, where it was included in the Hazelton Group by Evenchick and Thorkelson (2005). Future studies may be able to place these Triassic-Jurassic conglomeratic rocks within the Hazelton or Stuhini Groups, however it is currently recognized by its distinctive lithology over broad areas and is mapped as a separate unit (Evenchick and Thorkelson, 2005). Successions of this unit include a coarse, matrix-supported sedimentary melange containing granule-size chert clasts and cobble to boulder size clasts of marble and limestone (Evenchick and Thorkelson, 2005). In the area of Red Chris, this unit occurs north and northwest of Todagin Mountain as coarse sediment gravity flows containing abundant clasts of hornblende-phyric andesite. Debris flows are 1 to 4 m thick and are composed of a dark brown, sandy matrix, and host sub-rounded to sub-angular clasts up to 20 cm in diameter.

2.3.1.4 Jurassic Hazelton Group

The Jurassic Hazelton Group (unit **EMJH** on Figure 2.6) includes all Early to Middle Jurassic volcanic and related sedimentary rocks on Stikinia (Evenchick and Thorkelson, 2005). The Hazelton Group contains a wide variety of rock types, including felsic to mafic lava, breccias, tuff, limestone and epiclastic rocks ranging from conglomerate to shale. Therefore, a single description of the group is difficult and the main criterion for this Group is an Early to Middle Jurassic age (Evenchick and Thorkelson, 2005). While age is not the most suitable distinguishing feature for defining this stratigraphic unit, it is the best available correlatable element for this unit where rock types are widely varied and usually laterally discontinuous (Evenchick and Thorkelson, 2005). The volcanic rocks of the Hazelton Group are divided into three distinct successions; the Griffith Creek volcanics, the Cold Fish volcanics and the Mount Brock volcanics. Much of the map area north of Ealue Lake mapped by Evenchick and Thorkelson (2005) as Hazelton Group includes maroon, grey and green aphyric to porphyritic breccias, tuff and flows. A bimodal succession of basalt-rhyolite occurs southwest of Todagin Mountain where the basalt forms massive flows and pillow breccias and the felsic rocks are ash, lapilli tuff-breccia and massive flows (Evenchick and Thorkelson, 2005). Intercalated with and overlying the volcanic rock is the Spatsizi Formation, a succession of rocks where fine to coarse-grained sedimentary rocks dominate over the volcanic rocks (Evenchick and Thorkelson, 2005). Only limited volumes of the Hazelton Group occur in the area of Red Chris, between the Red Stock and Kluea Lake as calcarenite (unit **EJHl** on Figure 2.7), feldspathic sandstone (unit **EMJs** on Figure 2.7) and siltstone of the Spatsizi Formation (unit **MJSs** on Figure 2.7). Facies

transitions and thinning of the Spatsizi Formation successions indicate that the depositional basin shallowed to the north where the Spatsizi Formation laps onto the topographically positive Stikine Arch (Thomson et al., 1986).
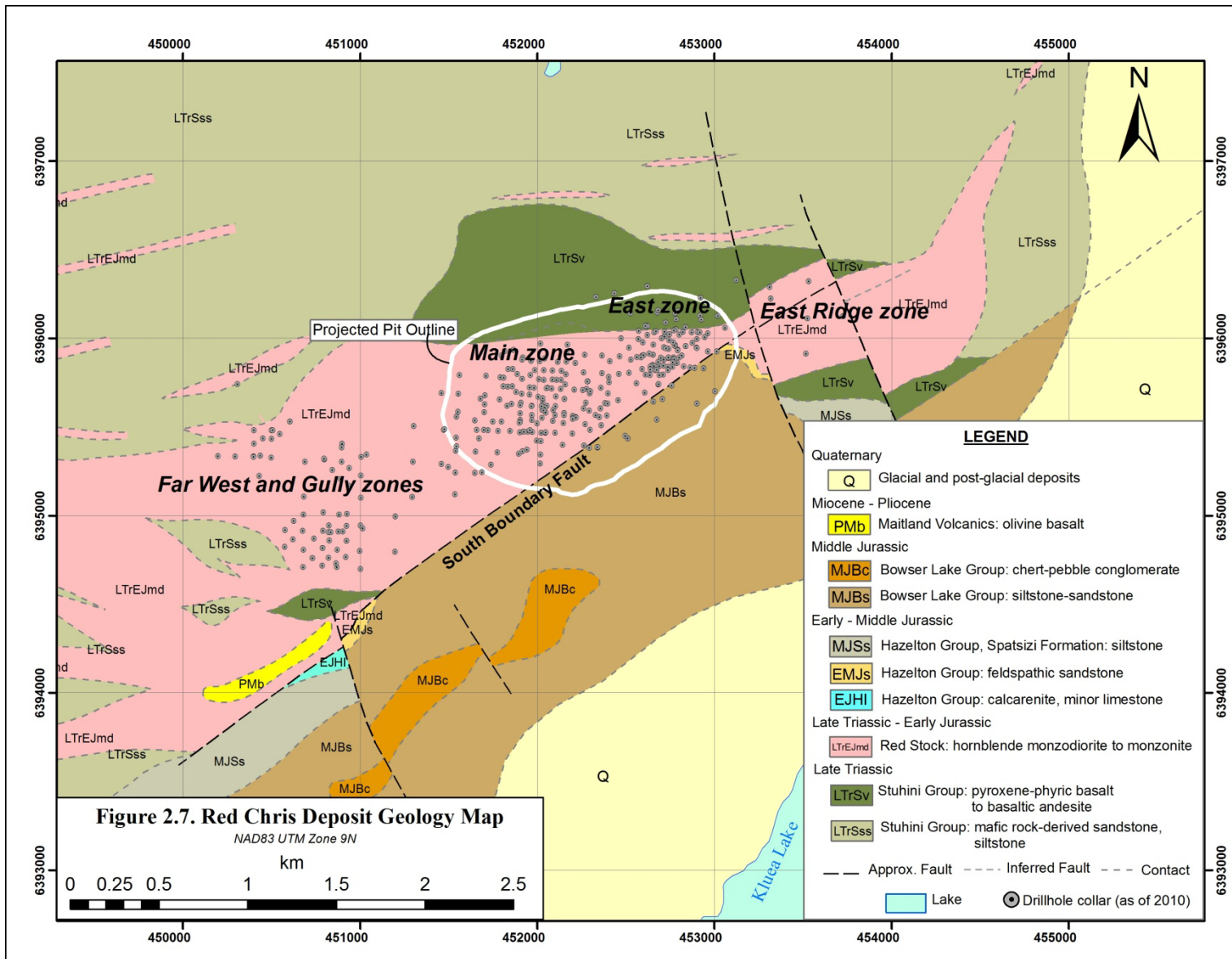
Figure 2.7 Geology map of Red Chris with mineralized centers of the Far West, Gully, Main, East, and East Ridge zones.

2.3.1.5 Middle Jurassic Bowser Lake Group

The contrast between the synorogenic deposition of the Bowser Lake Group from the eugeoclinal volcanism and sedimentation of the Spatsizi Formation signaled the beginning of a new tectonic regime for northern Stikinia (Tipper and Richards, 1976). Clastic sediments were deposited over a large area between the Skeena and Stikine Arches, termed the Bowser Basin (Figure 2.2). The Bowser Lake Group consists of marine and nonmarine shale, siltstone, sandstone and conglomerate. Chert clasts within the Bowser Lake Group were derived from the Cache Creek Terrane to the north, and provide a provenance link between Stikinia and Cache Creek (Evenchick and Thorkelson, 2005).

The Bowser Lake Group has been divided into several lithofacies units representing broad environments of deposition which are assumed to interfinger laterally, and repeated vertically on a range of scales (Evenchick and Thorkelson, 2005). Two lithofacies assemblages of the Bowser Lake Group occur south of Red Chris and Kluea Lake. The oldest and most widespread is the Todagin assemblage (unit **MJBs** on Figure 2.6) which is representative of a slope depositional environment and gradationally overlies siliceous siltstone of the Spatsizi Formation of the Hazelton Group (Evenchick and Thorkelson, 2005). The Todagin assemblage is dominantly dark-grey- or black-weathering, laminated to massive siltstone and shale with laterally continuous rusty orange-weathering claystone beds, fine-grained sandstone, rare limestone and lenses of light-grey-weathering chert-pebble conglomerate. The conglomerate lenses are commonly clast supported with a sandy matrix and contains rounded to well rounded clasts commonly 1 to 6 cm in diameter (Evenchick and Thorkelson, 2005).

Gradationally overlying the Todagin assemblage is the Muskaboo Creek assemblage (unit **MJBc** on Figure 2.7), which represents a shelf depositional environment and far less widespread than the Todagin (slope lithofacies) assemblage in the area south of Red Chris. The Muskaboo Creek assemblage (Green, 1992) is characterized by coarsening upward cycles, 5 to 10 m thick, of thinly bedded shale and minor mudstone at the base overlain by thinly layered micritic sandstone interbedded with siltstone to fine-grained sandstone. Some cycles are capped by 15 to 25 cm thick chert lithic conglomerate. Sedimentary structures in coarser-grained portions of the cycles are suggestive of a shallow-marine, shelf environment (Evenchick and Thorkelson, 2005). The occurrence of the Todagin (slope) and Muskaboo Creek (shelf) assemblages at the northern

margin of the Bowser Basin, immediately south and southeast of Red Chris, represent the stratigraphic overlap of more proximal (to source) facies over relatively distal ones.

2.3.1.6   Cenozoic Maitland Volcanics

The Cenozoic Maitland Volcanics are a suite of volcanic rocks and associated volcanic necks north, west and southwest of Maitland Creek (Evenchick and Thorkelson, 2005). These erosional remnants of Tertiary lava flows dominantly occur west of Klappan River, east of Iskut River and north of Burrage and Chismore Creeks, roughly 20 to 40 km south of Red Chris. The Maitland Volcanics are flat-lying lavas up to 400 m thick and contain up to 20 separate flow units (Evenchick and Thorkelson, 2005). The flows are dominantly aphyric to slightly feldspar-phyric basalt comprising thin, basal flow breccias, a brown-weathering, crudely columnar core and a horizon of scoriaceous reddish-brown flow-top breccias (Evenchick and Thorkelson, 2005). Discontinuous layer of intraflow fluvial gravel and unclassified fossil colluvium locally occur at the base of the lava successions and less commonly as recessive interbeds. An outlier of the Maitland Volcanics (unit **PMb** on Figure 2.6), located 5 km northeast of Todagin Mountain on the Red Chris property, consists of an olivine basalt (Newell and Peatfield, 1995). The Maitland Volcanics have been dated by K-Ar methods as 5.2 to 4.6 Ma and are correlated with the Nido stage of the Mount Edziza Volcanic Complex 40 km to the west (Souther, 1992; Evenchick and Thorkelson, 2005).

2.3.2   Intrusive Rocks

The oldest intrusive rocks in the region are Early Mississippian in age and intrude the Stikine assemblage 15 km north of Red Chris. Several suites of Late Triassic to early Middle Jurassic intrusions occur at, and within the vicinity of Red Chris. These suites are likely the intrusive equivalents of the Stuhini and Hazelton Group volcanic successions (Evenchick and Thorkelson, 2005). The intrusive rocks were emplaced into Stikinia before the amalgamation with Cache Creek and the subsequent docking with the ancient western North American margin.

2.3.2.1   Early Mississippian Granodiorite

North of Ealue Lake, a Mississippian granitic pluton (unit **EMgd** on Figure 2.6) intrudes metavolcanic rocks and metasedimentary rocks of the Paleozoic Stikine assemblage. The outcrop is granodiorite to diorite, light-grey to buff white, medium to coarse grained, equigranular to locally foliated near intrusive contacts (Ash et al., 1997a). Mafic minerals are replaced by

chlorite. Ages from U-Pb analysis on zircon of 353 to 342 Ma indicates that this intrusion is early Mississippian (Ash et al., 1997a).

2.3.2.2 Red Stock, Ealue Stock and Related Intrusions

The Red Stock (unit **LTrEJmd** on Figure 2.6) occurs 3 km northwest of Kluea Lake at the northern margin of the Bowser Basin. This Late Triassic hornblende monzonite and quartz monzonite porphyry intrudes the Stuhini Group volcanic and sedimentary rocks and hosts the Red Chris Cu-Au porphyry deposit (Schink, 1977; Friedman and Ash, 1997). An age from U-Pb analysis on zircon from the Red Stock is 203.8 ± 1.3 Ma (Friedman and Ash, 1997) which lends to the Red Stock being referred to as a Late Triassic intrusion. The Red Stock is discussed in detail in the following chapter (3.2.2; Intrusive Monzodiorite (Red Stock)).

The Ealue Stock (unit **LTrJEmd** on Figure 2.6), 3 km east of Ealue Lake, and several dykes northeast of the Red Stock have a similar composition to the Red Stock and intrude the Stuhini Group. They are inferred to be a part of the same intrusive suite (Ash et al., 1996), however they are Early Jurassic in age. Two of the dykes were dated by U-Pb on zircon to be 200.4 +1.4/-1.3 Ma and 197.9 +1.8/-3.2 Ma (Ash et al., 1996).

2.3.2.3 Edon, Rose and Related Intrusions

North and East of Ealue Lake are several Early to early Middle Jurassic intrusions referred to as the Edon, Rose and related intrusions (unit **EJg** on Figure 2.6). The Edon and Rose plutons (Read, 1984) are mineralized and hydrothermally altered hornblende quartz monzonite intrusions emplaced into andesite and may also be overlain by maroon andesite (Cooper, 1978; Read, 1984). Four samples from the Edon intrusion were dated by K-Ar (whole rock) methods to be 163.6 Ma, 169.6 Ma, 170.4 Ma and 198.5 Ma (Read, 1984). The related intrusions are dyke swarms of alkali granite and were dated by U-Pb methods as 186 to 182 Ma (Ash et al, 1997a). Due to the lack of location information for the rocks of the related intrusions sampled by Ash et al. (1997a), the relationship of these dyke swarms with the Edon and Rose plutons is unknown (Evenchick and Thorkelson, 2005).

2.3.2.4 Regional Structures

Brittle faults cut the region, and the east-northeast trending Ealue Lake Fault is the most prominent feature in the map area (Ash et al., 1995). The Ealue Lake Fault was mapped by Read

and Psutka (1990) as the McEwan Creek Fault which occurs west of Figure 2.6 (Evenchick and Thorkelson, 2005). The Ealue Creek Fault is not considered an extension of the McEwan Creek Fault (east of Figure 2.6), and is well established by contrasting lithologies and styles of alteration on either side of the inferred contact (Ash et al., 1995). Ankerite and intense, pervasive carbonatization preserved in rocks south of the Ealue Lake fault is absent to the north of the fault and in the overlying sedimentary rocks of the Bowser Basin (Ash et al., 1995). East to northeast trending faults define structural contacts locally on the edge of the Bowser Basin and a number of less prominent, yet locally significant northwest-trending faults are prevalent throughout the area of Red Chris (Ash et al., 1995). The northeast- and northwest-trending steep faults in the region are commonly dip-slip, however the dip direction is difficult to determine and it is therefore unclear if they are normal or reverse faults (Evenchick and Thorkelson, 2005).

2.3.2.5 Red Chris Deposit Structures

At the scale of the Red Chris deposit, several post-mineral east-northeast-trending structures control the current distribution of the Red stock (Ash et al., 1995). Specifically, the South Boundary Fault separates the Red stock from the unconformably overlying Bowser Lake Group sedimentary rocks (Figure 2.7). The South Boundary Fault is one of several east-northeast-trending faults that define the northwestern margin of the Bowser Basin (Newell and Peatfield, 1995).

Fault slip occurred after the crystallization of the Red Stock as several structures are observed as centimeters to several meters of clay gouge and rehealed breccia zones. Angular fragments of altered Red Stock and mineralized veins occur within a matrix of dark grey fault gouge or mixtures of quartz/ankerite-dolomite cement. Pyrite and minor chalcopyrite occurs within clay-quartz-carbonate gouge (Schink, 1977) indicating that faults are post-mineral. A set of north-northwest striking faults are inferred from major offsets of stockwork zones and late dikes, from a major offset on the northern contact of the stock and from geophysical evidence (Newell and Peatfield, 1995). It is suggested that these west-side down normal faults result in the exposure of progressively higher levels of the porphyry system to the west (Newell and Peatfield, 1995). In drill core, individual fault zones are difficult to correlate between holes (Newell and Peatfield, 1995; this study). Breccia zones are commonly located at probable intrusive phase contacts, thereby commonly destroying any cross-cutting relationships.

2.3.3 Environment of Formation

The Red Stock and associated Red Chris porphyry deposit was emplaced into the Stuhini Group rocks at ~203.8 Ma in a predominantly submarine environment, indicated by the presence of marine fossils and turbidite sequences (Evenchick and Thorkelson, 2005). Lavas of the Stuhini Group rarely exhibit oxidation features indicative of subaerial deposition, such as reddish flow margins or iddingsitized olivine. The emplacement of the Red Stock and the formation of the Red Chris porphyry deposit occurred during a period of inactivity of the volcanic arc, forming after the eruption of the Stuhini Group volcanic rocks and subsequent erosion and deposition of the Stuhini Group sedimentary rocks. Minor volcanic activity occurred ~40 km East and Southeast of Red Chris as the Griffith Creek Volcanics (205.8 Ma, Thorkelson et al., 2005). The Griffith Creek Volcanics were deposited roughly 2 million years before the formation of Red Chris, indicating porphyry emplacement during the waning stages of the volcanic arc. Volcanic activitiy resumed with the eruption of the Cold Fish Volcanics (Hazelton Group) ~60 to 80 km East and Southeast of Red Chris around 194 to 197 Ma (Thorkelson et al., 1995). The Griffith Creek Volcanics and Cold Fish Volcanics were deposited subaerially, indicated by densely welded ingnimbrite, reddened lava flows, and the absence of indicators of aqueous deposition (Evenchick and Thorkelson, 2005).

2.4 Comparison of Selected Northern Stikinia Porphyry Deposits with Red Chris

Northern Stikinia hosts several major pre-accretionary porphyry deposits including Kemess, Kerr, Schaft Creek, Sulphurets, Copper Canyon, Galore Creek and Red Chris in addition to numerous other porphyry occurrences. Many of these deposits share a similar geological framework, and formed over a small time interval. They, however, represent a range in porphyry deposit types and exhibit very different styles of alteration and mineralization. The GJ, Schaft Creek and Galore Creek porphyry deposits of northern Stikinia exhibit span a range in porphyry deposit types, and will be compared to the Red Chris deposit in terms of regional geology, timing and composition of host intrusions, alteration and mineralization (Figure 2.8, Table 2.2).
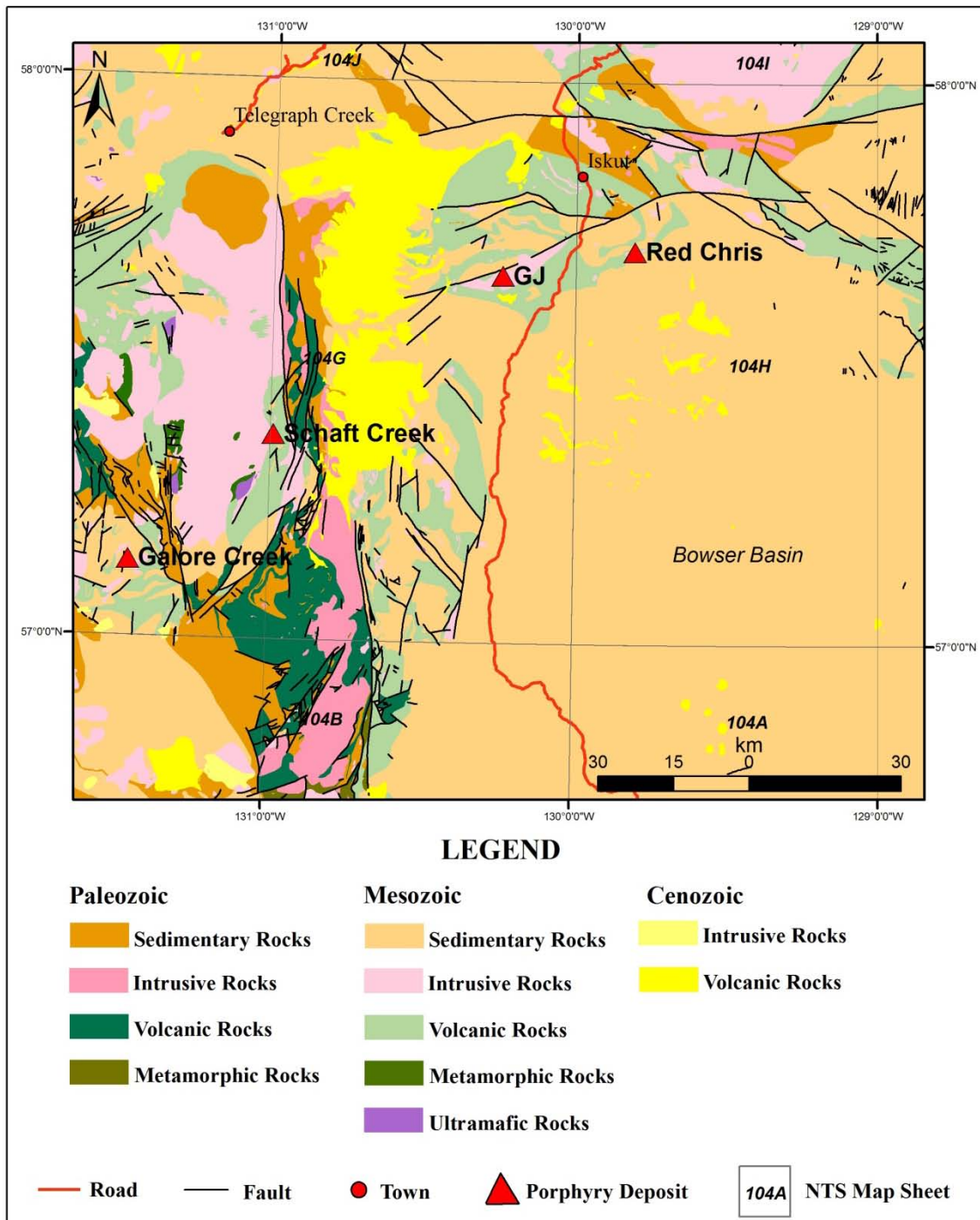
Figure 2.8 Select porphyry deposits of northern Stikinia (Red Chris, GJ, Schaft Creek, and Galore Creek) and associated geology (NTS 104G/H). Modified from BC Geological Survey Map of Massey et al., (2005).

Table 2.2 Comparison of Major Features of Red Chris, GJ, Schaft Creek and Galore Creek

	Red Chris	**GJ**	**Schaft Creek**	**Galore Creek**
'Type'	Alkalic / Calc-alkalic?	Alkalic / Calc-alkalic?	Calc-alkalic	Alkalic (silica undersaturated)
Metals	Cu-Au	Cu-Au	Cu-Mo-(Au)	Cu-Au
NTS Map Sheet	104H/12W	104G/9	104G/7W	104G/3,4
Age (Ma)	~203.8 (U-Pb)	~205.1 (U-Pb)	~222.1 (U-Pb)	~210 (U-Pb, Pb-Pb)
Host Intrusion(s)	*Red Stock* Hornblende monzonite to quartz monzodiorite	*Groat Stock* Quartz diorite to quartz monzodiorite	*Hickman Batholith* Hornblende gabbro to plagioclase hornblendite, hornblende biotite granodiorite to quartz monzonite, diorite	*Hickman Plutonic Suite* Pseudoleucite dykes, syenite porphyry, megaporphyry, minor fine-grained syenite
Host Volcanic Rocks	Stuhini Group	Stuhini Group	Stuhini Group	Stuhini Group
Mineralization	Quartz veins and stockworks *Py, Cp, Bn >> Mo*	Quartz veins and stockworks *Py, Cp > Bn >> Mo*	Veins, breccias, disseminations *Bn, Cp, Mo, Py ± quartz-carbonate* Veins *Mo, Cu-Pb-Zn, specularite ± quartz*	Disseminated and minor fracture controlled *Cp, Bn > Py Minor malachite and azurite*
Alteration	Early potassic, phyllic, intense illite overprint (intermediate argillic), minor phyllic and propylitic, pervasive carbonate	Early potassic, phyllic and propylitic overprint, silicification, ankerite flooding	Potassic, sericite-chlorite, propylitic, late carbonate and hematite	Potassic, calc-potassic, calcic, spdoc, sericite-anhydrite-carbonate, minor propylitic

(Py = pyrite, Cp = chalcopyrite, Bn = bornite, Mo = molybdenite)

2.4.1 **GJ**

The GJ Cu-Au porphyry deposit is located at the northeast end of Kinaskan Lake on NTS mapsheet 104G/9 at the southwestern end of the Groat Pluton (Ash et al., 1996; Figure 2.8). Located 20 km from the Red Stock, the Groat Stock has a similar regional geologic framework to Red Chris; located in northern Stikinia between the Skeena and Stikine Arches at the northern margin of the Bowser Basin. The Groat Stock intrudes Late Triassic fine-grained clastic and pelagic sedimentary rocks associated with the Stuhini Group including bedded sandstone, siliceous siltstone, chert and graphitic chert (Ash et al., 1996). The Stuhini Group is unconformably overlain by volcanic rocks of the Jurassic Hazelton Group. To the south, the

Stuhini and Hazelton Groups are unconformably overlain by chert pebble conglomerate, grit, greywacke and siltstone of the Middle Jurassic Bowser Lake Group (Ash et al., 1997b).

The Late Triassic Groat Stock is similar to the compositionally variable, texturally equigranular to porphyritic, elongate, and southwest-trending nature of the Red Stock. The Groat Stock ranges from quartz diorite to quartz monzodiorite and contains plagioclase and lesser hornblende phenocrysts in a microcrystalline groundmass of anhedral granular quartz and feldspar (Ash et al., 1996). Analysis of U-Pb on zircon and titanite from a sample from the southeastern part of the Groat Stock returned a crystallization age of 205.1 ± 0.8 Ma (Friedman and Ash, 1997). The elongated nature of the Groat Stock is not a primary feature, as the length of the pluton is increased by dextral offset along two northeast-trending strike slip faults which may represent a western extension of the regionally significant Ealue Lake Fault (Ash et al., 1996).

The GJ Cu-Au porphyry deposit is hosted in intrusive rocks and siliceous sedimentary rocks and is characterized by disseminated, fracture, quartz vein and quartz stockwork controlled pyrite, with variable chalcopyrite, rare bornite and trace molybdenite (Ash et al., 1996; Mehner, 2005). Ankerite and quartz flooding are the prominent alteration types observed on the GJ property (Ash et al., 1996) with early potassic alteration overprinted by later phyllic and propylitic alteration (Dunne and Thompson *in* Mehner et al., 2007). Following the 2007 drill program, a substantial portion of the indicated resource outlined in Mehner et al., (2007) was upgraded to an NI 43-101 compliant measured and indicated resource, at a cut-off of 0.20 % copper, of 153.3 million tonnes grading 0.321 % copper and 0.369 g/t gold containing 1.09 billion pounds of copper and 1.82 million ounces of gold at the Donnelly and North-Donnelly zones (Canadian Gold Hunter Corporation, 2008).

2.4.2 Schaft Creek

The Schaft Creek Cu-Mo ± Au porphyry deposit is located approximately 60 km south of Telegraph Creek on NTS mapsheet 104G/07W between the Mess Creek and Schaft Creek valleys (Scott et al., 2008; Figure 2.8). Located in Stikinia, at the northwestern margin of the Bowser Basin, Schaft Creek is hosted in the Hickman batholith, which intruded rocks of the Triassic Stuhini Group and the Paleozoic Stikine assemblage. The Schaft Creek deposit is hosted in the Mess Lake facies of the Stuhini Group, composed of subaerial basaltic to andesitic tuffs and mafic flows (Scott et al., 2008). Conglomerates of the Early Jurassic Hazelton Group

unconformably overlie the Mess Lake facies east and west of Schaft Creek (Brown et al., 1996; Logan et al., 2000). To the south, the Stuhini Group is in fault contact with the Stikine assemblage and is intruded by the Late Triassic Hickman pluton and Yehiniko pluton to the west (Brown et al., 1996; Logan et al., 2000).

The Hickman batholith is a complex zoned, north-trending intrusive body composed of three distinct plutons: the Hickman, Yehiniko and Nightout (Souther, 1972; Scott et al., 2008). The Nightout pluton occurs north of the Schaft Creek area. The Hickman pluton is composed of three distinct phases: the main phase, a southerly mafic phase and a western diorite phase (Brown et al., 1996). The southern mafic phase is predominantly a medium-grained, equigranular hornblende gabbro to plagioclase-bearing hornblendite (Brown et al., 1996). The main phase is a medium- to fine-grained hornblende biotite granodiorite to quartz monzonite that grades into the diorite phase to the west where it intrudes the Stuhini Group (Brown et al., 1996; Logan et al., 2000). The age of the Hickman batholith is approximately constrained by a U-Pb (zircon) date of 222.1 ± 9.6 Ma which is in agreement with a well-constrained age of mineralization (Re-Os molybdenite) at the Schaft Creek deposit of 222.0 ± 0.8 Ma (Scott et al., 2008).

The calc-alkalic Schaft Creek Cu-Mo ± Au porphyry deposit has been divided into three mineralized zones where granodioritic dykes from the Hickman batholith intrude and locally brecciated the mafic volcanic sequence (Scott et al., 2008). Mineralization occurs on the eastern slopes above the Schaft Creek valley in the Paramount, Main and West Breccia zones (Scott et al., 2008). These zones exhibit a range of alteration and mineralization styles that are distinct in each zone. However, there is also significant overlap between the zones in terms of geology, alteration and mineralization (Scott et al., 2008). Two mineralization main phases are observed at Schaft Creek: a hydrothermal vein, breccia and disseminated style consisting of bornite, chalcopyrite, molybdenite, and pyrite associated with potassic and sericite-chlorite alteration; and a second, minor mineralization style of veins of molybdenite ± specularite and Cu-Pb-Zn sulphide veins without any significant alteration (Scott et al., 2008). Widespread hydrothermal alteration is common at Schaft Creek with potassic alteration occurring in a north-south linear trend at the Paramount zone and in an irregular pattern in the core of the Main zone (Scott et al., 2008). The potassic zone is broadly encompassed by sericite-chlorite alteration and propylitic alteration forming a halo over several hundred meters around the inner alteration zones (Scott et al., 2008). Late stage carbonate and hematite overprint the older alteration assemblages. The

deposit has been extensively structurally deformed during and after its formation (Scott et al., 2008). A measured mineral resource for Schaft Creek (at 0.2 % copper equivalent cut-off) is estimated to be 40.3 million tonnes grading 0.36 % copper, 0.023 % molybdenum, and 0.25 g/t gold (copper equivalent of 0.61 %) containing 319.6 million pounds copper, 20.5 million pounds molybdenum and 0.32 million ounces gold (Copper Fox Metals Incorporated, 2011).

2.4.3 **Galore Creek**

Galore Creek is a silica-undersaturated alkalic Cu-Au porphyry district located in the lower Stikine River region of northwestern British Columbia at the headwaters of Galore Creek on NTS mapsheets 104G/3,4, roughly 150 km northeast of Stewart, British Columbia (Enns, et al., 1995; Lang et al., 1995b; Schwab et al., 2008: Figure 2.8). Galore Creek lies in Stikinia at the western margin of the Intermontane Belt. In the area of Galore Creek, extensive units of Mississippian and Permian carbonate of the Stikine assemblage are exposed to the northeast of the district (Enns, et al., 1995). Unconformably overlying the Stikine assemblage is a variety of flows, tuffs, volcanic breccias and sedimentary rocks of the Middle to Upper Triassic Stuhini Group (Kerr, 1948; Schwab et al., 2008). North of Galore Creek, rocks equivalent to the Hazelton Group are recognized (Logan et al., 1989). Significant intrusive activity occurred in the Late Triassic to earliest Jurassic including the calc-alkaline Hickman pluton and the alkaline intrusions at Galore Creek, Copper Canyon and similar bodies to the north and south (Enns et al., 1995). Intrusive activity is interpreted to be more or less contemporaneous with parts of the Stuhini Group volcanic rocks (Logan and Koyanagi, 1989). There are also several distinct granitoid phases to the west of Galore Creek belonging to the Cretaceous and Eocene Coast Plutonic Complex (Enns et al., 1995; Schwab et al., 2008). At the scale of the deposit, major structures are east, northwest and north-trending faults (Schwab et al., 2008) that divide the region into a series of fault-bounded blocks.

At Galore Creek, multiple intrusions were emplaced into volcanic rocks of similar composition and are divided based on cross-cutting relationships, degree of alteration and mineralization, as well as phenocryst mineralogy, texture and grain size of least altered samples (Enns et al., 1995). Previous work had outlined intrusions as pre-, syn-, or post-mineral, however this sequence has been discontinued as at least two mineralizing events have been recognized (Schwab et al., 2008). The oldest intrusive rocks are pseudoleucite-phyric syenites in addition to early- and late-phases of orthoclase and pseudoleucite-phyric syenite which can contain

megacrysts of pseudoleucite and orthoclase (Schwab et al., 2008).These oldest intrusions contain accessory magnetite, apatite and minor clinopyroxene phenocrysts. The youngest intrusive rocks at Galore Creek are orthoclase syenites with orthoclase megacrysts, significant plagioclase and biotite phenocrysts, local hornblende phenocrysts and accessory magnetite and apatite (Schwab et al., 2008). These orthoclase megacrystic syenite intrusions are recognized as post-mineral to many of the mineralized centers, but pre-mineral to others. Post-mineral plagioclase-phyric diorites, biotite-phyric lamprophyres and aphanitic mafic, intermediate and felsic dykes are the youngest intrusive phases present (Schwab et al., 2008). Several intrusions were analyzed for U-Pb and Pb-Pb geochronology on zircon and titanite, respectively by Mortensen et al. (1995). A probable crystallization age from an early to syn-mineral pseudoleucite-orthoclase syenite intrusion was dated at 210 ± 1 Ma (U-Pb on zircon). Additionally, two intrusions of an orthoclase megacrystic syenite (late to post-mineral in some centers, pre-mineral in others) returned an age of 205 ± 2.3 Ma (U-Pb on zircon) and an age of 200.1 ± 2.2 Ma (U-Pb on titanite). Six large and numerous smaller breccia bodies are noted around Galore Creek as both clast- and matrix-supported hydrothermal and diatreme breccias, locally containing both altered and mineralized clasts (Enns et al., 1995). Hydrothermally cemented breccias commonly contain abundant sulphide minerals (Schwab et al., 2008).

Twelve Cu-Au mineralized zones are recognized at Galore Creek, mostly occurring in highly altered volcanic rocks (Central, North Junction, Junction, Middle Creek, West Rim, Butte and South 110 zones) and to a lesser degree in syenite intrusions (North Rim zone), with the Southwest and Saddle zones occurring in breccias (Enns et al., 1995). Recent exploration has discovered additional zones such as the Bountiful and West Fork zones, peripheral to the Central zone (Schwab et al., 2008). Mineralization at Galore Creek consists mostly of disseminated and minor fracture-controlled hypogene copper sulphides of chalcopyrite and bornite (Enns et al., 1995; Schwab et al., 2008). Chalcopyrite is the dominant sulphide however significant disseminated bornite is present in several of the high-grade zones. Pyrite is not abundant within the mineralized zones however it is associated with elevated gold grades in the Southwest zone. In the Central zone, bornite is associated with increased gold grades at a location where Ca-K-silicate alteration (core of central replacement zone) grades into K-silicate alteration (North and South Gold Lenses; Enns, et al., 1995; Schwab et al., 2008). Minor supergene Cu is present as malachite and azurite on fracture surfaces within 60 m of the surface (Chamberlain et al., 2007). As of 2011, measured and indicated resource estimates at Galore Creek are 286.7 million tonnes

grading 0.33 % copper, 0.27 g/t gold, and 3.64 g/t silver, and proven and probable reserves of 528 million tonnes grading 0.6 % copper, 0.32 g/t gold and 6.02 g/t silver (Gill et al., 2011).

The hydrothermal alteration at Galore Creek is significantly different from alteration described at other alkalic porphyry deposits of British Columbia, specifically lacking quartz alteration and veins (Micko et al., In Press). Five main styles of alteration are reported in terms of mineral associations, as reported at the Central zone, the largest prospect at Galore Creek. Early and main stage potassic alteration is recognized, characterized by orthoclase, biotite, magnetite, hematite, anhydrite and apatite and affects the volcanic rocks and the pseudoleucite-phyric syenites (Micko et al., In Press). Main stage calc-potassic alteration is associated with breccias bodies in the core of the central zone and mineralized fractures in the wall-rocks (Micko et al., In Press). Calc-potassic alteration is characterized by garnet, diopside and anhydrite. The silicate minerals are later replaced by biotite, magnetite and rare orthoclase. Several additional potassic alteration zones formed after the cessation of calc-potassic alteration. A late stage calcic alteration zone is restricted to the eastern portion of the Central zone and is characterized by the presence of red-brown garnets with a distinctive 'oatmeal' texture (Micko et al., In Press). Late stage sodic alteration is spatially confined to within 50 m of the South Fault at the South Gold Lens and is characterized by texturally destructive albite. Sericite-anhydrite-carbonate alteration overprints earlier alteration phases (Ca-K-silicate and K-silicate) particularly on the periphery of the Central zone (Enns et al., 1995; Micko et al., In Press). This style of alteration is not recognized in other alkaline porphyry deposits in British Columbia (Enns et al., 1995). A minor propylitic alteration assemblage of epidote and chlorite is recognized to overprint calcic and phyllic alteration (Micko et al., In Press).

2.4.4 Comparisons with Red Chris

Red Chris and GJ are located 20 km apart and share many features (Table 2.2). The regional context is similar, forming in Stuhini Group volcanic rocks on top of the Paleozoic Stikine assemblage near the current northern margin of the Middle Jurassic Bowser Basin. The Late Triassic to Early Jurassic timing and composition of the host intrusions is also very similar. GJ is hosted in the Groat Stock, a quartz diorite to quartz monzodiorite dated at 205.1 ± 0.8 Ma (U-Pb on zircon) while Red Chris is hosted in the Red Stock, a quartz monzonite to monzonite dated at 203.8 ± 1.3 Ma (U-Pb on zircon). Both intrusive rocks contain hornblende and plagioclase phenocryst phases and are bounded by north-east trending faults. Mineralization at

both deposits occurs as disseminated, fracture-controlled, quartz veins containing chalcopyrite, bornite, pyrite and minor molybdenite, however the relative abundances of these copper-iron-sulphides varies between the two deposits. Alteration at GJ and Red Chris is similar with an early potassic zone overprinted by a later 'phyllic' type alteration. Late stage carbonate alteration is recognized intensely at Red Chris and in moderate amounts at GJ.

Red Chris and the calc-alkalic Schaft Creek porphyry deposit have several features in common (Table 2.2), including a very similar regional geologic framework. Similar to Red Chris, Schaft Creek is hosted in the Stuhini Group, overlying the Stikine assemblage, and is unconformably overlain by the Hazelton Group. Schaft Creek is located at the northwestern margin of the Bowser Basin, southwest of Red Chris. The major batholith associated with Schaft Creek is the Hickman batholith, comprised of three distinct plutons. The Hickman pluton is the intrusion responsible for mineralization at Schaft Creek and has a varied composition. However, the main phase is a hornblende biotite granodiorite to quartz monzonite, similar to the quartz monzonite to monzonite composition of the Red Stock. The Hickman batholith is dated at 222.1 ± 9.6 Ma, roughly 18 million years older than the Red Stock, and is considered a Late Triassic intrusion. Whereas Schaft Creek contains two different styles of mineralization, only one is recognized at Red Chris. Both Schaft Creek and Red Chris contain mineralization in hydrothermal, quartz-bearing veins, however the disseminated and breccia hosted mineralization observed at Schaft Creek is minor and absent at Red Chris, respectively. Bornite, chalcopyrite, pyrite and molybdenum are observed at both deposits however Schaft Creek contains significantly greater volumes of molybdenite than Red Chris. Both Red Chris and Schaft Creek contain potassic alteration zones overprinted by sericite-chlorite, and have some form of propylitic halo. Late-stage carbonate alteration is a feature common to both deposits.

Of the porphyry deposits compared in this section, Galore Creek shares the fewest similarities with Red Chris. Galore Creek and Red Chris have a similar regional geological framework, occurring within the Stuhini Group in northern Stikinia. The intrusive rocks at Galore Creek are however, predominantly syenitic and silica-undersaturated, unlike the quartz monzonite to monzonite composition of the Red Stock. The different intrusive suites are relatively close in age, between 210 ± 1 Ma and 200.1 ± 2.2 Ma for Galore Creek syn-mineral and post-mineral intrusions, and 203.8 ± 1.3 Ma for the Red Stock. Few of the alteration styles observed at Galore Creek coincide with alteration at Red Chris. The K-silicate (potassic)

alteration is common to both deposits. However, the characteristic calc-potassic alteration, associated garnet and late sericite-anhydrite-carbonate alteration overprint at Galore Creek are not features observed at Red Chris. Propylitic alteration is a feature common to both deposits. Red Chris and Galore Creek are both Cu-Au porphyry deposits with mineralization likely being structurally controlled. At Red Chris most of the mineralization occurs in quartz veins within intrusive rocks and only in minor amounts in the surrounding volcanic rocks. Much of the mineralization at Galore Creek occurs in altered volcanic rocks and to a lesser extent within intrusions and breccias. Another significant difference between the deposits is that quartz veins do not occur at Galore Creek.

2.4.5   **Discussion**

The porphyry deposits of northern Stikinia all have a similar regional geological framework yet represent a range of deposit types. The deposits described and compared above all formed on the Paleozoic Stikine assemblage, and are hosted in Stuhini Group and/or Hazelton Group volcanic rocks and associated sedimentary rocks. The intrusive rocks are all Late Triassic, ranging from the oldest (Schaft Creek) at 222.1 ± 9.6 Ma, to the youngest (Red Chris) at 203.8 ± 1.3 Ma. The composition of these intrusions however has a wide range, typically from diorite to syenite with varying amounts of primary quartz. These deposits also represent a diverse set of porphyry deposit types, ranging from the calc-alkalic Cu-Mo $\pm$ Au Schaft Creek deposit, the silica-undersaturated alkalic Cu-Au Galore Creek deposit and the Red Chris Cu-Au deposit with both calc-alkaline and alkaline affinities. Such a range in intrusive composition and contained metals suggests that in Late Triassic to Early Jurassic time, magmatic activity in northern Stikinia may have evolved from a calc-alkalic to a more alkalic source over a relatively short period of time (less than 20 Ma).

At Red Chris, the sericite (illite)-chlorite overprint is extensive and the most dominant alteration style at the surface. It is not known if the sericite associated with this alteration at Schaft Creek and Galore Creek is represented by illite, or not. The presence of illite as a major alteration mineral at porphyry deposits is not well documented or understood. If illite is present in significant amounts at Schaft Creek and Galore Creek; it indicates that a lower temperature form of sericite (illite) is a more common feature of porphyry deposits than previously observed.

A late-stage carbonate alteration event has been recognized at Red Chris, GJ, and Schaft Creek in varying intensities. A late carbonate alteration overprint is also recognized at Galore Creek in addition to sericite and anhydrite. Carbonate alteration could represent a late-stage feature characteristic to porphyry deposits of northern Stikinia.

3 Red Chris and the Porphyry Cu Model: Lithology, Alteration, Veins and Mineralization

Recent deep drilling at Red Chris provided extensive drill-core for examination of the rocks of the East zone in order to create a detailed description of the lithology, alteration mineralogy, veins, and sulphide mineralogy. The following descriptions are primarily based on observations from drill core in addition to the previous descriptions of Schink (1977), Ash et al. (1995), Blanchflower (1995) and Baker et al. (1997). The alteration zones recognized at Red Chris are generally consistent with characteristics of many porphyry deposits, as described by Meyer and Hemley (1967), Lowell and Guilbert (1970), Seedorff et al. (2005) and Sillitoe (2010). Additionally, descriptions of different groups of veins are broadly consistent with the A-B-D vein classification system of Gustafson and Hunt (1975), terminology that has been applied to veins at numerous porphyry deposits. These comparisons, drawn from field-based and subsequent lab-based observations (petrography, short wave infrared spectroscopy, X-ray diffractometry) establish a paragenesis of the evolution for the East zone at Red Chris.

3.1 Methods: Field Data Collection

A total of 13,980 m of core was logged over 13 drillholes in the East zone (Figure 3.1) using an adapted version of the Anaconda field mapping method (Einaudi, 1997). This method was developed by Anaconda geologists in the 1960's working on copper porphyry deposits such as El Salvador, Chile and Yerington, Nevada. Logged holes represent 5 drillholes along a north-south cross-section 452700E, including RC07-335, a 1029 m vertical drillhole grading 1.02 % Cu and 1.26 g/t Au over the entire length of the hole (Imperial Metals Corporation, 2007), in addition to drillholes RC94-079, RC94-106, RC95-140 and RC95-224. An additional 8 drillholes were logged along a N50E cross-section, nearly parallel to the axial trend of the elongated intrusive host rocks. Drillholes RC09-345, RC09-348, RC09-349, RC09-350, RC09-351, RC09-352, RC08-353 and RC09-354 lie along the N50E section line. Drillhole RC07-335 lies on both cross-sections.
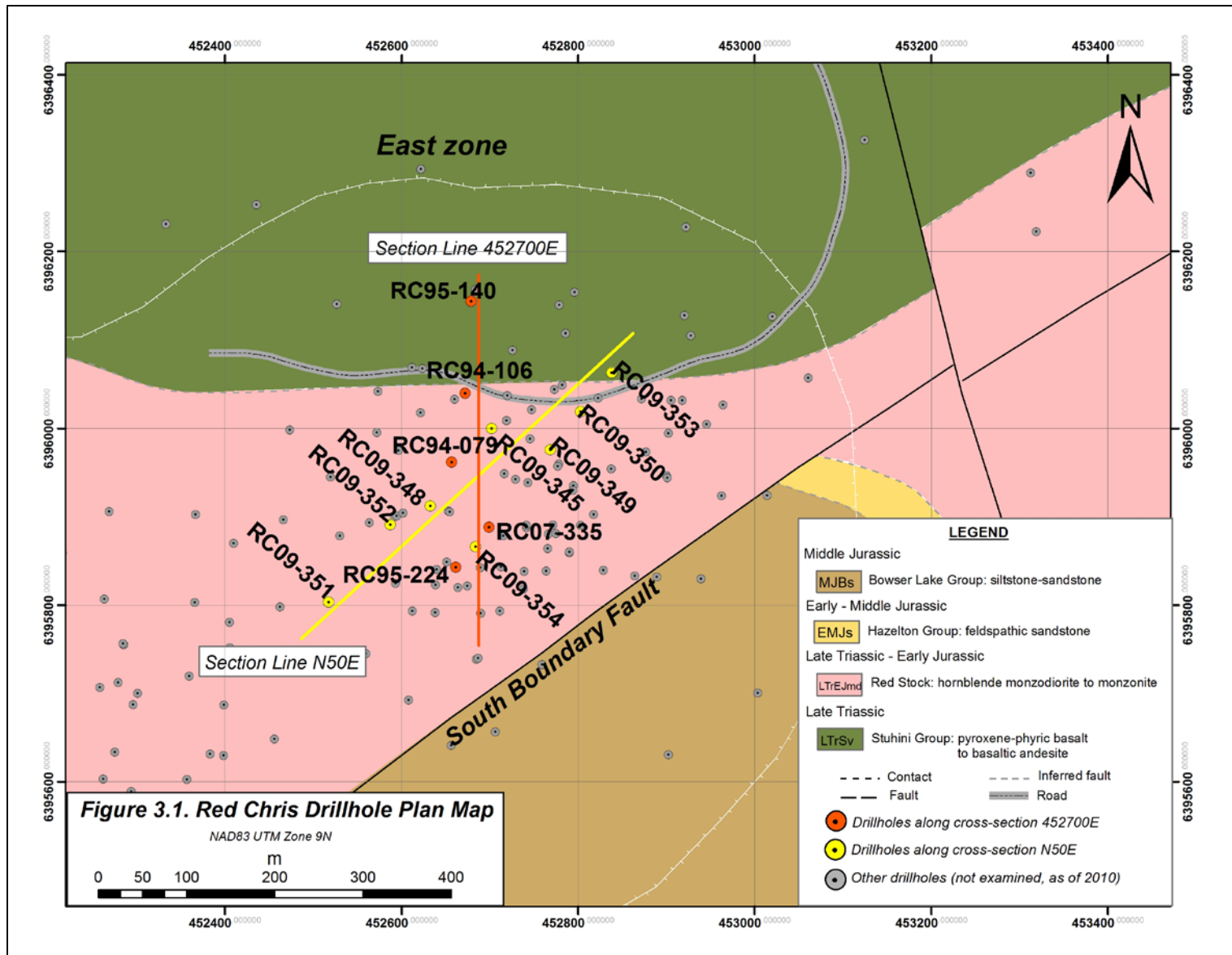
Figure 3.1 Drillhole plan map of the East zone at Red Chris and the two cross-sections (452700E and N50E) examined in this study.

Across the 13 drillholes examined, collar elevations are generally consistent, between 1504 and 1521 m above sea level. Eight of the drill holes were drilled vertically, where as five drillholes were angled, drilled at dips of -60, -65 and -71 degrees with an azimuth of 180 degrees. In general, down hole depths are consistent across drillholes, especially along the N50E cross-section. Throughout the following descriptions, locations of alteration zones, veins, and mineralization are reported as down-hole depth locations, unless otherwise specified as an elevation.

Drill core was logged at a scale of 1:500 (1 mm = 50 cm). The logs document the rock types, presence and intensity of alteration of felsic and mafic material, vein material, sulphide and iron oxide minerals in veins, phenocryst size and density and the visually estimated density of quartz veins. Locations, intensity and nature of faults and fractures are documented in addition to breccias. Additional notes describe the drill core including cross-cutting vein relationships. Core logs are provided as Appendix A1. A total of 504 samples were selected approximately every 50 m as 10 to 20 cm slabs (1-2 cm thick) of drill core for analysis and reference. A sample list and descriptions are provided in Appendix A2.

Specifically, the core logs record: 1) alteration of felsic material to sericite, K-feldspar and carbonate (ankerite-dolomite); 2) alteration of mafic minerals/sites to sericite, chlorite, secondary biotite, carbonate (ankerite-dolomite), hematite, magnetite, pyrite, chalcopyrite and epidote; and 3) vein infill material of quartz, carbonate (ankerite-dolomite), anhydrite and chlorite. The presence of sulphide and iron oxide minerals occurring in the veins such as pyrite, chalcopyrite, bornite, molybdenite, magnetite and hematite are also recorded. Specific minerals logged in the field were confirmed by petrographic, short-wave infrared spectroscopic, and X-ray diffraction techniques.

3.2   Lithology

3.2.1   Stuhini Group Volcanic Rocks and Mafic-Derived Sedimentary Rocks

The Stuhini Group is composed of basaltic to basaltic andesitic volcanic flows and derivative sedimentary rocks. At Red Chris, the supracrustal sequence is intruded by the Red Stock, the main host to the porphyry Cu deposit. The volcanic and mafic-derived sedimentary

rocks currently lie to the north and northwest of the Red Stock, where only sparse outcrops are present.

The volcanic and volcaniclastic rocks are medium to dark fine-grained rocks with local phenocrysts up to 3 mm in diameter (Figure 3.2A). These rocks are concentrated in the upper 100 m of drillhole RC95-140 where they form large rafts up to 20 m thick (apparent thickness, in drillcore) within intrusive rocks of the Red Stock. The mafic-derived sedimentary rocks are beige to dark brown, very fine-grained and are rarely bedded (Figure 3.2B, C, D). They form isolated, 0.3 to 30 m thick rafts within the Red Stock, below 500 m depth on the flanks of the East zone.
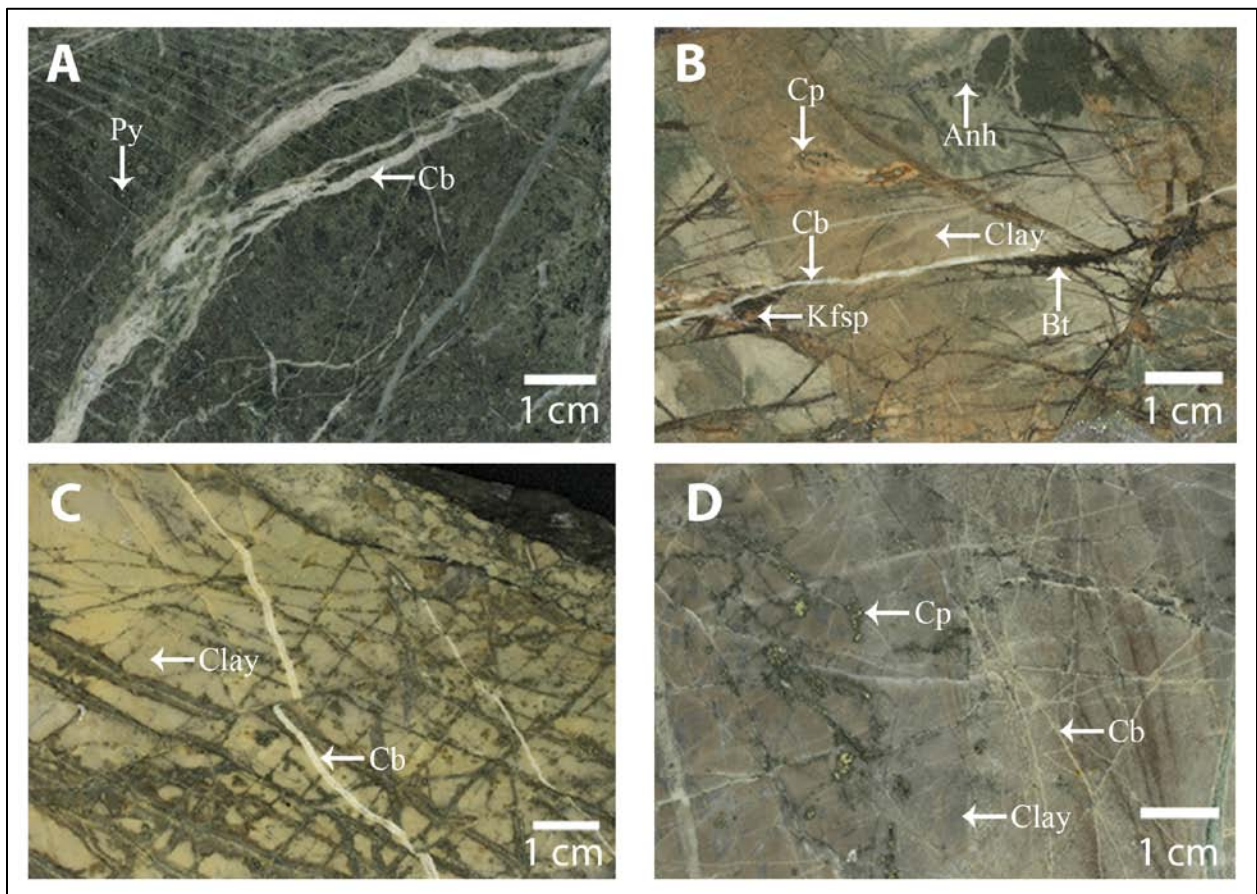
Figure 3.2 Stuhini Group volcanic rocks (A: RC95-140, 14 m) and derived sedimentary rocks with K-silicate and clay alteration (B: RC09-351, 1127 m, C: RC09-345, 628 m, D: RC09-351, 1352 m). (Cb = carbonate, Py = pyrite, Cp = chalcopyrite, Anh = anhydrite, Kfsp = K-feldspar, Bt = secondary biotite)

The Stuhini Group volcanic rocks and derivative sedimentary rocks are variably altered across the East zone, with very few fresh rocks preserved. In drillhole RC95-140 the volcanic rocks are weakly to intensely clay altered, as pale grey to white rocks with abundant pyrite clots. The mafic rock-derived sedimentary rocks are most commonly intensely clay altered, but locally dark brown biotite hornfels is preserved; the hornfels reflects thermal metamorphism. The

sedimentary rocks are altered to secondary biotite and rare pink K-feldspar alteration, particularly as vein halos. The volcanic rocks commonly contain pyrite stringers and pyrite replacing mafic phenocrysts. The mafic rock-derived sedimentary rocks contain abundant <1 mm microfractures commonly filled with pyrite and chalcopyrite, purple anhydrite ±quartz veins in addition to minor chlorite, usually below 1000 m depth. Sparse carbonate and quartz veins cut both the volcanic and mafic-derived sedimentary rocks of the Stuhini Group.

3.2.2 **Intrusive Monzodiorite (Red Stock)**

The Red Stock is an east-northeast trending, roughly 4.5 by 1.5 km elongated body (Ash et al., 1995; Ferreira, 2009) and intrudes the Stuhini Group volcanic rocks and mafic rock-derived sedimentary rocks which outcrop to the north-northwest (Figures 2.6 and 2.7). The South Boundary fault truncates the Red Stock at its southern margin at the surface where it juxtaposes the plutonic rocks against the post-mineral chert-pebble conglomerate and siltstone-sandstone of the Upper Jurassic and Cretaceous Bowser Lake Group. There is extensive glacial till covering much of the Red Stock, however limited outcrop occurs southwest of the East and Main zones in creek valleys of the Far West and Gully zones.

The Red Stock is medium grey with phenocrysts of plagioclase and hornblende in a very fine-grained groundmass. The groundmass typically accounts for 50 % of the rock and consists of anhedral microcrystalline alkali feldspar and minor quartz (Schink, 1977). The plagioclase feldspar phenocrysts are generally buff-white to grey, 2 to 4 mm euhedral to subhedral crystals (Figure 3.3A). Hornblende phenocrysts are black, euhedral, 2 to 10 mm crystals with distinct crystal boundaries (Figure 3.3B). Trace amounts of primary, 2 mm long biotite flakes are noted in the deepest, least altered rocks. The phenocrysts are randomly oriented with weakly trachytic textured hornblende phenocrysts within the grey aphanitic groundmass (Schink, 1977). Estimated visually, phenocryst abundance typically varies between 35 and 50 %, but can be as high as 65 % (Figure 3.3C, D). Ash et al. (1995) tentatively classify the Red Stock as an altered equivalent of a hornblende-plagioclase-porphyritic quartz monzodiorite similar in texture, geometry and spatial proximity to other stocks and dykes north of the Bowser Basin. Previously, the Red Stock was determined to be monzonitic in composition by Schink (1977) based on petrographic analysis and point counting. Following Ash et al. (1995) it is uncertain if the fine-grained quartz and K-feldspar in the groundmass is primary or of secondary origin due to K-silicate alteration. Therefore the composition of the Red Stock is equivocal, and it could be a

quartz monzodiorite to monzonite. Assuming the groundmass K-feldspar is dominantly a product of alteration the Red Stock will be herein referred to as a monzodiorite. The alteration and veins of the Red Stock are discussed in detail in sections 3.3 and 3.4 respectively.
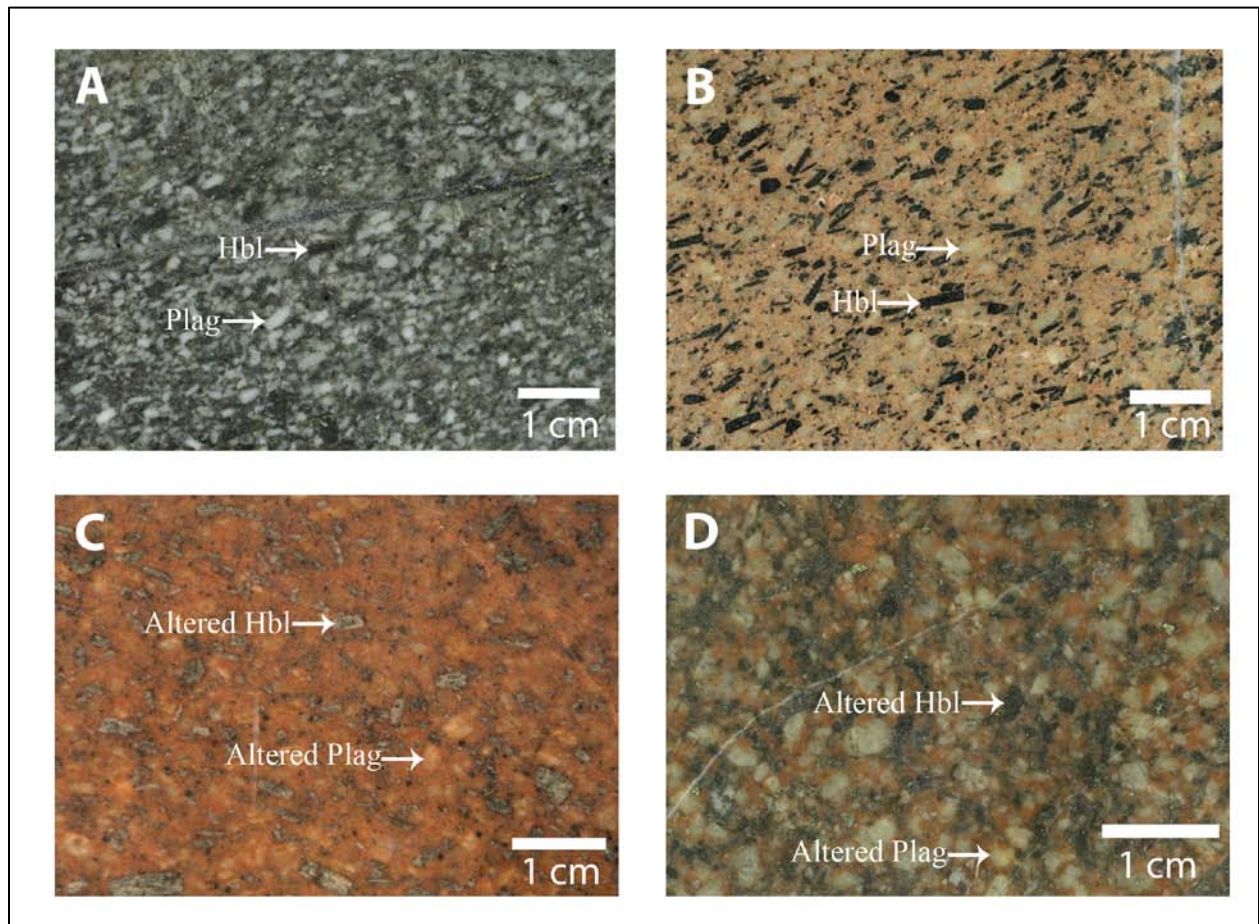
Figure 3.3 Red Stock. A: plagioclase feldspar phenocrysts (white) and weakly altered hornblende phenocrysts (black) in a grey groundmass (RC09-353, 1026 m); B: hornblende phenocrysts (black, weakly altered) and plagioclase feldspar phenocrysts (white-pale beige, weakly altered) in a moderately K-silicate altered groundmass (RC09-351, 1461 m); C: secondary biotite and sericite altered phenocrysts: density of roughly 35 % (RC07-335, 462 m); D:secondary biotite and sericite altered phenocrysts: density of roughly 65 % (RC09-354, 837 m). (Plag = plagioclase feldspar, Hbl = hornblende)

Minor breccias zones occur within the Red Stock at all depths within the East zone but are concentrated in the upper 300 m along the NE and SW extents of section N50E, as well as along the northern contact of the Red Stock with the Stuhini Group volcanic rocks. The origin and true extent of these breccia zones are difficult to quantify and correlate in drill core. The observations of the breccia zones are generally consistent with a magmatic-hydrothermal breccia, as outlined by Sillitoe (2010) and may also represent xenolith-rich intrusive margins. The breccias are both clast and matrix supported with angular to subrounded, monomictic clasts, commonly > 1 cm in size. Both the matrix and clasts have a similar composition where the

matrix likely represents recrystalized rock flour. Zones of breccia are variably altered (Figures 3.4A, B) and are intensely clay altered in the upper 400 m. Intense clay alteration masks the clast-matrix relationship and makes it difficult to determine possible compositional or textual variations between them. The matrix is intensely clay altered monzodiorite where the clasts are also intensely clay altered. Where the clasts have relict K-silicate alteration with weak clay overprinting, the matrix is typically fine-grained and dark grey to black with intact beige plagioclase phenocrysts. Veins also obscure the recognition of breccia zones. Some veins are brecciated, however other veins cross-cut both clasts and the matrix of the breccia. Only minor to no sulphide minerals are introduced during these breccias events; however they occasionally contain clasts of moderate sulphide-bearing veins.
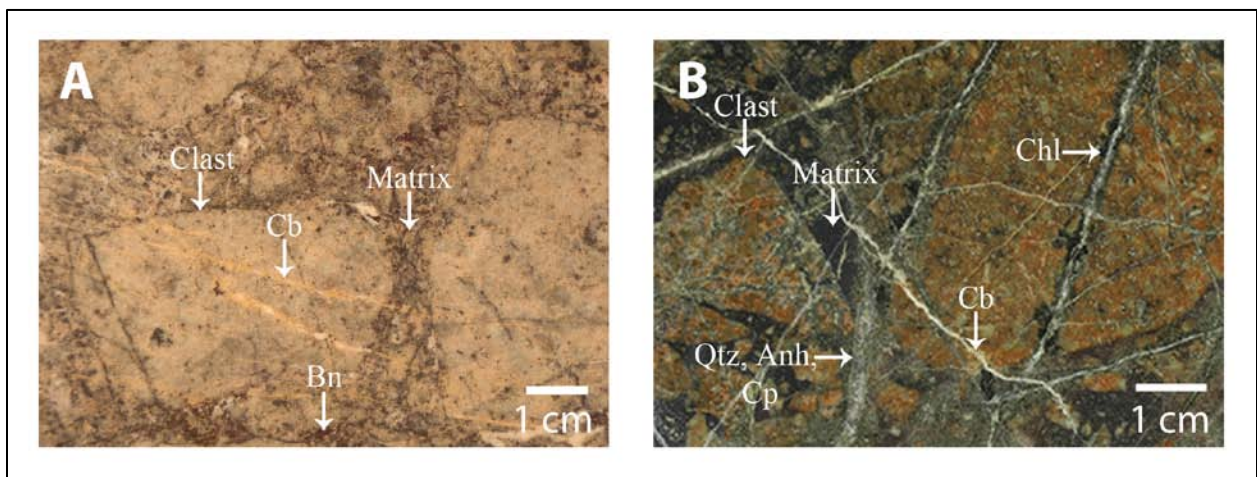
Figure 3.4 Magmatic-hydrothermal breccias cut by carbonate ± quartz veins. Clay (kaolinite) altered with minor bornite in matrix (A: RC94-106, 213.59 m) and K-silicate-illite altered clasts in a recrystalized rock flour matrix (B: RC09-349, 669.59 m). (Cb = carbonate, Bn = bornite, Chl = chlorite, Qtz = quartz, Anh = anhydrite, Cp = chalcopyrite)

Crosscutting relationships and breccias indicate at least two pulses of intrusive activity within the Red Stock. However younger faults, veins and alteration minerals complicate the identification and classification of discrete units. Only a few crosscutting relationships between intrusive phases are preserved but these contacts cannot be correlated between drillholes in either cross-section. Most intrusive contacts are either reactivated by younger brittle faults or are intensely carbonate cemented, or both. Intense clay alteration in these zones greatly obscures any textural or compositional differences between intrusive units. Minor primary igneous relationships are more easily recognized in deeper portions of the East zone where alteration is weaker and changes in phenocryst size and density and groundmass texture are quantifiable. However, these relationships are difficult to extrapolate into the upper portions of the East zone due to extensive overprinting clay alteration (see below). Historically, the composite Red Stock

in the East zone (see Schink, 1977) was considered to comprise main and late intrusive phases, both of which are cut by post-mineral dikes. However, this study failed to conclusively identify discrete intrusive phases that can be correlated at all depths and locations across the East zone.

3.2.3 Post-Mineral Dykes

Two types of post-mineral, 1 to 20 m wide (measured in drill core) diorite to monzodiorite dykes intrude the Red Stock. These dykes are present throughout the East zone, but are mostly located between 400 and 800 m in depth. The amygdaloidal monzodiorite dykes are beige to locally light green and very fine-grained, with carbonate > quartz amygdules 2 to 10 mm in size (Figure 3.5A). Minor euhedral hornblende phenocrysts, up to 4 mm long and altered to clay and/or chlorite are also present (< 3 %). The hornblende-biotite diorite dykes are light to medium green and are very fine-grained, with up to 10 % biotite, along with minor hornblende phenocrysts, which occur up to 5 mm long and are locally altered to clay and/or chlorite (Figure 3.5B). The post-mineral dykes compose < 2 % of the stock, are not mineralized, are variably altered and are cut by minor, late, buff-white carbonate veins and local chlorite veins.
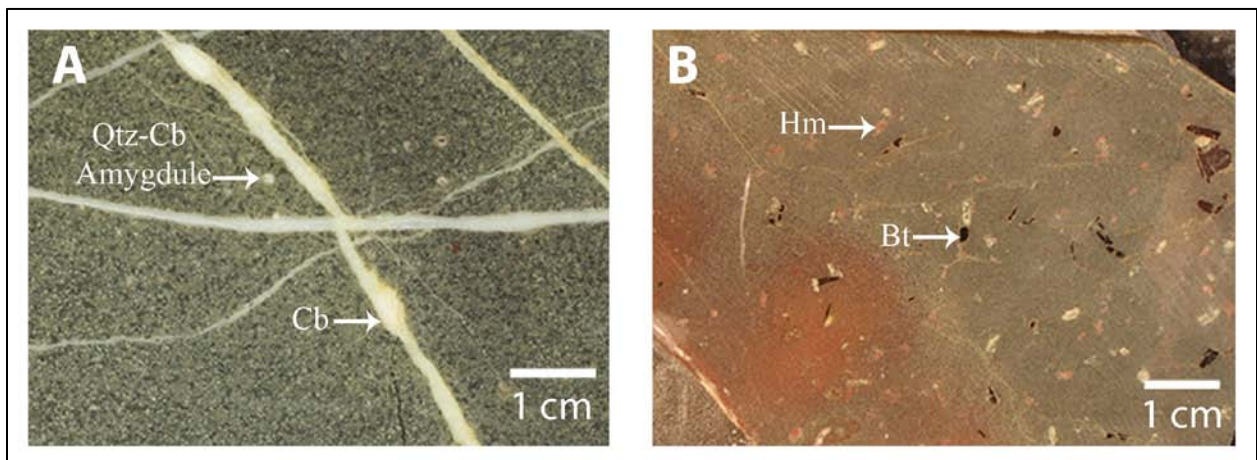
Figure 3.5 Post-mineral dykes. Quartz-carbonate amygdaloidal monzodiorite dyke (A: RC09-345, 958.79 m) and hornblende-biotite diorite dyke (B: RC94-079, 232.75 m) weakly hematite and clay altered. (Qtz = quartz, Cb = carbonate, Hm = hematite, Bt = biotite)

3.3 Hydrothermal Alteration

3.3.1 Overview

Hydrothermal alteration of the Red Stock in the East zone is intense and pervasive, as all of the rocks along sections N50E and 452700E (Figures 3.6 and 3.7) exhibit various forms of alteration. Several alteration zones are present and are variably overprinted by younger alteration events. There are very few fresh rocks and the least altered rocks occur along the deepest flanks of the East zone. A few, localized sections of chlorite-pyrite-epidote altered rocks are weakly

preserved on the deep flanks of the East zone; these rocks are locally slight to moderately K-silicate and clay altered. The core of the East zone is characterized by intense K-silicate alteration to an assemblage of secondary biotite, magnetite and lesser K-feldspar. A relict lens of quartz-sericite-pyrite alteration zone is preserved at a shallow depth near the contact with the Stuhini Group volcanic rocks; these rocks likely formed a part of a larger zone forming a halo around the K-silicate altered core. The K-silicate and quartz-sericite-pyrite altered zones are intensely overprinted by illite-kaolinite which forms the dominant alteration association currently present in shallow levels of the East zone. Whereas most of the quartz-sericite-pyrite alteration is overprinted by illite-kaolinite, the K-silicate alteration is preserved at depth where the illite overprint diminishes. Illite-kaolinite is widespread across the East zone and at depth where the even the least altered rocks exhibit minor illite-kaolinite alteration.
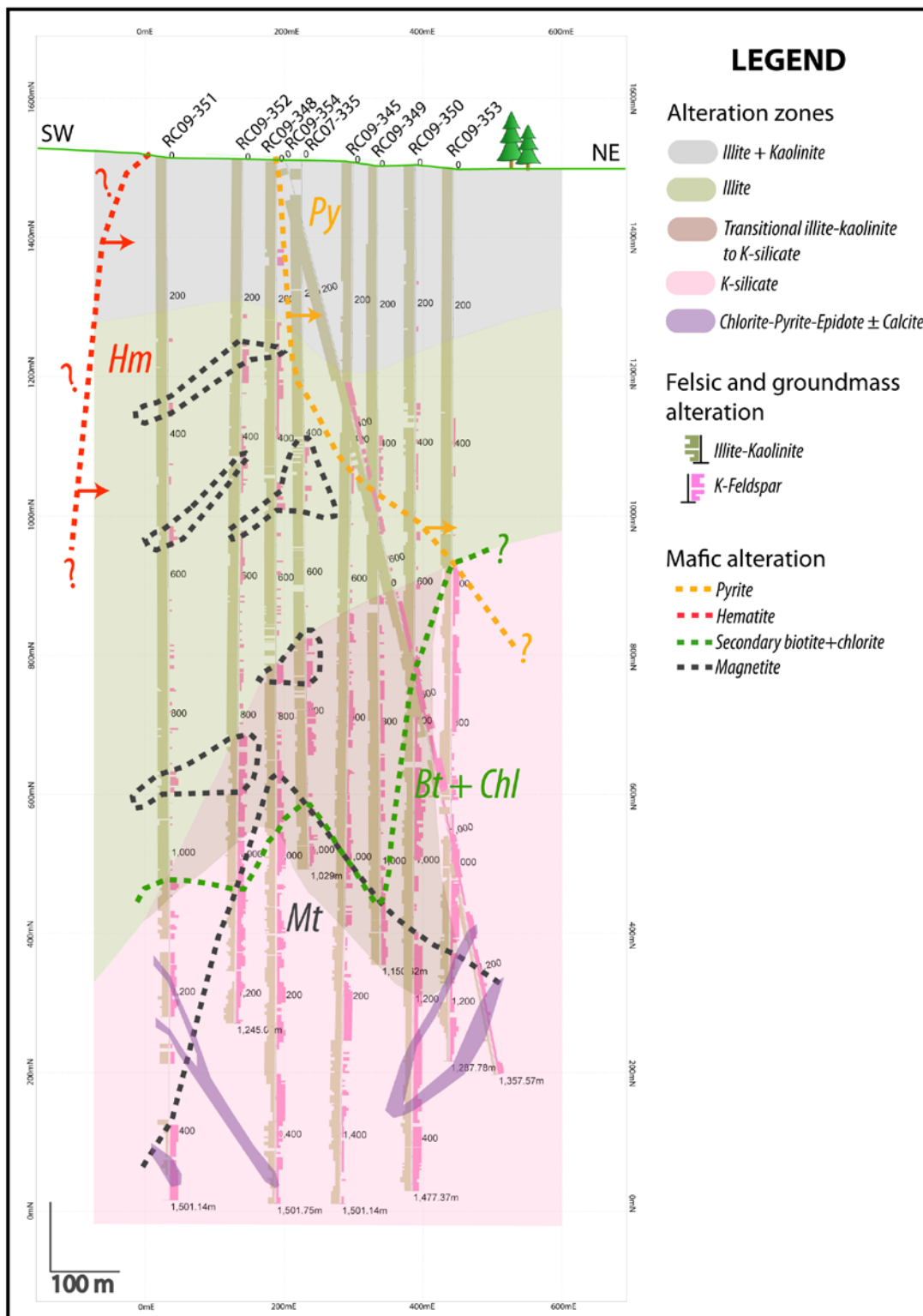
Figure 3.6 Alteration zonation across section N50E of K-silicate, transitional K-silicate to illite, illite and kaolinite. Histograms on drillhole traces show alteration of felsic phenocrysts and groundmass to illite-kaolinite and of the groundmass to K-feldspar. Heavy dashed lines indicate zones of mafic site alteration to magnetite, secondary biotite, chlorite, hematite and pyrite.
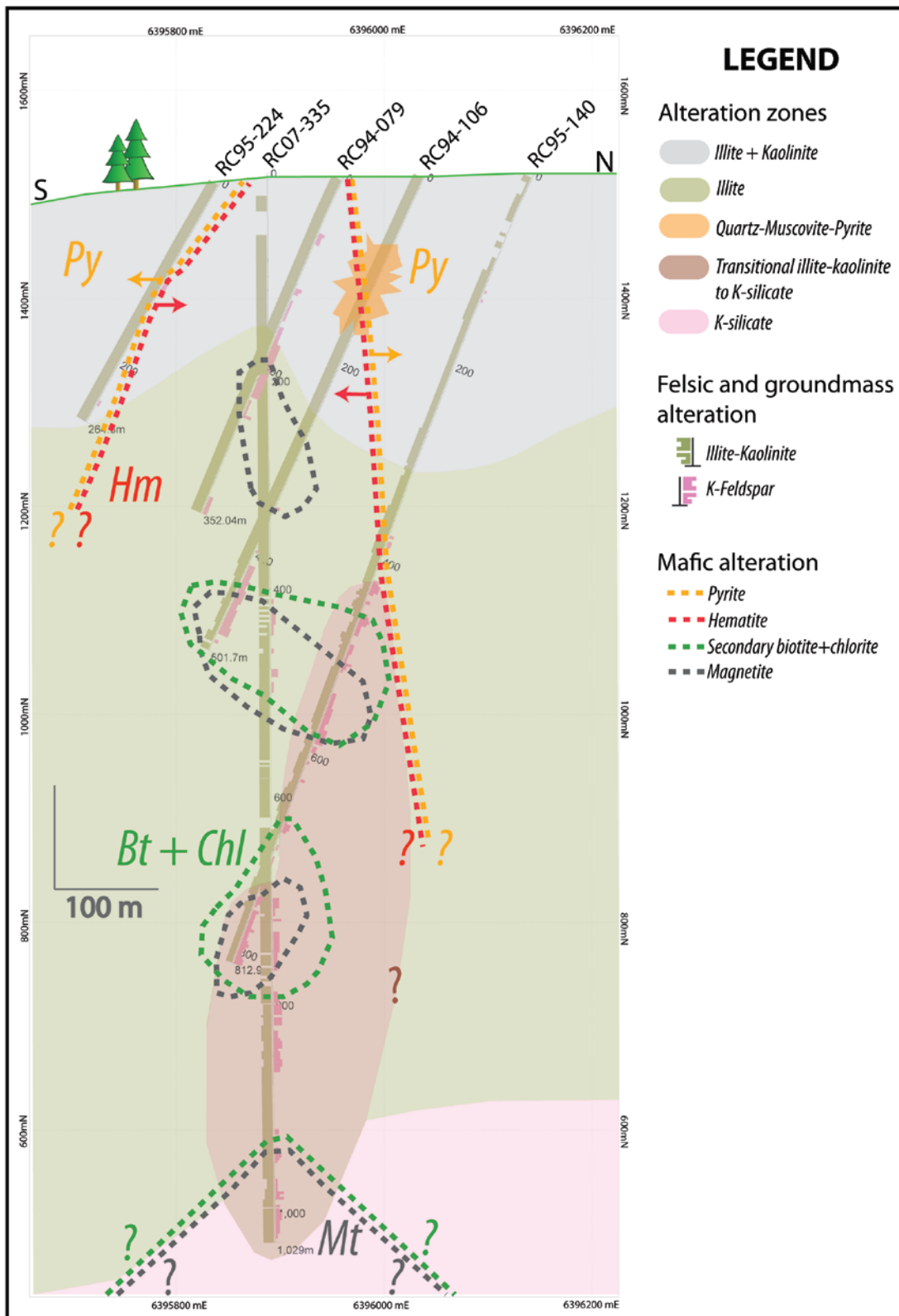
Figure 3.7 Alteration zonation across section 452700E of K-silicate, transitional K-silicate to illite, illite, kaolinite and quartz-muscovite-pyrite. Histograms on drillhole traces show alteration of felsic material to illite-kaolinite and of the groundmass to K-feldspar. Heavy dashed lines indicate zones of mafic site alteration to magnetite, secondary biotite, chlorite, hematite and pyrite.

3.3.2 **Least Altered Monzodiorite**

No fresh, unaltered monzodiorite is present, as all of the rocks exhibit at least minor clay or K-silicate alteration. The least-altered rocks occur below 1200 m depth along section N50E on the SW and NE flanks of the East zone. These rocks are white-light grey with localized pink-orange tint due to primary K-feldspar in the groundmass (Figure 3.8A).
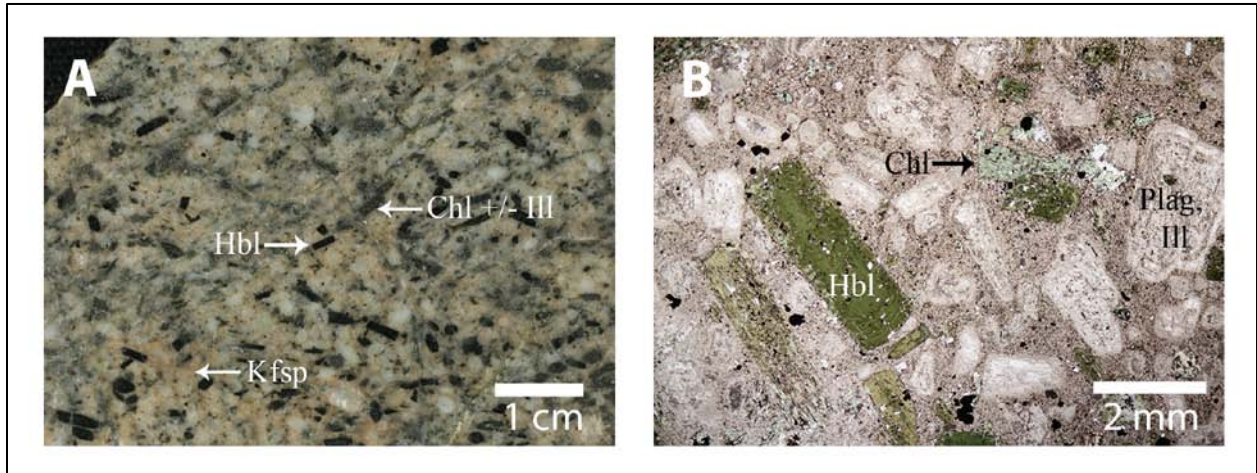
Figure 3.8 Least altered monzodiorite: Weakly K-silicate and illite altered (A) with hornblende phenocrysts weakly altered to chlorite ± illite, minor K-feldspar alteration of groundamss (RC09-353, 1244 m); B: weak chlorite ± illite alteration of horblende phenocrysts, weak illite alteration of plagioclase phenocrysts and groundmass (transmitted, plane polarized light, RC09-350, 1230 m). (Hbl = hornblende, Chl = chlorite, Kfsp = K-feldspar, Plag = plagioclase feldspar, Ill = illite)

Plagioclase phenocrysts are white to beige, tabular crystals, typically 2 to 4 mm long and exhibit oscillatory zoning, simple twinning and minor polysynthetic twinning in thin section. All plagioclase phenocrysts in the least altered monzodiorite are weakly altered to fine-grained illite, typically in the center of the phenocrysts (Figure 3.8B). The groundmass is a mixture of fine-grained quartz and minor K-feldspar with weak fine-grained clay alteration. Mafic igneous minerals are dominantly 3 to 6 mm long hornblende and minor 1 to 2 mm long biotite flakes. There is trace secondary biotite alteration of the hornblende phenocrysts in the least altered monzodiorite. Most of the alteration of mafic minerals is to minor to moderate amounts of chlorite. Minor fine-grained subhedral magnetite crystals with localized fine hematite rims are locally present within the mafic mineral sites where associated with significant illite alteration. Trace, very fine-grained chalcopyrite is locally observed in the magnetite. These likely represent products of K silicate alteration. In contrast, fine-grained magnetite locally within the groundmass could be igneous or hydrothermal in origin. Minor purple anhydrite-quartz-sulphide veins and pyrite ± chalcopyrite veins are associated with the least altered monzodiorite.

3.3.3 **Chlorite-Pyrite-Epidote Alteration**

A minor, weak zone of chlorite-pyrite-epidote ± calcite alteration is preserved in the deep flanks of the East zone (Figure 3.6). Chlorite-pyrite-epidote is locally moderately to intensely overprinted by K-silicate and by illite alteration in the core and along the flanks of the East zone. Chlorite is observed to replace primary hornblende in the absence of secondary biotite in a few deep, least altered samples (Figure 3.9A). Chlorite is generally dominant over secondary biotite and illite alteration in mafic sites below ~1000-1100 m depth across the East zone. Pyrite is observed as minor, fine-grained clots within mafic sites (Figure 3.9B) below 1480 m in the SW flank of the East zone (drillholes RC09-351, RC09-348) and between 1375 and 1501 m near the core of the deposit in RC09-345. Pyrite is located in mafic sites in localized, trace amounts across the East zone below 1000 m depth. Minor pyrite-only veinlets are also observed at these depths. Epidote occurs over localized, 5 m intervals as minor fine-grained clots within mafic sites and along boundaries of purple anhydrite veins. Epidote occurs below 1450 m in the SW flank (drillholes RC09-351, RC09-348) and between 1150 and 1350 m depth in the NE flank, in drillholes RC09-350, RC09-353 and RC09-354 and is associated with chlorite and minor secondary biotite alteration (Figure 3.9C). Calcite is rare, but is noted in thin section to form as minor clots with chlorite and epidote alteration of mafic sites.
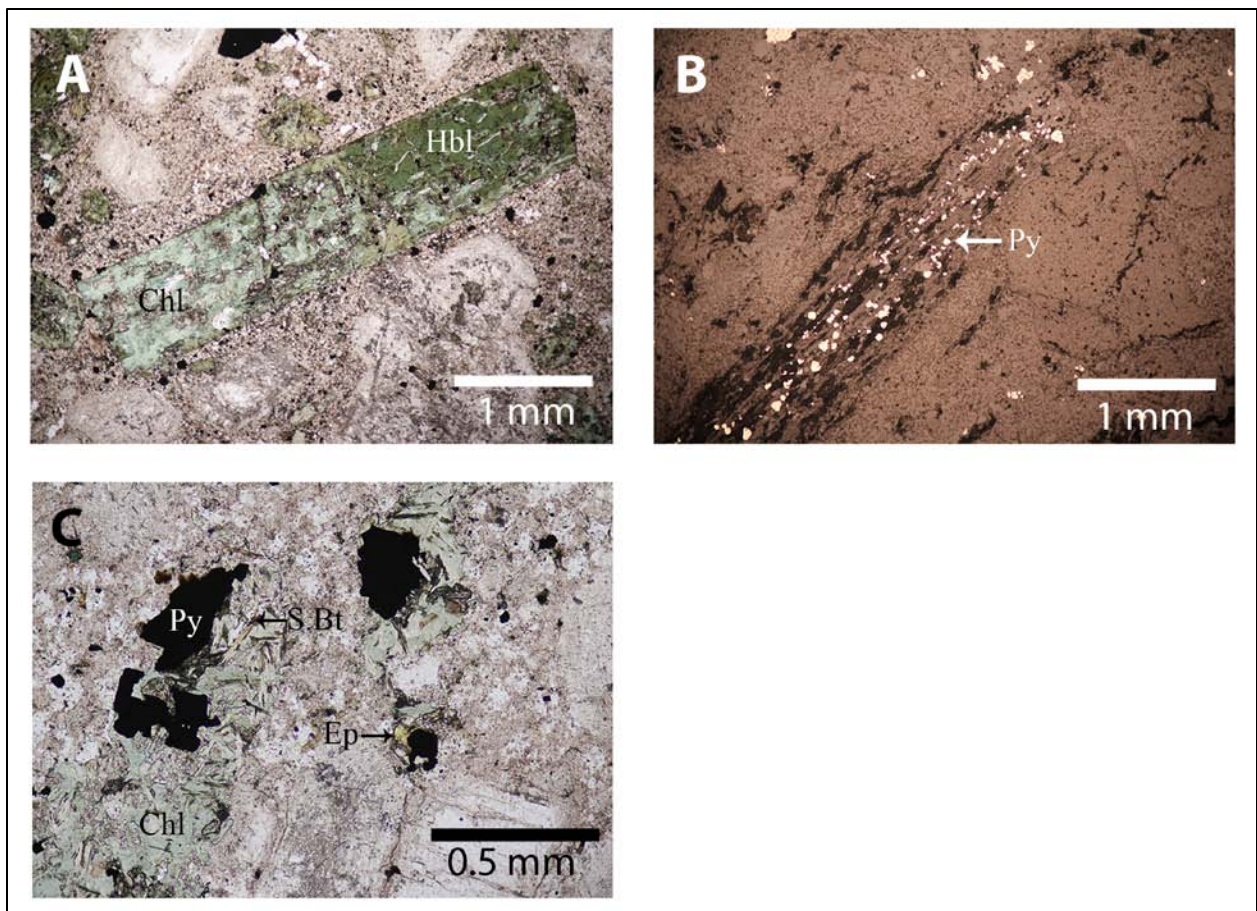
Figure 3.9 Chlorite-pyrite-epidote alteration: A: hornblende altered to chlorite (RC09-350, 1230 m); B: pyrite alteration of mafic sites (RC09-351, 1006 m); C: secondary biotite altered to chlorite, pyrite and epidote (RC09-354, 1256 m). (Chl = chlorite, Py = pyrite, S.Bt = secondary biotite, Ep = epidote)

3.3.4 **K-Silicate Alteration**

The K-silicate alteration zone is visible along section N50E, and is only preserved below 1000 m depth in section 452700E. In section N50E, the remnant K-silicate zone currently has a broadly arching geometry, deepest in the westernmost portion of the section (~1000 m depth) and shallowest in the easternmost (~600 m depth) (Figure 3.6). The shallowest portions of K-silicate alteration are overprinted by illite-kaolinite alteration, making it difficult to determine the original extent of the K-silicate zone. Lenses of relict K-silicate altered rock are present in the core and south-western flank of the East zone in holes RC07-335, RC09-348, RC09-352 and RC09-351 between 200 and 900 m depth where illite-kaolinite alteration is not pervasive. A transitional zone of weak, residual K-silicate alteration with a moderate to strong illite-kaolinite overprint directly overlies the intense K-silicate zone and below a zone of intense illite-kaolinite alteration. The upper contact of the transitional zone is irregular, varying in depth between 600 and 800 m along section N50E (Figure 3.6) and at 400 m depth along section 452700E (Figure 3.7).

3.3.4.1 Secondary Biotite, Magnetite, K-Feldspar

Secondary biotite, magnetite and texturally destructive K-feldspar that replaces the groundmass characterize the K-silicate alteration zone (Figure 3.10A, B). Hornblende is replaced by secondary biotite, magnetite, and by younger chlorite (Figure 3.10A, B); locations in which they dominate are mapped along section line N50E (heavy dashed lines in Figure 3.6). Secondary biotite and chlorite are preserved below a depth of 950 m in the eastern portion of the section and at 600 m in the western portion, creating a sharp boundary between holes RC09-349 and RC09-350. A localized zone of moderate secondary biotite and chlorite in holes RC07-335 and RC09-348 at depths of 400 and 450 m, respectively, is continuous to the west through holes RC09-352 and RC09-351 at a depth of 800 m. Moderate to abundant amounts of hydrothermal magnetite is present within the mafic sites and groundmass below 900 m in the core, and at gradually deeper depths towards the flanks of the East zone. The magnetite zone lies at a depth of 1150 m in the eastern portion of the section and at 1100 to 1400 m in the west, with an apex at 900 m in drillhole RC09-348. Lenses of relict K-silicate alteration where magnetite is preserved in mafic sites occurs in the upper 1000 m, in the core of the East zone. Relict magnetite is noted as shallow as ~200 m depth, which is evidence for K-silicate alteration having once extended to at least such depths, prior to any subsequent alteration overprinting events.
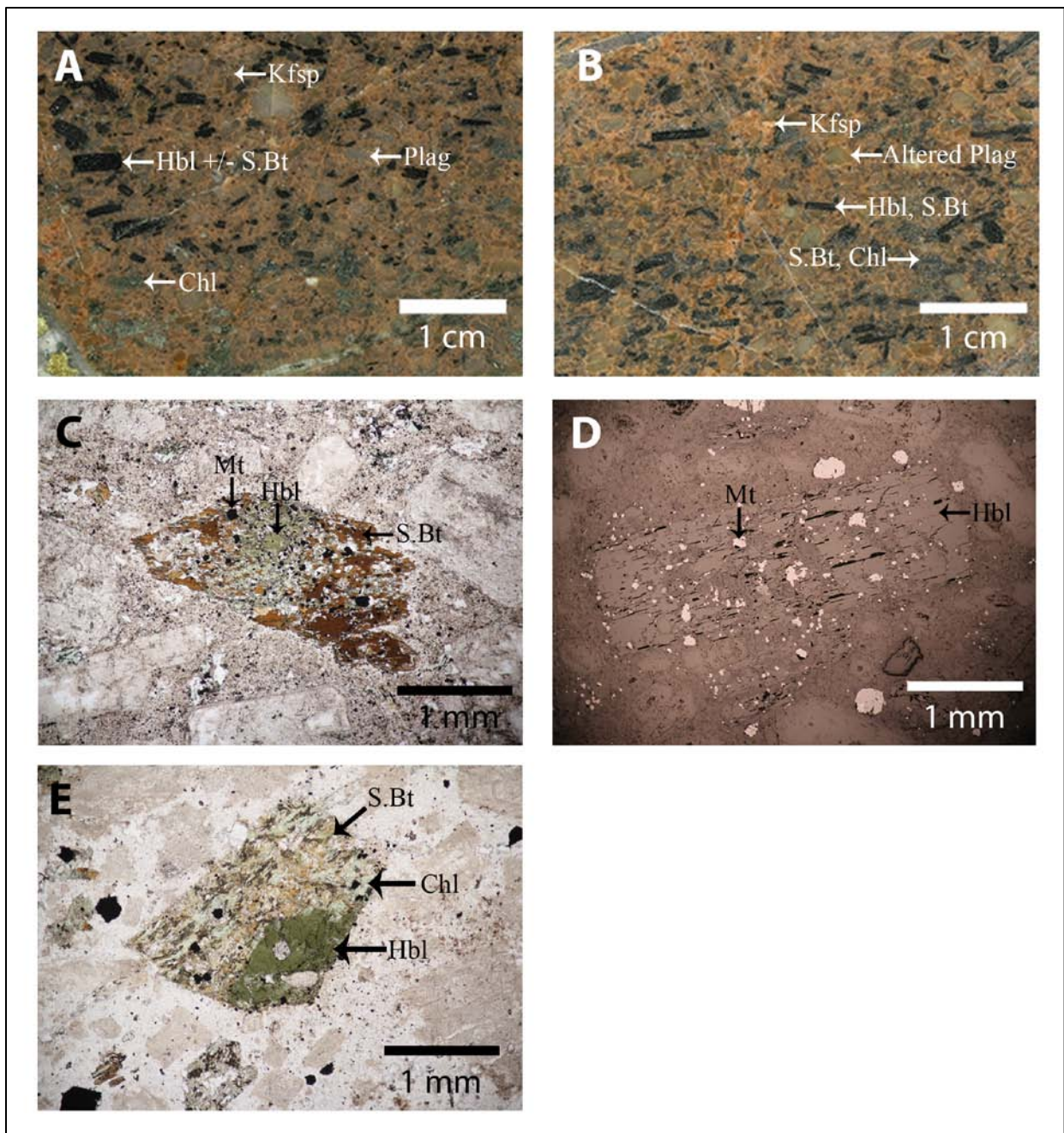
Figure 3.10 K-silicate alteration. A: K-feldspar altered groundmass, mafic sites are hornblende variably altered to secondary biotite and chlorite, felsic minerals are weakly clay altered plagioclase feldspar (RC09-348, 1128 m); B: K-feldspar altered groundmass, mafic sites are hornblende variably altered to secondary biotite and chlorite, felsic minerals are clay altered plagioclase feldspar (RC09-352, 1062 m); C: secondary biotite and magnetite altering a primary hornblende phenocryst (RC09-354, 1168 m); D: magnetite clots within a weakly altered hornblende phenocryst (RC09-348, 1128 m). E: weak illite-kaolinite alteration with hornblende altered to secondary biotite and overprinted by chlorite (RC09-353, 1244 m). (Hbl = hornblende, S.Bt = secondary biotite, Chl = chlorite, Kfsp = K-feldspar, Plag = plagioclase, Mt = magnetite)

Secondary biotite replaces primary hornblende as shreddy, fine-grained sheets that in many locations may retain the original hornblende crystal shape (Figure 3.10C). Chlorite

typically alters secondary biotite prior to clay alteration however few samples show illite-kaolinite alteration of secondary biotite with no obvious chlorite present. Magnetite occurs as subhedral, subrounded blebs within mafic sites and locally within the groundmass (Figure 3.10D). Chalcopyrite occurs as trace, very-fine-grained blebs within magnetite, and as isolated blebs in mafic sites. Hydrothermal K-feldspar intensely alters the groundmass which is best indentified by K-feldspar staining, as the fine-grained K-feldspar is difficult to identify in thin-section and the reddish colour in hand samples may also be due to disseminated hematite. Only minor primary K-feldspar is present in the least altered rocks (Figure 3.11A, B) and significant addition of K-feldspar is present in the K-silicate zone (Figure 3.11C, D). Gradually increasing intensity of illite-kaolinite alteration overprinted and replaced hydrothermal K-feldspar (Figure 3.11E, F, G). Primary plagioclase phenocrysts are weakly clay altered and are not altered to K-feldspar. Where preserved, plagioclase phenocrysts are equant, coarse-grained and occur in their least altered form below 1200 m depth.
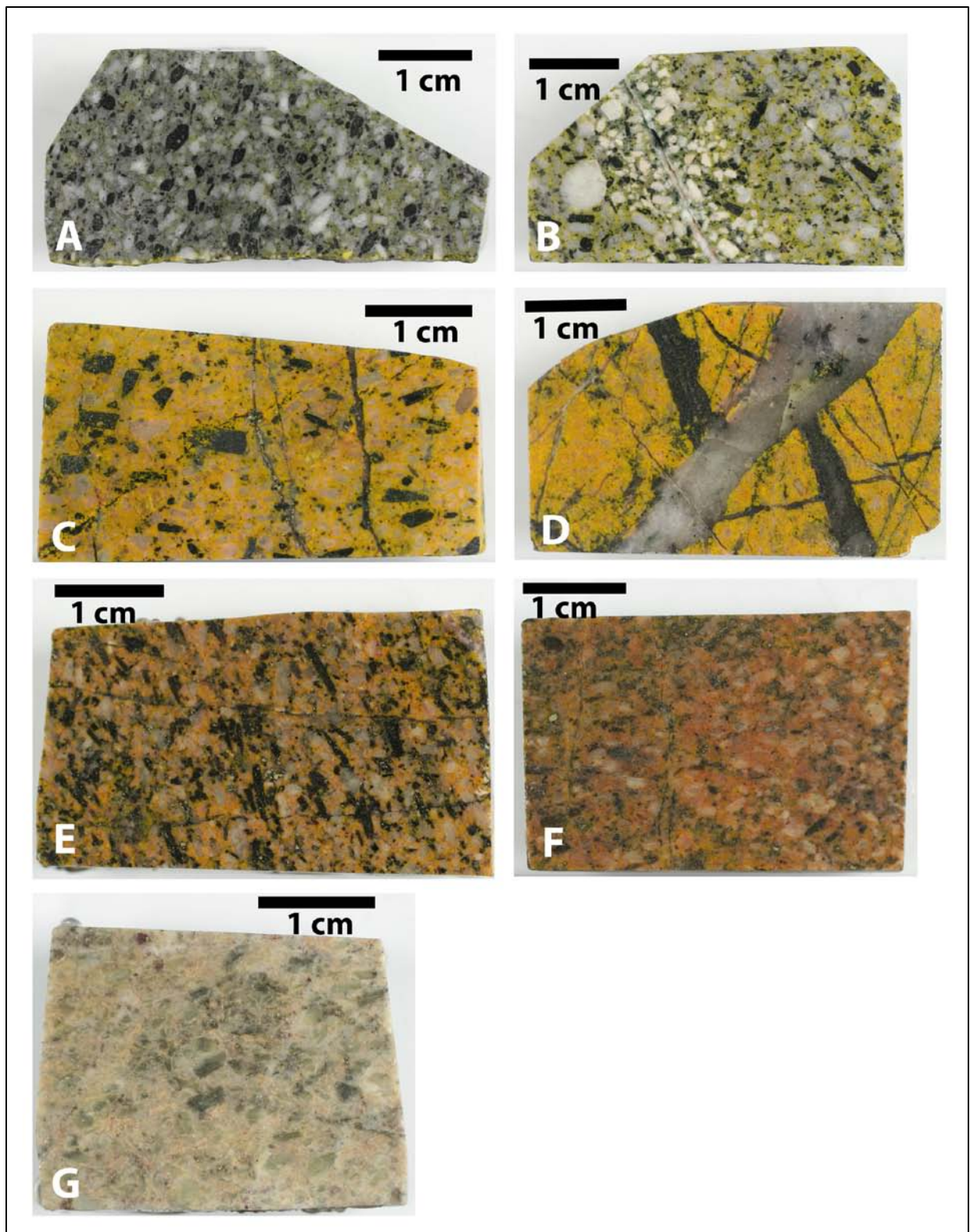
Figure 3.11 K-feldspar (bright yellow) stained offcuts. Least altered rock with minor K-feldspar in groundmass (A: RC09-354, 1168 m; B: RC09-350, 1230 m); Intense K-feldspar alteration of groundmass (C: RC09-350, 1398 m ; D: RC07-335, 864 m); Weak illite overprint with moderate relict K-feldspar in groundmass (E: RC09-354, 917 m); Moderate illite overprint with minor relict K-feldspar in groundmass (F: RC09-351, 550 m); Intense illite overprint with no K-feldspar remaining (G: RC09-354, 630 m).

3.3.4.2 Chlorite

Chlorite is present in varying amounts within mafic sites throughout much of the East zone in areas of weak to moderate illite-kaolinite overprint. Chlorite alters secondary biotite and/or igneous hornblende (Figure 3.10E). Chlorite replaces secondary biotite prior to being altered to muscovite or illite. Chlorite is a transitional alteration mineral between hornblende or secondary biotite and muscovite and/or illite.

3.3.4.3 Hematite

Minor to moderate hematite dusted groundmass and plagioclase feldspar phenocrysts are occasionally observed with K-silicate alteration and can be mistaken as K-feldspar. Applying a K-feldspar stain to a rock is the best way to distinguish between K-feldspar and hematite dusting. It is not conclusive as to how or when the rocks become dusted by hematite, however it is assumed to form with K-silicate alteration, as proposed by Meyer and Hemley (1967). Hematite dusting is not related to magnetite alteration to hematite during illite-kaolinite alteration (discussed below), but rather is destroyed by illite-kaolinite. Hematite dusting is recognized at the Cadia District, southeastern Australia where it is an important component of propylitic alteration (Wilson et al., 2003; Wilson et al., 2007).

3.3.5 Quartz-Sericite (Muscovite)-Pyrite Alteration

A localized section within drillhole RC94-106 identified a continuous zone of quartz-muscovite-pyrite alteration. The presence of muscovite was determined by interpretations of short-wave infrared (SWIR) spectroscopy and confirmed by X-Ray diffraction (XRD) analysis. The full-width half-maximum (FWHM) method was used on XRD patterns to determine that the mineral near the 10 °2θ CuKα (mica) peak is muscovite (See Appendix A3). Between ~70 and 165 m down-hole depth in RC94-106, SWIR spectroscopy identified muscovite and minor local kaolinite as the dominant clay minerals within this section. No illite was identified in this section. XRD analysis on sample RC106-007 taken at a down-hole depth of 72.23 m identified only quartz, muscovite and pyrite as minerals contained in the rock. Further, XRD analysis also reported quartz, muscovite, kaolinite, ankerite, pyrite and minor chalcopyrite in samples RC106-012 (107.57 m depth) and RC106-018 (138.99 m depth, Figure 3.12A) within this zone. Samples of kaolinite ± illite altered breccias occur above and below the quartz-muscovite-pyrite dominant section and the original spatial extent of this quartz-muscovite-pyrite zone is not known.
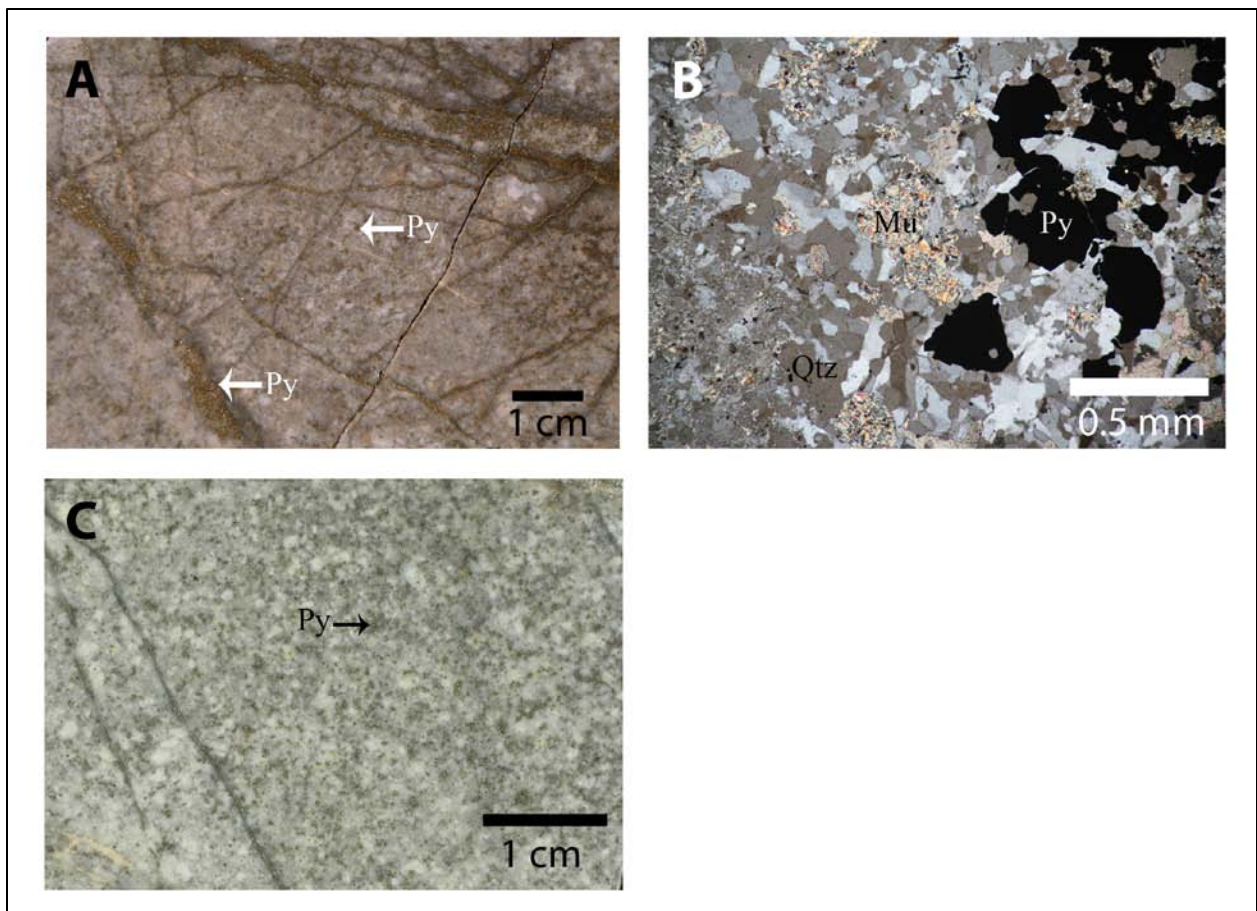
Figure 3.12 Quartz-muscovite-pyrite alteration in RC94-106 (139 m) in hand sample (A) and in transmitted light (crossed polars; B). Muscovite laths (B) are slightly coarser grained than illite-kaolinite alteration. C: pyrite alteration of mafic sites (RC09-345, 44 m). (Qtz = quartz, Mu = muscovite, Py = pyrite)

Petrographic analysis demonstrates pervasive, fine-grained, lath-like muscovite alteration (Figure 3.12B), which appears slightly coarser-grained than very fine-grained illite-kaolinite alteration. Original plagioclase and hornblende phenocryst grain boundaries are nearly indistinguishable in hand sample and thin section. Quartz commonly forms fine-grained, subhedral grains within the groundmass and locally in clots and along vein margins. Fine to medium grained, anhedral pyrite crystals commonly replace mafic minerals and also form veinlets (Figure 3.12C). Carbonate in this sample forms fine-grained clots associated with muscovite and fine-medium grained subhedral pyrite.

Pyrite associated with the quartz-sericite-pyrite zone dominates in the shallowest portion of sections N50E (Figure 3.6) and 452700E (Figure 3.7). Along section N50E, pyrite dominates the northeast portion of the section at a depth of 580 m in RC09-353 and gradually at shallower depths westward toward RC07-348, where it replaces mafic minerals in the upper 10 m of the

drillhole. Along section 452700E, pyrite forms in the upper 400 m along the north and south flanks of the section.

3.3.6   Illite-Kaolinite Alteration

Illite-kaolinite alteration was logged in the field as sericite. Sericite is a field term widely used to describe alteration to fine-grained hydrous white mica minerals and may include muscovite, pyrophyllite, paragonite, phlogopite and occasionally illitic mica and interlayered disordered micas with other sheet-structured minerals such as montmorillonite, chlorite and vermiculite (Meyer and Hemley, 1967). Results of SWIR analysis on all of the samples identified the clay alteration minerals as dominantly illite and lesser kaolinite accompanied by minor muscovite. These results were confirmed by XRD techniques.

Illite-kaolinite intensely overprints the K-silicate alteration assemblage and locally chlorite-pyrite-epidote in the East zone along section lines 452700E (Figure 3.7) and N50E (Figure 3.6), altering both groundmass and phenocrysts. Minor to moderate chlorite and moderate pervasive carbonate, as ankerite-dolomite, are associated with illite-kaolinite. Hematite alteration of magnetite is also associated with clay alteration.

Intense illite-kaolinite alteration occurs in both sections (N50E and 452700E) in the upper 600 to 800 m. In a transitional zone between 600 and 1000 m depth in the core of the system, plagioclase phenocrysts are moderately to strongly illite-kaolinite altered yet K-feldspar remains in the groundmass. Lenses of relict K-silicate alteration occur in the core and western flank of the East zone above 1000 m depth within areas of intense to transitional illite-kaolinite alteration. The intensity of illite-kaolinite alteration overprint decreases with depth, to minor amounts below 1000 m on the flanks and to moderate amounts in the deepest drilled holes (1500 m) in the core of the East zone.

3.3.6.1   Illite and Kaolinite

Illite and kaolinite pervasively alter plagioclase and alkali feldspars, hornblende phenocrysts and secondary biotite in the least- and K-silicate–altered zones. Alteration is commonly buff-white (Figure 3.13A), locally pale green (illite; Figure 3.13B) and rarely pale orange (ankerite-dolomite). The groundmass is also clay altered in areas of moderate to intense alteration. The original porphyritic texture is locally completely destroyed by illite-kaolinite

alteration in hand sample (Figure 3.13C). The extent of the illite-kaolinite alteration overprinting K-silicate alteration is variable (Figure 3.13D, E). Kaolinite alteration dominates in the upper 200 to 300 m of sections N50E and 452700E and illite dominates below the kaolinite zone to depths of 600 to 800 m in the core and eastern flank, and to 1000 m on the western flank of the East zone (Figure 3.6).
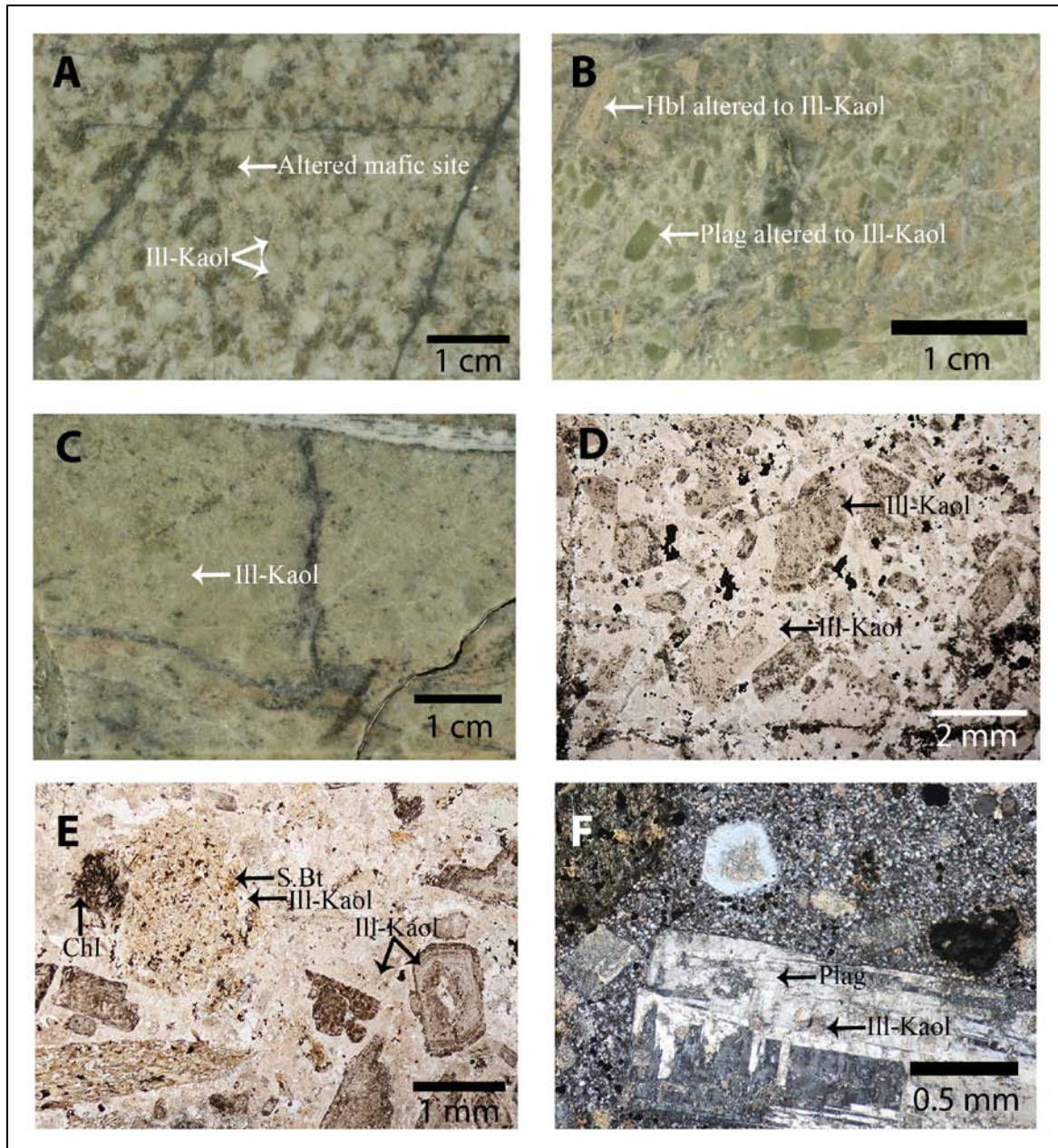
Figure 3.13 Illite-kaolinite alteration. A: plagioclase phenocrysts altered white, mafic phenocrysts altered beige-brown, goundmass is altered grey-white (RC09-349, 200 m); B: plagioclase phenocrysts altered pale green, mafic phenocrysts altered pale beige, groundmass altered grey (RC09-350, 1099 m); C: intense illite-kaolinite alteration nearly destroying the poprhyritic texture (RC09-354, 434 m); D: intense illite-kaolinite alteration of phenocrysts and groundmass (RC09-350, 346 m); E: weak illite-kaolinite alteration overprinting secondary biotite (RC09-350, 997 m); F: weak illite-kaolinite alteration of plagioclase phenocrysts (RC09-350, 1132 m). (Ill = illite, Kaol = kaolinite, Hbl = hornblende, Plag = plagioclase, S.Bt = secondary biotite, Chl = chlorite)

73

Illite and kaolinite alteration is characterized by pervasive, very-fine-grained clay alteration of plagioclase phenocrysts. In less altered crystals, clay alteration is observed in the center of the grain (Figure 3.13F). Remnant oscillatory zoning, Carlsbad twins and polysynthetic twinning are preserved in weak to moderately-clay altered plagioclase phenocrysts. The groundmass is altered to very-fine grained clay thereby obscuring any previous alteration. Hornblende phenocrysts are commonly entirely altered to clay and are identified primarily by crystal shape. Once containing mafic minerals (hornblende ± secondary biotite), these clay altered phenocrysts are referred to as mafic sites, as little to no trace of the original mafic mineral remains. Mafic sites have irregular grain boundaries and, where intensely clay altered are hard to distinguish from the groundmass and highly altered plagioclase phenocrysts. Where mafic sites have irregular grain boundaries and shreddy-textures, the original hornblende was altered to secondary biotite prior to chlorite and illite alteration, as chlorite and illite alteration of primary hornblende will retain the sharp crystal boundaries of the hornblende phenocryst.

Illite and kaolinite alteration was confirmed by the use of the TerraSpec analyzer, which uses short-wave infrared (SWIR) spectroscopy that detects energy generated by vibrations within molecular bonds of minerals (Thompson et al., 1999). These bonds vibrate between 1300 nm and 2500 nm of the electromagnetic spectrum and diagnostic absorption features at certain wavelengths can be used to identify alteration minerals, particularly white micas. A study was undertaken on 42 samples to compare the results of the TerraSpec with X-ray diffraction (XRD) methods. Samples of whole-rock were taken from areas that were not influenced by vein material, so as to not contaminate the sample with any possible vein alteration halo material. Whereas the presence of kaolinite was readily identifiable in both TerraSpec and XRD, differentiation between illite and muscovite required additional analysis.

3.3.6.2   Illite vs. Muscovite

Illite and muscovite are different minerals with distinct crystal structures, chemical compositions and form under different conditions. Whereas illite may be considered the clay-sized (< 2 μm) fraction of a micaceous mineral, it contains H_2O in its crystal structure, which muscovite does not. The presence of water should allow for the identification of illite versus muscovite by SWIR based on the depth and intensity of the H_2O absorption feature at 1900 nm. A sharp 1900 nm absorption feature on illite spectra indicate molecular water is present and is

located within well-defined and well-ordered sites (Kruse and Hauff, 1991). However the 1900 nm feature often appears shallow when potassium mica (muscovite) is present (Hunt and Ashley, 1979). Therefore, the depth of the H_2O feature, when compared to the depth of the 2200 nm (Al-OH) feature, is best diagnostic tool for differentiating between illite and muscovite; a sharp, deep 1900 nm feature for illite (Figure 3.14A) and a broader, shallow feature for muscovite (Figures 3.14B). This technique may not be applicable everywhere, such as at the Ann Mason porphyry deposit of the Yerington district, Nevada, where by muscovite determined by electron microprobe analysis also can have a deeper 1900 nm feature similar to those characterizing illite (Cohen, 2011).
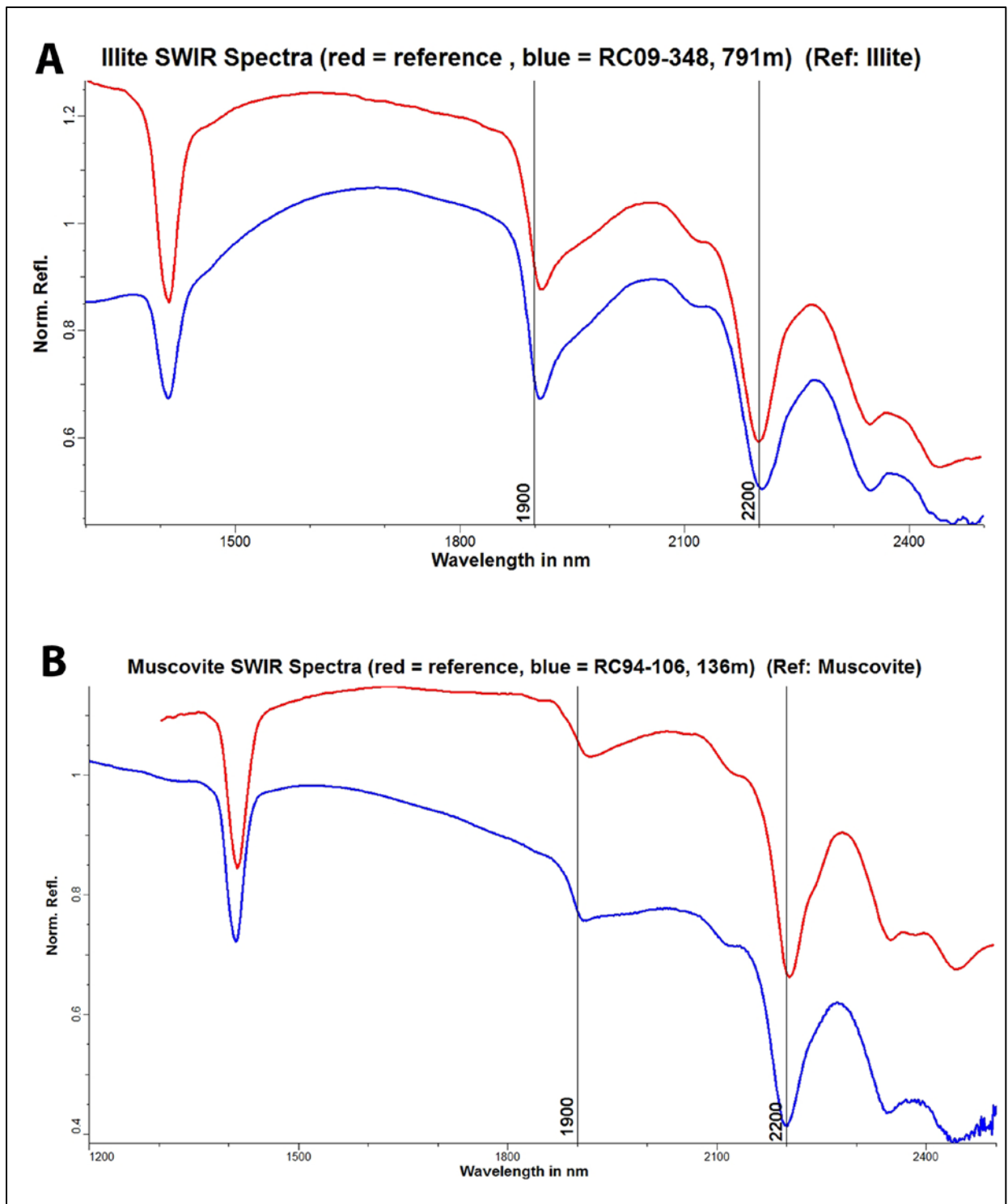
Figure 3.14 TerraSpec short-wave infrared spectroscopic spectra with 1900 nm (H_2O) and 2200 nm (Al-OH) absorption features labeled. A: illite reference spectra (red) and illite alteration pattern (blue) from RC09-348 at 791 m depth; B: muscovite reference spectra (red) and muscovite alteration pattern (blue) from RC94-106 at 136 m depth.

After visually interpreting the SWIR data, it was determined that much of the clay alteration is illite. However, in many instances, the depth of the 1900 nm feature was neither

deep nor shallow and the interpretation of the SWIR data was inconclusive for illite or muscovite. XRD methods were employed to test the ability of the TerraSpec to identify clay minerals at Red Chris, as well as to distinguish the difference between illite and muscovite where the interpreted TerraSpec results were inconclusive. The result of the XRD study confirmed that the samples clearly identified as illite by the TerraSpec were also illite by XRD analysis. Additionally, samples clearly identified as muscovite by the TerraSpec were also muscovite by XRD analysis. Where TerraSpec analysis was inconclusive for illite or muscovite (moderate 1900 nm features), the XRD reported illite, however it is possible that both illite and muscovite were present in these samples.

3.3.6.3 Hematite

Hematite is associated with the intense illite-kaolinite alteration overprint and its presence has been mapped along section line N50E (Figure 3.6) and section 452700E (Figure 3.7). Throughout the illite-kaolinite zone, pervasive but minor hematite occupies the mafic sites and within veins and has both sharp and diffuse crystal boundaries. The hematite is very fine grained and dark grey (specular), and earthy-red to maroon (Figures 3.15A, B). Magnetite associated with the K-silicate alteration zone is altered to hematite by the illite-kaolinite alteration fluids (Figure 3.15C). This hematite is different from hematite dusting observed in the K-silicate alteration zone.
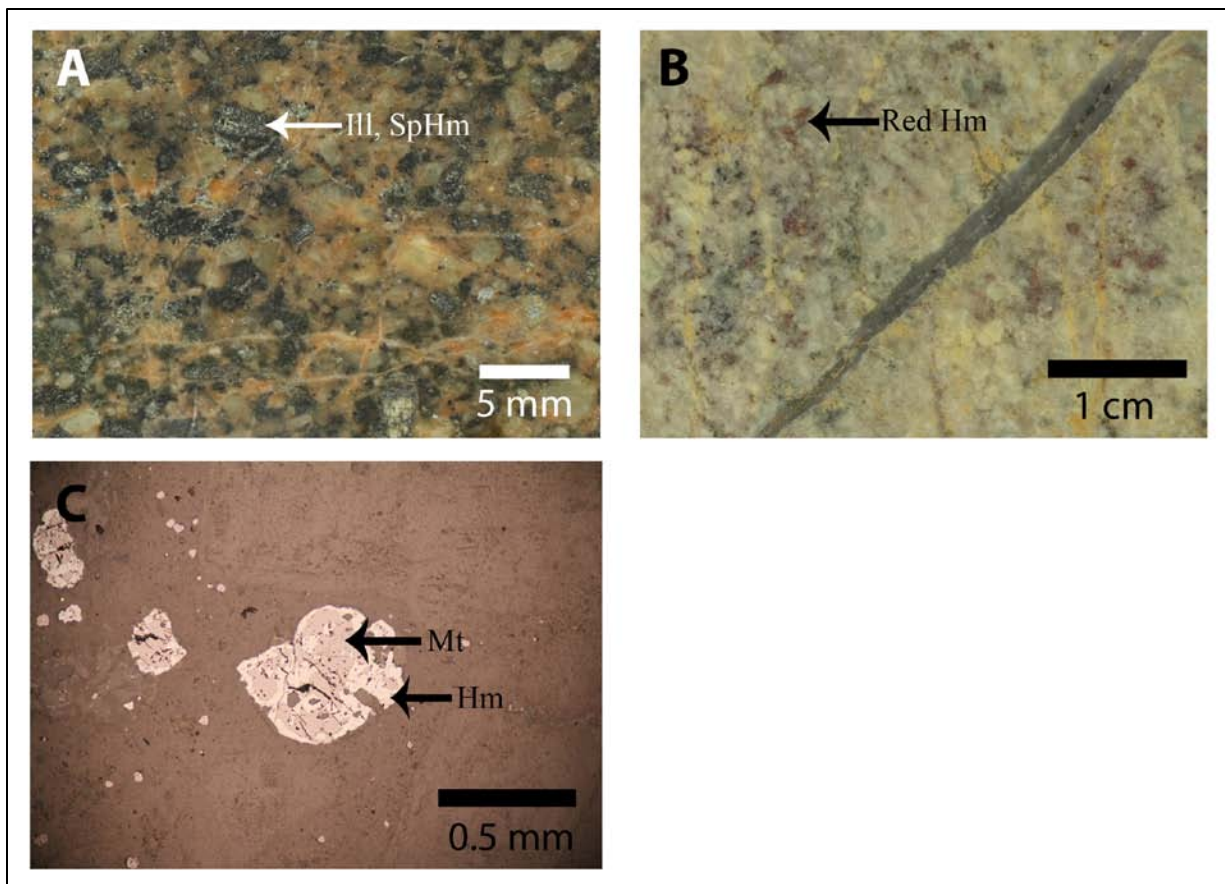
Figure 3.15 Hematite alteration. A: illite-kaolinite alteration with mafic sites altered to illite and specular hematite (RC09-351, 264 m); B: illite-kaolinite alteration with red-pink hematite stain in mafic sites (RC09-351, 216 m); C: magnetite bleb with hematite alteration rims in reflected light (RC09-350, 1132 m); (Py = pyrite, Ill = illite, SpHm = specular hematite, Hm = hematite, Mt = magnetite)

Along the southwest portion of section N50E (drillholes RC09-351, RC09-352 and RC09-348) hematite is the dominant oxide in the mafic sites and veins, extending to a depth of 900 m in RC09-348, marking the apex of a deeper, magnetite-dominant zone. Localized isolated pods of magnetite as the dominant oxide in the mafic sites occur throughout the hematite-dominant zone, reflecting areas with a less intense illite-kaolinite alteration overprint. A zone of sub-equal hematite and magnetite within the mafic sites indicates a transitional oxide zone between depths of 550 and 1100 m in the easternmost part of the section, in drillholes RC09-353 and RC09-350.

Along section 452700E, hematite occurs with illite-kaolinite in the core of the section where pyrite (quartz-sericite-pyrite alteration) occurs in the upper 400 m along the north and south flanks of the section. As in section N50E, magnetite and secondary biotite associated with K-silicate alteration are altered to hematite, chlorite and illite-kaolinite. Lenses of relict K-

78

silicate alteration characterized by magnetite, secondary biotite and chlorite are present along section 452700E in drillholes RC07-335, RC94-079, RC94-106 and RC95-140 but have a weak illite-kaolinite overprint.

3.3.6.4 Carbonate

Pervasive carbonate is spatially associated with the illite-kaolinite in the upper portions of the East zone. Baker et al. (1997) reported a ferroan-dolomite composition for this carbonate. Locally, phenocrysts are preferentially altered to a buff beige carbonate that oxidizes to a pale orange over time (Figure 3.16A). As much of the core was drilled in the mid-1990's and at least one year prior to logging, the orange carbonate alteration was readily visible. Some samples from the East zone show a moderate pervasive orange carbonate alteration in all of the phenocrysts and the groundmass of the sample, which also appear to be intensely illite-kaolinite altered (Figure 3.16B). The pervasive carbonate alteration is very fine-grained and hard to distinguish from fine-grained clay alteration in thin-section.
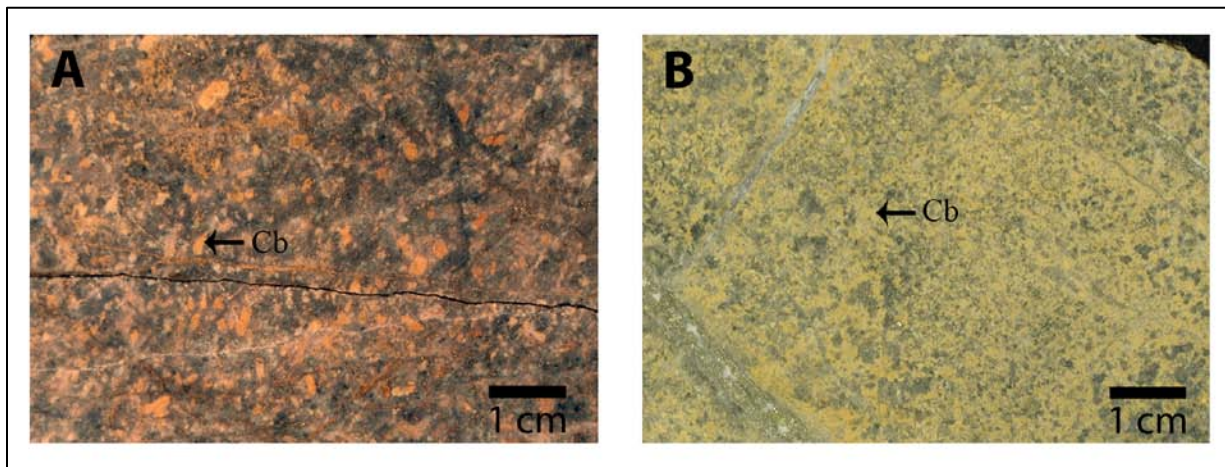
Figure 3.16 Carbonate alteration with orange (iron) oxidation. A: pervasive carbonate alteration of phenocrysts (RC94-106, 133 m); B: pervasive carbonate alteration of the groundmass ± phenocrysts (RC09-348, 178 m). (Cb = carbonate)

Although the greatest intensity of pervasive carbonate alteration was logged in the upper 500 m of the East zone, XRD analysis indentified carbonate in nearly all of the samples analyzed for clay mineralogy, occurring at ~1100 m at the deepest extent. The carbonate is referred to as ankerite however the mineral is likely a ferroan-dolomite or an ankerite-dolomite mixture. Ankerite and dolomite are difficult to distinguish by XRD. The TerraSpec did not identify ankerite as an alteration mineral of the monzodiorite as carbonates are a low-reflectance mineral and there is less than 30 % carbonate in the sample.

3.3.7 **Alteration Zonation**

Alteration zonation is dominant in the vertical extent and lesser laterally across the East zone (Figures 3.6 and 3.7). Minor lateral zonation of weakly preserved chlorite-pyrite-epidote alteration occurs at the SW and NE flanks of the East zone, as observed along section N50E. The core of the East zone at depth does not exhibit pyrite or epidote and represents a K-silicate altered core with variable illite alteration. The flanking chlorite-pyrite-epidote zones are occasionally moderately overprinted by illite and lesser kaolinite and carbonate.

In the vertical dimension, the alteration zonation is distinct. There is a gradation of illite-kaolinite and carbonate alteration overprint, which decrease with depth. The K-silicate alteration zone once had a much greater extent prior to the clay overprint but currently is best preserved below 1000 m depth. Above this zone, up to about 800 m at the SW flank and up to 600 m at the NE flank, there is a transitional zone of moderate illite overprinting the K-silicate zone where clay and K-silicate alteration minerals are present roughly in equal amounts. The upper 600 to 800 m of the East zone is intensely overprinted by illite with the top 200 to 300 m being dominated by kaolinite alteration. Minor to moderate carbonate is associated with illite-kaolinite and is present at its greatest extent in the upper 500 m and decreases in intensity with depth. A localized, minor quartz-muscovite-pyrite alteration zone is located between 63 and 150 m depth in drillhole RC94-106. This zone represents a relict lens of phyllic alteration that probably formed a halo around the core of the East zone, and has been significantly overprinted by illite.

3.4 Veins

Seventeen vein types recognized in the East zone at Red Chris are divided into 5 major groups based on cross-cutting relations. These are, in decreasing age: Early, Sulphide, Anhydrite-Gypsum, Pyrite and Late Carbonate-Chlorite. Cross-cutting relationships between all the vein types are not observable as the vein groups are generally constrained to specific locations and depths across the East zone. Nonetheless, sufficient relative relationships are visible to conclude that these groups generally record the hydrothermal evolution of the porphyry system through time and with depth. In this section the nature, distribution, vein-relationships, and sequence of the 5 vein sets are described. The major characteristics are outlined in Table 3.1.

Table 3.1 Vein Sets and Characteristics of the East Zone at Red Chris

Vein Set	Silicate Assemblage and Texture	Alteration Halo	Age and Structural Style	Sulphide-Oxide Assemblage and Texture
Early (E1-3)	Quartz, Anhydrite-Sulphide, trace Biotite • Equigranular quartz with variable amounts of medium to coarse grained purple anhydrite • Quartz-only as first stage, then anhydrite only with increasing sulphide and quartz content and decreasing anhydrite • Latest stage forms sulphide ± iron oxide veinlets with minor granular quartz • Occasional carbonate infill and rare fine-grained secondary biotite along centerlines	K-feldspar ± Epidote • Occasional K-feldspar halos up to 2 mm wide altering groundmass • Rare, weak epidote altering primary mafic phenocrysts and secondary biotite along vein margins	Earliest vein set, cut by Sulphide Veins (S1) • Quartz-only veins are irregular and wavy to straight walled sheeted veins • Anhydrite-sulphide ± quartz veins are commonly straight edged with parallel walls and become more so with increasing quartz content • Sulphide-iron oxide veinlets typically, discontinuous irregular to wavy • ~1-20 mm wide	E1 – Barren E2 – Common Cp with lesser Py and Mo • Disseminated, up to 2 mm grains and clots E3 – Sulphide-iron oxide dominant veinlets • Up to two sulphide minerals or sulphide iron-oxide mixtures. • Equigranular sulphide ± iron oxide up to 2 mm • Mt>Cp>MtCp>Py>CpMo, MtBn, Bn, Mo
Sulphide (S1-6)	Sulphide-Iron Oxide-Quartz ± Carbonate • Fine-grained to massive, commonly equigranular with rare 'cockscomb' texture perpendicular to vein walls • Minor to moderate carbonate commonly as centerline or margin infill, locally patchy and disseminated with sulphides-iron oxides	Weak K-feldspar ± chlorite (after secondary biotite) halos, up to 2 mm wide on S1, S2 and S3 veins No halos observed on S4, S5 and S6 veins due to illite alteration overprint	Younger than Early Veins, Older than Pyrite and Late Carbonate-Chlorite Veins • Occasionally wavy or irregular (S1) • Commonly straight walled, sheeted veins (S2-6) to stockworks (S2, S3), locally massive • ~1-2 mm wide (S1, S4) • ~2-20 mm wide (S3, S5, S6) • ~2-50 mm wide (S2)	Cp, Bn, Mt, Hm, Py, trace Cv • Common banding of sulphide-iron oxide minerals as centerlines and cross-cutting veinlets • Commonly up to 2 mm disseminations throughout quartz ± carbonate, occasionally up to 4 mm • Cp predominant, Bn never with Py • Mt altered to Hm in areas of illite alteration overprint

Vein Set	Silicate Assemblage and Texture	Alteration Halo	Age and Structural Style	Sulphide-Oxide Assemblage and Texture
Anhydrite-Gypsum (AG1-3)	Anhydrite-Gypsum, Chlorite • Anhydrite is white to peach, fine to medium grained, and partially hydrated to gypsum • Rare, minor, fibrous, translucent gypsum veinlets • Medium to dark green chlorite as shear-like veinlets	Local K-feldspar halos (~2 mm) on anhydrite veins No halos on gypsum or chlorite veinlets	Timing/age poorly constrained, Anhydrite veins cross-cut E2 veins • Straight-walled to slightly irregular (AG1, AG2) • Wavy to irregular (AG3) • ~1-20 mm wide (AG1) • ~1-2 mm wide (AG2, AG3)	Trace amounts of fine-grained disseminated Cp within Anhydrite (AG1) veins
Pyrite (P1-2)	Quartz-Pyrite ± Chalcopyrite ± Carbonate ± Tourmaline • Pale grey, equigranular quartz with local infill and centerlines of carbonate and sulphides • Rare, minor very fine-grained dark grey to black tourmaline as acicular, radiating mats associated with pyrite veinlets (P2)	Occasional mottled grey quartz (± sericite?) alteration halos up to 3 mm wide	Not observed to cut older veins, older than LC veins, some overlap of P2 and LC1 • P2 veins cross-cut P1 veins • Straight-walled (P1) to slightly irregular (P2) • ~2-10 mm (P1) • <1-3 mm (P2) • Tourmaline as <1 mm veins	Py predominant with local Cp • Py ± Cp as 1-3 mm grains forming disseminations or centerlines in quartz, or as Py-only veinlets • Clots of ~1 mm sized Py replacing mafic sites
Late Carbonate-Chlorite (LC1-3)	Carbonate OR Chlorite • Pale beige to white carbonate veins (LC1, LC2) and breccia cement, locally banded ± vuggy with possible calcite infill • Carbonate locally exhibits orange oxidation • Carbonate predominantly ankerite-dolomite with trace calcite and rare siderite • Chlorite (LC3) as dark to pale green fine-grained veins, locally fills in vugs in carbonate and occasionally forms on minor shear or fracture surfaces	No alteration halos observed	Youngest vein set observed • All veins cut mineralized and post-mineral dykes • Carbonate veins (LC1 ± LC2) cut/infill older veins types (Early, Sulphide, Pyrite) and are straight-walled and continuous • Chlorite (LC3) not constrained but may be same as AG3 • ~1-5 mm wide (LC1) and thicker where forming breccia cement • ~1-3 mm wide (LC3), straight-walled to wavy	Rare Py and Cp • Minor to moderate amounts of medium to coarse (1-5 mm) grains, likely remobilized from earlier veins (P1, P2?)

(Py = pyrite, Cp = chalcopyrite, Bn = bornite, Mo = molybdenite, Mt = magnetite, Hm = hematite)

3.4.1 **Early Veins (E1, E2, E3)**

Three vein types compose the oldest veins in the East zone. These are, in decreasing age, quartz-only veins (E1); purple anhydrite veins which evolve in sulphide and quartz content (E2); and veins of sulphide- iron oxide minerals (magnetite, chalcopyrite, pyrite, molybdenite, bornite) with accessory quartz (E3). The veins typically are present in the deepest portions of the East zone below 1000 m depth except for the sulphide- iron oxide veins (E3) which are also preserved at shallower depths. Overall, the dominant vein types in this set are E2 and E3.

3.4.1.1 Quartz (E1)

Quartz forms the oldest vein type. The veins are 1 to 4 mm wide (Figure 3.17A), commonly have straight, parallel walls or irregular walls forming wavy veins. The commonly sheeted quartz veins are white to pale grey in colour and locally faintly banded. No alteration halos are associated with these veins.
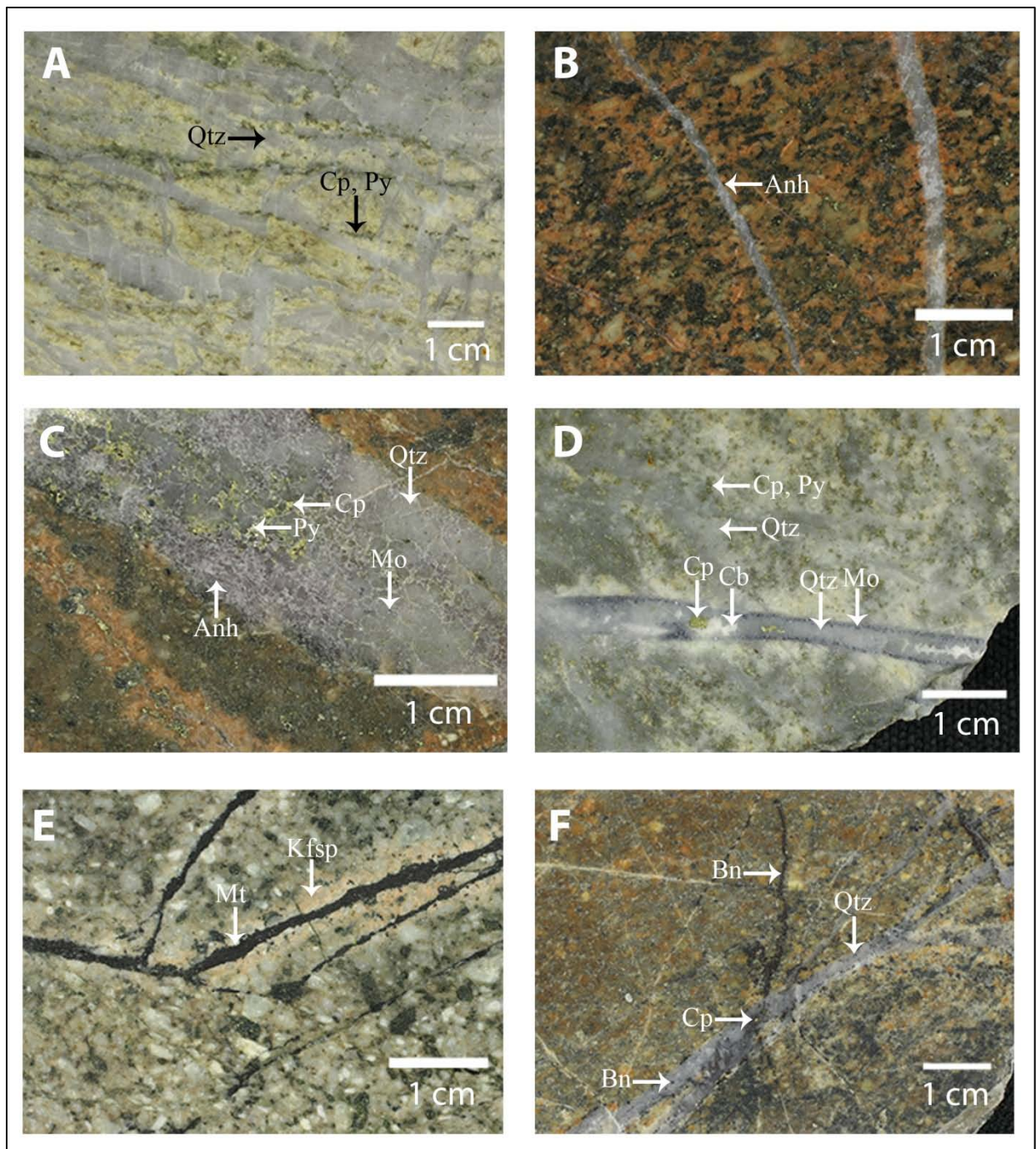
Figure 3.17 Early Veins. A: quartz-only veins (E1) cut by Py-Cp veins (E3) (RC09-345, 1142 m); B: purple anhydrite veins (E2) (RC09-354, 917 m); C: purple anhydrite, quartz, Cp, Py and Mo vein (E2) (RC09-350, 1140 m); D: quartz veins (E1) cut by Cp veins (E3) cut by quartz vein with Cp and carbonate center and Mo on margins (E2) (RC09-350, 1055 m); E: Mt vein (E3) with weak K-feldspar alteration halo (RC09-350, 1213 m); F: Bn-quartz vein (E3) cut by quartz-Bn-Cp vein (S3) (RC09-348, 683 m). (Py = pyrite, Cp=chalcopyrite, Bn= bornite, Mo= molybdenite, Mt = magnetite, Qtz = quartz, Cb = carbonate, Kfsp = K-feldspar, Anh = anhydrite)

The rare quartz-only veins do not occur in significant abundance or volume throughout the deeper parts of East zone. They are however concentrated in drillhole RC09-345 below 1150 m depth where the rocks are variably K-silicate altered with varying intensities of late illite

overprint. Due to the spatial irregularity of the quartz-only veins, their relationship with other veins is not well constrained. Minor common chalcopyrite or pyrite veinlets (E3) cross-cut and exploit these veins.

3.4.1.2 Purple Anhydrite ± Quartz-Sulphide (E2)
(± Purple Anhydrite ± Qtz ± Cp > Py > Mo ± Carbonate)

Veins containing varying amounts of purple anhydrite, quartz and sulphide minerals are present throughout the East zone where they consistently cut the quartz-only veins (E1). These range from purple anhydrite-only veins to anhydrite veins with sulphide minerals and minor quartz and finally to quartz dominant veins with common sulphide minerals and minor to rare purple anhydrite. The abundance of anhydrite, sulphide minerals, and quartz varies throughout the deposit.

Anhydrite-only veins appear to be the oldest, areally widespread and dominant vein-type. Purple to lavender, medium to coarse-grained anhydrite fill straight walled veins, 1 to 2 mm wide; rare irregular vein walls are present (Figure 3.17B). Minor fine-grained secondary biotite is present along centerlines. Rare, minor epidote alteration of mafic minerals adjacent to the vein walls is locally present where the rocks are weakly K-silicate altered. The anhydrite veins occur below 1200 m in the least altered rocks as well as in rocks that are intensely K-silicate altered with varying degrees of illite overprint.

Anhydrite-sulphide ± quartz veins are dominantly medium- to coarse-grained purple anhydrite with up to 2 mm disseminated chalcopyrite ± pyrite ± molybdenite (Figure 3.17C). They are 2 mm to 2 cm wide with straight vein boundaries. Minor quartz occurs as massive pale grey translucent grains throughout the vein, commonly as clots and locally along the margins. Rare, fine-grained secondary biotite is present. Minor epidote is present along vein boundaries within mafic sites in the least altered rocks. Local alteration halos of orange-pink K-feldspar up to 2 mm wide occur in K-silicate altered rock.

These veins cut the purple anhydrite-only veins as well as cut and are cut by sulphide-oxide veins (E3). The purple anhydrite-sulphide-quartz veins are distributed across the East zone between 1100 m and 1400 m depth.

Quartz, sulphide and minor to trace anhydrite with accessory carbonate veins form the final combination within this vein type (E2). These 2 mm to 2 cm pale grey quartz veins have fine grained disseminated sulphides and local 1 to 3 mm clots of medium grained purple anhydrite (Figure 3.17D). Chalcopyrite and local pyrite occurs as 1 to 2 mm clots disseminated throughout the veins. Molybdenite forms 1 mm grains along the margins of the vein, where present. Locally ankerite-dolomite form 1 to 2 mm clots in the center of the quartz veins and commonly contains disseminations of fine-grained molybdenite and/or chalcopyrite. Minor, 2 mm K-feldspar alteration halos are associated with these veins, which occur in K-silicate altered rocks and locally where there is a moderate to intense illite overprint. These veins occur across the East zone and are concentrated between 1000 m and 1200 m depth. These quartz-sulphide-anhydrite veins cut and are cut by sulphide-iron oxide dominant veins (E3).

3.4.1.3   Iron Oxide - Sulphide (E3)
(Mt > Cp > MtCp > Py > CpMo, MtBn, Bn, Mo, Accessory Qtz)

Thin, < 1 mm wispy and discontinuous veinlets of iron oxide-sulphide ± quartz veins are composed of up to two sulphides or iron oxide-sulphide mineral mixtures of chalcopyrite, magnetite, lesser bornite, pyrite and molybdenite (Figure 3.17A, E, F). Accessory fine-grained quartz is also present. Magnetite ± chalcopyrite are common. Chalcopyrite, molybdenite, pyrite and bornite form < 1 mm to 1 mm in diameter grains. Magnetite and less commonly sulphide minerals form veinlets up to 2 mm wide. Alteration halos are overprinted by illite at shallow depths. However, in least altered rocks at depth, narrow 1 to 2 mm K-feldspar halos are associated with magnetite veinlets. Minor chlorite is present in mafic mineral sites previously altered to secondary biotite, as up to 1 mm wide halos on chalcopyrite and magnetite veinlets in the K-silicate altered zone.

Distinct iron oxide-sulphide mineral assemblages characterize the E3 vein type in parts of the East zone. Pyrite veinlets are common in the deepest, most distal peripheral parts of the East zone, where the veins are associated with the least altered rocks. Chalcopyrite veinlets characterized the core and marginal areas but lie inboard of pyrite veinlets in zones of weak to intense K-silicate alteration. Molybdenite, where present always occurs with chalcopyrite, and rarely forms as the only sulphide in K-silicate altered rocks. The highest concentrations of molybdenite are present in drillhole RC09-353 between 840 to 1250 m depth. Magnetite veinlets with local chalcopyrite are present throughout the K-silicate altered rocks and locally within

weak to least altered rocks. Magnetite is commonly replaced by specular hematite in areas of illite overprint. Bornite is most common in the core of the East zone within K-silicate altered rocks, where it forms bornite only veins or is associated with magnetite and chalcopyrite. The relationship between these iron oxide-sulphide-dominant veins (E3) and another type of iron oxide-sulphide-dominant veins (S1) is not conclusive (see below). It is possible that vein type (S1) may be a continuation of the vein type (E3) and not represent a separate event. Iron oxide-sulphide-dominant veins (E3) have only been documented to cross-cut anhydrite ± quartz-sulphide veins (E2).

3.4.2 **Sulphide Veins (S1, S2, S3, S4, S5, S6)**

Six vein types (S1, S2, S3, S4, S5 and S6) composed of sulphide and iron oxide minerals (chalcopyrite, magnetite, bornite, hematite and pyrite) in addition to significant quartz dominate the upper 1000 m of the East zone. Minor to moderate carbonate is also present locally. This group has the greatest abundance and volume of veins, with vein-types S1, S2 and S3 responsible for the majority of the high-grade copper-gold in the East zone. The veins extend to surface in drillholes RC07-335 and RC09-354. Above 1000 m depth, there are few examples of Sulphide Veins cross-cutting Early Veins. Aside from minor ambiguity regarding vein-types E3 and S1, no Sulphide Veins are cut by Early Veins.

3.4.2.1 **Iron Oxide - Sulphide (S1)**
(Mt(Hm) > Cp > Bn ± Qtz)

A distinct set of iron oxide-sulphide veins occur at shallower depths than the iron oxide-sulphide veins (E3). The shallower veinlets are 1 to 2 mm wide, straight to slightly discontinuous in nature and are composed of combinations of chalcopyrite, bornite and magnetite altered to specular or earthy-red hematite (Figure 3.18A, B). The sulphide minerals are fine to medium-grained (up to 2 mm) and commonly associated with minor fine-grained quartz. These veinlets in moderately illite overprinted K-silicate altered rocks contain magnetite and specular hematite. There is minor, 1 to 2 mm chlorite (after secondary biotite) or K-feldspar alteration halos in the least altered and K-silicate altered rock.
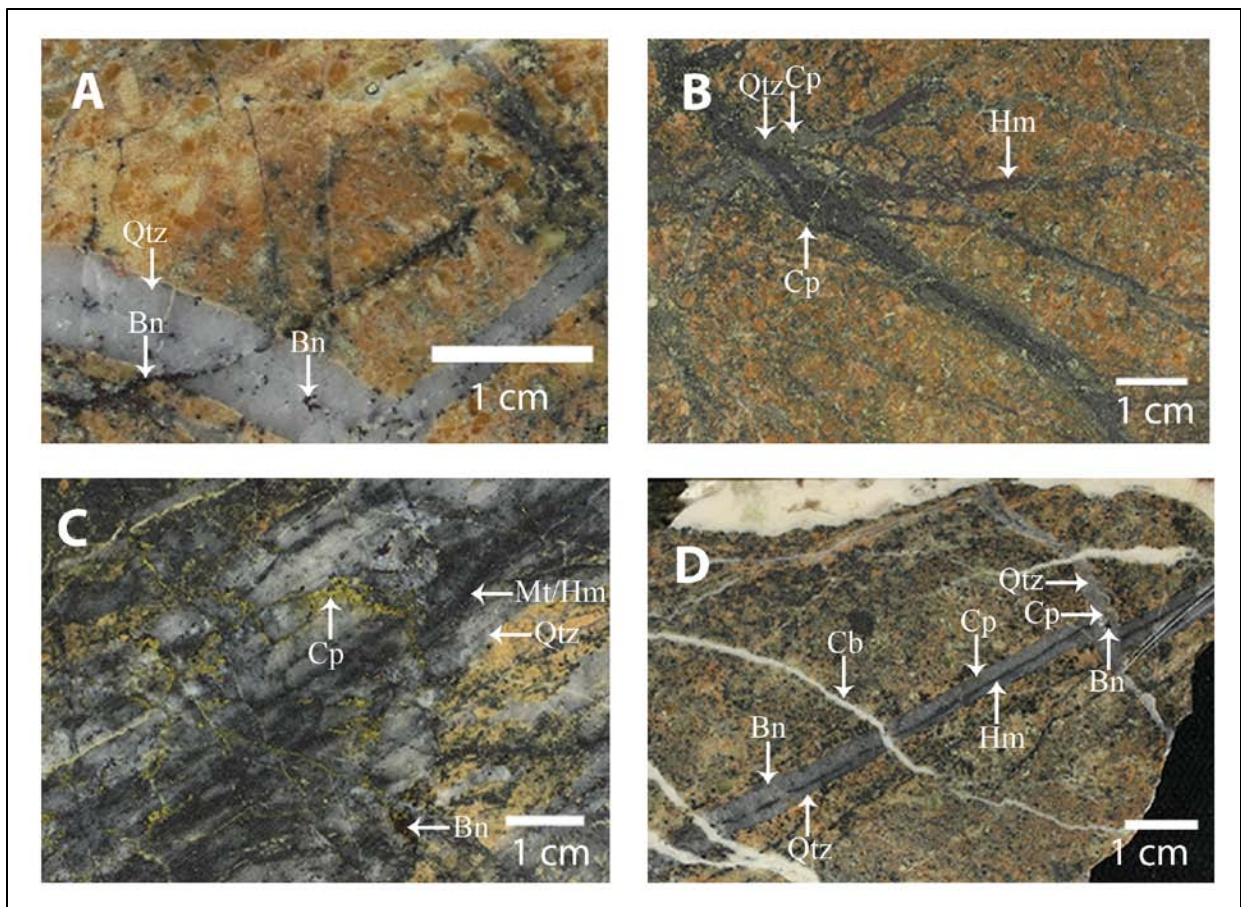
Figure 3.18 Sulphide Veins. A: quartz with Bn ± Cp centerlines (S3) cut by Bn ± quartz (S1) vein (RC09-352, 749 m); B: quartz-Cp veins (E2) exploited by Hm (E3) and crosscut by Cp-quartz (S1) (RC09-350, 528 m); C: banded quartz-Mt-Hm vein (S2) cut by Cp-Bn veinlets (S1) (RC09-345, 842 m); D: quartz-Bn-Cp vein with Hm centerline (S3) cut by quartz-Bn-Cp vein (S3) cut by carbonate (LC1) (RC09-352, 603 m). (Bn= bornite, Cp= chalcopyrite, Hm= hematite, Mt = magnetite, Qtz = quartz, Cb = carbonate)

The iron oxide-sulphide veinlets (S1) are concentrated in the upper 800 m of the East zone. Chalcopyrite and magnetite/hematite veinlets crosscut zones of intensely banded quartz veins and quartz stockwork (S2 and S3). The quartz stockwork veins (S2 and S3) host varying amounts of disseminated chalcopyrite, magnetite/hematite, and bornite, and are cut by chalcopyrite, magnetite ± bornite veinlets (S1), that commonly form 1 mm-scale centerlines and cross-cutting fractures within the quartz veins. The sequencing of vein-sets (E3) and (S1) is not fully conclusive as crosscutting relationships between them were not observed.

3.4.2.2   Quartz - Iron Oxide - Sulphide (S2)
(Qtz, Mt(Hm) > Cp > Py)

The 2 mm to 5 cm straight walled quartz veins of S2-type vein are composed pale to medium grey with chalcopyrite, magnetite/specular hematite and local pyrite (Figure 3.18C).

Chalcopyrite forms < 1 mm disseminated grains or up to 1 mm thick centerlines whereas magnetite or specular hematite forms 1 to 3 mm bands along the margins or center of the vein. Hairline, < 1 mm fractures crosscut the veins perpendicular to the vein and locally contain chalcopyrite. Pyrite is rare and, where present, forms fine-grained disseminations or is present locally along centerlines with chalcopyrite. These quartz veins commonly form sheeted sets that are banded with multiple sulphide centerlines. Weak, minor 1 to 2 mm K-feldspar alteration halos are associated with these veins which are widely overprinted by illite alteration.

S2-type veins are concentrated in the core of the East zone, between ~400 and 1000 m depth. This vein-type formed in rocks characterized by intense K-silicate alteration, and are preserved in rocks with varying degrees of illite overprint. These quartz-sulphide-iron oxide (S2) veins form at shallower depth and thus overlie the level of anhydrite (E2) veins. They also cut iron oxide-sulphide- dominant veinlets (E3 and S1).

3.4.2.3   Quartz-Sulphide-Iron Oxide ± Carbonate (S3)
(Qtz, Cp > Mt(Hm) > Bn ± Ankerite-Dolomite)

The S3 veins host a significant portion of the high-grade copper-gold grades in the East zone. The 2 mm to 2 cm wide straight edged grey quartz veins have accessory chalcopyrite, magnetite/specular hematite, bornite and local carbonate (Figure 3.18A, D). The veins are commonly banded, with multiple sulphide-iron oxide centerlines. Chalcopyrite is almost always present as 1 to 2 mm disseminations and/or centerlines; it is the only sulphide mineral present with quartz in the massive stockwork zone in RC09-350. Magnetite or specular hematite is present in a significant portion of the veins as < 1 to 2 mm wisps and bands and more commonly as 1 mm disseminations. Most bornite forms 1 mm disseminations throughout the quartz, but locally forms irregular 1 to 2 mm centerlines associated with chalcopyrite and magnetite/specular hematite. Thin veinlets up to 1 mm thick of carbonate locally form the vein centers or clots associated with chalcopyrite ± bornite ± magnetite. Moderate to intense orange oxidation of the carbonate-bearing veins indicate the carbonate is iron-rich, being ankeritic or sideritic. Localized weak 1 to 2 mm alteration halos of K-feldspar and < 1 mm chloritization of mafic sites are common along the vein margins. The veins and alteration halos are overprinted by illite alteration.

Zones of massive banded quartz veins (S3) are mapped in drillhole RC09-350 at ~500 m depth and in the upper ~70 m of drillholes RC07-335 and RC09-354. These areas form much of the high-grade copper-gold zones of the East zone. Veins of type S3 cross-cut vein-sets E3, S1 and S2, and are observed to be cut by vein-set S1, which likely form most of the centerlines and banded nature of the quartz-stockwork veins (S3). The exploitation of these veins by chalcopyrite and bornite of vein-type S1 likely upgraded the metal tenor this vein-type.

3.4.2.4   Quartz Bornite (S4)
(Qtz, Bn ± Mt ± Ankerite-Dolomite)

Two mm wide, straight to gently wavy, pale grey quartz veins with disseminated 1 to 2 mm bornite grains form vein type S4 (Figure 3.19A). Minor carbonate, likely as younger infill and magnetite/hematite along the vein margins are associated with these veins. Covellite formed and inclusion in one bornite crystal in the East zone in sample RC348-008 (276 m depth; Figure 3.19B). The quartz-bornite veins are volumetrically insignificant, being present in a few locations in the core of the East zone. No alteration halos are observed as they occur within rocks that have experienced moderate to intense illite overprint. The timing of these veins is not constrained however they do crosscut the vein-set S3.
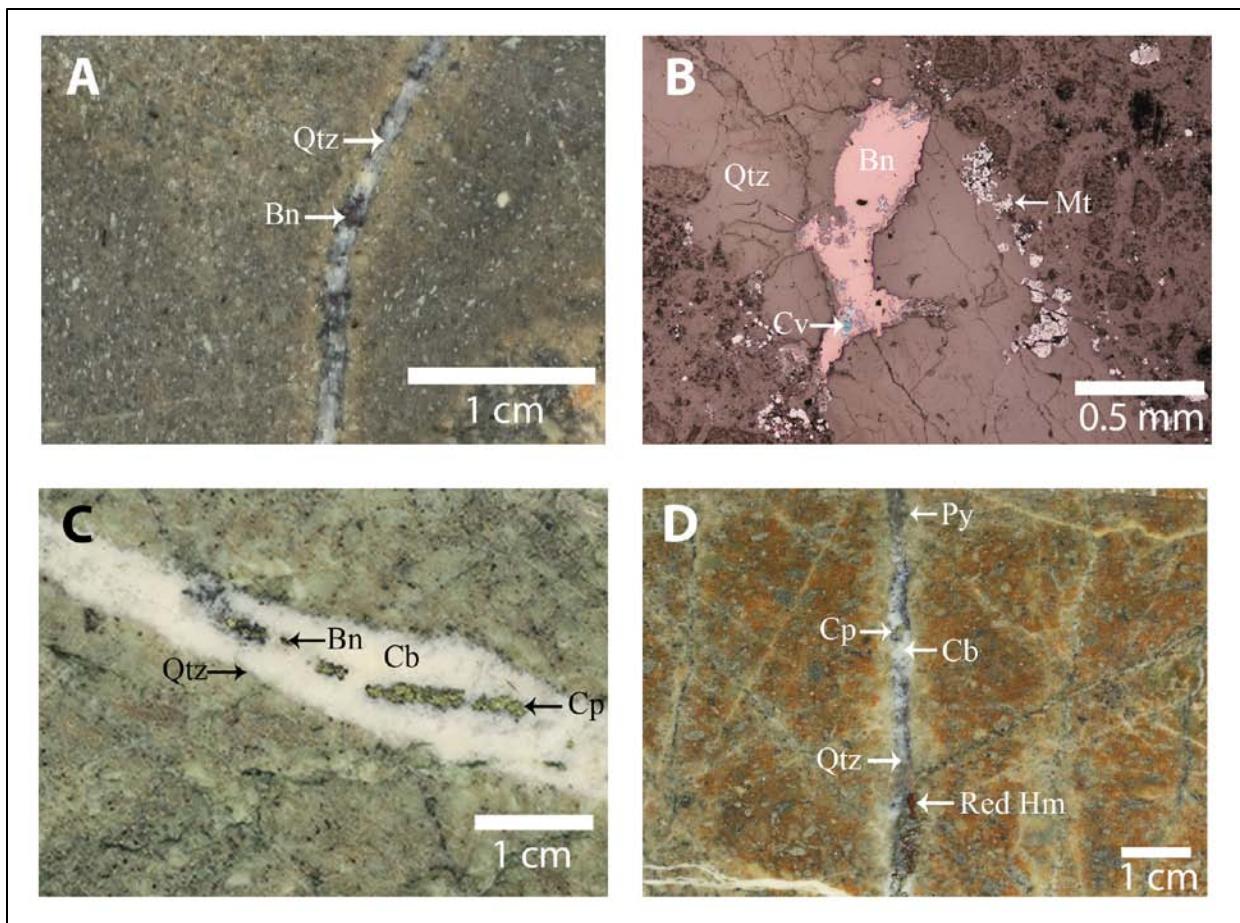
Figure 3.19 Sulphide Veins. A: quartz-bornite ± magnetite vein (S4) (RC09-348, 276 m); B: quartz vein containing magnetite blebs and bornite containing a small grain of covelite (RC09-348, 276 m); C: carbonate, chalcopyrite with bornite rims and minor quartz vein (S5) cut by irregular chlorite veinlet (AG3) (RC09-351, 846 m). D: quartz-red hematite-carbonate vein (S6) with chalcopyrite and minor pyrite (RC09-345, 749 m). (Qtz = quartz, Bn = bornite, Mt = magnetite, Cv = covelite, Cb = carbonate, Cp = chalcopyrite, Py = pyrite, Hm = hematite)

3.4.2.5 Carbonate – Quartz - Sulphide (S5)

(Ankerite-Dolomite > Qtz-Cp > Bn)

Carbonate veins with pale grey quartz, chalcopyrite and bornite make up vein-set S5. These veins are 1 to 2 cm wide and contain carbonate in the center of the veins, with 1 to 2 mm chalcopyrite and lesser bornite grains (Figure 3.19C). Bornite commonly forms rims on the chalcopyrite. The amount of quartz varies within the vein-type and occurs along the margins of the vein as well as throughout the carbonate material. It is likely that the carbonate infilled fractures in earlier quartz-sulphide veins. These veins have straight edges and no alteration halos. They cross-cut and locally exploit the S3 vein-set. The relative timing with other vein-sets is not constrained.

3.4.2.6 Quartz-Carbonate- Iron Oxide-Sulphide (S6)
(Qtz, Ankerite-Dolomite, Hm > Cp > Py)

Veins of dominantly quartz-carbonate with moderate hematite, chalcopyrite ± pyrite that are 2 mm to 1 cm wide with straight edges compose vein-set S6. The quartz is massive and pale grey with > 2 mm centerlines of locally red- stained ankerite-dolomite and 2 to4 mm coarse grains of chalcopyrite and lesser pyrite (Figure 3.19D). In some veins, carbonate is more voluminous than quartz and contains significant amounts of chalcopyrite. Few carbonate veins have 1 mm intense orange oxidation rims, suggesting Fe-rich carbonate preceded ankerite-dolomite infill. No bornite or magnetite is associated with this vein-set. The abundant hematite is an alteration product of magnetite. Alteration halos are not observed as they occur in the upper 450 m of the core of East zone where intense illite-kaolinite alteration has overprinted any higher temperature alteration assemblages. It is possible that this vein-set represents an altered version (magnetite replaced by specular and red hematite) of vein-type S2 which has experienced some degree of younger carbonate infilling.

3.4.3 Anhydrite-Gypsum (AG1, AG2, AG3)

The third vein set consists of anhydrite (AG1), gypsum (AG2) and chlorite (AG3) veins which typically occur at depths below 1000 m and rarely in the upper 500 m. These veins compose a very small portion of the total vein material across the East zone and very few relationships with other vein types are observed. Overall, the general timing of these veins is poorly constrained with regards to the rest of the vein-sets.

3.4.3.1 Anhydrite (AG1)

Fine to coarse grained white to peach anhydrite form 1 mm to 2 cm thick veins (Figure 3.20A). The veins are straight to slightly irregular and contain trace amounts of fine-grained chalcopyrite. The peach-white anhydrite is partially altered to gypsum, and may represent the hydration of older purple anhydrite veins. The white to peach anhydrite veins locally exhibit 1 to 2 mm K-feldspar alteration halos. In intermediate to shallow depths in the East zone, a 2 to 3 cm vein of peach anhydrite has been reopened by younger carbonate. Whereas most white to peach anhydrite is concentrated in the deeper portions of the East zone in least altered to strongly K-silicate altered rocks, it also cuts vein-sets S2 and S3 locally in the upper 500 m where illite alteration dominates. The majority of this vein-type is observed to crosscut purple anhydrite (E2) veins in the deep K-silicate altered regions of the East zone, below 1000 m depth.
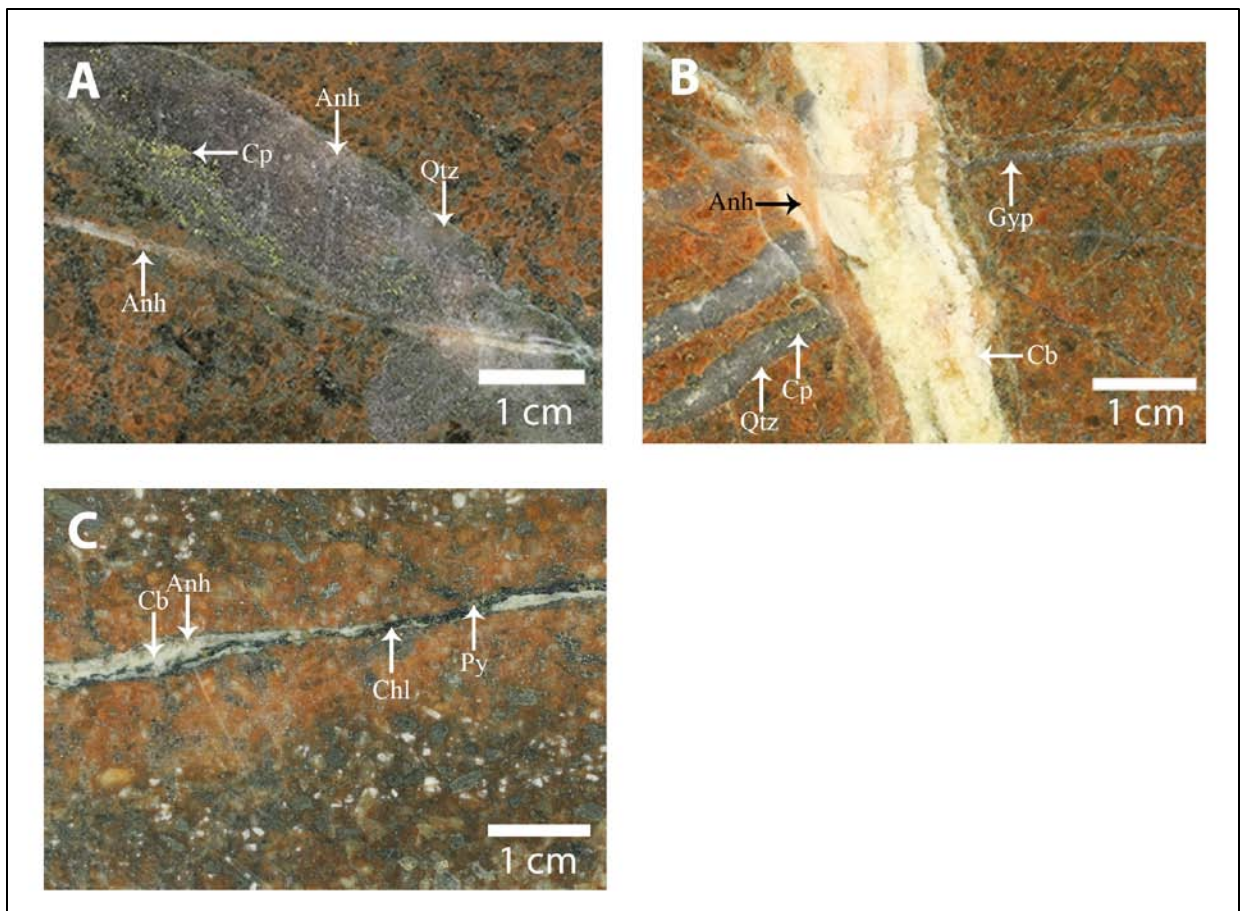
Figure 3.20 Anhydrite-Gypsum Veins. A: purple anhydrite-chalcopyrite-quartz vein (E2) cut by white-peach anhydrite vein (AG1) (RC09-352, 1159 m); B: quartz-chalcopyrite-molybdenite-carbonate vein (E2) cut by peach-white anhydrite vein ± carbonate (AG1) cut by gypsum veins (AG2) (RC09-350, 766 m); C: chlorite ± pyrite (AG3) exploiting a peach-white anhydrite ± carbonate vein (AG1) (RC09-349, 1147 m). (Anh = anhydrite, Qtz = quartz, Cp = chalcopyrite, Cb = carbonate, Gyp = gypsum, Chl = chlorite, Py = pyrite)

3.4.3.2 Gypsum (AG2)

Rare, minor gypsum forms fibrous, 2 mm wide veins within weakly illite overprinted lenses of relict K-silicate altered rock in the upper 500 m of the East zone, for example in drillhole RC09-352 at 320 m depth. Gypsum veins cross-cut white to peach anhydrite veins (Figure 3.20B) and may represent anhydrite veins which have been hydrated. The relationship between these veins and younger vein-sets is not constrained as no other veins cross-cut the gypsum veins.

3.4.3.3 Chlorite (AG3)

Rare, minor dark to medium green chlorite forms 1 to 2 mm thick shear-like veinlets (Figure 3.20C) below ~1000 m depth in the least altered to intensely K-silicate altered rocks.

Much of the chlorite is concentrated on the flanks of the East zone. The chlorite may have exploited older white to peach anhydrite ± gypsum vein (AG1, AG2). The chlorite veins are not cut by any other veins and the relationship with other chlorite veins (LC3) is not known.

3.4.4   Pyrite Veins (P1, P2)

The fourth major vein set consists of quartz, pyrite, occasional minor chalcopyrite, variable amounts of carbonate and rare tourmaline. No iron oxide minerals are present. These veins are restricted to the pyrite-rich halo on the upper 200 to 600 m flanks of the East zone and are not observed to cross-cut any of the quartz-sulphide-iron oxide stockwork veins (S2, S3). Veins of set four are cross-cut by carbonate veins associated with the fifth and youngest major vein set (Late Carbonate-Chlorite).

3.4.4.1   Quartz-Pyrite ± Carbonate ± Chalcopyrite (P1)

Quartz-pyrite veins are pale grey quartz, 2 mm to 1 cm wide with straight edges (Figure 3.21A). Pyrite forms 1 to 3 mm coarse-grained centerlines, occasionally with beige carbonate (ankerite-dolomite) interstitial to the pyrite grains. Also present are 1 to 3 mm wide coarse-grained pyrite veins with up to 3 mm wide mottled grey quartz alteration halos (Figure 3.21B). Rare moderate medium-grained chalcopyrite blebs occur with pyrite in quartz-carbonate-bearing veins. The veins lie in the upper 600 to 400 m of the northeastern flank of the East zone and in the upper 200 m of the southwestern flank. Abundant pyrite replacement of mafic minerals is observed where quartz-pyrite veins are present. These veins are not observed to cut any other vein-types, but they are cut by younger pyrite-only (P2) and carbonate veins (LC1, LC2). The P1 veins contain visible quartz as vein material or halos, whereas quartz associated with pyrite E3 veins is very fine-grained (microscopic).
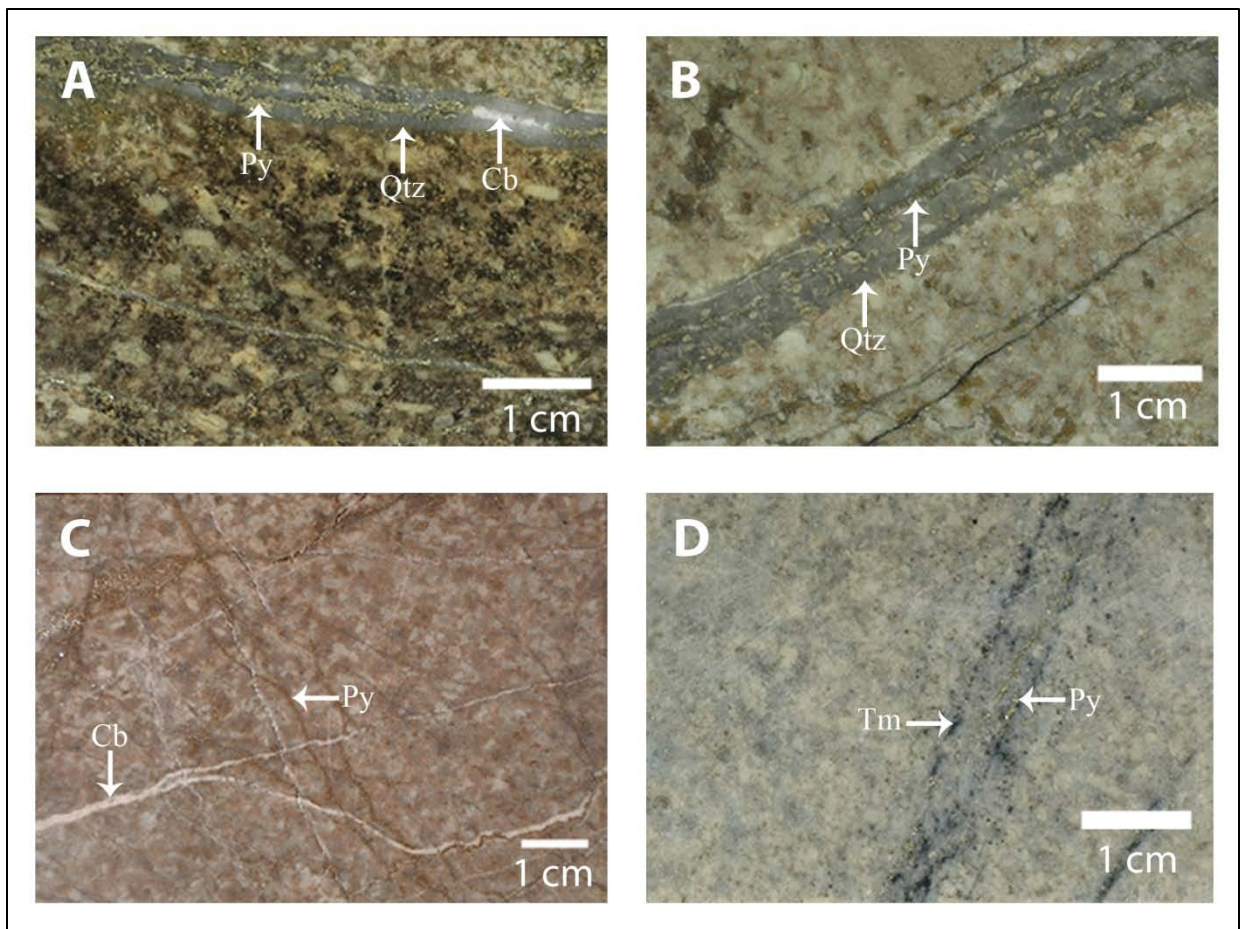
Figure 3.21 Pyrite Veins. A: quartz-pyrite vein (P1) with minor carbonate in center (RC09-345; 390 m); B: pyrite vein (P1) with quartz halo (RC09-345; 417 m); C: pyrite veins (P2) cut by carbonate veins (LC1) (RC94-106, 113 m); D: fine-grained dark black tourmaline associated with pyrite veins (P2) (RC09-353, 54 m). (Py = pyrite, Qtz = quartz, Cb = carbonate, Tm = tourmaline)

3.4.4.2   Pyrite ± Tourmaline (P2)

Fine- to coarse-grained pyrite forms < 1 to 3 mm wide, veins that cut quartz-pyrite veins (Figure 3.21C). These veins are cospatial in the East zone with the quartz-pyrite veins and are also associated with intense pyrite within the mafic mineral sites of the host rock. Pyrite veins hosted in the monzodiorite and the Stuhini Group volcanic rocks have no visible alteration halos. Locally, pyrite veins cut the late carbonate veins (LC1). Rarely associated with the pyrite veins are minor localized irregular < 1 mm veinlets of dark grey to black tourmaline (Figure 3.21D). Tourmaline forms very fine-grained acicular, radiating mats. Pyrite-tourmaline veinlets are only found in areas of intense illite-kaolinite in the upper 50 m, typically on the flanks of the East zone, and near zones of breccias. The P2 veins are differentiated from the pyrite E3 veins by overall width and grain-size.

3.4.5   **Late Carbonate-Chlorite Veins (LC1, LC2, LC3)**

The fifth major vein set is dominated by significant carbonate (ankerite-dolomite) veins cross-cutting other vein sets, and thus where seen represents the youngest vein stage. Carbonate in older veins may be related, but this cannot be conclusively demonstrated. Carbonate veins are present across the East zone, even in minor amounts at depth. Carbonate commonly forms breccia in-fill, concentrated along the contacts between different intrusive phases, and also fills in fault zones. Carbonate forms veins cutting post-mineral dykes.

3.4.5.1   **Carbonate Veins and Breccia Cement (LC1)**

Veins of ankerite-dolomite are commonly 1 to 5 mm wide and are widespread across the East zone (Figure 3.22A). Locally, the veins contain central vugs, 1 to 3 mm in size rimmed by comb textured carbonate. The carbonates range in colour from beige-white to beige and orange (oxidized ankerite) and usually are banded or zoned. The veins locally contain minor to moderate amounts of medium to coarse-grained chalcopyrite and pyrite, which likely are relicts from older veins. Carbonate is common as cement throughout zones of intense brecciation; angular clasts are of volcanic or sedimentary rocks, K-silicate altered monzodiorite and illite-kaolinite altered monzodiorite (Figure 3.22B, C), and in one location, angular carbonate clasts. Textural, colour, and banded character of the carbonate veins suggest a range of carbonate species present.
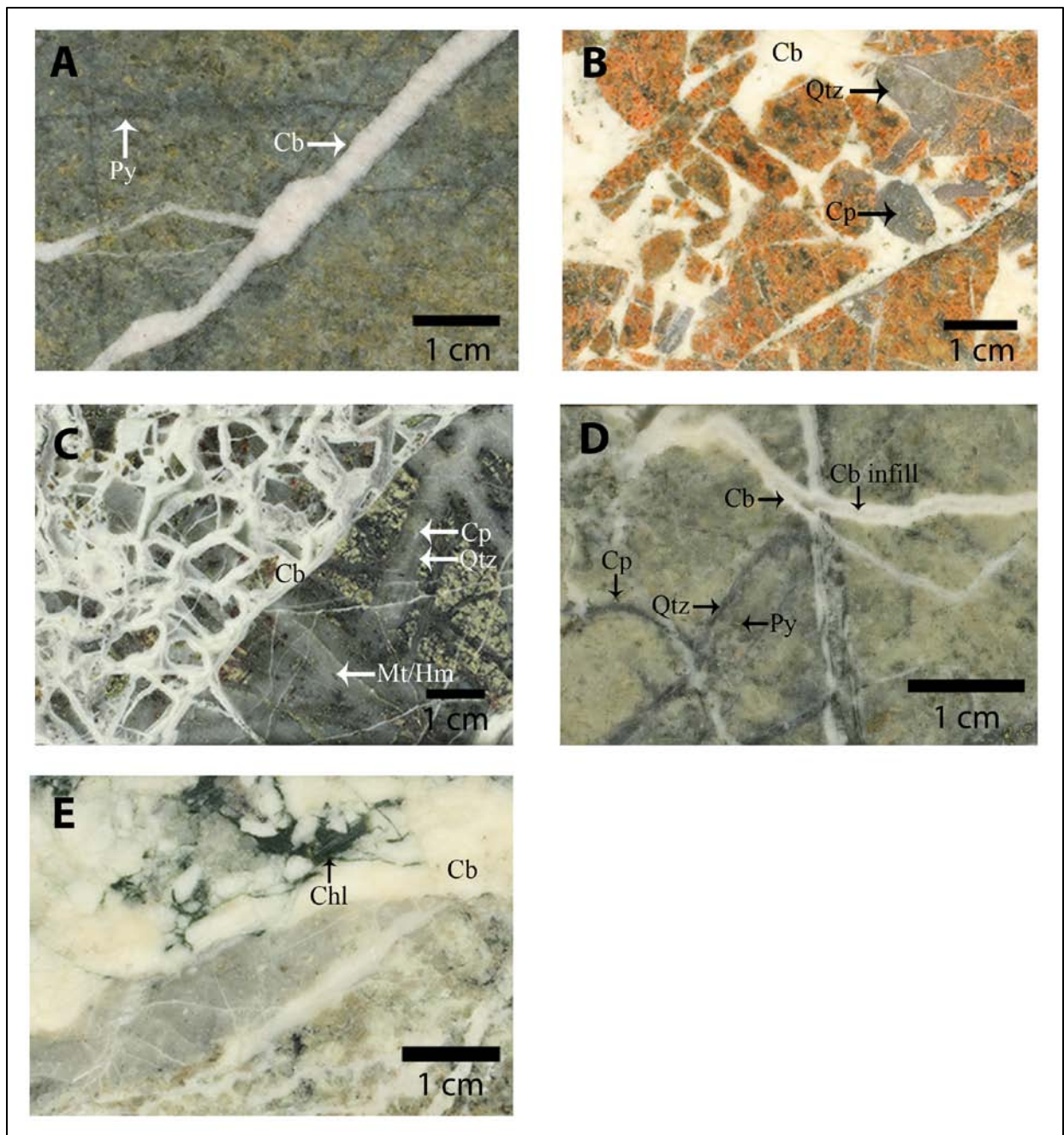
Figure 3.22 Late Carbonate-Chlorite Veins. A: carbonate vein (LC1) cross-cutting pyrite veinlets (P2) (RC09-349, 178 m); B: carbonate breccia (LC1) of K-silicate altered rock and quartz-chalcopyrite veins (RC09-350, 917 m); C: carbonate breccia (LC1) cross-cutting banded quartz-chalcopyrite-magnrtite-hematite ± bornite veins (S3) (RC09-354, 202 m); D: carbonate vein (LC1) with carbonate infill (LC2) cross-cutting quartz-carbonate-pyrite ± chalcopyrite veins (P1) (RC09-353, 557 m); E: chlorite (LC3) infilling vugs in carbonate veins/breccia (LC1) (RC09-352, 1002 m). (Cb = carbonate, Qtz = quartz, Cp = chalcopyrite, Py = pyrite, Chl = chlorite)

Carbonate (LC1) veins cross-cuts all other veins in the East zone, penetrating several hundreds of meters deep into the monzodiorite. Carbonate veins and breccias occur at all levels of the East zone, but are concentrated between 500 and 700 m depth. Thin 1 mm veinlets of a still younger carbonate cut older carbonate cemented breccias (LC2).

Post-mineral dykes are not brecciated by carbonate, being emplaced after the majority of the carbonate material. However, minor 1 to 3 mm wide veins of pale beige carbonate cut the late dykes, suggesting carbonate veins are broadly associated temporally with the emplacement of the dykes.

3.4.5.2   Carbonate Infill (LC2)

Minor carbonate (calcite?) appears as near-translucent to creamy white minerals filling the vugs within ankerite-dolomite (Figure 3.22D). This vein infill is commonly difficult to visually discern from other vein carbonate in hand sample.

3.4.5.3   Chlorite (LC3)

Dark to pale green massive chlorite usually forms minor 1 to 3 mm wide veins cutting ankerite-dolomite (LC1) veins in post-mineral dykes and monzodiorite and also locally fills vugs in carbonate veins (LC1) (Figure 3.22E). The chlorite veins locally form along minor shear or fracture surfaces. The relationship with this vein-set and the other chlorite event (AG3) is not constrained. These chlorite veins are the last vein event at Red Chris.

3.5   Sulphide Mineral Distribution

3.5.1   Overview

Hypogene sulphide minerals are zoned laterally across the East zone, centered on drillhole RC07-335 (Figures 3.23, 3.24). No supergene minerals are observed. Copper and gold in the East zone is concentrated in disseminated and vein-hosted bornite and chalcopyrite that are mostly within banded quartz-stockwork veins. Minor gold is associated with pyrite-chalcopyrite-quartz veins and also with quartz only or quartz alteration halos in the pyritic halo around the core of the East zone. Molybdenite is present throughout the deposit in minor amounts with quartz, chalcopyrite and carbonate veins. Magnetite and hematite throughout the East zone are zoned on the basis of the intensity of illite-kaolinite overprinting the K-silicate alteration zone.
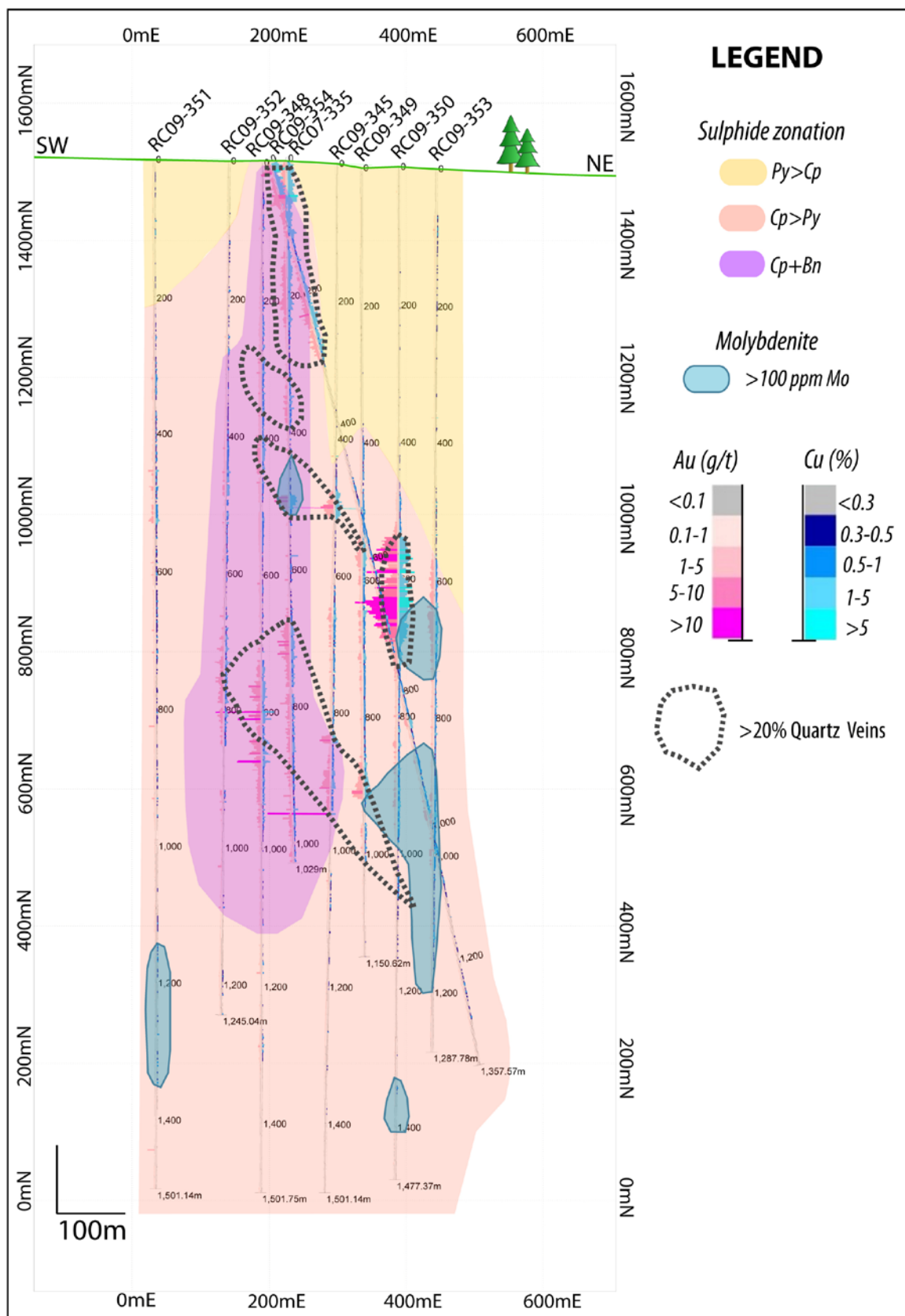
Figure 3.23 Sulphide zonation across section N50E. Central bornite + chalcopyrite core with a chalcopyrite > pyrite shell and a pyrite > chalcopyrite halo. Histograms along drill traces show gold grade (g/t) and copper grade (%). Blue zones are areas of > 100 ppm Mo. Heavy dashed lines show zones of > 20 % quartz vein density (estimated visually, over ~5 m intervals).
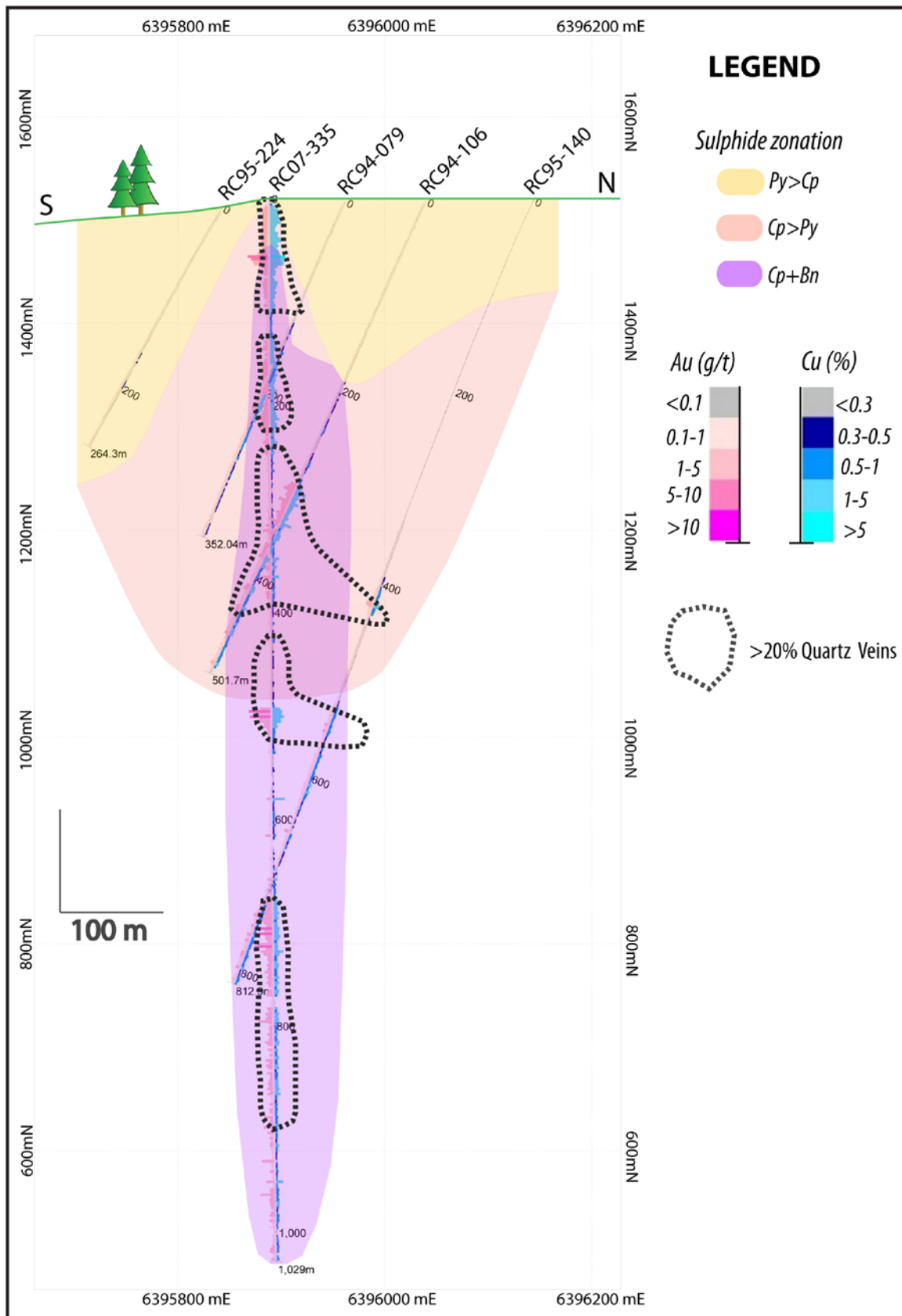
Figure 3.24 Sulphide zonation across section 452700E. Central bornite + chalcopyrite core with a chalcopyrite > pyrite shell and a pyrite > chalcopyrite halo. Histograms along drill traces show gold grade (g/t) and copper grade (%). Heavy dashed lines show zones of > 20 % quartz vein density (estimated visually, over ~5 m intervals).

3.5.2 Nature of Hypogene Sulphide Mineralization

3.5.2.1 Bornite

Bornite forms fine anhedral crystals and local aggregates in 5-10 mm thick quartz veins (Figure 3.25A), and also as wavy, 1-2 mm wide bornite ± quartz veins. At depth, bornite is deep purple with local blue reflections. Bornite is commonly associated with chalcopyrite and magnetite (Figure 3.25B) however it can form sulphide-only veins. Bornite locally forms <1 mm rims on 1 mm scale chalcopyrite grains where there is moderate amounts of carbonate present with the quartz-sulphide veins (Figure 3.25C). Bornite ± quartz veins are cut by and also exploit quartz-sulphide veins, indicating a mutually cross cutting relationship.
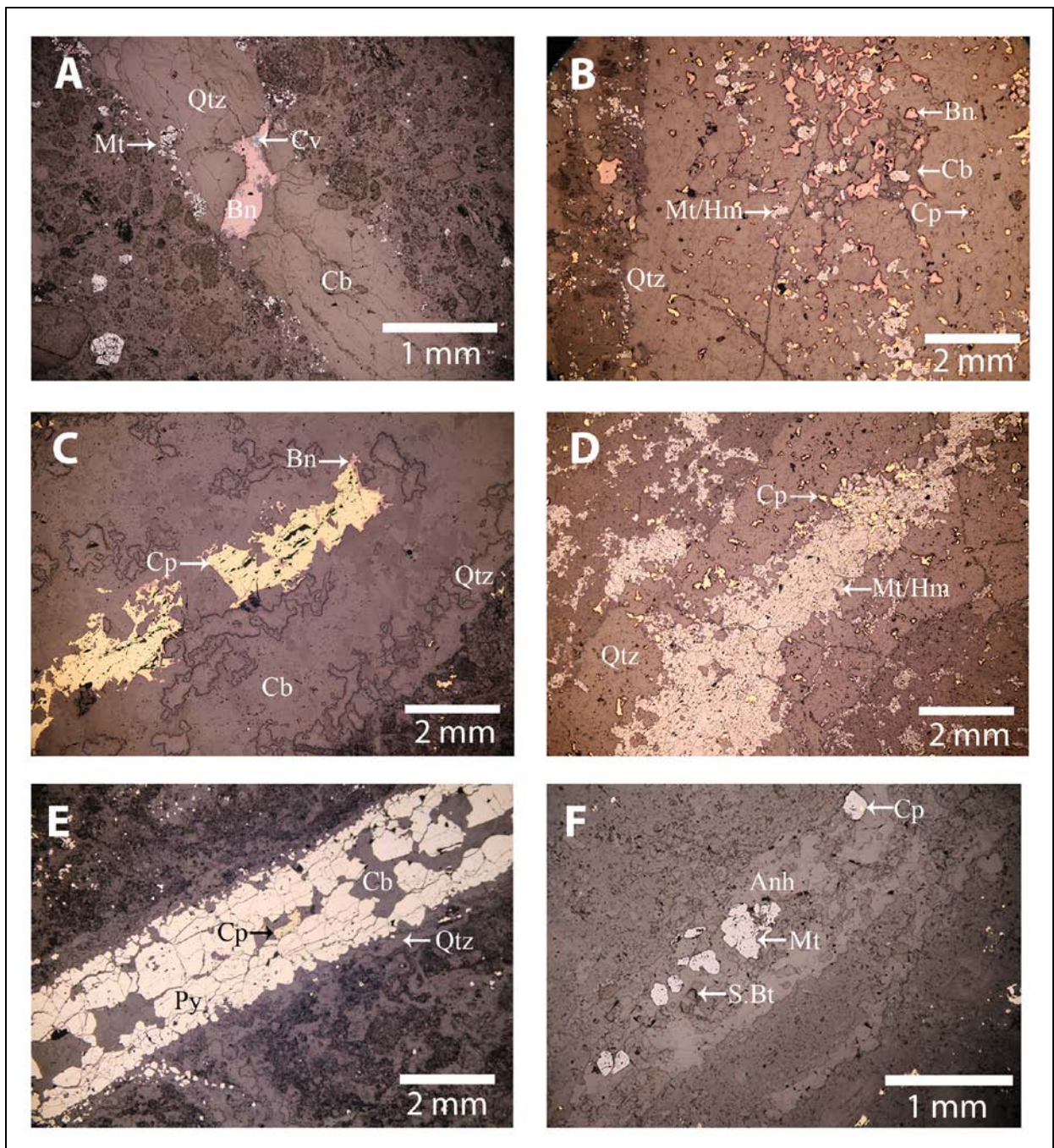
Figure 3.25 Bornite and chalcopyrite in reflected light. A: magnetite, bornite and covelite in a quartz vein with minor central carbonate (RC09-348, 276 m); B: quartz vein with disseminated bornite, magnetite (with weak hematite alteration) and chalcopyrite with interstitial carbonate (RC09-352, 840 m); C: carbonate-quartz vein with central chalcopyrite with bornite rims (RC09-351, 846 m); D: quartz veins with disseminated chalcopyrite and central magnetite weakly altered to hematite (RC09-350, 528 m); E: pyrite with minor chalcopyrite in a carbonate vein with minor quartz margins (RC09-345, 178 m); F: anhydrite vein with minor central secondary bitotie and magnetite clots with internal chalcopyrite blebs (RC09-354, 1256 m). (Qtz = quartz, Cb = carbonate, Bn = bornite, Cp = chalcopyrite, Mt = magnetite, Hm = hematite, Py = pyrite, Cv = covelite, Anh = anhydrite, S.Bt = secondary biotite)

3.5.2.2 Chalcopyrite

Chalcopyrite forms fine anhedral grains, local aggregates in quartz veins (Figure 3.25D), and also as wavy 1 to 2 mm wide chalcopyrite ± quartz veins. Chalcopyrite is the dominant sulphide in the East zone, is almost always present within quartz veins, and commonly forms fine-grained aggregates in purple anhydrite and quartz-purple anhydrite veins. Chalcopyrite locally is present in carbonate veins with pyrite (Figure 3.25E). Chalcopyrite is occasionally present within mafic mineral sites and rarely within magnetite blebs (Figure 3.25F) in illite altered rocks of the upper 700 m of the eastern flank. Chalcopyrite is also locally present in mafic mineral sites and magnetite blebs below 1000 m depth in K-silicate altered rocks throughout the East zone.

3.5.2.3 Pyrite

Pyrite dominantly forms medium to coarse grains within quartz veins or pyrite-only veins in the upper 200 to 400 m of the flanks of the East zone (Figure 3.26A, B). Pyrite also forms minor fine-grained disseminations in quartz veins with chalcopyrite and local carbonate. Pyrite is common as fine to medium grains within mafic sites as an alteration product with illite ± muscovite ± kaolinite and dominates the upper 400 to 600 m of the eastern flank along section N50E and in the upper 200 to 400 m of the northern part of section 452700E. Minor pyrite is also present in mafic sites with hornblende, secondary biotite and chlorite below 1250 m on the eastern flank of section N50E.
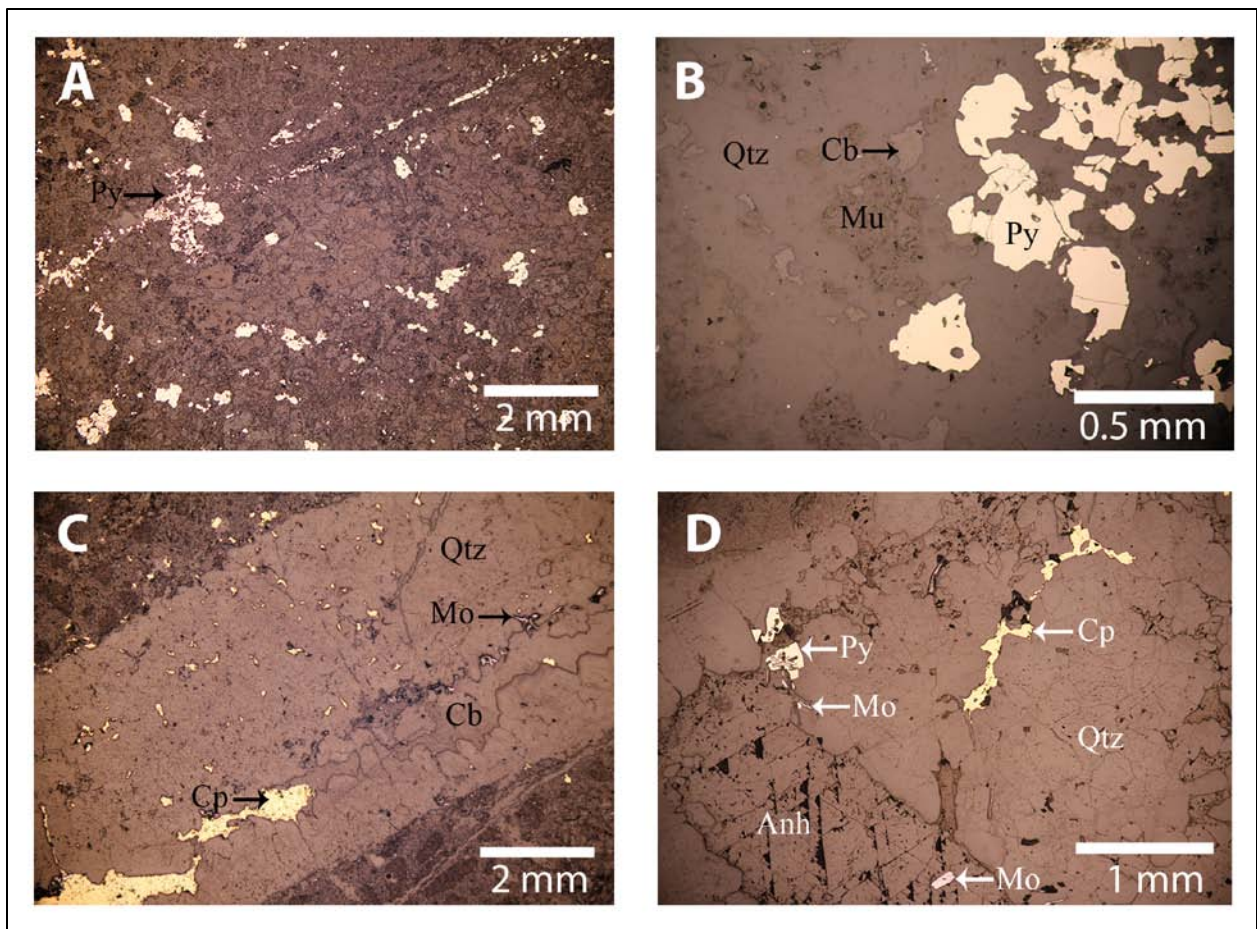
Figure 3.26 Pyrite and molybdenite in reflected light. A: pyrite-only veinlets and pyrite clots (RC09-353, 8 m); B: quartz-pyrite vein with muscovite alteration (RC94-106, 139 m); C: quartz vein with disseminated chalcopyrite and molybdenite with central carbonate (RC09-349, 904 m); D: quartz-anhydrite vein with disseminated chalcopyrite, pyrite and molybdenite laths (RC09-350, 1140 m). (Qtz = quartz, Cb = carbonate, Mu = muscovite, Py = pyrite, Cp = chalcopyrite, Mo = molybdenite, Anh = anhydrite)

3.5.2.4 Molybdenite

Molybdenite is present in minor amounts as fine- to medium-grained, pale grey to shiny pale purple disseminations within quartz-carbonate veins and locally along the margins of quartz-carbonate ± anhydrite veins (Figure 3.26C, D). Chalcopyrite is typically associated with molybdenite. Molybdenite is sparsely present throughout the N50E section but is concentrated in moderate amounts in drillholes RC09-353 and RC09-350 below 600 m depth.

3.5.3 Sulphide Zonation

Bornite, chalcopyrite, pyrite and molybdenite are varyingly distributed along section N50E (Figure 3.23). A narrow, yet vertically significant zone of bornite + chalcopyrite dominates the central region of the section, extending to depths of 1100 m in drillhole RC09-

348. At 900 m depth, this zone is roughly 200 m wide and is intersected by four adjacent drillholes. The bornite + chalcopyrite zone narrows towards the surface, and is roughly 50 m wide at 50 m depth. Outboard of the bornite + chalcopyrite core, a zone of chalcopyrite > pyrite forms the bulk of the N50E section. A zone of pyrite > chalcopyrite forms an asymmetrical dome about the centre of the section around drillholes RC09-348, RC07-335. This pyrite zone is concentrated in the upper 200 m in the western flank of the N50E section and extends down to a depth of 400 to 600 m in the east. A similar sulphide zonation pattern is observed along section 452700E with a bornite + chalcopyrite core, a chalcopyrite > pyrite shell and a pyrite > chalcopyrite halo (Figure 3.24). Molybdenum is present in minor amounts within quartz-chalcopyrite-carbonate veins across the East zone below 600 m however it is concentrated in the chalcopyrite dominant zone of drillhole RC09-353.

3.5.4   Location of High-Grade Ore

Histograms of copper and gold grades plotted on section N50E (Figure 3.23) show that the highest gold grades are associated with the highest densities of banded quartz-stockwork veins. The core of the East zone has grades > 0.5% Cu and > 0.1 g/t Au from surface down to ~1000 m in depth, with localized sections of much higher grade values. The eastern portion of the section has grades typically > 0.5% Cu and > 0.1 g/t Au from 400 to 550 m down to ~1000 m, also with localized sections that are much higher in grade. An example is drillhole RC09-350, which has an intersection of 152 m thick, at 540 m in depth, of 4.12% Cu and 8.83 g/t Au. In the west (RC09-352), grades are typically > 0.5% Cu and > 0.1 g/t Au between depths of 400 and 850 m. The westernmost drillhole of the East zone (RC09-351) has localized sections grading > 0.5% Cu and > 0.1 g/t Au between 400 and 800 m in depth. The highest gold grades are associated with the chalcopyrite and bornite core in the centre of the East zone, and locally in flanking areas of dominantly chalcopyrite. Minor gold grade is associated with pyrite in the pyrite > chalcopyrite halo. Visible gold was not observed. Copper and gold have an average ratio of 1:1 (% Cu to g/t Au), and they are strongly correlated across all grades (Baker et al., 1997). Copper and gold grade is controlled by quartz veins.

3.5.4.1   Quartz Vein Density

An approximate density of quartz veins was estimated on 5 to 20 m intervals of drill core as volume percentages. This estimation was done visually, and is possibly overestimated, as vertical drillholes may have been drilled down the quartz veins. The vein-thickness measurement

method described by Gruen et al., (2010) is a more accurate estimation of quartz vein density. In the study at Red Chris, visual estimates of volume percent were divided into five bins (0–20, 20–40, 40–60, 60–80 and 80–100 vol %) and plotted as a histogram for each hole. Several isolated regions of high quartz-vein densities greater than 20 % cluster in the centre of the section (outlined by thick black dashed lines on Figure 3.23). The widest region occurs in the centre of the East zone around 800 m in depth. A region of very high density of quartz veins occurs isolated within drillhole RC09-350 between 540 and 700 m in depth grading 4.12 % Cu, 8.83 g/t Au and 10.46 g/t Ag over 152 m. Another region of very high density of quartz veins occurs at the surface and extending down to a depth of 65 m in drillholes RC07-335 and RC09-354. These areas of high quartz vein density correlate to the zones of the highest copper and gold grades in the East zone.

High quartz vein densities (> 20 vol %) reported in this study might be overestimated, as these values are not commonly reported at porphyry deposits. At Bingham Canyon, quartz veins typically account for 5 to 10 volume % of the rock in the quartz monzonite porphyry and equigranular monzonite (Gruen et al., 2010) and locally contain zones 1 to 10 m wide up to 25 volume % (Redmond and Einaudi, 2010). However, quartz vein densities reported at Ridgeway, where 20 to 30 vol % densities are typical and locally reach 80 vol % (Wilson et al., 2003) are generally consistent with densities reported at Red Chris.

3.6   Discussion

3.6.1   **Alteration**

Alteration zones at Red Chris have characteristics of propylitic, potassic, chlorite-sericite, sericitic and intermediate argillic alteration typical of porphyry Cu deposits (Meyer and Hemley, 1967; Lowell and Guilbert, 1970; Sillitoe, 2000; Seedorff et al., 2005, Sillitoe, 2010). Progressive alteration of phenocrysts, groundmass and iron oxide and sulphide minerals as a result of these alteration types is outlined in Table 3.2. Much ambiguity exists in the definition of sericite. In this study where the mineral has been determined (by SWIR and XRD) to be muscovite or illite, such names are used. However, the term sericite will be used where is it not conclusive if the mineral(s) in question is either illite or muscovite.

Table 3.2 Mineralogical Changes During Progressive Alteration by Magmatic and Thermally Driven External Fluids

	Least Altered	*MAGMATIC-DERIVED FLUID*	**Potassic**	**Chlorite-Sericite**	**Sericitic/Phyllic**	*MIXING OF MAGMATIC AND EXTERNAL FLUIDS*	**Intermediate Argillic**
Mafic Phenocrysts	Hornblende		Secondary biotite	Chlorite ± sericite (muscovite)	Sericite (muscovite) Pyrite		**Mafic Phenocrysts:** Illite – kaolinite
Felsic Phenocrysts	Plagioclase		± Sericite (muscovite)	± Sericite (muscovite)	Sericite (muscovite)		**Felsic Phenocrysts:** Illite – kaolinite
Groundmass	Quartz, Plagioclase and K-Feldspar		K-Feldspar	± Sericite (muscovite)	Sericite (muscovite) ± quartz		**Groundmass:** Illite – kaolinite
Oxides-sulphides	± Magnetite		Magnetite	Hematite	Pyrite		**Iron-Oxides:** Magnetite to Hematite
	Least Altered	*EXTERNAL FLUID*	**Propylitic**				
Mafic Phenocrysts	Hornblende		Chlorite ± epidote ± calcite				**Sulphides:** No change
Felsic Phenocrysts	Plagioclase		± Sericite (muscovite)				
Groundmass	Quartz, Plagioclase and K-Feldspar		± Sericite (muscovite)				
Oxides-sulphides	± Magnetite		Pyrite				

3.6.1.1 Propylitic

The deep, marginal zone of weak chlorite-pyrite-epidote alteration can be equated with propylitic alteration (Meyer and Hemley, 1967; Lowell and Guilbert, 1970) and appears to have a gradational contact with K-silicate alteration, a feature common to many porphyry Cu deposits (Sillitoe, 2010). Propylitic alteration forms a disseminated yet widespread fringe around the periphery of the ore deposit (Meyer and Hemley, 1967). Minor chlorite, pyrite, epidote and rare calcite alter both primary hornblende and locally secondary biotite, representing an alteration event before or shortly after the onset of K-silicate alteration.

3.6.1.2 K-Silicate

Secondary biotite, magnetite and K-feldspar form a K-silicate altered core (Meyer and Hemley, 1967; Lowell and Guilbert, 1970; Sillitoe, 2010) to the porphyry Cu system at Red Chris. Replacement of primary hornblende phenocrysts by shreddy biotite aggregates is the predominant alteration mineral with variable K-feldspar. At Red Chris, the K-feldspar alteration is restricted to the groundmass and does not alter primary plagioclase phenocrysts. The original spatial extent of K-silicate alteration was likely once more extensive than currently preserved. Relict lenses of K-silicate alteration within zones of intense illite-kaolinite suggest it extended to at least 200 m depth and possibly even closer to current surface.

The lack of K-feldspar alteration of plagioclase phenocrysts at Red Chris is uncharacteristic for K-silicate alteration zones at most porphyry deposits. Hollister (1978) proposed a 'diorite model' for porphyry deposits which describes a range in K-feldspar addition during potassic alteration whereby orthoclase might be absent, less inconspicuous than plagioclase or prominent. Additionally, biotite predominant over orthoclase is common of potassic alteration in diorite-type deposits (Beane and Titley, 1981). At the onset of potassic alteration of the Lost Horse dykes at Copper Mountain, mafic minerals were generally fresh or replaced by epidote and K-feldspar replaced plagioclase in the groundmass, however phenocrysts were only affected where alteration was intense (Stanley et al., 1995). Perhaps Red Chris represents a porphyry deposit in which K-Silicate alteration is dominated by secondary biotite and K-feldspar alteration is subordinate and simply does not alter plagioclase phenocrysts.

3.6.1.3 Chlorite-Sericite

Early reports on wall-rock alteration and alteration zoning associated with porphyry deposits note chlorite as being associated and intergrown with biotite during K-silicate alteration (Meyer and Hemley, 1967; Lowell and Guilbert, 1970). However, chlorite replacement of secondary biotite represents a transitional alteration zone between the potassic and sericitic alteration zones and can be equated with chlorite-sericite (Hedenquist et al., 1998; Sillitoe, 2010) and sericite-clay-chlorite alteration (SCC; Sillitoe and Gappe, 1984). Chlorite replacing secondary biotite at Red Chris is characteristic of the transitional chlorite-sericite alteration type. The current extent of chlorite-sericite alteration marks a transitional zone roughly between 1000 and 600 m depth where it overprints older potassic alteration. The nature and distribution of clay and sericite associated with this alteration type is unclear due to the intense illite-kaolinite overprint on all other (older) alteration types. It is likely that some amount of sericite (illite or muscovite) alteration of plagioclase phenocrysts and the groundmass accompanied the chlorite. The hydrothermal fluids associated with chlorite-sericite alteration altered magnetite to specular hematite. Chlorite-sericite alteration is not equivalent to intermediate argillic alteration of Meyer and Hemley (1967), discussed below.

3.6.1.4 Sericitic (Phyllic)

The localized zone of quartz-sericite (muscovite)-pyrite alteration is consistent with sericitic alteration (Meyer and Hemley, 1967) or phyllic alteration of Lowell and Guilbert (1970). This sericitic zone represents hydrolytic alteration forming late, yet still at elevated temperatures following K-silicate alteration. Secondary biotite, chlorite and sericite associated with chlorite-sericite are altered to sericite whereas the groundmass is altered to sericite ± quartz. Sericitic alteration is commonly texturally destructive and the formation of pyrite, typically within mafic mineral sites is characteristic.

The significant overprint by illite-kaolinite has masked much of the original extent of muscovite alteration, and resulted in the current limited extent of identifiable muscovite. It is likely that the sericitic zone was once more extensive, and formed a halo above and around the core of the deposit. XRD analysis of 5 samples (RC224-002, RC224-005, RC106-013, RC349-013 and RC353-004) from the upper ~300 m report kaolinite and muscovite as the dominant alteration minerals present in addition to pyrite, ankerite, siderite and chalcopyrite. These

samples suggest relict sericitic (muscovite) alteration at the margins of the East zone, which have also experienced younger kaolinite and carbonate alteration but not appreciable amounts of illite.

3.6.1.5 Intermediate Argillic

There is much confusion in literature regarding the terminology and characterization of intermediate argillic alteration. Hemley and Jones (1964) described an 'intermediate' association of hydrolytic alteration characterized by the formation of montmorillonite, kaolinite, sericite, biotite, pyrite and quartz. On the basis of Hemley and Jones (1964), Meyer and Hemley (1967) termed and described 'intermediate argillic' alteration as a distinct alteration type common at porphyry deposits that is predominated by kaolin- and montmorillonite-group minerals. Dickite and well-ordered kaolinite are not as abundant in intermediate argillic alteration as are disordered and mixed-layer clays, such as illite-montmorillonite (Tooker, 1963). The term 'intermediate' was added to 'argillic alteration' to distinguish it from the higher temperature 'advanced argillic' alteration assemblage, and from argillic alteration formed by supergene processes. Work by Sillitoe and Gappe (1984) equated sericite-clay-chlorite (SCC) alteration with intermediate argillic alteration. An alteration model by Sillitoe (2000) describes intermediate argillic alteration forming as a pale green overprint on K-silicate alteration, yet prior to sericitic/phyllic alteration. Further confusion surrounds the alteration assemblage of chlorite-sericite (Hedenquist et al., 1998) and its relationship to intermediate argillic alteration. Sillitoe (2010) discusses that equating chlorite-sericite alteration, the abbreviated name used by Hedenquist et al., 1998) for sericite-clay-chlorite alteration of Sillitoe and Gappe (1984) with intermediate argillic alteration should be discontinued. An intermediate argillic alteration assemblage outlined in this study is described below and the relationship with chlorite-sercite and sericitic/phyllic alteration assemblages is investigated in Chapter 4.

Illite and kaolinite at Red Chris can be equated with argillic alteration (Lowell and Guilbert, 1970) and intermediate argillic alteration (Meyer and Hemley, 1967), which formed late in the hydrothermal system as a lower temperature form of hydrolytic alteration as sericitic alteration waned (Seedorff et al., 2005). It must be noted that intermediate argillic alteration at Red Chris differs from the assemblage described by Meyer and Hemley (1967). Biotite recyrstallization from chlorite is not recognized at Red Chris. Further, Meyer and Hemley (1967) describe K-feldspar as being metastable with intermediate argillic alteration, which is recognized at Red Chris where the overprint in minor to moderate (below 400 to 600 m depth). However, in

shallow levels of the system K-feldspar is destroyed by intermediate argillic alteration and minor lenses of relict K-silicate alteration remain between 600 and 200 m depth. Intermediate argillic alteration recognized at Red Chris is not advanced argillic as distinguishing alteration minerals such as andalusite, diaspore, pyrophyllite, dickite and alunite (Meyer and Hemley, 1967; Seedorff et al., 2005) are not present.

At Red Chris, intermediate argillic alteration results from meteoric fluid mixing with the late, cooler, acidic hydrothermal fluid to form illite and kaolinite. Intermediate argillic alteration overprints all alteration types, even weakly overprinting portions of propylitic alteration, indicating that intermediate argillic alteration extended to areas well outside of the initial extent of high-temperature hydrothermal alteration.

Much of the intermediate argillic alteration is represented by illite or illite + kaolinite; however few samples are only kaolinite. These kaolinite-only altered rocks are restricted to post-mineral dykes at all depths and breccias zones in the upper 200 to 300 m. It is likely that the post-mineral dykes and zones of brecciation formed preferential pathways for the late acidic alteration fluids. Additionally, kaolinite likely formed after illite, weakly overprinting the major illite zone as the temperature continued to decrease with increased mixing with meteoric fluids.

Pyrite noted in areas of intense intermediate argillic alteration likely formed during sericitic alteration and remains unaltered during the overprint by illite-kaolinite. Alteration of magnetite to hematite during chlorite-sericite alteration was likely intensified during intermediate argillic alteration.

3.6.1.6 Carbonate

Pervasive carbonate alteration may be paragenetically related to intermediate argillic alteration as minor carbonate (ankerite-dolomite) weakly overprints the upper ~500 m of the East zone and gradually decreases with depth in a similar fashion to illite. Further, the pervasive carbonate variably alters all other alteration events similar to intermediate argillic alteration. However, the pervasive carbonate alteration may also be related to an event even younger than intermediate argillic alteration, having altered all precursor alteration types. Whether associated with intermediate argillic alteration, or as a later event, the carbonate alteration is likely related to the late stage carbonate veins (LC1, LC2) observed across the East zone.

111

3.6.2 **Veins**

Section 3.4 outlines seventeen discrete vein types in the East zone and a sequence of the vein formation is constructed on the basis of cross-cutting relationships (Figure 3.27). The veins are divided into five major groups, four of which can be assigned to the A-B-D vein classification system of Gustafson and Hunt (1975). This classification system, based on vein types observed at the El Salvador porphyry deposit in Chile, include early- (A Veins), transitional- (B Veins) and late alteration and mineralization (D Veins). The vein types and characteristics outlined by Gustafson and Hunt (1975) are outlined in Table 3.3.
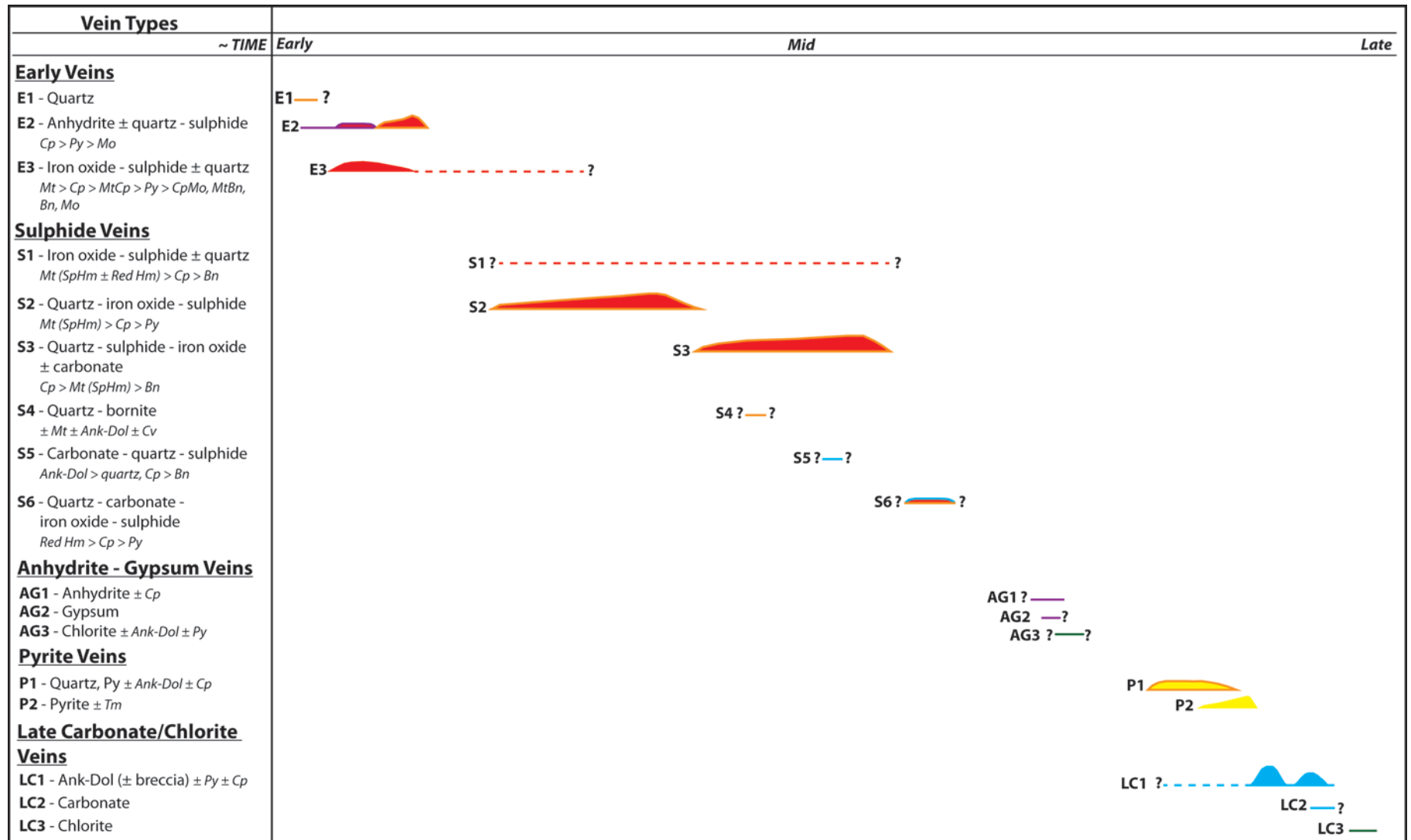
Figure 3.27 Vein paragenesis. Seventeen vein types grouped into five major groups: Early Veins (E1-3); Sulphide Veins (S1-6); Anhydrite-Gypsum Veins (AG1-3); Pyrite Veins (P1-2); and Late Carbonate/Chlorite Veins (LC1-3). (Py = pyrite, Cp = chalcopyrite, Mo = molybdenite, Bn = bornite, Mt -= magnetite, Hm = hematite, SpHm = specular hematite, Cv = covelite, Ank-Dol = ankerite-dolomite, Tm = tourmaline)

113

Table 3.3 Vein Types and Characteristics of the A-B-D Vein Classification System at El Salvador, Chile

Vein Type	Silicate Assemblage and Texture	Alteration Halo	Age and Structural Style	Sulphide Assemblage and Texture
'A Veins' *(Red Chris: Early Veins E1-3, Anhydrite-Gypsum Veins AG1-2 and Sulphide S1)*	Quartz – K-feldspar – Anhydrite – Sulphide ± Biotite • Quartz typically 50-90 % • Fine equigranular quartz with other disseminated minerals of similar size and shape • Typically no veins symmetry, but banding of K-feldspar at edges of center is not uncommon	K-feldspar (perthitic) more or less developed about most veins • May be very thin and inconspicuous especially in strong K-silicate altered rock • Strongest, most obvious about late veins in relatively fresh rock	Oldest of all veins, cut by B Veins • Earliest veins are most randomly oriented and discontinuous, commonly segmented and 'wispy' • Successively younger veins have more parallel walls and tend to occupy more continuous and systematically occupied breaks • ~1-25 mm wide	Disseminated Cp, Bn with traces of Mo • Similar size and shape to quartz
'B Veins' *(Red Chris: Sulphide Veins S2-6)*	Quartz – Anhydrite – Sulphide with K-feldspar characteristically absent • Quartz relatively coarse grained, tends to be elongated perpendicular to walls approaching 'cockscomb' texture • Granular quartz is common, especially in sheared bands • Vein symmetry, of sulphides, anhydrite or granularity along centerlines, margins or irregular parallel bands, is typical but unevenly developed	Lack of alteration halos is characteristic • Occasionally faint and irregular bleached halos present, likely due to superimposed veining	Younger than A Veins, older than D Veins • Characteristically regular and continuous and tend to have flat attitudes • ~5 -50 mm wide	Mo-Cp is characteristic with traces of Bn and common minor Py • Coarse-grained sulphides occupy banding parallel to walls or cracks perpendicular to them
'D Veins' *(Red Chris: Pyrite Veins P1-2)*	Sulphide-Anhydrite ± Quartz and occasional carbonate • More quartz where superimposed on B Veins • Quartz shows crystal form • Anhydrite locally forms coarse-crystalline masses and is commonly banded with sulphides	Feldspar destructive halos are characteristic • Patterns vary and have not been well documented • Sericite or sericite-chlorite halos may or may not have outer kaolinite-calcite halos	Cut all A and B Veins, youngest of all veins • Continuous, though locally irregular and 'lacing' and occupy systematic structure patterns • ~1-75 mm wide	Pyrite predominant with Cp, Bn, Enr, Tn, Sph and Gn common • Minor Mo and other sulphides locally • Proportions of sulphides other than Py tend to increase upward

(After Gustafson and Hunt, 1975. Py = pyrite, Cp = chalcopyrite, Bn = bornite, Mo = molybdenite, Enr = enargite, Tn = tennantite, Sph = sphalerite, Gn = Galena)

At Red Chris, the oldest veins (Early Veins) are vein sets E1, E2, and E3 and are observed in the deepest drilled sections of the East zone. These veins are equivalent to A-veins. They are irregular, discontinuous veins of quartz and anhydrite with varying amounts of chalcopyrite, pyrite, magnetite and molybdenite with local K-feldspar halos (where preserved). Sulphide-dominant veins are composed of magnetite, chalcopyrite and pyrite with minor molybdenite and quartz. Successively older A-veins tend to have more parallel walls, as noted by Gustafson and Hunt (1975) and are observed in type E2 with increasing quartz content. The veins of S1 may represent a continuation of vein-type E3 with changing fluid chemistry over time to account for the lack of pyrite and molybdenite and the increase in bornite in the later vein-set S1. S1 veins are respresentative of A-veins.

Sulphide Veins (S2, S3, S4, S5 and S6 vein-types) represent B-veins and cut A-veins. Veins S2-6 exhibit features of A-veins and B-veins, however are classified here as B-veins (Table 3.3). The coarse-grained quartz of the Sulphide Veins, along with the vein symmetry of the sulphide is characteristic of B-veins. Additonally, B-veins are typically continuous, planar structures with parallel vein walls and commonly exhibit internal banding (Gustafson and Hunt, 1975), features consistent with the Sulphide Veins. B-veins are commonly reopened by younger veins (Gustafson and Hunt, 1975) and much of the banding and sulphide-oxide centerlines observed in this group of veins is likely due to vein-type S1 exploiting quartz-sulphide-iron oxide veins (S2 and S3). The sulphide assemblage of chalcopyrite, bornite and minor pyrite in the Sulphide Veins is more characteristic of A-veins, whereas B-veins are characterized by molybdenite, chalcopyrite with trace bornite and common minor pyrite. These Sulphide Veins (S2-6) appear to lack disctinct alteration halos, as noted by Gustafson and Hunt (1975) in B-veins. However, the widespread K-silicate alteration in the system could not have formed from the deeper Early Veins and represents widespread alteration halos of the Sulphide Veins. Thus, in terms of alteration halos, Sulphide Veins are representative of A-veins.

Most of the copper and gold at Red Chris was deposited within the Sulphide Veins (S2 and 3), which are characterized as B-veins. In many porphyry deposits, much of the high-grade mineralization is associated with A-veins. It is possible that the temperature was too hot for sufficient copper-gold deposition during the Early Veins. As the temperature descreased, copper and gold were deposited in the latest stage of Early Veins (E3), through to the earliest stage of the Sulphide Veins (S1) and predominantly deposited in S2 and S3 veins.

The third set of veins (Anhydrite-Gypsum Veins) are AG1 and AG2 and AG3, of which AG1 and AG2 can also be classified as A-veins. These anhydrite veins cross-cut earlier coarser-grained anhydrite-sulphide-quartz veins (E2) and that have been partially (AG1) and fully (AG2) hydrated to gypsum. This set of veins may indicate the possible resurgence of the Early Vein stage, suggesting an onset of a second hydrothermal event in the East zone, however much smaller and less productive than the first. These veins contain trace sulphide minerals, are thinner than early E2–type veins and are only observed to cross-cut purple anhydrite-sulphide ± quartz veins (E2). The very minor amount and sparse distribution of these veins make it difficult to determine how they relate to other vein events in the system.

Pyrite Veins (P1 and P2) in the East zone represent the late-stage D-veins. These are continuous veins, dominantly pyrite with variable quartz, minor chalcopyrite and rare tourmaline. Carbonate (ankerite-dolomite) is typically present in minor to moderate amounts. D-veins are younger than the A and B veins and are located in a halo around the core of the East zone. These veins formed late at the deposit during the stage of hydrolytic alteration.

Some Late Carbonate-Chlorite veins (LC1) cross-cut Sulphide Veins and Pyrite Veins and likely infill open spaces in Sulphide Veins, accounting for the minor carbonate observed. Late, very fine-grained chlorite is observed to cross-cut, and to fill-in vugs in carbonate veins as vein-sets AG3 and LC3. It is likely that these are the same event. Although minor carbonate is associated with Pyrite Veins, much of the carbonate veins and breccias (LC1 and LC2), in addition to the late chlorite veins and infill (LC3) do not fit into the classic A-B-D classification of Gustafson and Hunt (1975) and likely represent a later fluid event.

Many similarities in the vein types exist between El Salvador and Red Chris, however a few differences remain. The most noted discrepancy is the lack of anhydrite in the B and D vein sets at Red Chris (Sulphide Veins and Pyrite veins, respectively). Carbonate (ankerite-dolomite) appears in place of the anhydrite in these vein sets. Carbonate is a common, yet variable mineral throughout the veins at Red Chris, and commonly fills in centers of, or occurs along margins of quartz-sulphide veins. At El Salvador, anhydrite formed along centers or margins of B Veins, suggesting that at Red Chris, carbonate may have replaced anhydrite associated with the Sulphide and Pyrite Veins sets. Further, minor carbonate is noted in the latest stages of E2 veins,

116

where the amount of anhydrite is decreased with regards to earlier stages. This supports the possibility that carbonate replaced anhydrite.

3.6.3   Mineralization

A copper-iron-sulphide zonation pattern has been described at other porphyry Cu deposits whereby a core of chalcopyrite-bornite grades outward to a chalcopyrite-pyrite annulus, and outward into a pyrite halo (Sillitoe, 2010). This sulphide zonation is consistent with the pattern recognized at Red Chris. Additionally, the distribution of molybdenum is also comparable at other porphyry deposits. Molybdenite is common in drillhole RC09-351 on the southwest flank and drillholes RC09-350 and RC09-353 on the northeast flank of the East zone, and is consistent with molybdenum exhibiting distinct halos to the molybdenum-poor, copper-gold zones observed at many deposits (Ok Tedi, Batu Hijau, Santo Tomas II, Far Southeast, Bajo de Alumbrera, Saindak; Sillitoe, 2000).

High grade mineralized zones within the East zone are contained within quartz stockwork veins (S2 and S3). The different nature and mineralogy between the high grade zones in RC09-350 and RC07-335/RC09-354 suggest different fluid events. The high grade intersection at 540 m depth in RC09-350 is massive quartz with randomly oriented chalcopyrite veinlets and cross-cutting carbonate (Figure 3.28A, B). The high grade intersection in the upper ~60 m of drillholes RC07-335 and RC09-354 are preferentially banded quartz, chalcopyrite, pyrite, magnetite and hematite with carbonates aligned along these bands (Figure 3.28C, D). The quartz stockworks near the surface are vertically oriented veins, parallel to the core-axis. The fluid events responsible for these high grade zones may be related to the emplacement of different porphyritic intrusive phases. Sillitoe (2010) mentions the presence of 'quartz cores', areas of high densities of quartz veins located in the core of orebodies in a few deposits such as Ok Tedi, Papua New Guinea. These 'quartz cores', may be equivalent to the areas of high-density quartz veins at Red Chris, notably the two zones of massive quartz veins (RC07-335 and RC09-350) marked by centers of different ore bodies. Additional lower-grade ore bodies might also be present, represented by gaps between isolated zones of high-density of quartz veins.
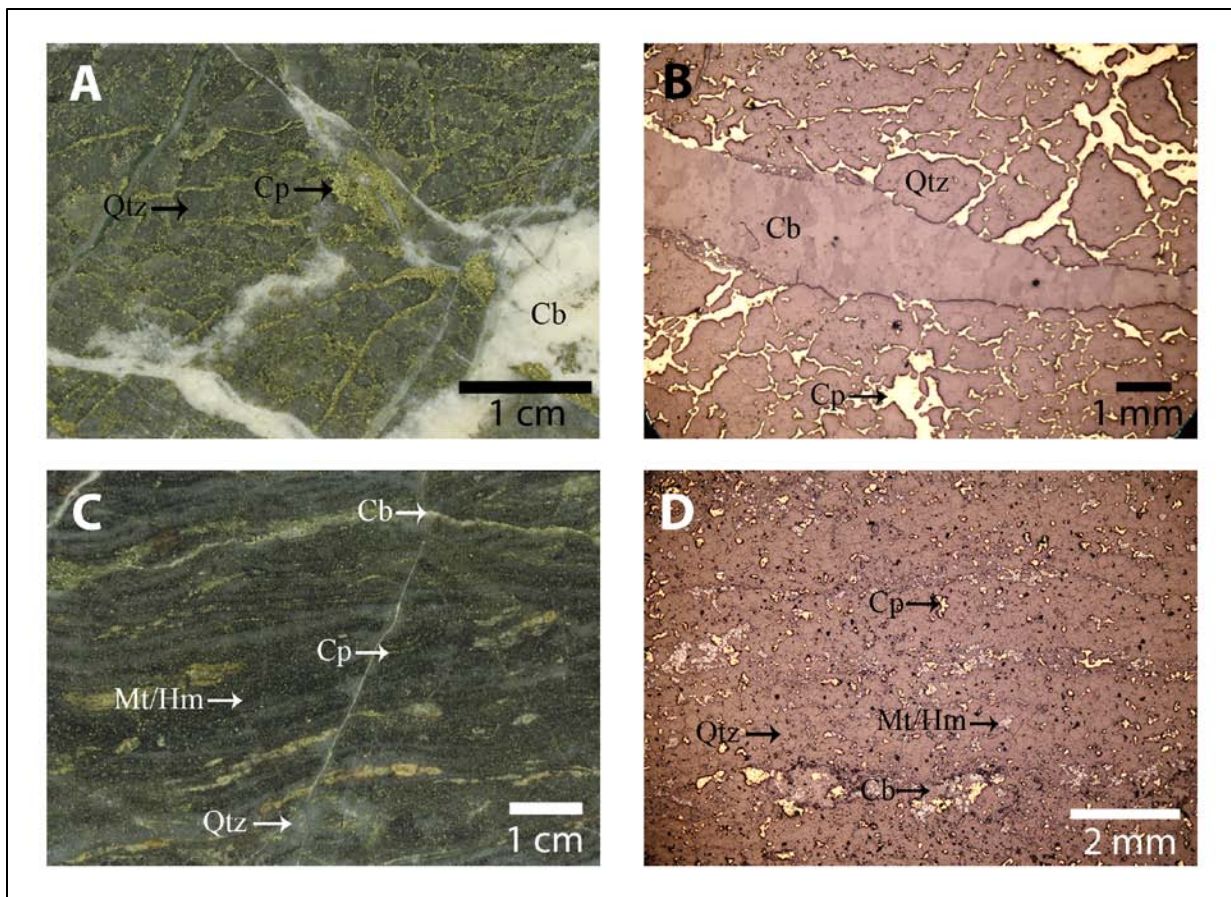
Figure 3.28 High-grade mineralization. Chalcopyrite in massive quartz stockwork with cross-cutting carbonate in hand sample (A) and thin section (B, reflected light), (RC09-350, 629 m, 6.06% Cu, 11.94 g/t Au); banded quartz-magnetite/hematite-chalcopyrite with minor interstitial carbonate in hand sample (C) and thin section (D, reflected light), (RC09-354, 15 m, 4.75% Cu, 4.54 g/t Au). (Qtz = quartz, Cb = carbonate, Cp = chalcopyrite, Mt = magnetite, Hm = hematite)

Most of the high-grade copper and gold ore is introduced with the banded quartz-sulphide B-veins, S2 and S3 and to a lesser extent S4, S5 and S6 (Figure 3.27). These veins are concentrated in the core of the East zone at depth and extend to surface with a limited lateral extent (< 50 m) near drillhole RC07-335. The ore-bearing veins are related to the K-silicate alteration event, which has been intensely illite-kaolinite overprinted. Additional minor grade occurs within the sulphide-bearing quartz-anhydrite veins (E2) at depth in weakly K-silicate and illite altered zones and also within pyrite-chalcopyrite of quartz ± carbonate veins (P1 and P2) in the upper 600 to 200 m pyrite halo of the East zone.

3.7   Conclusion

Whereas not currently visible due to alteration overprint, there is a direct relationship between alteration, veins and mineralization. K-silicate alteration is associated with A-veins and B-veins and their contained metals. Much of the high-grade ore is introduced into the system

118

during this stage. A portion of the B-veins and contained mineralization may also be associated with chlorite-sericite alteration; however this association is not constrained. Sericitic (phyllic) alteration is associated with D-veins which form much of the pyrite in the system. Minor grade is associated with pyrite and chalcopyrite contained within D-veins. Intermediate argillic alteration does not have a distinct set of associated veins nor mineralization. The late stage carbonate veins are associated with the pervasive carbonate alteration, however it is not conclusive if these are related to intermediate argillic alteration, or if they occur afterward. Carbonate minerals are present in nearly all veins observed throughout the system, however the mineral represents a late event which both cross-cuts and fills older veins and is not directly associated with ore mineralization.

4   Source and Evolution of Hydrothermal Fluids: Evidence from Stable Isotopes

Two major fluids are responsible for hydrothermal alteration observed at porphyry deposits. The magmatic fluid is a high temperature, magma-sourced fluid that is confined within a series of porphyry stocks whereby each event focused upward movement of magmatic fluid. The buoyantly rising magmatic fluid alters rock within and adjacent to the porphyry stocks and deposits sulphide minerals. The second major fluid is an external, meteoric fluid that circulates due to heat supplied by the underlying batholith. This external fluid alters rock material outboard of the stock as it flows upward along the margins of the stocks. Eventually, the external meteoric fluid enters the porphyry stock to mix with the cooling magmatic fluid. With continued cooling magmatic-meteoric fluid mixing continues and greater volumes of meteoric fluid are incorporated into the mixture. Generation of magmatic fluid and mixing with meteoric fluids is rarely a single event due to the multi-phase intrusive events supplying discrete pulses of magmatic fluid. Eventually the magmatic-hydrothermal system cools and the low temperature circulating fluids are entirely meteoric in origin.

Much of the hydrothermal alteration types at Red Chris prior to the late intermediate argillic overprint are generally well documented, described, and understood processes of porphyry systems (Meyer and Hemley, 1967; Lowell and Guilbert, 1970; Beane, and Titley, 1981; Sillitoe, 2010). Propylitic alteration formed outboard of the host porphyry stocks from the heated external, meteoric fluid. K-silicate alteration formed within the host porphyry stocks and in the surrounding rocks from the high temperature magmatic-derived fluids. Chlorite-sericite and sericitic (phyllic) alteration formed from cooling magmatic fluids and disproportionation of sulphate leading to hydrogen exchange (hydrolysis) with the rock material. The late stage, low temperature intermediate argillic alteration is the most widespread, pervasive alteration type recognized at Red Chris, however its significance is unknown. This distinguishing feature at Red Chris begs the question: does illite-kaolinite (intermediate argillic) alteration characterize the upper parts of an alkalic porphyry system? If illite-kaolinite is related to a hydrothermal alteration of a porphyry system, evidence of magmatic fluids would be expected? If illite-kaolinite alteration is unrelated to a porphyry system, evidence would only indicate the presence of meteoric fluid?

Studies on stable isotopes can provide evidence for the source and nature of magmatic and meteoric hydrothermal fluids present during the formation of Red Chris. Sulphur isotopes can be

used to interpret the evolution of the magmatic, Cu-Au bearing fluids as they interact with surrounding wall-rocks. Additionally, oxygen and deuterium isotopes on hydrosilicate minerals can be used to interpret a magmatic/meteoric source of the hydrothermal fluids and construct the sequence of alteration events. Further, carbon and oxygen isotope analysis can be used to interpret the source of carbonate minerals at Red Chris and place the carbonate veins and alteration into context with respect to other recognized alteration events.

4.1 Stable Isotope Analysis on Sulphides and Sulphates - $\delta^{34}S$

Distinctive sulphur isotopic zonation patterns recognized at porphyry deposits of the Cadia District in New South Wales, Australia, have been proposed to have potential as exploration vectors in alkalic porphyry provinces (Wilson et al., 2007). Lateral and vertical zonation patterns depict more negative $\delta^{34}S_{sulphide}$ values in high-grade mineralized cores of deposits that transition upwards and outwards to near-zero (magmatic) background $\delta^{34}S_{sulphide}$ values in the periphery (Wilson et al., 2007). Such zonation patterns are noted to generally correlate with high-grade mineralized zones and recognized alteration assemblages.

Galore Creek and Mt. Milligan are two alkalic porphyry deposits in northern and central British Columbia that exhibit zonation patterns in $\delta^{34}S_{sulphide}$ values related to mineralization and alteration. At Galore Creek, sulphur isotope analyses conducted by Micko (2010) on the North Gold Lens demonstrate a distinct zonation pattern, particularly with respect to the early mineralizing event. Highly negative $\delta^{34}S_{sulphide}$ values (-17.13 to -11.65 ‰) are localized in small centers associated with intense potassic alteration and the high-grade Au-enriched ore shell (Micko, 2010). Moderately negative $\delta^{34}S_{sulphide}$ values (-6.61 to -4.22 ‰) surround the high-grade Au-enriched shell and correlates with the Cu-dominated halo (Micko, 2010). The outer sericite-anhydrite-carbonate/propylitic zone, characterized by disseminated pyrite with $\delta^{34}S_{sulphide}$ values between +0.04 and +1.08 ‰ (Micko, 2010). A well developed sulphur isotopic zonation pattern is also recognized at Mt. Milligan, which correlates with lateral distance from the center of the vertically reoriented MBX Stock (Jago et al., In press). The potassic altered margin of the MBX Stock contains the lowest $\delta^{34}S_{sulphide}$ values (-5 to -3 ‰) where as the peripheral carbonate-phyllic, outer propylitic and chloritic assemblages have slightly higher $\delta^{34}S_{sulphide}$ values (-1.5 to +0.5 ‰). Galore Creek and Mount Milligan demonstrate that the sulphur isotopic zonation pattern observed in the Cadia porphyry district of New South Wales, Australia is also evident in alkali porphyry deposits of British Columbia.

A sulphur isotopic study was undertaken at the Red Chris Cu-Au porphyry deposit, in northwestern British Columbia to determine if a zonation pattern is present similar to Galore Creek, Mt. Milligan and the porphyry deposits of the Cadia district. The results of this study have implications for exploration targeting of alkalic porphyry deposits in British Columbia. Further, geothermometric calculations on co-precipitating sulphide-sulphide and sulphide-sulphate isotope pairs are used for estimating temperatures of fluid formation.

4.1.1 Systematics of Sulphur Isotopes

The examination of sulphur isotopes in combination with geological and mineralogical parameters within an ore deposit may help define the source(s) of the ore-forming fluids. Sulphur has four stable isotopes ^{32}S, ^{33}S, ^{34}S and ^{36}S which naturally occur in abundances of 95.018 %, 0.750 %, 4.215 % and 0.017 % respectively (MacNamara and Thode, 1950). The common isotopic notation for sulphur is reported as δ^{34}S in per mil units (‰) and compares the ratio of the two most abundant isotopes of sulphur (^{32}S and ^{34}S) in a sample with that of an internationally recognized standard. The δ^{34}S of a sample is measured by:

$$\delta^{34}S = \left[\frac{{}^{34}S_{sample} \big/ {}^{32}S_{sample}}{{}^{34}S_{std} \big/ {}^{32}S_{std}} - 1 \right] \times 1000$$

The standard for sulphur isotopic studies is from troilite (FeS) of the Canyon Diablo meteorite (CDT) with a ^{34}S/^{32}S value of 0.0450045 (Ault and Jensen, 1963). Sulphur species which reflect the isotopic composition of a fluid and precipitated minerals include H_2S, HS^-, S^{2-}, SO_4^{2-}, HSO_4^-, KSO_4^- and $NaSO_4^-$ and are largely controlled by T, pH, and fO_2 of the system (Ohmoto, 1972). The total isotopic value of sulphur in a sample is determined by the isotopic value of sulphur for each of the species involved. The effect of pressure on the fractionation of sulphur isotopes within a mineral is negligible at P < ~10 kbar. When in equilibrium, the heavier isotope (^{34}S) will preferentially fractionate into the sulphur species with the highest valence (most oxidized), resulting in $\delta^{34}S_{SO4 \text{ (and sulphate minerals)}} > \delta^{34}S_{SO2} > \delta^{34}S_{S2} > \delta^{34}S_{H2S \text{ (and sulphide minerals)}}$ (Ohmoto and Goldhaber, 1997). Variations in δ^{34}S within a system may be caused by temperature variations, changes in redox state and the incorporation of multiple sources of sulphur.

In magmatic systems, the $\delta^{34}S$ values of most igneous rocks was believed to be between 0 ± 5 ‰ (Ohmoto and Rye, 1979) however subsequent studies indicate that it is quite common for igneous rocks to have $\delta^{34}S$ values well outside this range. In many areas, the sulphur isotopic content of igneous rocks is similar to that of sulphides and sulphates of the associated country rocks (Ohmoto and Goldhaber, 1997). This suggests a bulk assimilation of country rock during the emplacement of granitoid (I-type) magmas. Ohmoto and Goldhaber (1997) outline sulphur isotopic characteristics of major ore deposit types (Table 4.1, for porphyry deposits associated with I-type magmas), and note that none of the major hydrothermal deposit types appear to have sulphur isotopic contents from a pristine mantle-derived magma source. Additionally, when sulphur bearing minerals in an ore deposit can be traced to a specific magma source, the ore-forming magmas appear to have acquired a significant amount of sulphur (and other elements) from the country rocks (Ohmoto and Goldhaber, 1997).

Table 4.1 Sulphur Isotopic Characteristics for Porphyry Deposits Associated with I-type Magmas

Host Lithology	Porphyries
Ore Mineralogy	Chalcopyrite, Bornite, Molybdenite, Scheelite, Gold
Associated Minerals	Pyrite, Anhydrite
Source of S^{2-} In Ore	Fluids from magmas that acquired most of their sulphur through assimilation of country rocks
$\delta^{34}S$ Mineral Range	Narrow $\delta^{34}S$ Range $\delta^{34}S_{ore\ sulphides} \approx \delta^{34}S_{local\ igneous\ rocks} \approx \delta^{34}S_{local\ country\ rocks}$ $\delta^{34}S$ sulphides $= 0 \pm 5$‰ for most deposits in western US and South America
$\delta^{34}S$ Relationship Between Ore Minerals	Equilibrium mostly between sulphides, occasional equilibrium between sulphides and sulphates
Examples	Butte, Bingham, Ajo, Morococha, El Salvador

4.1.2 Samples and Data

Thirty-four samples of sulphide and sulphate minerals from veins and pseudomorphed phenocrysts are distributed across a section (N50E) of the East zone at Red Chris (Figure 4.1). Fourteen chalcopyrite, nine pyrite, five bornite, five anhydrite and one molybdenite sample were selected on the basis of their location within the East zone. Samples are from the near-surface, down to a maximum downhole depth of 1440 m. Sulphide and sulphate minerals were selected from various vein types throughout the paragenetic sequence of the deposit in variably altered rocks. The vein types (see Chapter 3) include:

- anhydrite ± chalcopyrite ± molybdenite ±quartz (Early Veins);

- sulphide (pyrite, chalcopyrite, bornite) with minor quartz (Sulphide Veins);
- quartz-sulphide (chalcopyrite-bornite) veins with magnetite-hematite and local carbonate (Sulphide Veins);
- quartz-pyrite ±carbonate veins (Pyrite Veins);
- pyrite replacing mafic phenocrysts.

Five mineral pairs of sulphide-sulphide or sulphide-sulphate were included in this study.

In general, the data yield a range of δ^{34}S sulphide mineral values that are mostly between -1.9 ‰ and +1.9 ‰, and between +2.8 ‰ to 11.5 ‰ for sulphate minerals (Table 4.2). Generally, the pyrite has a higher average value (+0.75 ‰) than bornite (+0.12 ‰), with chalcopyrite being the lightest (-0.42 ‰). However, each mineral has a range greater than ±1 ‰, emphasizing significant overlap, and that factors other than mineral composition controls the isotopic composition. A single molybdenite is -0.2 ‰.
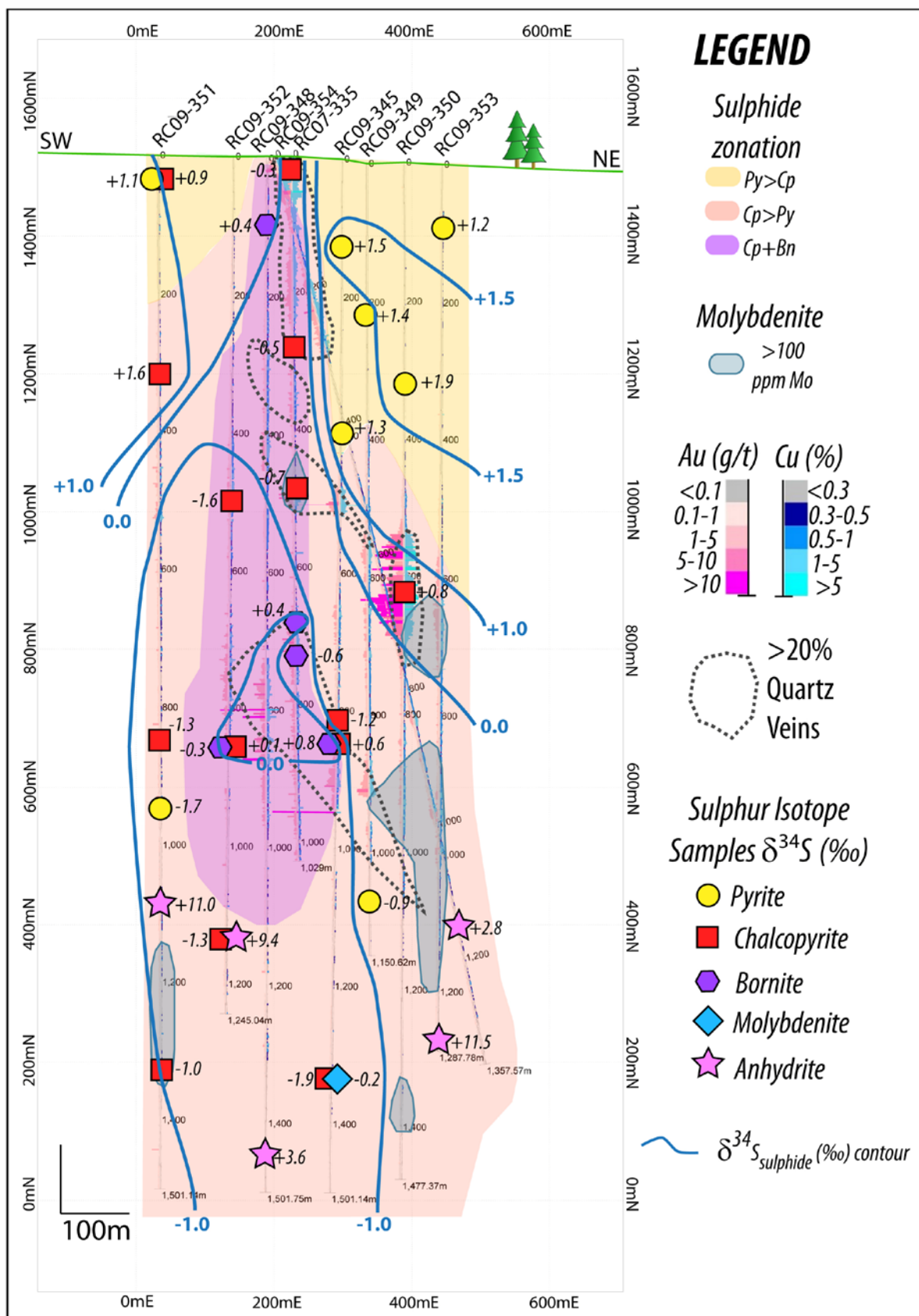
Figure 4.1 Sulphur isotope zonation on section N50E. δ³⁴S (‰) values plotted for various sulphur-bearing minerals: pyrite (yellow circle); chalcopyrite (red square); bornite (purple hexagon); molybdenite (blue diamond); anhydrite (pink star). More negative δ³⁴S at bottom of section and more positive δ³⁴S values near top and in pyrite halo. δ³⁴S_sulphide contours in blue.

125

Table 4.2 Sulphur Isotope Data and Results

Sample Name	Original Sample Name	Depth (m)	Cu (%)	Au (g/t)	Mineral	Approx. Total S (%)	$\delta^{34}S$ (CDT)
JNS-001	RC335-039	505	2.69	4.82	Chalcopyrite	31.9	-0.7
JNS-002	RC351-019	846	0.20	0.16	Chalcopyrite	41.8	-1.3
JNS-003	RC335-001	12	2.97	2.19	Chalcopyrite	24.7	-0.3
JNS-004	RC350-018	629	6.06	11.94	Chalcopyrite	35.1	0.8
JNS-005	RC351-032	1352	0.39	0.09	Chalcopyrite	41.3	-1.0
JNS-006	RC345-024	824	0.28	0.22	Chalcopyrite	31.9	-1.2
JNS-007	RC348-003	94	0.71	0.52	Bornite	24.0	0.4
JNS-008	RC335-048	665	0.44	0.52	Bornite	28.3	0.4
JNS-009	RC352-021	840	0.46	0.91	Chalcopyrite	34.8	0.1
JNS-010	RC352-021	840	0.46	0.91	Bornite	25.7	-0.3
JNS-011	RC335-050	700	1.24	2.52	Bornite	20.4	-0.6
JNS-012	RC345-025	842	2.78	5.18	Chalcopyrite	36.9	0.6
JNS-013	RC345-025	842	2.78	5.18	Bornite	29.0	0.8
JNS-014	RC352-027	1159	0.25	0.33	Chalcopyrite	37.8	-1.3
JNS-015	RC352-027	1159	0.25	0.33	Anhydrite	30.7	9.4
JNS-016	RC349-046	1088	0.00	0.23	Pyrite	54.6	-0.9
JNS-017	RC140-005	132	0.00	0.00	Pyrite	59.9	0.9
JNS-018	RC351-021	931	0.66	1.34	Pyrite	58.3	-1.7
JNS-019	RC349-008	200	0.07	0.07	Pyrite	63.4	1.4
JNS-020	RC345-011	390	0.16	0.11	Pyrite	63.8	1.3
JNS-021	RC345-003	113	0.01	0.04	Pyrite	57.8	1.5
JNS-022	RC345-041	1342	0.14	0.08	Molybdenite	27.8	-0.2
JNS-023	RC345-041	1342	0.14	0.08	Chalcopyrite	31.0	-1.9
JNS-024	RC348-038	1441	0.04	0.02	Anhydrite	4.9	3.6
JNS-025	RC353-030	1279	0.19	0.08	Anhydrite	2.9	11.5
JNS-026	RC354-027	1126	0.26	0.10	Anhydrite	37.7	2.8
JNS-027	RC351-026	1081	0.11	0.12	Anhydrite	24.9	11.0
JNS-028	RC351-001	24	0.41	0.21	Pyrite	52.6	1.1
JNS-029	RC351-001	24	0.41	0.21	Chalcopyrite	46.0	0.9
JNS-030	RC353-003	95	0.58	0.91	Pyrite	73.6	1.2
JNS-031	RC350-007	335	0.31	0.20	Pyrite	74.9	1.9
JNS-032	RC335-025	285	0.40	0.36	Chalcopyrite	59.6	-0.5
JNS-034	RC351-007	321	0.79	0.84	Chalcopyrite	57.1	1.6
JNS-035	RC352-012	472	0.95	0.77	Chalcopyrite	49.3	-1.6

4.1.3 Results: Sulphide $\delta^{34}S$ Values

The range of $\delta^{34}S$ values for sulphide minerals demonstrates a vertical zonation since all of the positive values > +1.0 ‰ are shallower than 400m, and the most negative values (< -1.0 ‰) all occur below 450m depth, along section N50E (Figure 4.1). The values from the upper 400 m of the deposit also display a lateral zonation in $\delta^{34}S$ values whereby the core of the deposit

126

(RC07-335) has a value of -0.3 ‰ δ^{34}S, and the flanks have values of > +0.9 ‰. Data below 800 m depth are generally less than 0.0 ‰ δ^{34}S (negative), however there is a cluster of positive values between +0.1 and +0.8 ‰ in the central core of the deposit, associated with a zone of intense quartz-sulphide stockwork veins. A previous study on sulphur isotopes from sulphide minerals in the upper 350 m of the Main zone at Red Chris (along Section line 50000East; Dyell and Tosdal, 2005) indicated a similar range in δ^{34}S mostly between +0.9 ‰ and -2.0 ‰, with a few outliers to -5 ‰ measured on pyrite and chalcopyrite.

There are no apparent relationships between sulphur isotope ratios and grade however some of the lowest grades from this study are associated with the most negative δ^{34}S values. This is reflective of the vertical zonation within the deposit, as the lowest δ^{34}S values occur in the deepest portions of the East zone where grades are typically low. A weak relationship between δ^{34}S value and the paragenetic sequence is noted however the paragenetic sequence is broadly correlated with depth and relative lateral distance from the core of the deposit.

In general, the deepest portions of the deposit (below 800 m) have values at or below -0.9 ‰. The ore-bearing portion of the East zone shallower than 800 m depth have δ^{34}S values between -0.7 and +0.9 ‰ with a subset of δ^{34}S values between 0.0 and +0.9 ‰ where there is great density of quartz-sulphide stockwork veins. One sample of chalcopyrite is not consistent with this trend with a δ^{34}S value of -1.6 at 472 m depth within the bornite + chalcopyrite core. The flanks of the deposit in the pyritic halo have δ^{34}S values greater than +0.9 ‰.

4.1.4 Results: Sulphate δ^{34}S Values

The values of δ^{34}S in purple anhydrite of this study are consistent with the values of sulphate minerals examined in the study by Dyell and Tosdal (2005). The δ^{34}S samples for anhydrite were taken from veins of purple and peach-white anhydrite below 1080 m depth. Petrographic analysis indicates that the purple material is pure anhydrite however the peach-white material is anhydrite that has been variably hydrated to gypsum. The lowest δ^{34}S$_{sulphate}$ values of +2.8 ‰ and +3.6 ‰ were taken from peach-white anhydrite veins and the greater values of +9.4 ‰, +11.0 ‰ and +11.5 ‰ were taken from purple anhydrite veins. The samples of purple anhydrite with the highest δ^{34}S$_{sulphate}$ values represent unaltered sulphate indicative of the primary fluids that formed them and do not reflect any later sulphur fractionation during alteration of anhydrite to gypsum. The high values of δ^{34}S$_{sulphate}$ in purple anhydrite of this study

are consistent with the values of sulphate minerals examined in the study by Dyell and Tosdal (2005). Higher $\delta^{34}S_{sulphate}$ values reported in sulphate minerals compared to sulphide minerals is consistent with ^{34}S preferentially fractionating into the most oxidized sulphur species (sulphate; Ohmoto and Goldhaber, 1997).

4.1.5 Geothermometry Using Sulphur-bearing Mineral Pairs

Sulphur isotopic content from sulphur-bearing minerals that precipitated from the same fluid can be used to estimate the temperature of mineral formation. Minerals pairs must have formed in equilibrium with one another, meaning they were co-deposited from the same fluid at the same temperature in order to extract true fluid temperature information (Campbell and Larson, 2005). Further, the sulphur isotope content of these minerals must have been retained after formation and not changed due to loss or addition of sulphur during subsequent processes. Mineral pairs not formed in equilibrium, or have not retained their isotopic composition will result in unreasonable formation temperatures.

4.1.6 Fractionation Factors and Geothermometric Equations

Fractionation of sulphur isotopes within a mineral is pressure insensitive and is heavily dependent on temperature. In order to calculate the temperature of formation for two co-precipitated sulphur-bearing minerals, individual fractionation factors must first be obtained and then can be combined to form a fractionation equation from which a temperature can be determined. Fractionation factors of sulphur isotopes are commonly given with respect to H_2S. In this study, mineral pairs include anhydrite, molybdenite, chalcopyrite, pyrite and bornite. Fractionation factors for these minerals are listed in Table 4.3, after Ohmoto and Rye (1979).

Table 4.3 Equilibrium Isotopic Fractionation Factors of Sulphur Compounds with Respect to H_2S

Mineral	Fractionation Factor (T in K)	T (°C)
Anhydrite *(CaSO₄)*	Anh-H_2S: $10^3 ln\alpha_{Anh-H2S} = 8.0(10^6/T^2)$	> 400
Molybdenite *(MoS₂)*	Mo-H_2S: $10^3 ln\alpha_{Mo-H2S} = 0.45(10^6/T^2)$	
Chalcopyrite *(CuFeS₂)*	Cp-H_2S: $10^3 ln\alpha_{Cp-H2S} = -0.05(10^6/T^2)$	200-600
Bornite *(Cu₅FeS₄)*	Bn-H_2S: $10^3 ln\alpha_{Bn-H2S} = -0.25 (10^6/T^2)$	
Pyrite *(FeS₂)*	Py-H_2S: $10^3 ln\alpha_{Py-H2S} = 0.4(10^6/T^2)$	200-700

Two individual fractionation equations for co-deposited sulphur-bearing minerals can be combined to form a geothermometric fractionation equation. For example, a pyrite-chalcopyrite pair would have the following fractionation equation:

$$(10^3 ln\alpha_{Py\text{-}H2S}) - (10^3 ln\alpha_{Cp\text{-}H2S}) = (0.4(10^6/T^2)) - (-0.05(10^6/T^2))$$

Therefore:

$$10^3 ln\alpha_{Py\text{-}Cp} = 0.45(10^6/T^2) \approx \delta_{Py} - \delta_{Cp} = \Delta_{Py\text{-}Cp}$$

So:

$$T(K) = \left(\frac{0.45 \times 10^6}{\Delta_{Py-Cp}} \right)^{1/2}$$

Careful note must be taken when defining α and therefore Δ as either $\alpha_{Py\text{-}Cp}$ or $\alpha_{Cp\text{-}Py}$. Mineral pair fractionation equations used in this study have been calculated and given in Table 4.4.

Table 4.4 Sulphur Isotopic Thermometers

Mineral Pair	Fractionation Equation (T in K)
Anhydrite-Chalcopyrite	$T = \left(\dfrac{8.05 \times 10^6}{\Delta_{Anh-Cp}} \right)^{1/2}$
Molybdenite-Chalcopyrite	$T = \left(\dfrac{0.50 \times 10^6}{\Delta_{Mo-Cp}} \right)^{1/2}$
Chalcopyrite-Bornite	$T = \left(\dfrac{0.20 \times 10^6}{\Delta_{Cp-Bn}} \right)^{1/2}$
Pyrite-Chalcopyrite	$T = \left(\dfrac{0.45 \times 10^6}{\Delta_{Py-Cp}} \right)^{1/2}$

4.1.7   Geothermometry: Samples, Data and Results

Five mineral pairs from this study were examined as geothermometers: one pair of anhydrite-chalcopyrite, one pair of molybdenite-chalcopyrite, two pairs of chalcopyrite-bornite and one pair of pyrite-chalcopyrite as outlined in Table 4.5. All mineral pairs appeared to be in equilibrium. Temperature estimates were calculated using equations outlined in Table 4.4. Overall, only four temperature estimates were obtained as one mineral pair (Cp-Bn from RC345-025) did not return a temperature value due to mathematical limitations. The calculated temperature estimate was 596 °C for the anhydrite-chalcopyrite pair, 273 °C for molybdenite-chalcopyrite, 380 °C for chalcopyrite-bornite and 1152 °C for the pyrite-chalcopyrite pair.

Table 4.5 Formation Temperature Estimates from Sulphur-Bearing Mineral Pairs

Mineral Pair		Original Sample	Depth (m)	Δ_{1-2}	T (K)	T (°C)
Minerals	Samples					
[1]Anhydrite-[2]Chalcopyrite	JNS-015 JNS-014	RC352-027	1159	10.652	869	**596**
[1]Molybdenite-[2]Chalcopyrite	JNS-022 JNS-023	RC345-041	1342	1.675	546	**273**
[1]Chalcopyrite-[2]Bornite	JNS-012 JNS-013	RC345-025	842	-0.145	*N/A*	*N/A*
[1]Chalcopyrite-[2]Bornite	JNS-009 JNS-010	RC352-021	840	0.470	653	**380**
[1]Pyrite-[2]Chalcopyrite	JNS-028 JNS-029	RC351-001	24	0.222	1425	**1152**

4.2 Stable Isotopes on Hydrosilicates - δD and δ^{18}O

Direct samples of hydrothermal fluids circulating at the time of porphyry formation cannot be taken. However, minerals that formed from hydrothermal alteration preserve the oxygen and hydrogen isotopic signature of the hydrothermal fluid. Analyzing the oxygen and hydrogen isotopic signature of alteration minerals formed by hydrothermal fluids, along with estimates of temperatures of formation, the isotopic content of the associated hydrothermal fluids can be inferred. The possible source(s) of these hydrothermal fluids can then be evaluated.

4.2.1 Systematics of δD and δ^{18}O Stable Isotopes

As H_2O is the dominant constituent of most ore-forming fluids, examining the oxygen and deuterium isotopic character of hydrothermal minerals is useful for determining the source and history of the hydrothermal fluids involved (Taylor, 1997). Oxygen has three stable isotopes: ^{16}O, ^{17}O, and ^{18}O and occur in 99.763 %, 0.0375 % and 0.1995 % natural abundance, respectively (Hoefs, 1997). The common isotopic ratio for oxygen is reported as δ^{18}O in per mil units (‰) and involves comparing the ratio of $^{18}O/^{16}O$ in a sample with that of an internationally recognized standard. The δ^{18}O of a sample is measured by:

$$\delta^{18}O = \left[\frac{^{18}O_{sample}/^{16}O_{sample}}{^{18}O_{std}/^{16}O_{std}} - 1 \right] \times 1000$$

The standard for oxygen is Vienna Standard Mean Ocean Water (VSMOW) which is set at a value of 0 ‰. An isotopic composition of δ^{18}O is reported as a value relative to this standard. Deuterium (^2D), the heavy isotope of hydrogen (^1H) naturally occurs in 0.0156 % abundance compared to 99.9844 % of ^1H (Hoefs, 1997). Similar to oxygen, the common isotopic ratio of

deuterium is reported as δD in per mil units (‰) and involves comparing the ratio of D/H in a sample to VSMOW (0 ‰). The δD of a sample is measured by:

$$\delta D = \left[\frac{\left(D/H \ sample \right)}{\left(D/H \ std \right)} - 1 \right] \times 1000$$

Once the oxygen and deuterium isotopic composition of a compound is measured, these values must be manipulated in order to extract the isotopic composition of the associated hydrothermal fluid. The fractionation factor (α) between two phases A and B (such as a hydrothermal mineral and associated H_2O) is:

$$\alpha_{A-B} = \frac{R_A}{R_B}$$

where R is the ratio of D/H or $^{18}O/^{16}O$. The fractionation (in per mil notation) between the two phases (A and B) can be equated with the isotopic composition in δ notation:

$$1000 \ ln \ \alpha_{A-B} = \delta_A - \delta_B$$

Equilibrium H- and O-isotope fractionation equations have been determined for different mineral-fluid phases based on experimental, empirical and/or theoretical data. In the oxygen isotope example of kaolinite-H_2O, the fractionation equation (Sheppard and Gilg, 1996) is:

$$1000 \ln \alpha_{Kaol-H_2O} = \left(2.76 \times \frac{10^6}{T^2} \right) - 7.7$$

Temperature (T) is in Kelvin. With a known oxygen isotopic composition of kaolinite and an estimate of the temperature of formation, or a temperature value obtained from directly measuring the fluid (e.g. fluid inclusion study) the oxygen isotopic content of the associated hydrothermal fluid (H_2O) can be calculated. The isotopic fractionation equations used in this study are given in Table 4.6.

Table 4.6 Oxygen and deuterium isotope fractionation equations for mineral-H$_2$O systems

Fractionation Equation	T (°C)	Reference	Isotope
$10^3 \ln \alpha_{Biotite-H_2O} = \left(3.84 \times 10^6 T^{-2}\right) + \left(-8.76 \times 10^3 T^{-1}\right) + 2.46$	0-1200	Zheng, 1993	Oxygen
$10^3 \ln \alpha_{Biotite-H_2O} = \left(-21.3 \times 10^6 T^{-2}\right) - 2.8$	450-800	Suzuoki and Epstein, 1976	Hydrogen
$10^3 \ln \alpha_{Illite/musc-H_2O} = \left(2.39 \times 10^6 T^{-2}\right) - 3.76$	0-700	Sheppard and Gilg, 1996	Oxygen
$10^3 \ln \alpha_{Illite/musc-H_2O} = -25 \pm 5$	120-400	Sheppard and Gilg, 1996	Hydrogen
$10^3 \ln \alpha_{Kaolinite-H_2O} = \left(2.76 \times 10^6 T^{-2}\right) - 6.75$	0-350	Sheppard and Gilg, 1996	Oxygen
$10^3 \ln \alpha_{Kaolinite-H_2O} = \left(-2.2 \times 10^6 T^{-2}\right) - 7.7$	0-300	Sheppard and Gilg, 1996	Hydrogen

4.2.2 **Methods of Analysis and Sample Data**

Twenty samples analyzed for δD and δ^{18}O isotopes include four secondary biotite-chlorite, three muscovite, seven illite and six kaolinite samples. Results are listed in Table 4.7. Secondary biotite-chlorite samples were drilled out of mafic phenocrysts whereas muscovite, illite and kaolinite samples underwent clay separation techniques in order to isolate the appropriate mineral from the rest of the sample (Appendix A4). All samples were analyzed by XRD to ensure the separation techniques were effective. Samples were weighed (~20-25 mg) and sent to the stable isotope laboratory at GNS Science in Gracefield, New Zealand.

Table 4.7 Oxygen and Hydrogen Isotope Data from Hydrosilicate Minerals at Red Chris

Mineral	Sample Number	Depth (m)	$\delta^{18}O_{mineral}$	$\delta D_{mineral}$	T (°C)	$\delta^{18}O_{H2O}$	δD_{H2O}
Secondary Biotite	RC354-022	916	5.8	-81.9	550	8.3	-47.7
Secondary Biotite	RC350-033	816	6.4	-80.4	550	8.9	-46.2
Secondary Biotite	RC353-025	1075	7.7	-77.8	550	10.2	-43.6
Secondary Biotite	RC350-042	997	6.8	-78.1	550	9.3	-43.9
Muscovite	RC345-001	44	9.9	-79	350	7.5	-54.0
Muscovite	RC106-018	139	10.3	-90.4	350	7.9	-65.4
Muscovite	RC348-010	335	10.7	-92.7	350	8.3	-67.7
Illite	RC349-003	84	11.5	-78.2	250	6.5	-53.2
Illite	RC349-003B	84	10.8	-76.6	250	5.8	-51.6
Illite	RC224-011	189	11.3	-78.5	250	6.3	-53.5
Illite	RC351-016	690	9.4	-80.9	250	4.4	-55.9
Illite	RC350-034	825	9.0	-80.6	250	4.0	-55.6
Illite	RC335-018	216	10.7	-85.1	250	5.7	-60.1
Illite	RC348-023	791	10.2	-79.1	250	5.2	-54.1
Kaolinite	RC349-009	248	8.7	-83.0	150	0.0	-63.0
Kaolinite	RC224-015	233	12.4	-83.1	150	3.7	-63.1
Kaolinite	RC345-012	417	11.3	-79.7	150	2.6	-59.7
Kaolinite	RC352-016	636	10.0	-79.5	150	1.3	-59.5
Kaolinite	RC351-032	1352	8.2	-77.0	150	-0.5	-57.0
Kaolinite	RC106-042	497	9.8	-78.8	150	1.1	-58.8

At the laboratory, oxygen was extracted from sample powders for isotope analyses using a CO_2-laser and BrF_5 (Sharp, 1990). Oxygen isotope values are reported in the familiar $\delta^{18}O$ notation, relative to VSMOW (Vienna Standard Mean Ocean Water, absolute isotope ratio (2005.20 ($\pm$ 0.45) x 10^{-6}; Baertschi, 1976). Samples were normalized to the international quartz standard NBS-28 using a value of +9.6 ‰. Values for four NBS-28 analyzed with the samples had values that varied by less than 0.15 ‰. Samples and standards were heated overnight to 150 °C prior to loading into the vacuum extraction line. These were then evacuated for approx 6 hours. Blank BrF_5 runs were done until yield was less than 0.2 µmoles oxygen. Oxygen yields were recorded and CO_2 gas analyzed on a Geo20-20 mass spectrometer.

For deuterium analysis, samples were analyzed on a HEKA tech high temperature elemental analyzer coupled with a GV Instruments IsoPrime mass spectrometer. Samples were pyrolyzed at 1450 °C, in silver capsules. All samples were analyzed in triplicate. All results are reported in δD notation, relative to VSMOW (Vienna Standard Mean Ocean Water, absolute isotope (155.76 ($\pm$ 0.05) x 10^{-6} Hagemann et al., 1970), normalized to international standards

IAEA-CH-7, NBS30 and NBS22 with reported δD values of -100 ‰, 66 ‰ and 118 ‰. The precision on the standards is 1.5 ‰.

No temperature data is currently available on minerals or mineral associations at Red Chris however such estimates could be attained through future fluid inclusion studies. All temperature estimates used in calculating δD$_{H2O}$ and δ^{18}O$_{H2O}$ are obtained from other studies undertaking similar analyses in similar environments. In the absence of known fluid temperatures, a range of temperature estimates was selected for each mineral-H$_2$O sample analyzed.

4.2.3   Results: Secondary Biotite-Chlorite (K-Silicate Alteration)

The four samples of secondary biotite-chlorite were analyzed for δD and δ^{18}O isotopes from coherent rocks of the Red Stock exhibiting K-silicate alteration and little to no clay (intermediate argillic) alteration. Mafic phenocrysts altered to secondary biotite ± chlorite were separated from the hand sample by a handheld Dremmel microdrill. The resultant powdered sample material was analyzed by XRD to ensure the presence of secondary biotite. Abundant chlorite was present in the samples as well as minor quartz, orthoclase, chalcopyrite and trace albite, pyrite, anhydrite, gypsum and dolomite-ankerite. It is assumed that the majority of the isotopic composition obtained was from secondary biotite-chlorite.

The secondary biotite-chlorite samples contain δ^{18}O$_{biotite}$ values between +5.8 and +7.7 ‰ and δD$_{biotite}$ values between -77.8 and -81.9 ‰. The temperature estimate used to calculate the fluid (H$_2$O) isotopic composition was based on temperatures used at Bajo de la Alumbrera of 550 to 700 °C (Harris et al., 2005). Using the calculations of Zheng (1993) and Suzuoki and Epstein (1976) listed in Table 4.6 and a formation temperature estimate of 550 °C, isotopic compositions were determined to be between +8.3 and +10.2 (‰) δ^{18}O$_{H2O}$ and between -43.6 and -47.7 (‰) δD$_{H2O}$ (Table 4.7). If a lower temperature is used to estimate fluid isotopic composition (~400 °C), there is a minimal (-0.4 ‰) shift in δ^{18}O, however there is a +15.6 ‰ shift in δD.

4.2.4   Results: Muscovite (Sericitic/Phyllic Alteration)

The three muscovite samples were selected on the basis of SWIR and XRD analyses from the isolated phyllic alteration zone (drillhole RC94-106) and from other areas that may be extensions of this zone. All samples are from altered rocks of the Red Stock. Clay separation

techniques isolated muscovite from the rest of the sample material. After clay separation, XRD analysis identified that muscovite was the dominant mineral in each sample along with minor quartz and carbonate as well as trace kaolinite in one of the samples. It is assumed that the majority of the isotopic composition obtained was from muscovite.

The muscovite samples contain $\delta^{18}O_{muscovite}$ values between +9.9 and +10.7 ‰ and $\delta D_{muscovite}$ values between -79.0 and -92.7 ‰. Temperature estimates on muscovite from Oyu Tolgoi (Khashgerel, 2009) range from 250 to 350 °C whereas temperature estimates are up to 400 °C at Bajo de la Alumbrera (Harris et al., 2005) for illite. Assuming the muscovite at Red Chris formed at or above formation temperatures of illite, a range of 250 to 400 °C is used for muscovite. Using the calculations of Sheppard and Gilg (1996) and a formation temperature estimate of 350 °C, $\delta^{18}O_{H2O}$ and δD_{H2O} isotopic compositions were determined to be between +7.5 and +8.3 (‰) $\delta^{18}O_{H2O}$ and between -54.0 and -67.7 (‰) δD_{H2O} (Table 4.7).

4.2.5   Results: Illite (Intermediate Argillic Alteration)

The seven illite samples from various locations and depths across the East zone were selected on the basis of SWIR and XRD analyses whereby illite was reported as the only clay mineral. All samples are from altered rocks of the Red Stock. Following clay separation, XRD analysis confirmed isolation of illite. Three of the seven samples reported minor kaolinite and six of the seven samples reported trace carbonate. It is assumed that the majority of the isotopic composition obtained was from illite.

The illite samples contain $\delta^{18}O_{illite}$ values between +9.0 and +11.5 ‰ and δD_{illite} values between -76.6 and -85.1 ‰. Temperature estimates on illite from Far Southeast-Lepanto (Hedenquist et al., 1998) range from 275 to 350 °C where as estimates are between 200 to 400 °C at Bajo de la Alumbrera (Harris et al., 2005). The formation temperature of illite may even be much lower than reported estimates. Assuming the illite at Red Chris formed at or below formation temperatures of muscovite, a range of 100 to 350 °C is used for illite. Using the calculations of Sheppard and Gilg (1996) and a formation temperature estimate of 250 °C, $\delta^{18}O_{H2O}$ and δD_{H2O} isotopic compositions were determined to be between +4.0 and +6.5 (‰) $\delta^{18}O_{H2O}$ and between -51.6 and -60.1 (‰) δD_{H2O} (Table 4.7).

4.2.6   **Results: Kaolinite (Intermediate Argillic Alteration)**

The six kaolinite samples were selected on the basis of TerraSpec analysis from various locations and depths across the East zone as well as different rock types. Two samples are from coherent Red Stock, two samples are magmatic-hydrothermal breccias of the Red Stock, one sample is from a deep raft of altered mafic-derived sedimentary rock and one sample is from a post-mineral dyke. The SWIR spectra for these samples appeared to have no interference from other minerals. However, after clay separation it became evident that five of the six samples contained significant sericite (illite or muscovite), minor quartz and trace carbonate, pyrite and chalcopyrite. Clay separation greatly distorts the true nature of illite/muscovite peak and the FWHM method is thus no longer suitable for distinguishing muscovite from illite. The isotopic composition, therefore, is obtained from a mixture of kaolinite and illite/muscovite.

The kaolinite samples contain $\delta^{18}O_{kaolinite}$ values between +8.2 and +12.4 ‰ and $\delta D_{kaolinite}$ values between -77.0 and -83.1 ‰. A temperature estimate of one late vug-filling kaolinite sample from Far Southeast-Lepanto (Hedenquist et al., 1998) is 100 °C however other kandite minerals (nacrite and dickite) have a temperature estimate of 150 °C and can form up to 200 °C (Reyes, 1990). Assuming the kaolinite at Red Chris formed at or below formation temperatures of illite, a range of 100 to 200 °C is used for kaolinite. Using the calculations of Sheppard and Gilg (1996) and a formation temperature estimate of 150 °C, $\delta^{18}O_{H2O}$ and δD_{H2O} isotopic compositions were determined to be between -0.5 and +3.7 (‰) $\delta^{18}O_{H2O}$ and between -57.0 and -63.1 (‰) δD_{H2O} (Table 4.7).

4.3   **Stable Isotopes on Carbonates –$\delta^{13}C$ and $\delta^{18}O$**

Analysis of carbon and oxygen isotopes in carbonate minerals at Red Chris can be used to identify the source for the carbonate-forming fluids. The carbonate alteration and veins may be related to the magmatic-hydrothermal fluids responsible for mineralization and associated alteration or may be from a later, cooler, unrelated fluid.

4.3.1   **Overview of Carbonates at Red Chris**

Carbonate alteration at Red Chris is locally pervasive in the upper portions of the East zone. The groundmass and local phenocrysts are altered to a ferroan-carbonate, imparting a dull beige and pale orange colour to the rock. Abundant carbonate veins (LC1, LC2) are seen throughout the East zone, at all depth levels investigated, commonly filling in pre-existing veins.

In sulphide deposits, carbonate minerals frequently occur later in the paragenetic sequence than the sulphide minerals. It is believed that carbonate found within quartz ± sulphide ± oxide veins (E3, S1-6) earlier in the paragenetic sequence is the result of infill by later carbonate and not part of the sulphide-precipitating fluid. Carbonate veins range from straight to discontinuous, white to beige-orange and are locally vuggy. Carbonate also occurs as breccia cement with clasts of altered monzodiorite and contained quartz ± sulphide ± oxide veins. Most of the carbonate veins appear late in the paragenetic sequence cross-cutting all other vein types in the system except for the latest chlorite veinlets (LC3).

The carbonate compositions vary spatially and temporally (Baker et al., 1999) and it is believed that the iron content in the carbonate veins generally decreases through the paragenetic sequence. Baker et al. (1999) analyzed carbonate material using an electron microprobe and determined that carbonate occurring with K-silicate alteration was siderite, the carbonate formed during quartz-sericite-carbonate alteration (quartz-muscovite-pyrite in this study) was ankerite, and the late stage carbonate alteration formed an ankerite-dolomite composition. Additionally, the carbonate formed during chlorite-carbonate alteration (propylitic?) in the study by Baker et al. (1999) was calcite. XRD analysis on carbonate vein material identified ankerite-dolomite as the predominant carbonate species along with minor siderite and calcite. Ankerite-dolomite was also reported in XRD analysis of carbonate altered host rock. An evolution through siderite-ankerite-dolomite-calcite is recognized in cross-cutting vein relationships of this study. Where visible, siderite forms darker orange oxidation rims on beige ankerite-dolomite veins, suggesting that siderite was a pre-existing vein which was later exploited by a less Fe-rich ankerite-dolomite vein. Calcite is pale to near translucent carbonate which locally filled in vugs and centerlines in ankerite-dolomite veins. Ankerite and dolomite are difficult to distinguish from one another in XRD patterns, thus the term ankerite-dolomite is used. In fact, the carbonate present is likely a mixture of an ankerite-dolomite composition as reported by Baker et al. (1999). Analysis of δ^{13}C and δ^{18}O on carbonate minerals may suggest a source fluid for the carbonate and possibly indicate whether the carbonate alteration/veins are associated with intermediate argillic alteration.

4.3.2 Systematics of δC and δ^{18}O Isotopes in Carbonates

Carbon has two stable isotopes ^{12}C and ^{13}C which naturally occur in 98.89 % and 1.11 % abundance respectively (Hoefs, 1997). The common isotopic notation for carbon is reported as

$\delta^{13}C$ in per mil units (‰) and involves comparing the ratio of $^{13}C/^{12}C$ in a sample with that of an internationally recognized standard. The $\delta^{13}C$ of a sample is measured by:

$$\delta^{13}C = \left[\frac{^{13}C_{sample} / ^{12}C_{sample}}{^{13}C_{std} / ^{12}C_{std}} - 1 \right] \times 1000$$

The standard for carbon isotopic studies is from the Chicago PDB (Belemnite from the Peedee Fm.) which is defined to have a $^{13}C/^{12}C$ value of 0.0112372 (Craig, 1957) or Vienna Peedee Belemnite (VPDB). Aqueous carbon species important in ore-forming fluids may include $CO_{2(aq)}$, H_2CO_3, HCO_3^-, CO_3^{2-} and $CH_{4(aq)}$ and their isotopic character is largely controlled by T, $f O_2$ and pH (Ohmoto, 1972). The total isotopic value of carbon in a sample is determined by the isotopic value of carbon for each of the species involved. The effect of pressure on the isotopes of carbon is negligible at P ~< 10 kbar. When in equilibrium, the heavier isotope (^{13}C) will preferentially fractionate into the carbon species with the highest valence (most oxidized), resulting in $\delta^{13}C_{CO2 \text{ (and carbonate minerals)}} > \delta^{13}C_{C \text{ (organic matter, graphite, diamond)}}$ (Ohmoto and Goldhaber, 1997). The isotopic signature of a sample may incorporate carbon derived from magmatic fluids (CO_2), from carbonate-bearing rocks (limestone), or due to reduced carbon from organic matter or graphite. Each of these carbonate reservoirs has a distinct range of $\delta^{13}C$ values which may be useful for identifying carbon source(s).

Oxygen has three stable isotopes: ^{16}O, ^{17}O, and ^{18}O and occur in 99.763 %, 0.0375 % and 0.1995 % natural abundance, respectively (Hoefs, 1997). The common isotopic ratio for oxygen is reported as $\delta^{18}O$ in per mil units (‰) and involves comparing the ratio of $^{18}O/^{16}O$ in a sample with that of an internationally recognized standard. The $\delta^{18}O$ of a sample is measured by:

$$\delta^{18}O = \left[\frac{^{18}O_{sample} / ^{16}O_{sample}}{^{18}O_{std} / ^{16}O_{std}} - 1 \right] \times 1000$$

The standard for oxygen is Vienna Standard Mean Ocean Water (VSMOW) which is set at a value of 0 ‰. An isotopic composition of $\delta^{18}O$ is reported as a value relative to this standard. Oxygen within a carbonate mineral may originate from a range of sources, with isotopic signatures varying between +40 and -55 ‰ (Campbell and Larson. 2005). Meteoric water has the lightest isotopic signature, ranging from 0 ‰ (sea water) to -55 ‰. Igneous rocks and fluid

generally have oxygen isotope contents of 5-10 ‰, but have been recorded to range from 0 to over 15 ‰ (Campbell and Larson, 2005). Modern marine limestone has a signature of ~30 ‰ $\delta^{18}O$ whereas old limestone can be lighter, ~20 ‰. Atmospheric CO_2 is the heaviest reservoir of $\delta^{18}O$, with a signature near 40 ‰.

4.3.3 **Samples**

Thirty-eight samples of vein carbonate material were analyzed for $\delta^{18}O$ and $\delta^{13}C$. These samples were selected on the basis of containing enough material for analysis, the location within the East zone as well as the relative position in the paragenetic sequence. Most of samples analyzed are from LC1 ± LC2 vein-sets as they are the most abundant and contain the most carbonate material. Of the vein carbonate samples, 13 were mechanically separated from the host rock by hammer and ground to a powder using mortar and pestle. The 25 other vein carbonate samples were drilled out of the host rock using a hand-held Dremmel micro-drill. All of the 13 samples that were mechanically separated from host rock material by hammer were contaminated by some degree by pyrite from the vein carbonate material, whereas the 25 samples that were separated by micro-drill were not contaminated by pyrite. The presence of pyrite was determined by XRD.

4.3.4 **Comparison of Two Methods of $\delta^{18}O$ and $\delta^{13}C$ Analysis**

All 38 samples were initially analyzed using the prototype Los Gatos Research (LGR) high-CO_2 concentration isotopic analyzer at the University of British Columbia, Canada. However the results indicated that pyrite contamination might have skewed the carbon and oxygen isotopic signature. Two samples with visible pyrite contamination reported erroneous isotopic concentrations and the data was discarded. In order to determine the effect of pyrite contamination on carbon and oxygen isotopic analysis by the LGR, a subset of 10 samples was selected for analysis on the Delta PlusXL mass spectrometer at the University of British Columbia, Canada. Of the 10 samples run on the Delta, 4 were contaminated with pyrite and 6 samples were not.

Samples analyzed on the prototype Los Gatos Research (LGR) high-CO_2 concentration isotopic analyzer were acidified with phosphoric acid to convert carbonate to CO_2, which is then analyzed and the CO_2 concentration is used to calculate final $\delta^{18}O$ and $\delta^{13}C$ values. Approximately 35 mg of pure carbonate material is required for accurate and precise analyses

and samples containing other minerals may require more amount of material to be acidified to obtain the optimum CO_2 concentration for analysis. It is known that the presence of sulphide minerals in the sample, particularly chalcopyrite and arsenopyrite, will produce H_2S when acidified with phosphoric acid and will yield unreliable isotopic results. The precision of the analyzer is approximately $\pm$ 0.3 ‰ for $\delta^{13}C$ and $\pm$ 0.5 ‰ for $\delta^{18}O$, depending on the care with which the analyses are undertaken. Analyses were corrected for fractionation using repeat analyses of UBC internal carbonate standard BN 13. Results were corrected for ankerite fractionation (for $\delta^{18}O$) and are reported in relation to standards; PDB for $\delta^{13}C$ and VSMOW for $\delta^{18}O$.

The additional analyses of 10 samples were carried out using the gas bench and a Delta PlusXL mass spectrometer in continuous flow mode. Samples were acidified with 99 % phosphoric acid in helium-flushed sealed vials, and the headspace gas was measured in a helium flow. The analyses were corrected for fractionation using repeat analyses of UBC internal carbonate standards BN 13, BN 83-2, H6M. These have been calibrated against international standards NBS 18 and 19. Results were corrected for ankerite fractionation and are reported in relation to standards; VPDB for $\delta^{13}C$ and VSMOW for $\delta^{18}O$.

Of the 10 samples analyzed by the Delta, the 4 samples that contain pyrite experienced significant shifts in $\delta^{18}O$ values (average 10.0 ‰ shift) and moderate shifts in $\delta^{13}C$ values (average 1.3 ‰ shift) when compared to results of the LGR (Figure 4.2A, Table 4.8). The 6 samples (and 2 duplicate runs) lacking pyrite contamination experienced minor shifts in $\delta^{18}O$ values (average 0.5 ‰ shift) as well as minor shifts in $\delta^{13}C$ values (average 0.5 ‰ shift) when compared to results of the LGR (Figure 4.2B, Table 4.8). Results of this method comparison are twofold: 1) pyrite contamination can lead to significant errors in carbon and oxygen isotopic analysis by the LGR; and 2) results from the Delta are consistent with values reported by the LGR (~0.5 ‰ differences in $\delta^{18}O$ and $\delta^{13}C$) on non-pyrite contaminated samples and therefore confirm the applicability of the LGR as a valid method for carbon and oxygen isotopic analysis.

Table 4.8 Comparison of Two Methods of Carbon and Oxygen Isotopic Analysis

Sample Number	Delta PlusXL Mass Spectrometer		LGR Desktop Analyzer		Absolute Difference	
	$\delta^{13}C$ (‰, VPDB)	$\delta^{18}O$ (‰, VSMOW)	$\delta^{13}C$ (‰, PDB)	$\delta^{18}O$ (‰, VSMOW)	$\delta^{13}C$ (‰)	$\delta^{18}O$ (‰)
Pyrite Contaminated Samples						
JNS-001	-1.8	12.5	-3.1	8.0	1.3	4.5
JNS-002	-2.3	14.2	-3.3	11.8	1.0	2.4
JNS-006	-3.7	17.7	-5.4	-0.6	1.7	18.3
JNS-011	-4.4	18.5	-3.1	3.9	1.3	14.6
				Average	**1.3**	**10.0**
Non-Contaminated Samples						
JNS-021	-3.4	14.3	-3.4	14.4	0	0.1
JNS-024	-4.4	14.9	-4.4	15.1	0	0.2
JNS-024 *(duplicate)*	-4.1	14.7	-4.4	15.1	0.3	0.4
JNS-033	-1.8	12.1	-2.2	11.1	0.4	1.0
JNS-035	-5.8	11.6	-6.5	11.9	0.7	0.3
JNS-040	-3.1	13.4	-4.1	12.5	1.0	0.9
JNS-042	-3.6	18.2	-4.3	18.6	0.7	0.4
JNS-042 *(duplicate)*	-3.7	18.1	-4.3	18.6	0.6	0.5
				Average	**0.5**	**0.5**

4.3.5 **Results of $\delta^{18}O$ and $\delta^{13}C$ Analysis**

Overall, 36 samples yielded reliable $\delta^{18}O$ and $\delta^{13}C$ results (Table 4.9), either from results of LGR (n=32) or Delta (n=4) analyses. Two additional samples were discarded due to the presence of visible sulphide. Samples that were contaminated by pyrite but were not re-analyzed using the Delta are included with the results as they plot within the ranges of the rest of the data. The actual isotopic signature of these samples may be skewed and any interpretation based on these samples is carried out with caution. The reported results from all uncontaminated carbonate samples are from the LGR analysis. The final $\delta^{13}C$ values range between -1.8 and -6.5 ‰ (average -3.9 ‰) and the $\delta^{18}O$ values range between +9.9 and +19.0 ‰ (average +14.1 ‰).

Table 4.9 Carbon and Oxygen Stable Isotope Data from Carbonate Samples at Red Chris

Sample	Original Sample	Depth (m)	Sample Weight (mg)	$\delta^{13}C$ (PDB)	$\delta^{18}O$ (SMOW)	XRD Results - Carbonate Species ± Sulphide	Method Of Analysis	Notes
JNCO-001	RC224-009	163	90	-1.8	12.5	ankerite-dolomite, siderite, calcite, **pyrite**	Delta	
JNCO-002	RC224-010	183	85	-2.3	14.2	siderite, ankerite-dolomite, calcite, **pyrite**	Delta	
JNCO-003	RC079-012	269	82	-5.2	11.0	ankerite-dolomite, **pyrite**	LGR	Data used, plots in range
JNCO-004	RC079-014	305	48	-4.9	16.2	ankerite-dolomite, calcite, **Pyrite**	LGR	Data used, plots in range
JNCO-005	RC106-002	13	109	-5.0	19.0	ankerite-dolomite, calcite, **pyrite**	LGR	Data used, plots in range
JNCO-006	RC106-033	323	161	-3.7	17.7	ankerite-dolomite, calcite, **pyrite**	Delta	
JNCO-007	RC106-037	404	84	-4.7	-18.4	N/A	LGR	Visible sulphide, discarded
JNCO-008	RC335-021	255	80	-4.5	13.1	ankerite-dolomite, calcite, **pyrite**	LGR	Data used, plots in range
JNCO-009	RC335-025	285	124	-3.1	9.9	ankerite-dolomite, calcite, **pyrite**	LGR	Data used, plots in range
JNCO-010	RC335-028	313	83	-3.5	13.8	ankerite-dolomite, calcite, **pyrite**	LGR	Data used, plots in range
JNCO-011	RC335-008	88	252	-4.4	18.5	ankerite-dolomite, **pyrite**	Delta	
JNCO-012	RC335-039	505	320	N/A	N/A	N/A	LGR	Visible sulphide, discarded
JNCO-013	RC335-062	887	85	-3.9	17.3	ankerite-dolomite, calcite	LGR	
JNCO-019	RC351-019	846	40	-3.2	11.9	ankerite-dolomite	LGR	
JNCO-020	RC351-021	931	42	-2.8	11.9	ankerite-dolomite	LGR	
JNCO-021	RC352-009	370	39	-3.4	14.4	ankerite-dolomite, siderite	LGR	
JNCO-022	RC352-013	505	41	-3.6	15.3	ankerite-dolomite, calcite ± siderite	LGR	
JNCO-023	RC352-020	800	42	-3.1	12.9	ankerite-dolomite	LGR	
JNCO-024	RC352-026	1105	40	-4.4	15.1	ankerite-dolomite, calcite	LGR	
JNCO-025	RC348-002	59	42	-3.5	15.1	ankerite-dolomite	LGR	
JNCO-026	RC348-017	548	41	-3.0	13.0	ankerite-dolomite	LGR	
JNCO-027	RC348-032	1176	41	-4.0	11.7	ankerite-dolomite, calcite	LGR	
JNCO-028	RC354-005	202	42	-4.2	17.2	ankerite-dolomite, calcite	LGR	
JNCO-029	RC345-008	295	40	-4.7	16.8	ankerite-dolomite	LGR	
JNCO-030	RC345-016	574	42	-4.6	11.5	ankerite-dolomite	LGR	
JNCO-031	RC345-032	1043	41	-5.5	15.8	ankerite-dolomite, calcite	LGR	

Sample	Original Sample	Depth (m)	Sample Weight (mg)	$\delta^{13}C$ (PDB)	$\delta^{18}O$ (SMOW)	XRD Results - Carbonate Species ± Sulphide	Method Of Analysis	Notes
JNCO-032	RC349-015	368	41	-3.6	15.0	ankerite-dolomite	LGR	
JNCO-033	RC349-026	636	39	-2.2	11.1	ankerite-dolomite	LGR	
JNCO-034	RC349-028	653	41	-3.3	15.4	ankerite-dolomite	LGR	
JNCO-035	RC349-048	1142	40	-6.5	11.9	ankerite-dolomite, calcite	LGR	
JNCO-036	RC350-021	725	41	-3.6	12.9	ankerite-dolomite	LGR	
JNCO-037	RC350-025	757	40	-3.4	15.4	ankerite-dolomite	LGR	
JNCO-038	RC350-039	917	41	-5.1	13.6	ankerite-dolomite, calcite	LGR	
JNCO-039	RC350-041	970	39	-3.9	12.2	ankerite-dolomite	LGR	
JNCO-040	RC353-005	187	39	-4.1	12.5	ankerite-dolomite	LGR	
JNCO-041	RC353-012	495	40	-4.1	12.8	ankerite-dolomite	LGR	
JNCO-042	RC140-002	14	39	-4.3	18.6	ankerite-dolomite	LGR	
JNCO-043	RC140-021	657	40	-2.5	10.5	ankerite-dolomite	LGR	

Stable isotope data from vein material plotted as δ^{13}C ‰ vs. δ^{18}O ‰ displays a reasonable spread in results (Figure 4.2). Samples are divided into six categories on the basis of carbonate species (ankerite-dolomite, calcite, siderite) and the presence of pyrite, identified by XRD analysis. Nineteen samples contain ankerite-dolomite (blue), 13 contain ankerite-dolomite + calcite (red), and 4 samples contain ankerite-dolomite + siderite ± calcite (green). Squares (n=10) represent samples which were analyzed after the first field season (from above 325 m depth) and due to the method of carbonate separation, vein pyrite was inadvertently incorporated into the sample. Four of these samples were analyzed on the Delta, likely reporting more accurate results. Additionally, 6 samples contain pyrite and were not analyzed on the Delta and the reported isotopic composition is from the LGR and likely reports inaccurate results however they plot within the range of the rest of the data. Circles (n=26) represent samples analyzed after the second field season (from above 1175 m depth) and do not contain any vein pyrite as the method of carbonate separation was refined.
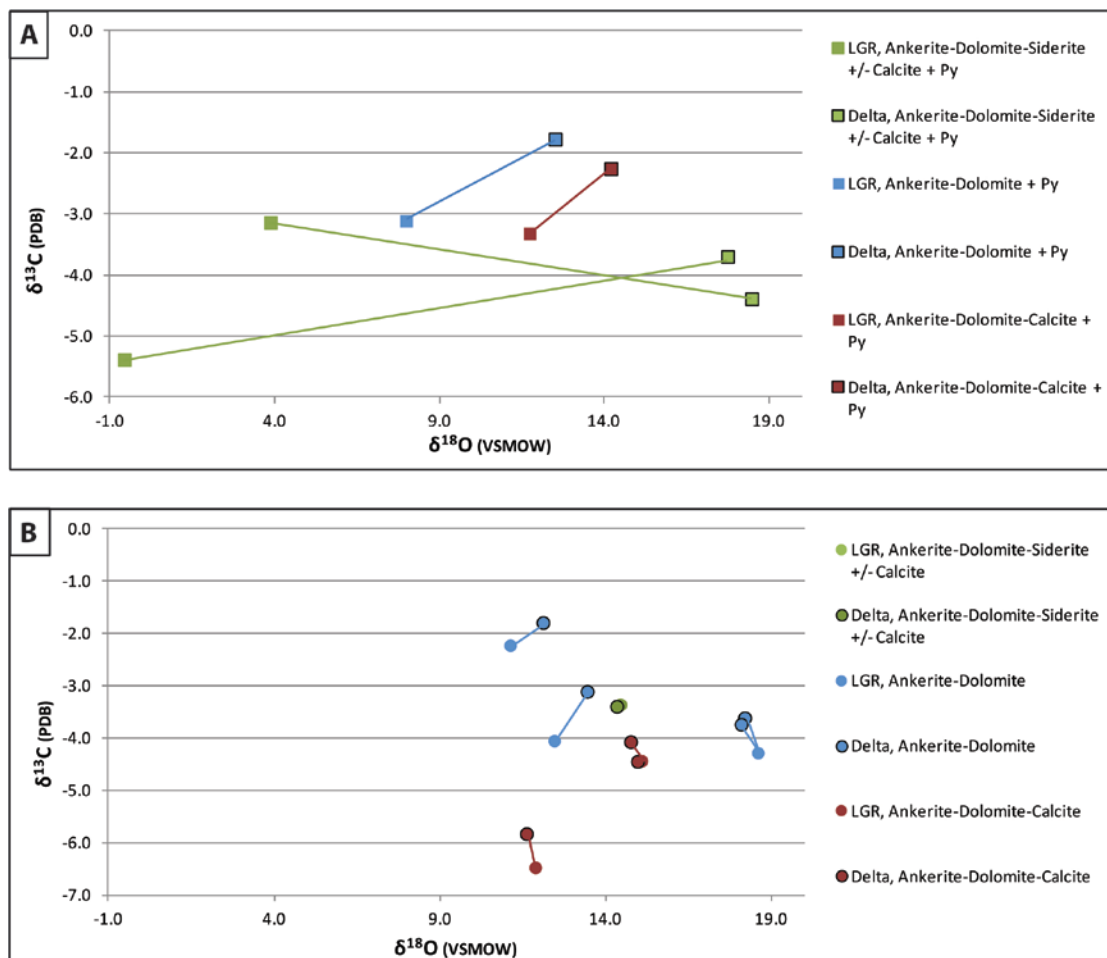
Figure 4.2 Comparison of carbon and oxygen isotopic data on carbonate material between the Los Gatos Research Desktop Analyzer (LGR) and the Delta Mass Spectrometer. A: Pyrite contaminated samples display moderate and significant shifts in δ^{18}O and moderate shifts in δ^{13}C; B: Carbonate-only samples display minor to moderate shifts in δ^{18}O and δ^{13}C. Solid lines link individual samples.

144

The data displays a broad cluster between +9.9 and +19.0 δ^{18}O ‰ and between -1.8 and -6.5 δ^{13}C ‰. The ankerite-dolomite + calcite samples (red circles and squares on Figure 4.3) appear to be slightly more depleted in δ^{13}C than the other samples (blue and green circles and squares on Figure 4.3). This depletion may result from the late calcite infill having a depleted δ^{13}C signature compared to the ankerite-dolomite ± siderite, and when the minerals were analyzed in a mixture, the result is only slight δ^{13}C depletion.
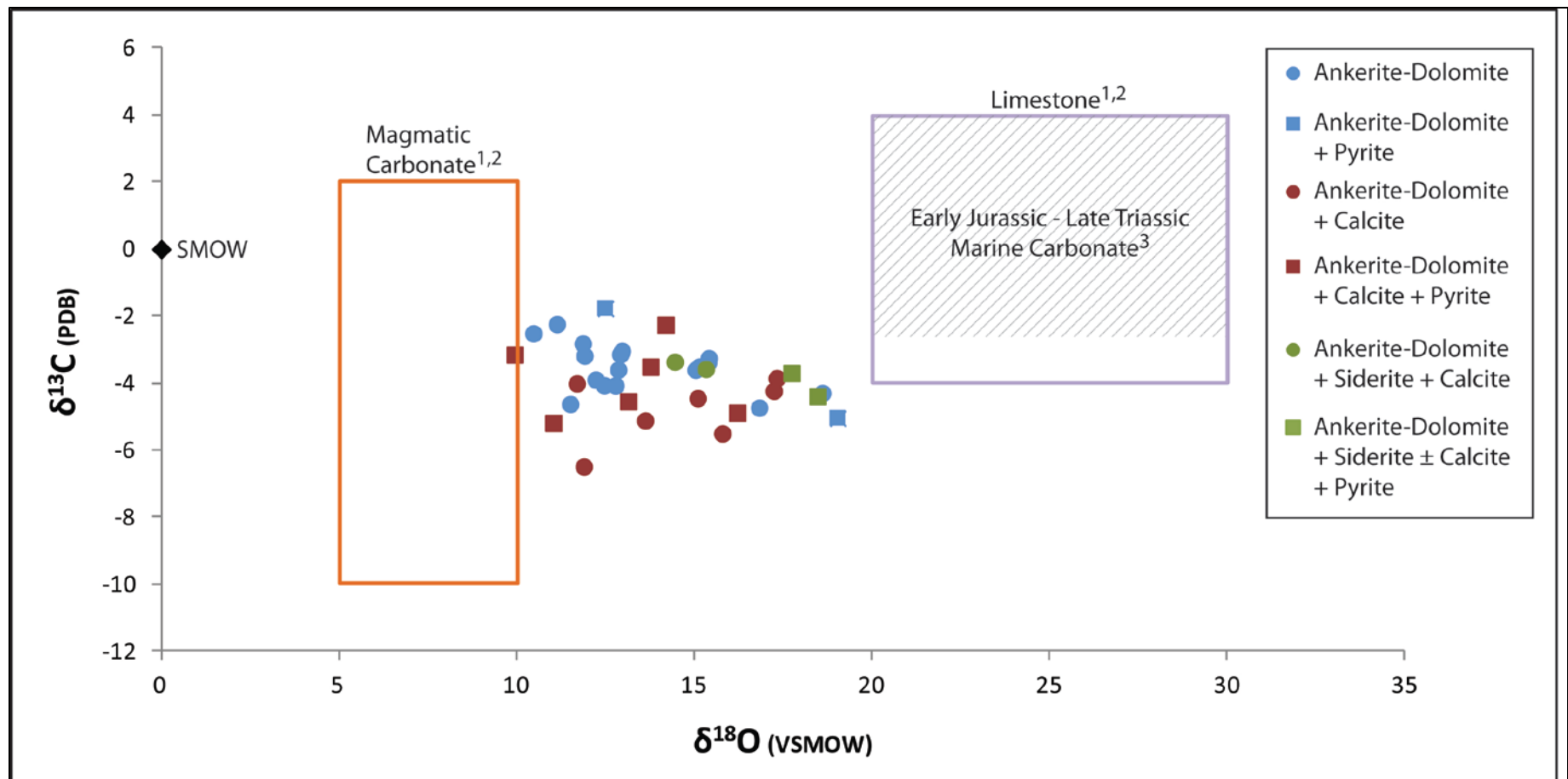
Figure 4.3 Stable isotope data from vein-carbonate material at Red Chris on a plot of $\delta^{13}C$ ‰ (PDB) vs. $\delta^{18}O$ ‰ (VSMOW) with boxes of carbon and oxygen resevoirs: magmatic carbonate (orange) and limestone (purple); after [1]Ohmoto and Rye (1979) for $\delta^{13}C$, [2]Campbell and Larson (2005) for $\delta^{18}O$, and [3]Veizer et al., (1999) for $\delta^{13}C$ ‰ of Early Jurassic-Late Triassic marine carbonate (diagonal lines). Samples contain varying species of carbonate, as identified by X-ray diffraction: ankerite-dolomite (blue); ankerite-dolomite + calcite (red); and ankerite-dolomite + siderite ± calcite. Samples are further differenatiated as those containing carbonate (circles) and carbonate + pyrite (squares).

There is no relationship between carbonate isotopic signature and paragenesis, as most of the carbonate was sampled from Late Carbonate veins (LC1 ± LC2). Carbonate from veins earlier in the paragenetic sequence is infill from these later veins. There is however, some notable features when carbonate mineralogy, δ^{13}C (Figure 4.4A) and δ^{18}O (Figure 4.4B) are compared with elevation of the sample. Ankerite-dolomite is always present and is therefore found at all depths sampled. Siderite was only reported in samples above ~1000 m elevation however this could reflect a sampling bias. Notably, calcite is present in two restricted locations: between 1200 and 1500 m elevation; and below ~600 m elevation. This may also indicate a sampling bias yet is still an intriguing distribution. The slight depletion in δ^{13}C in ankerite-dolomite + calcite samples is more pronounced in the samples below ~600 m elevation, however overall, δ^{13}C values are consistent across all elevations. Samples below 1100 m elevation have δ^{18}O values between 10 and 16 ‰ and samples above 1100 m elevation generally have δ^{18}O values between 12 and 20 ‰ (pyrite-bearing samples not analyzed on the Delta are excluded from this observation).
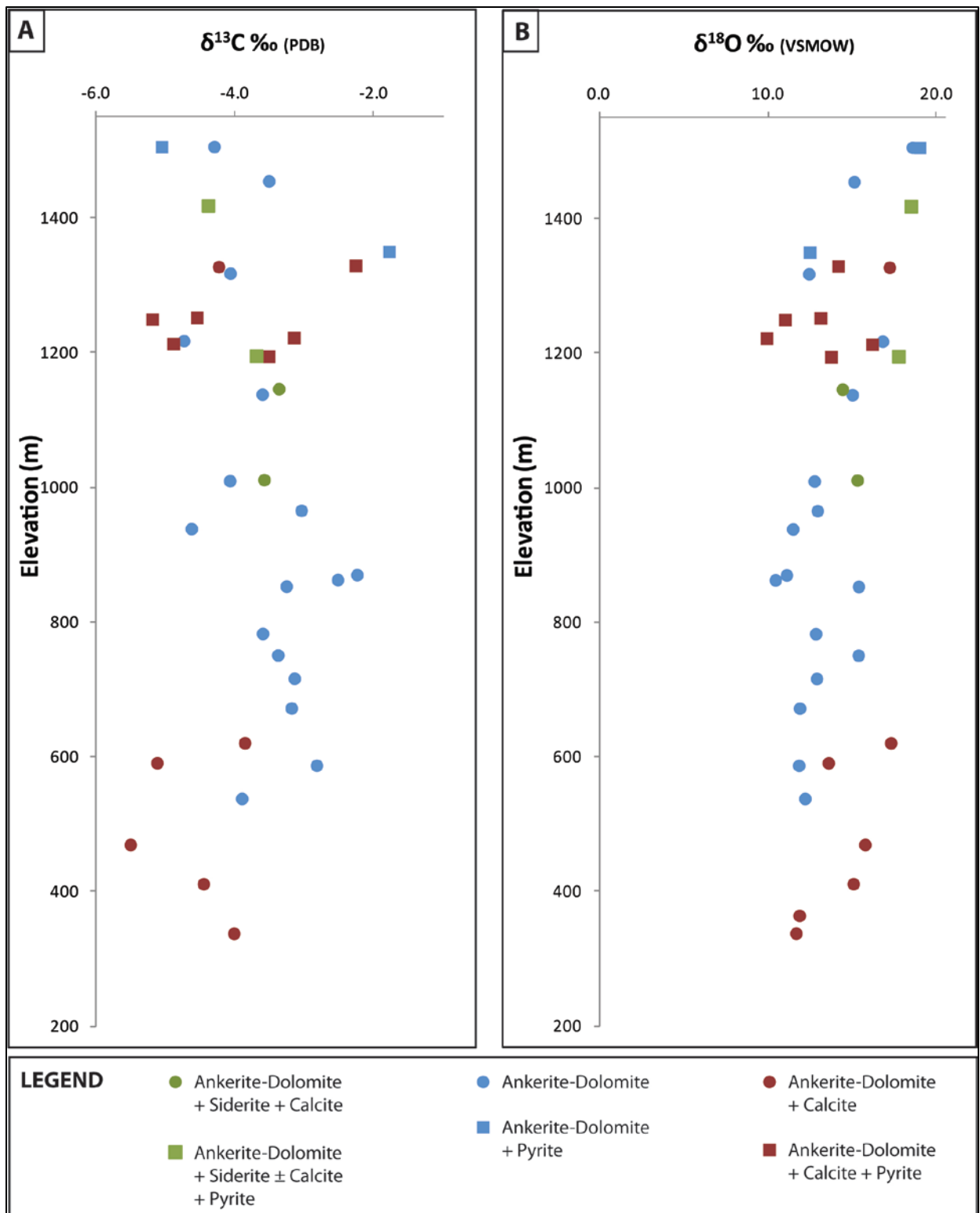
Figure 4.4 Variation in carbon and oxygen isotope data with elevation (m). A: $\delta^{13}C$ ‰ (PDB) vs. sample elevation (m); and B: $\delta^{18}O$ ‰ (VSMOW) vs. sample elevation (m).

148

4.4   Discussion

Results from stable isotopic studies on sulphur, hydrosilicate, and carbonate minerals provide information on the source and evolution of the internal magmatic and external meteoric fluids during the formation of Red Chris. Stable isotopic studies on sulphate and sulphide minerals indicate the temperature and oxidation state of magmatic fluids that produced a distinct sulphur zonation pattern. Isotopic analysis of oxygen and deuterium on hydrosilicate minerals provides evidence for high temperature alteration from a magmatic fluid and for the influx of meteoric fluid responsible for low temperature, late stage clay alteration. Additionally, isotopic studies on carbon and oxygen from carbonate minerals are consistent with a magmatic fluid that possibly experienced some degree of mixing with a meteoric fluid. Each of these stable isotopic studies help to constrain different stages in the evolution of the hydrothermal system at Red Chris.

4.4.1   Sulphur Isotope Studies at Porphyry Deposits

Sulphur isotopic studies of both alkalic and calc-alkalic porphyry deposits report that the majority of $\delta^{34}S$ values range between -3 and +1 ‰ for sulphides and between +8 and +15 ‰ for sulphates (Ohmoto and Rye, 1979). Diversions outside the $\delta^{34}S_{sulphide}$ range, especially to more negative values, are more common in alkalic porphyry deposits.

Negative $\delta^{34}S_{sulphide}$ values reported in the core of mineralized zones at several alkalic porphyry deposits such as Galore Creek, Mt. Milligan and the Cadia district can be explained by two processes. The depletion may be a result of magmatic-hydrothermal processes, or by incorporation of an additional highly depleted, external sulfur source, such as biogenic sulphide (Wilson et al., 2007). It is assumed that there is no sedimentary sulphide in the volcano-sedimentary wall-rocks at Red Chris, and that the negative $\delta^{34}S_{sulphide}$ values reported are a result of magmatic-hydrothermal processes. Additionally, at Galore Creek, no evidence of a biogenic sulphur source exists and ^{34}S fractionation may have been influenced by the volcanic wall-rocks (Micko, 2010). Further, there is no evidence for the addition of a biogenic sulphur source at the Cadia district or at Mt. Milligan (Wilson et al., 2007; Jago et al., In Press).

4.4.2   Effect of Temperature and Oxidation State on ^{34}S Fractionation

Temperature and oxidation state control fractionation of ^{34}S and resultant sulphur isotopic zonation patterns observed at porphyry deposits. Due to the preferential fractionation of ^{34}S into

the more oxidized aqueous sulphur species (Ohmoto and Goldhaber, 1997), under equilibrium conditions, an abundance of oxidized sulphur in a hydrothermal fluid can result in lower $\delta^{34}S_{sulphide}$ values (Ohmoto and Rye, 1979; Rye et al., 1992; Rye 1993). H_2S and SO_2 are the dominant sulphur species present in high-temperature (> 400 °C) magmatic fluids associated with porphyry copper deposits (Rye, 1993) and can produce aqueous sulphate at temperatures below 400 to 350 °C from the following hydrolysis reaction (Rye et al., 1992):

$$4\ H_2O + 4\ SO_2 = H_2S + 3\ H^+ + 2\ HSO_4^-$$

Therefore, a highly oxidized (sulfate-rich) magmatic fluid could deposit sulphide minerals with negative $\delta^{34}S_{sulphide}$ values. The oxidation state of the fluid is therefore controlled by the ratio of H_2S/SO_4 in a fluid. Under oxidizing conditions ($H_2S/SO_4=0.2$), cooling of a magmatic fluid from 600 through 250 °C will produce a wide-range in $\delta^{34}S_{sulphide}$ values that become increasingly depleted in ^{34}S with decreasing temperature (Wilson et al., 2007, Rye, 1993). Additionally, the same conditions will result in a narrow range in $\delta^{34}S_{sulphate}$ values. However, under reducing conditions ($H_2S/SO_4=5$) the range in $\delta^{34}S_{sulphide}$ will be narrow and the range of $\delta^{34}S_{sulphate}$ will be large (Wilson et al., 2007; Rye, 1993).

At Red Chris, the overall range and value (positive or negative) $\delta^{34}S_{sulphide}$ and $\delta^{34}S_{sulphate}$ values do not definitively indicate a highly oxidized or highly reduced magmatic fluid. Although the narrow range in $\delta^{34}S_{sulphide}$ values (-1.9 to +1.9 ‰) suggest a reduced magmatic fluid, the narrow range in $\delta^{34}S_{sulphate}$ values (+9.4 to +11.5 ‰, from pure anhydrite) and the weakly negative $\delta^{34}S_{sulphide}$ values (below ~1000 m depth) suggest that the magmatic fluid was oxidized. The magmatic fluids at Red Chris are interpreted to have been weakly oxidized and contained minor sulphate compared to alkalic porphyry deposits that exhibit greater depletion in $\delta^{34}S_{sulphide}$ such as at Galore Creek (-17 to -4 ‰, Micko, 2010), the Cadia District (-10 to -4 ‰, Wilson et al., 2007) and Mt. Milligan (-5 to -3 ‰, Jago et al., In Press) which represent highly oxidized, sulphate-rich fluids. Compiled by Ohmoto and Rye (1979), major calc-alkalic porphyry deposits such as Butte, Bingham, Chino, Ajo, Sierrita, Twin Butte, and Morococha have $\delta^{34}S_{sulphide}$ values commonly ranging between -3 and +5 ‰. The values are consistent with the $\delta^{34}S_{sulphide}$ values reported at Red Chris, representing weakly oxidized, minor sulphate-bearing magmatic fluids.

4.4.3   Geothermometry of Magmatic Fluids Using Sulphur Isotope Mineral Pairs

The best mineral pairs for geothermometry are those that have the largest temperature dependence of fractionation (Campbell and Larson, 2005). This is demonstrated in Figure 4.5

(after Ohmoto and Rye, 1979), illustrating the fractionation of various sulphur minerals and compounds with respect to H₂S. Mineral pairs which have the greatest difference in slope have the greatest dependence on temperature, and therefore make the best geothermometers. For example, pyrite (FeS) and galena (PbS) have the most different slopes in Figure 4.5 and is therefore the best geothermometer, whereas chalcopyrite (CuFeS₂) and sphalerite (ZnS) have the most similar slopes and do not make a very good geothermometer.
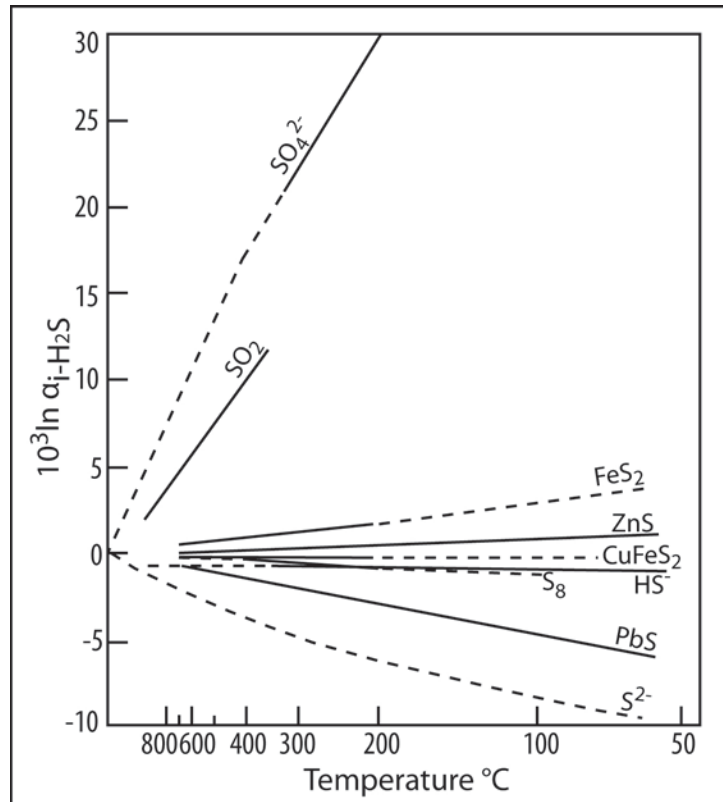
Figure 4.5 Equilibrium fractionation of various sulphur compounds relative to H₂S. Dashed lines are extrapolated or theoretically calculated. Solid lines are experimentally determined (redrafted from Ohmoto and Rye, 1979).

From Figure 4.5, it would be expected that sulphide-sulphate mineral pairs would make the best geothermometers, however it has been demonstrated by Ohmoto and Lasaga (1982) that aqueous sulphide and sulphate components are not likely to be in equilibrium below 300 °C (Campbell and Larson, 2005). In this study however, the sulphate-sulphide pair (anhydrite-chalcopyrite, sample RC352-027) from vein material of Early Vein (E2) was interpreted to be deposited in equilibrium during high-temperature, potassic alteration at temperatures above 300 °C and therefore anhydrite-chalcopyrite is a suitable geothermometric pair and the 596 °C temperature estimate is a reasonable value.

The chalcopyrite-bornite pair (sample RC352-021), reporting a formation temperature of 380 °C was taken from Sulphide Vein (S3). As the chalcopyrite-bornite pair was deposited after the anhydrite-chalcopyrite pair, a lower formation temperature for the chalcopyrite-bornite pair is expected. The 380 °C formation temperature reflects the gradual cooling of the porphyry system and indicates that chalcopyrite and bornite was deposited during a high, albeit not the highest temperature regime. In a study of fluid inclusions from the Bajo de la Alumbrera Cu-Au porphyry deposit, Ulrich et al. (2001) reported that efficient (85 %) deposition of copper ore by chalcopyrite precipitation from magmatic brines occurred as fluid inclusions were cooled from ~400 to 320 °C. Overall, the study proposed that much of the copper and gold was precipitated from magmatic brines below saturation temperatures near 400 °C, which is consistent with the 380 °C formation temperature of high grade copper and gold-bearing S3 veins at Red Chris.

A temperature estimate could not be calculated from the other chalcopyrite-bornite mineral pair (sample RC345-025) due mathematical constraints. The difference between the $\delta^{34}S$ values of bornite and chalcopyrite in this sample was very small. It is possible that these minerals were not deposited in equilibrium or that the contained sulphur isotopic content had been modified after deposition. Additionally, due to the nature of cross-cutting veins, the chalcopyrite and bornite of this sample may have inadvertently been sampled from different vein sets.

The molybdenite-chalcopyrite pair (sample RC345-041), reporting a formation temperature of 273 °C was sampled from a quartz-molybdenite-chalcopyrite ± pyrite vein of Early Vein set E2. This temperature is lower than expected as the Early Veins are considered to have formed at the highest-temperature. Molybdenite is known to form halos around the high-temperature, mineralized cores of porphyry deposits (Sillitoe, 2000), and this mineral pair was taken from a sample at 1342 m depth, suggesting that the lower than expected temperature could be a result of the molybdenite and chalcopyrite forming outboard (although spatially deeper) from the higher-temperature core. This calculated temperature may also reflect the unsuitability of a molybdenite-chalcopyrite mineral pair as an accurate geothermometer.

The pyrite-chalcopyrite pair (sample RC351-001) was taken from a quartz-pyrite-chalcopyrite vein (P1) in the pyrite halo. The reported value of 1152 °C is extremely high and likely not a true temperature of formation. The pyrite halo and associated veins are some of the youngest veins to form and a much lower formation temperature would be expected from this

zone. It is likely that the pyrite and chalcopyrite from this sample were not deposited in equilibrium, or may have had their sulphur isotopic content adjusted after formation.

Geothermometry using sulphur isotopes from sulphur-bearing mineral pairs provides evidence for cooling of the magmatic system through time. Three of the five sulphur-bearing mineral pair samples reported reasonable temperature of formation estimates. The anhydrite-chalcopyrite mineral pair (vein set E2) reported the highest temperature (596 °C), consistent with forming from high-temperature fluid, at or before the onset of K-silicate alteration. A chalcopyrite-bornite pair (vein set S3) reported an intermediate formation temperature (380 °C), which also are consistent with the paragenetic sequence and reflects cooling of the system. These sulphide minerals formed after the highest-temperature Early Veins during K-silicate and chlorite-sericite alteration and represent most of the high-grade ore in the deposit. The molybdenite-chalcopyrite pair reported a slightly-lower than expected value (273° C) and likely reflects the unsuitability of a molybdenite-chalcopyrite geothermometer. The pyrite-chalcopyrite mineral pair reported an unreasonable temperature estimate, indicating disequilibrium and/or sulphur isotopic adjustment. Overall, the three mineral pairs that yielded reasonable temperature estimates are consistent with the vein paragenesis and associated alteration and indicate the gradual temporal and spatial cooling of the magmatic-hydrothermal system.

4.4.4   Effect of Fluid-Rock Interaction on Sulphur Isotopes

The negative $\delta^{34}S_{sulphide}$ values occurring below ~1000 m depth can be explained by an oxidized (sulphate-bearing) magmatic fluid, however, cooling of this magmatic-hydrothermal fluid alone will not produce the transition to positive $\delta^{34}S_{sulphide}$ values reported upward and outward from the ^{34}S depleted, deeper region of the deposit. The interaction of magmatic-hydrothermal fluid with the rock it encounters and resultant chemical reactions is responsible for the change in ^{34}S fractionation, which produces the observed sulphur isotopic zonation pattern. As the magmatic fluid interacts with iron-bearing minerals (hornblende) in the rock, aqueous sulphate is inorganically reduced to sulphide at the same time ferrous iron is oxidized to ferric iron (Wilson, et al., 2007). At Red Chris, ferrous iron (Fe^{2+}) of hornblende phenocrysts was altered to ferric iron (Fe^{3+}) to form secondary biotite and magnetite during K-silicate alteration. Inorganic reduction of sulphate to sulphide and the formation of magnetite were produced as follows:

$$12\ FeO_{(rock)} + SO_4{}^{2-}{}_{(aq)} + 2\ H^+{}_{(aq)} = 4\ Fe_3O_4 + H_2S_{(aq)}$$

153
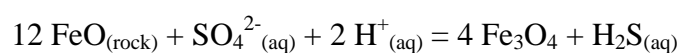
As sulphate is continually reduced to sulphide, ^{34}S will preferentially fractionate into sulphide as the amount of sulphate in the system decreases and the H_2S/SO_4 ratio changes, which in turn, increases $\delta^{34}S_{sulphide}$ values towards 0 ‰. The magmatic-hydrothermal fluid continues to react with increasing volumes of rock and greater amounts of ferrous iron are reduced and eventually no sulphate remains in the fluid. ^{34}S will then preferentially fractionate into H_2S, producing positive $\delta^{34}S_{sulphide}$ values.

Overall, the sulphur isotopic zonation observed at Red Chris can be explained by an initial high-temperature (~596 °C) oxidized magmatic-hydrothermal fluid that undergoes inorganic sulphate reduction caused by oxidation of ferrous iron-bearing minerals during fluid-rock interaction. The negative $\delta^{34}S_{sulphide}$ values observed in the deep regions of the deposit formed under high-temperature oxidizing conditions however the oxidation state changed about the same time as the onset of K-silicate alteration whereby the magmatic-hydrothermal fluid interacted with iron in hornblende phenocrysts to form magnetite. Simultaneously, sulphate was inorganically reduced to sulphide which gradually incorporated greater amounts of ^{34}S during K-silicate and chlorite-sericite alteration as the system cooled through ~380 °C and produced $\delta^{34}S_{sulphide}$ values towards 0 ‰. Eventually, after significant interaction between the rock and magmatic-hydrothermal fluid and cooling of the system around the time of sericitic (phyllic) alteration, sulphide minerals (especially pyrite) formed with positive $\delta^{34}S_{sulphide}$ values.

4.4.5 $\delta^{18}O$ and δD Evidence for a Magmatic Fluid from Alteration Minerals

Additional evidence for the presence of magmatic hydrothermal fluids is preserved in the isotopic signature of hydrothermal alteration minerals produced during fluid-rock interaction. Oxygen and deuterium incorporated into secondary biotite, chlorite and muscovite during different stages of alteration can be measured and compared to known fluid reservoirs.

Results of δD and $\delta^{18}O$ fluid compositions are plotted in Figure 4.6 in relation to the meteoric water line (Craig, 1961) and the kaolinite line (Savin and Epstein, 1970; Zhou, 1994). Further, results are compared to a range of fluid compositions from various sources: water discharged from high temperature fumaroles on andesitic volcanoes, termed 'volcanic vapour' (Giggenbach, 1992); water dissolved in 'felsic magmatic melts' (Taylor, 1992); and water dissolved in 'primary magmatic melts' (Taylor, 1974). Error bars on samples represent

calculated δD and δ^{18}O fluid compositions over a range in possible formation temperatures (See Legend, Figure 4.6).
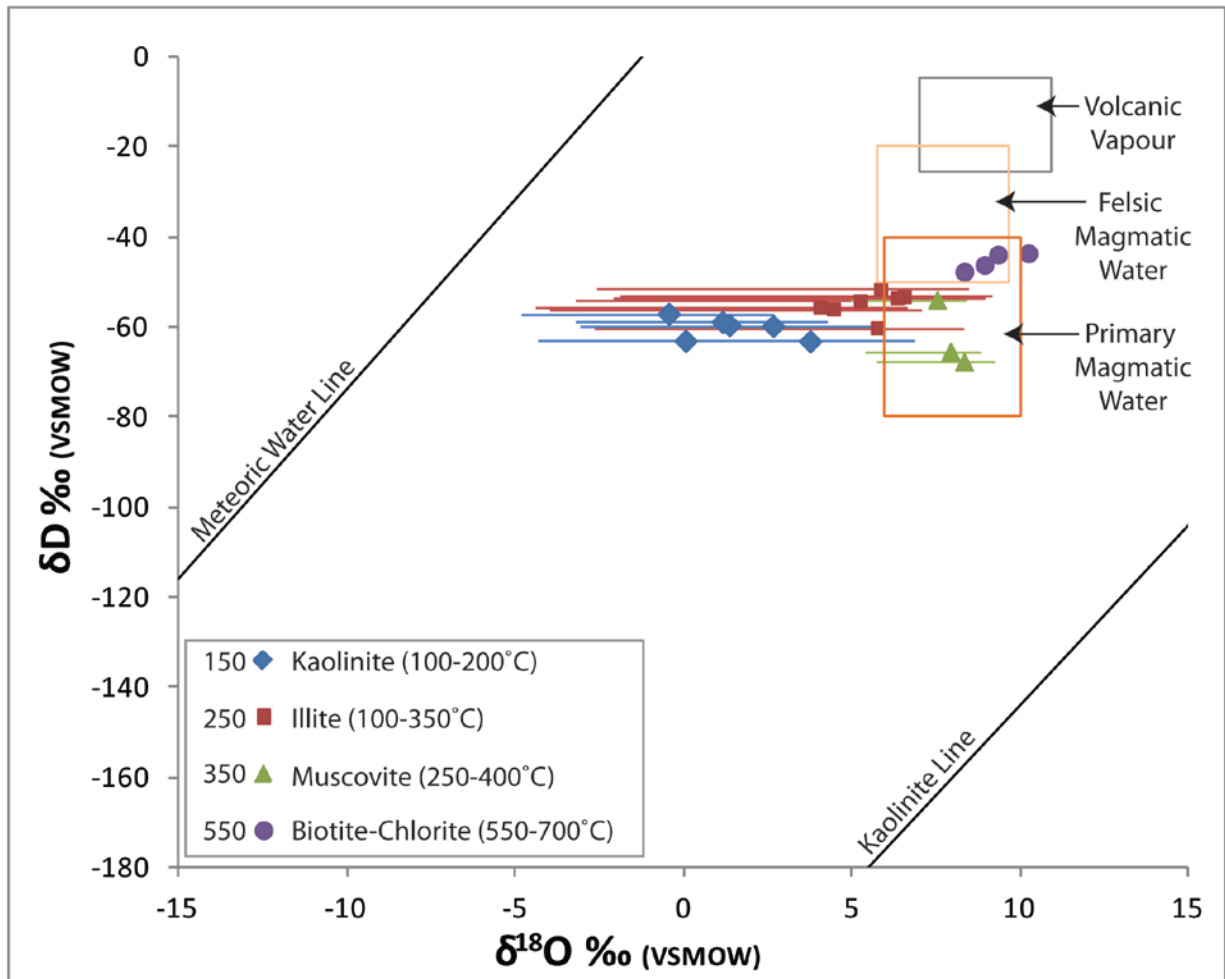
Figure 4.6 Plot of δD vs. δ^{18}O (‰, VSMOW) for H$_2$O calculated from mineral samples: biotite-chlorite (550 ˚C); muscovite (350 ˚C); illite (250 ˚C) and kaolinite (150 ˚C) at Red Chris. The range of compositions of water discharged from high temperature fumaroles on andesitic volcanoes if outlined by the box labelled 'volcanic vapour' (Giggenbach, 1992), and range of composition of water dissolved in felsic and primary melts are outlined by the boxes labelled 'felsic magmatic water' (Taylor, 1992) and 'primary magmatic water' (Taylor, 1974). Meteoric water line (Craig, 1961) and kaolinite line (Savin and Epstein, 1970; Zhou, 1994) plotted for reference.

The fluid associated with the formation of secondary biotite (K-silicate alteration) and chlorite (chlorite-sericite alteration) plots on Figure 4.6 within (or adjacent to) the compositional ranges of 'felsic magmatic water' and 'primary magmatic water' (Taylor, 1992; Taylor, 1974). When a lower temperature of formation is assumed for secondary biotite (400 °C), the δD fluid values shift +15.6 ‰, plotting well within the range of 'felsic magmatic water' of Taylor (1992). This indicates that the fluid associated with K-silicate alteration and subsequent chlorite-sericite alteration is of magmatic origin, as expected from fluids of a porphyry deposit.

Further to the evidence from K-silicate and chlorite-sericite alteration, the fluid associated with the formation of muscovite (sericitic/phyllic alteration) plots on Figure 4.6 below the box of 'felsic magmatic water' (Taylor, 1992) yet within the box of 'primary magmatic water' (Taylor, 1974). This suggests muscovite formed from a magmatic-hydrothermal fluid that was depleted in δD compared to the magmatic fluid that formed K-silicate and sericite-chlorite alteration. Within a shallow intrusive environment, as exsolution proceeds, the δD of the remaining dissolved H_2O will become increasingly depleted and, it follows, that so must the δD of the expelled aqueous phase (Taylor, 1997; Hedenquist and Richards, 2005). Thus, the fluid that forms an alteration mineral assemblage that has exsolved from a highly degassed magma (late-stage) will have a uniformly depleted δD_{H2O} signature compared to fluids associated with earlier stages of alteration (Hedenquist and Richards, 2005). A 10 to 20 ‰ δD_{H2O} depletion is observed between muscovite and biotite-chlorite samples and is interpreted as a result of the degassing phenomenon. The δD_{H2O} depletion indicates that the fluids associated with sericitic/phyllic alteration formed during a late-stage, degassed fluid sometime after K-silicate alteration. Overall, the δD_{H2O} and $\delta^{18}O_{H2O}$ composition indicates that the hydrothermal fluid associated with sericitic/phyllic alteration is of magmatic origin.

4.4.6 $\delta^{18}O$ and δD Evidence for Magmatic-Meteoric Fluid Mixing

Evidence for mixing of the magmatic fluid with an external meteoric fluid is reflected in the oxygen and deuterium isotopes incorporated into illite and kaolinite during the late-stage intermediate argillic alteration. The fluids associated with the formation of illite (intermediate argillic alteration) plot on Figure 4.6 just within and outside of the box of primary magmatic water (Taylor, 1974). The depletion of $\delta^{18}O_{H2O}$ in illite samples compared to muscovite samples is a result of magmatic fluid mixing with meteoric fluid at the time of illite formation. This shift towards the meteoric water line indicates that intermediate argillic alteration is associated with mixed magmatic-meteoric fluids.

The fluids associated with the formation of kaolinite (intermediate argillic alteration) plot on Figure 4.6 outside of the box of primary magmatic water (Taylor, 1974). Further $\delta^{18}O_{H2O}$ depletion occurs in the kaolinite samples suggesting that the greatest extent of magmatic- and meteoric-fluid mixing recorded by hydrothermal alteration minerals occurred during kaolinite formation. Although illite and kaolinite both compose the intermediate argillic alteration association, kaolinite exhibits an isotopic signature indicative of greater fluid mixing and is

generally restricted to the upper 300 m of the East zone. These phenomena are likely due to the temperature of formation of kaolinite being lower than that of illite. Below 300 m depth the temperature of the cooling porphyry system favoured the formation of illite, whereas above 300 m depth the temperature favoured the formation of kaolinite. Any residual magmatic fluid that circulated at such a shallow level in the system would also likely experience a greater degree of mixing with meteoric fluid and therefore have a more depleted $\delta^{18}O_{H2O}$ isotopic composition. Minor amounts of kaolinite alteration noted in the system at significant depths indicate that cool, magmatic-meteoric mixed fluid circulated deep into the system, likely along preferential fluid pathways, such as lithological contacts after the porphyry system cooled. After the system cools to pre-porphyry intrusion temperatures, fluids circulating through the rocks are entirely meteoric.

4.4.7 $\delta^{18}O$ and $\delta^{13}C$ Evidence for a Magmatic ± Meteoric Fluid Source of Carbonate

Carbonate material at Red Chris could have been sourced from various reservoirs: a local limestone unit; magmatic fluid; or a magmatic fluid mixed with a low-temperature meteoric fluid. Using known $\delta^{18}O$ and $\delta^{13}C$ signatures from these reservoirs, possible carbonate reservoirs can be plotted on a $\delta^{13}C$ vs. $\delta^{18}O$ diagram and compared to analyzed data (Figure 4.3). Limestone has a $\delta^{18}O$ composition between +20 and +30 ‰ (Campbell and Larson, 2005) and a $\delta^{13}C$ composition between -3 and +4 ‰ (Ohmoto and Rye, 1979). At Red Chris, a small body of calcarenite and minor limestone of the Hazelton Group (unit **EJHl** on Figure 2.7) has been mapped adjacent to the South Boundary Fault near its southwest contact with the Red Stock. Additionally, several thin, linear units of limestone (unit **LTrSl** on Figure 2.6) have been mapped north of Ealue Lake. Carbonate forming in a marine environment in Late Triassic to Early Jurassic time would have carbon isotopic values between -1.5 and +4 ‰ $\delta^{13}C$, as measured from brachiopod shells (Veizer et al., 1999). If the carbonates at Red Chris formed as a result of incorporating carbonate from a local limestone unit, the $\delta^{13}C$ values would reflect this. If this were the case at Red Chris, as the system cooled (increase in $\delta^{18}O$) and incorporated more carbon from limestone, the $\delta^{13}C$ values would indicate a trend toward more enriched (positive) values. Such a trend is not recognized in the $\delta^{13}C$ values at Red Chris and indicates that the carbonate material is not sourced from a local limestone unit.

Carbon in granitic, mafic and ultramafic rocks commonly have $\delta^{13}C$ compositions between -10 and +2 ‰ (Ohmoto and Rye 1979) and fresh igneous rocks have a $\delta^{18}O$

composition between +5 and +10 ‰ (Campbell and Larson, 2005). Whereas carbonate minerals at Red Chris reflect a magmatic source on the basis of their $\delta^{13}C$ signature the $\delta^{18}O$ signature does not correlate with reported values. Although magmatic fluids have a typical $\delta^{18}O$ composition between +5 and +10 ‰, values to 0 ‰ and greater than 15 ‰ have also been reported (Campbell and Larson, 2005). The +10 to +20 ‰ $\delta^{18}O_{mineral}$ range of carbonate minerals at Red Chris may in fact reflect a magmatic fluid.

Using the $\delta^{18}O$ composition for magmatic fluids that formed secondary biotite during K-silicate alteration, along with fractionation factors of carbonate species, a carbonate-forming magmatic fluid $\delta^{18}O_{mineral}$ range can be calculated for temperatures below 400 °C. The oxygen isotope fractionation equation for biotite-H_2O (see section 4.2.1) can be used to calculate a magmatic fluid composition at 400 and 550 °C. Four samples of secondary biotite return $\delta^{18}O_{H2O}$ values between 7.9 and 10.2 ‰, representing the range in oxygen isotopic signature of the magmatic fluid. Assuming that the magmatic hydrothermal fluid which formed the secondary biotite also formed the carbonate, the $\delta^{18}O_{H2O}$ signature is the same. Thus, the following holds true:

$$\delta^{18}O_{Ankerite} = \delta^{18}O_{H2O(magmatic\ from\ biotite)} + 10^3 ln\alpha_{Ankerite\text{-}H2O}$$

Using fractionation equations for ankerite from Zheng (1999) at 100, 200, 300 and 400 °C, a range of $\delta^{18}O_{Ankerite}$ values is calculated and tabulated in Table 4.10.

Table 4.10 Calculated $\delta^{18}O_{carbonate}$ for a Carbonate-Forming Magmatic Fluid

Ankerite $10^3 ln\alpha_{Ankerite\text{-}H2O} = (4.120 \times 10^6 T^{-2}) + (-4.62 \times 10^3 T^{-1}) + 1.71$ (Zheng, 1999)					
T (°C)	$\delta^{18}O_{H2O(magmatic)}$ LOW T	$\delta^{18}O_{H2O(magmatic)}$ HIGH T	$10^3 ln\alpha_{Ankerite\text{-}H2O}$	$\delta^{18}O_{Ankerite}$ LOW T	$\delta^{18}O_{Ankerite}$ HIGH T
100	7.9	10.2	18.92	26.8	29.1
200	7.9	10.2	10.35	18.3	20.6
300	7.9	10.2	6.19	14.1	16.4
400	7.9	10.2	3.94	11.8	14.1

Overall, calculated $\delta^{18}O_{Ankerite}$ values range between +26.8 and +29.1 ‰ (100 °C), +18.3 and +20.6 ‰ (200 °C), +14.1 and 16.4 (300 °C) and +11.8 and +14.1 ‰ (400 °C). Thus, depending on temperature the magmatic fluid forming the carbonates could have a $\delta^{18}O$ composition between +11.8 and 29.1 ‰. Much of the $\delta^{18}O$ and $\delta^{13}C$ data plot in this range and indicates that the carbonates at Red Chris could have formed from a cooling magmatic fluid between 100 and 400 °C (Figure 4.7).
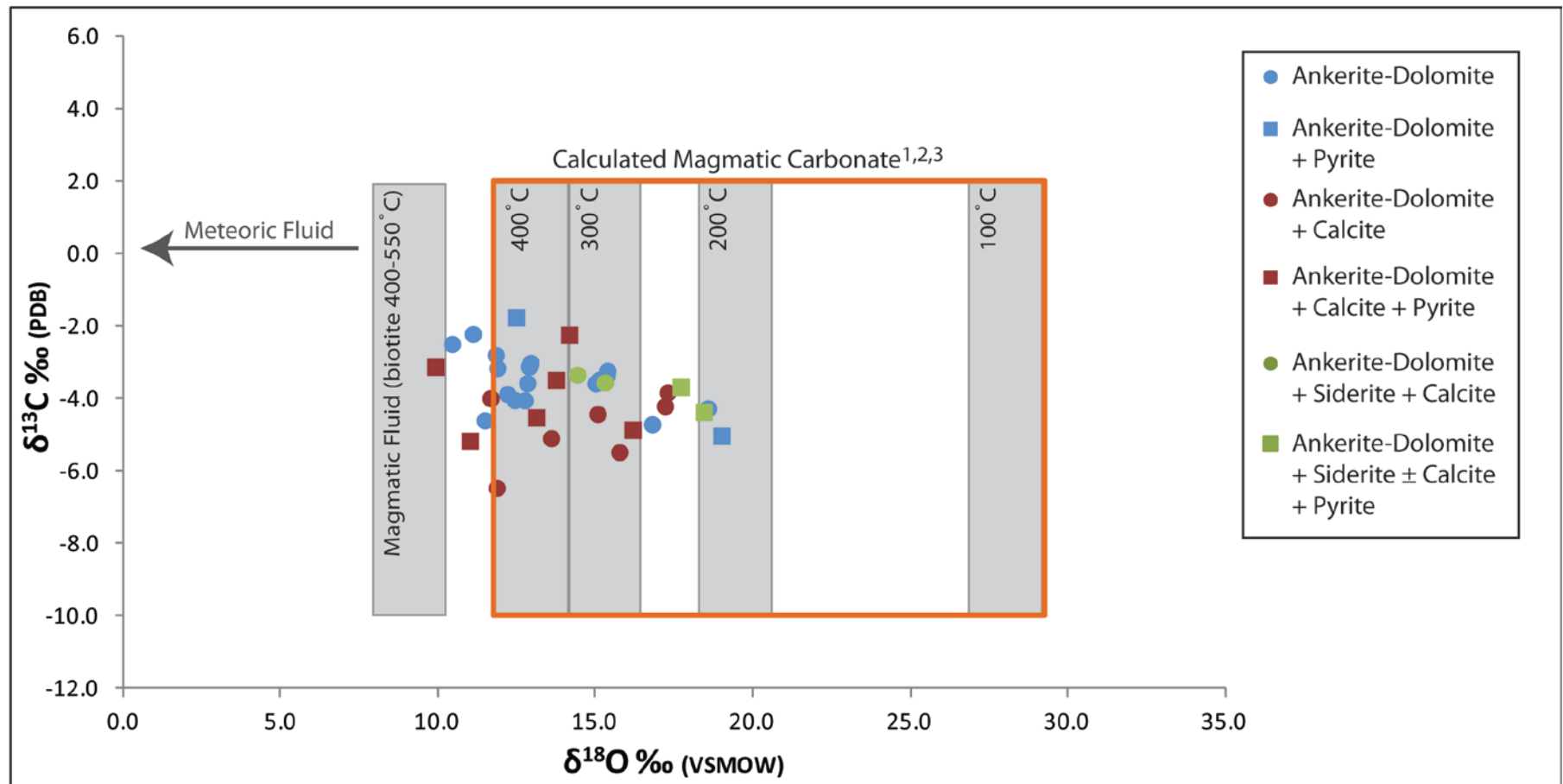
Figure 4.7 Stable isotope data from vein-carbonate material at Red Chris on a plot of $\delta^{13}C$ ‰ (PDB) vs. $\delta^{18}O$ ‰ (SMOW). The 'calculated magmatic carbonate' box is drafted from values of magmatic fluid whereby $\delta^{13}C$ ‰ is taken from [1]Ohmoto and Rye (1979) and [2]Campbell and Larson (2005) and $\delta^{18}O$(carbonate) ‰ is calculated from hydrothermal biotite at 400-550 °C taken to be equivalent to carbonate forming fluids between 100 and 400 °C ([3]Zheng, 1999). Samples contain varying species of carbonate, as identified by X-ray diffraction: ankerite-dolomite (blue); ankerite-dolomite + calcite (red); and ankerite-dolomite + siderite ± calcite. Samples are further differenatiated as those containing carbonate (circles) and carbonate + pyrite (squares).

A slight increase in δ^{18}O signature occurs above ~1100 m elevation (Figure 4.4). Samples below 1100 m elevation have δ^{18}O values between 10 and 16 ‰ and samples above 1100 m elevation generally have δ^{18}O values between 12 and 20 ‰ (pyrite-bearing samples not analyzed on the Delta are excluded from this interpretation). It is possible that this increase in δ^{18}O in the upper 400 m of the East zone may have undergone oxygen exchange during low temperature intermediate argillic alteration. Intermediate argillic alteration formed from a mixed magmatic-meteoric fluid and any oxygen exchange of such fluids with carbonate would likely impart a partial meteoric oxygen isotopic signature on the carbonate minerals. Isotopic exchange with a meteoric fluid would shift carbonate values towards 0 ‰ δ^{18}O, not towards more enriched values toward 20 ‰, as observed. Therefore, this slight shift in the upper 400 m is likely not related to isotopic exchange with a meteoric fluid (which partially formed intermediate argillic alteration). The slight increase in δ^{18}O reflects a temperature gradient within the system whereby the carbonates forming closer to the surface contain oxygen isotopic signatures reflective of a lower temperature regime.

Overall, the carbon and oxygen isotopic analyses of vein carbonate material are consistent with a magmatic fluid with possibly some degree of mixing with a meteoric fluid. Without temperature estimates on the carbonate minerals (which could be investigated in the future by fluid inclusion studies) the carbonate isotopic study can be interpreted in two ways: 1) the carbonates formed from a magmatic fluid at temperatures between 200-400 °C and higher with little to no mixing with meteoric fluid or 2) the carbonates formed from a magmatic fluid at temperatures below 200 °C and mixed with meteoric fluid to reflect the current isotopic composition, shifted towards a meteoric signature (0 to -55 ‰ δ^{18}O, Campbell and Larson, 2005).

4.4.8 Relationship of Carbonate to Other Recognized Alteration Assemblages

It has been indicated through oxygen and deuterium isotopic analysis of illite and kaolinite (intermediate argillic alteration) that there is evidence for mixing of magmatic and meteoric fluids; therefore it is possible that carbonates also formed under these mixed-fluid conditions. Additionally, both carbonate veins and intermediate argillic alteration are recognized as late-stage events in the evolution of the porphyry system. However, minor chlorite veinlets (LC3) are observed to locally cross-cut carbonate veins, indicating that the system was under the influence of higher temperature (chlorite-forming) fluids after carbonate formation and thus,

carbonate alteration and veins are likely not formed from a significantly mixed magmatic-meteoric fluid event (similar to intermediate argillic alteration) but are a part of the late stage hydrothermal system, higher in temperature than intermediate argillic alteration.

Additionally, it is not likely that carbonate veins and alteration are directly associated with intermediate argillic alteration, as the conditions of formation are very different for carbonate minerals and clay minerals, especially kaolinite. Fluid temperature estimates from isotopic analysis on carbonates at Red Chris suggest a 400 to 200 °C magmatic fluid. However, the stability of lower temperature minerals, illite and kaolinite in the absence of high temperature minerals, such as muscovite and dickite, restricts formation of intermediate argillic alteration to temperatures below ~200 °C (Seedorff et al., 2005).

4.5   Conclusions

Analysis of sulphur, oxygen, deuterium, and carbon isotopes have led to an understanding of the evolution of the hydrothermal fluids involved in the mineralization and alteration of Red Chris. Sulphur isotopes provide evidence for the temperature and oxidation state of the magmatic fluid responsible for the deposition of Cu and Au-bearing sulphide minerals. Oxygen and deuterium isotopic analysis on hydrosilicate minerals were used to interpret magmatic and mixed magmatic-meteoric fluid sources responsible for the various stages of hydrothermal alteration. Additionally, carbon and oxygen isotopes were used to interpret a magmatic ± meteoric source of carbonate minerals and ultimately place the carbonate veins and alteration in context with relation to other alteration events in the system. Ultimately, an understanding of the fluid sources, their interaction with the wall-rocks and the resultant alteration can be compiled into a series of distinct alteration events.

Zonation in $\delta^{34}S$ is a feature that has been recognized in the East zone at Red Chris as well as in other alkalic porphyry deposits in British Columbia such as Mount Polley, Galore Creek, Mt. Milligan, Afton and Lorraine (Dyell and Tosdal, 2005, Jago et al., In Press). The vertical and lateral zonation at Red Chris provides evidence for fluid evolution at the deposit and also has implications for the utilization of sulphur isotopes in exploration in the area. Occurring below ~800 m depth, the most negative $\delta^{34}S$ values (-0.9 to -1.9 ‰) indicate a high temperature (~596 °C), weakly oxidized, sulphate-bearing magmatic fluid produced sulphide ± sulphate minerals at the onset of K-silicate alteration. The oxidation state changed within the magmatic fluid as

inorganic reduction of sulphate to sulphide was triggered by the oxidation of ferrous iron in the wall rock (hornblende) to ferric iron (magnetite). As the high-temperature alteration progressed, the proportion of sulphate to sulphide changed, thus affecting fractionation of ^{34}S and produced increasingly enriched δ^{34}S values within sulphide minerals. The most positive δ^{34}S$_{sulphide}$ values (+0.9 to +1.5 ‰) occur near surface, within the pyrite-dominant halo along the flanks of the high-grade core of the East zone. Although the overall range in δ^{34}S is narrow, values decrease from weakly positive values in the pyritic halo to weakly negative δ^{34}S values towards the higher grade ore zones and become more negative with depth. This zonation effectively indicates the applicability of this technique to high grade targeting.

Additionally, the evolution of the hydrothermal system associated with Red Chris is isotopically preserved within the hydrosilicate alteration minerals. Calculations on δD and δ^{18}O analyses from alteration minerals and the resultant δD$_{H2O}$ and δ^{18}O$_{H2O}$ values indicate the presence of both a magmatic and meteoric fluid. Consistent with the alteration zonation and isotopic evidence at Red Chris, a model has be discussed by Sheppard et al. (1969, 1971) and Taylor (1974, 1997) to explain the relationship between observed alteration events in porphyry copper environments and the fluids that formed them.

The model discusses that throughout the crystallization of a porphyry stock, both internal and external hydrothermal systems are simultaneously present. During late stages of crystallization, the magmatic-derived hydrothermal system operates under lithostatic pressure within the upper and interior portions of a porphyry stock, (forming the high-temperature K-silicate alteration). Outside the stock, external waters (meteoric groundwaters ± saline formation waters) operate under hydrostatic pressures as a convective-hydrothermal system circulates due to heat supplied by the underlying batholith (and forms propylitic alteration). The external hydrothermal system is prevented from entering the stock due to the higher lithostatic pressures and the increasing influx of the magmatic-derived fluid (Taylor, 1987). The porphyry stock eventually cools (forming chlorite-sericite and sericitic/phyllic alteration) as the heat and fluid supply of the magmatic-derived hydrothermal system gradually fades away. However the lower-temperature external system still circulates outside of the stock and is then able to invade the porphyry stock. The external hydrothermal system 'collapses' onto the higher-temperature hydrothermally altered rocks such that the mixed magmatic-meteoric hydrothermal argillic

alteration (with their distinct isotopic compositions) are locally overprinted upon the K-silicate altered rocks ± the fresh pluton.

Field, petrologic and geochemical evidence from various studies of the Yerington porphyry copper district in Nevada support a model of two distinct fluid sources as the cause for hydrothermal wall-rock alteration and ore deposition (Dilles et al., 2000). Magmatic-hydrothermal fluids sourced from the underlying Yerington batholith are responsible for K-silicate alteration and copper-iron sulphide mineral deposition. These fluids generally flow upward and outward from porphyry centers and are also the source of acids and sulphur responsible for sericitic and advanced argillic alteration in higher levels of the system (Dilles et al., 2000). Additionally, sedimentary brines that are trapped as pore fluids within Triassic-Jurassic sedimentary stratigraphy become heated by intrusion of the Yerington batholith. These fluids convectively circulated through the contact aureole and flowed along complex pathways, generally inward, into crystalline parts of the batholiths and then upward and locally outward (Dilles et al., 2000). Upward flow of sedimentary brines occurred along porphyry dyke margins, separate from the upward flow of hydrothermal magmatic fluids (Dilles et al., 2000). Sedimentary brines are interpreted to have formed sodic-calcic alteration deep in the system, widespread propylitic-actinolite alteration at intermediate depths (~2.5 to 4.5 km) and chlorite-rich alteration in high-levels of the system (Dilles et al., 2000). Surficial ground water or meteoric water is suggested to have a minimal role in hydrothermal alteration at Yerington.

The two-fluid model, together with an understanding of general flow paths and evolution of hydrothermal alteration reported at Yerington, can be combined with the isotopic data and geologic constraints from Red Chris. A schematic alteration model through a series of figures can be constructed, outlining the formation and evolution of the alteration zones at Red Chris as the system cooled during interaction with magmatic and meteoric fluids (Figure 4.8).
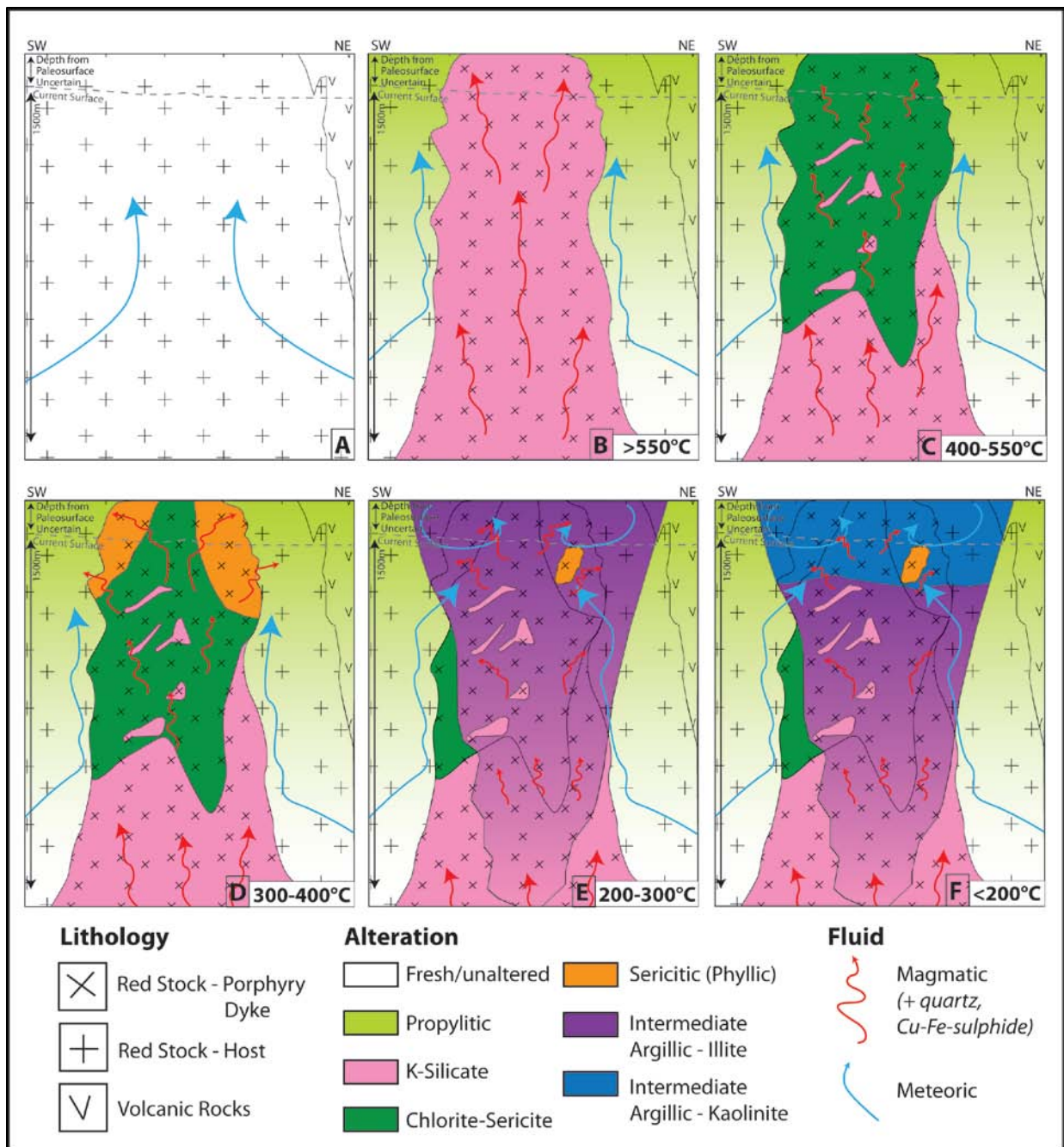
Figure 4.8 Schematic diagram of evolution of alteration zones at different temperatures and associated magmatic and/or meteoric fluids. A: Precursor Red Stock host; B: K-silicate and propylitic alteration; C: Chlorite-sericite alteration; D: Sericitic (phyllic) alteration; E: Intermediate argillic (illite) alteration; and F: Intermediate argillic (kaolinite) alteration.

Prior to the emplacement of the mineralized porphyry stock, meteoric fluid was present within the Stuhini Group rocks. Due to heat supplied by the underlying batholith, circulation and convection of the meteoric fluids was initiated (Figure 4.8A). After intrusion of the mineralized porphyry stock(s), during late-stage crystallization, internal magmatic hydrothermal fluids produced high-temperature, K-silicate alteration of the wall-rock along with deposition of

164

copper-iron-sulphide minerals (Figure 4.8B). Simultaneously, the external (meteoric) fluid flowed inward and upward, outboard of the mineralized porphyry stock forming weak propylitic alteration (Figure 4.8B). During the cooling of the porphyry stock, along with the vertical movement of magmatic-derived fluids, the chlorite-sericite zone formed (Figure 4.8C). Chlorite-sericite overprinted upon cooler portions of the K-silicate zone and a few relict lenses of K-silicate alteration remained. With continued cooling and fluid-rock interaction, the sericitic (phyllic) alteration zone formed in the upper peripheries of the porphyry stock(s) (Figure 4.8D). After the magmatic-hydrothermal system faded, the external meteoric-hydrothermal system persisted and eventually entered the cool porphyry stock(s), marking the onset of the collapse of the hydrothermal system. A mixture of low-temperature magmatic and meteoric fluid formed the pervasive illite (intermediate argillic) alteration, which overprinted upon much of the pre-existing alteration zones (Figure 4.8E). The intensity of illite alteration gradually decreased with depth, a function of the depth to which the external meteoric fluid could penetrate into the hydrothermal system. Continued cooling and mixing of magmatic and meteoric fluid, whereby the meteoric fluid increasingly dominated the fluid mixture in the upper ~300 m of the system lead to the formation of kaolinite (Figure 4.8F). Kaolinite formed within and possibly outboard of the illite alteration zone and may indicate the transition towards advanced argillic alteration.

Evidence from sulphur, carbon, oxygen, and deuterium stable isotope analysis provide the basis for the understanding and interpretation of the nature and evolution of the hydrothermal system at Red Chris. From sulphur isotopes, it has been interpreted that magmatic fluids responsible for Cu-Fe-sulphide mineral deposition and K-silicate alteration were weakly oxidized and contain minor sulphate. Carbon and oxygen isotopic analysis of carbonate minerals suggest a magmatic fluid source with some degree of meteoric fluid mixing possible. Oxygen and deuterium isotopic analysis of hydrothermal alteration minerals provide evidence for a magmatic source for K-silicate, chlorite-sericite and sericitic/phyllic alteration whereas a mixed magmatic-meteoric fluid is responsible for intermediate argillic alteration. The presence of a mixed magmatic-meteoric fluid indicates that the illite-kaolinite alteration is a late stage, low temperature alteration event associated with the high-temperature hydrothermal system. This association provides evidence that intermediate argillic alteration characterizes the upper parts of an alkalic porphyry system.

5 Conclusions, Implications for Exploration, and Suggestions for Future Work

5.1 Conclusions

The major objectives of this study were to investigate the evolution of the hydrothermal system of the East zone at Red Chris, with the ultimate goal of characterizing the upper parts of a porphyry Cu-Au deposit. This study described lithology, alteration mineralogy, vein-types, and copper-gold bearing sulphide mineralogy to construct a paragenesis of the East zone. The nature of the hydrothermal fluids of the porphyry system at Red Chris are characterized by several stable isotopic studies ($\delta^{34}S$, $\delta D/\delta^{18}O$, $\delta^{13}C/\delta^{18}O$) in order to determine an evolution of the hydrothermal system in relation to the observed alteration, veins, and copper-iron sulphide mineral distribution. Ultimately Red Chris exhibits many features representative of the well established porphyry model however has other features that are not as fully understood. The major conclusions from this study are summarized below.

Red Chris exhibits characteristics of alkalic and calc-alkalic porphyry deposits and represents a deposit that is transitional between the two types.

- Major alkalic features of Red Chris include the high-K calc-alkalic to alkalic chemistry of the host rocks, the cluster of deposits (East, Main, Far West, and Gully zones), the gold-rich nature with only minor molybdenum, the poorly developed phyllic alteration zone, and the significant volume of carbonate alteration.
- Major calc-alkalic features of Red Chris include the copper-iron sulphide mineralization being hosted in quartz veins and stockworks, the minor amounts of sphalerite and galena in shallow levels, and the presence of the low temperature clay (intermediate argillic) alteration assemblage. Additionally the phyllic alteration zone may have once been more extensive, consistent with the calc-alkalic model, yet currently restricted due to the intermediate argillic overprint.

5.1.1 Alteration

Red Chris exhibits alteration zones that are characteristic of porphyry copper deposits, as described by Meyer and Hemley (1967), Lowell and Guilbert (1970), Gustafson and Hunt (1975), Sillitoe (2000), Seedorff et al. (2005), and Sillitoe (2010). K-silicate, chlorite-sericite, sericitic/phyllic, and weak propylitic alteration zones are present yet have been pervasively overprinted by late-stage intermediate argillic alteration in the shallow levels of the system that diminishes intensity with depth. Additionally weak yet locally pervasive carbonate alteration and

166

abundant carbonate veins are also recognized shallow in the system. The mineral assemblages for each recognized alteration zone are:

- Propylitic: chlorite, pyrite, epidote ± calcite.
- K-silicate: secondary biotite, K-feldspar, magnetite.
- Chlorite ± sericite: chlorite alteration of secondary biotite, minor sericite.
- Sericitic/Phyllic: quartz, sericite (muscovite), pyrite.
- Intermediate argillic: illite, kaolinite.
- Carbonate: ankerite-dolomite ± calcite ± siderite.

Evidence from δD and $\delta^{18}O$ analysis on hydrothermal alteration minerals confirms the presence of both a magmatic and meteoric fluid. High temperature hydrothermal alteration to secondary biotite (K-silicate alteration), chlorite (chlorite-sericite alteration), and muscovite (sericite/phyllic alteration) formed from a magmatic fluid. Late-stage, low temperature, pervasive hydrothermal alteration of illite and kaolinite formed from a mixed magmatic-meteoric fluid. The evolution of the porphyry system, with respect to hydrothermal fluid-rock interaction, mineralization, and alteration types occurred as follows (Figure 4.8).

- Propylitic alteration: meteoric fluid heated by underlying batholith convected and circulated outboard of the porphyry stock.
- K-silicate alteration: high temperature magmatic flowed upward and deposited copper-iron-sulphide minerals (formed simultaneously as propylitic alteration).
- Chlorite-Sericite: locally overprinted K-silicate alteration as magmatic fluids flowed upward and began to cool.
- Sericitic/Phyllic alteration: locally overprinted chlorite-sericite and formed a minor halo in upper portions of deposit as magmatic fluids continued to cool and flow upward.
- Intermediate Argillic alteration: cool meteoric fluids mixed with low temperature magmatic fluids and produced pervasive illite alteration, extending deep into the system. As the system continued to cool, and with further fluid mixing, kaolinite alteration formed in the upper portions of the system.
- Carbonate alteration: cooling magmatic fluids in veins and throughout the host rock precipitated multiple events of carbonate that descreased in iron content through time. Minor mixing with meteoric water could have occurred during cooler, later stages of carbonate deposition.

- High-temperature K-silicate alteration was once more widespread than currently recognized and extended to at least within 200 m of the current surface. This zone was overprinted by later alteration events, especially the significant late-stage, low temperature intermediate argillic alteration overprint. Relict lenses of K-silicate alteration are still present. Additionally, most of the copper-iron-sulphide deposition occurred during K-silicate alteration.

- Chlorite-sericite alteration represents a transitional high-temperature alteration stage between K-silicate and sericite/phyllic alteration events. At Red Chris chlorite is dominant over sericite. Sericite noted in this alteration zone could be illite-kaolinite, a result of the younger intermediate argillic overprint. Precursor sericite (muscovite) may have been significant prior to alteration to illite-kaolinite.

- Sericitic/phyllic alteration is characterized by quartz-muscovite-pyrite, where muscovite represents a high-temperature, magmatic sourced version of sericite. Sericitic/phyllic alteration could have been more extensive, as evidenced by the presence of the pyrite-rich halo. Pervasive intermediate argillic alteration nearly destroyed the sericitic/phyllic zone, replacing muscovite with illite-kaolinite. Only a small relict lens remains, identifiable by the presence of quartz-muscovite-pyrite alteration. Alternatively, formation of the sericitic/phyllic zone could have been restricted, buffered by the abundant carbonate in the system. A poorly developed or absent phyllic zone is common to alkalic porphyry deposits.

- Low temperature intermediate argillic alteration is not equivalent to sericitic/phyllic alteration or to chlorite-sericite alteration. It formed by mixing of magmatic and meteoric fluids sometime after the formation of sericitic/phyllic alteration. Intermediate argillic alteration nearly destroyed the sericitic/phyllic zone and pervasively overprinted high-temperature K-silicate and chlorite-sericite alteration zones. Magnetite associated with K-silicate alteration is altered to hematite a feature also recognized at the Dinkidi porphyry deposit (Wolfe and Cooke, 2011). The mixed magmatic-meteoric isotopic signature indicates that intermediate argillic alteration is a late-stage alteration event, yet directly

related to the evolution of the porphyry system. Further, intermediate argillic alteration does not appear to destroy grade.

- Pervasive intermediate argillic alteration is most intense in the shallowest levels of the system due to cooling and increased mixing with meteoric fluid. As the magmatic-derived hydrothermal system cools and begins to mix with cooler (and closer to neutral) meteoric fluid, illite alteration forms. At higher levels in the system the temperature is cooler and a greater degree of magmatic-meteoric fluid mixing promotes a greater intensity of illite alteration. Even further mixing and cooling in the uppermost levels of the system produces kaolinite alteration and intensifies the overall effect of pervasive alteration.

- The timing of carbonate veins and alteration is not constrained with respect to intermediate argillic alteration. The carbonate veins dominantly formed after sericitic/phyllic alteration as they mostly cross-cut the associated Pyrite (D-veins). Evidence from carbon and oxygen isotopic analyses of vein carbonate material are consistent with a magmatic fluid with possibly minor mixing with a meteoric fluid. Carbonate veins and alteration likely formed by one of two ways: 1) carbonate formed from a magmatic fluid at temperatures between 200 and 400 °C and higher with little to no mixing with meteoric fluid or 2) the carbonates formed from a magmatic fluid at temperatures below 200 °C and mixed with meteoric fluid to reflect the isotopic compositions that are shifted towards a meteoric signature.

- The presence of moderate carbonate during and significant carbonate after sericitic/phyllic alteration suggests that carbonate at Red Chris acted as a buffer in the hydrothermal system and restricted the formation of a widespread phyllic alteration zone. Poorly developed or absent sericitic/phyllic zones in alkalic porphyry deposits could be a result of buffering in the system, inherent to the CO_2 and carbonate-rich nature of an alkalic porphyry deposit.

5.1.1.1 Intermediate Argillic Alteration at Porphyry Deposits

Late-stage, low-temperature alteration may directly overprint high-grade, high-temperature alteration zones at many porphyry deposits, however the low temperature overprint might not be

sufficiently recognized. The term 'sericite' is a textural term often used to describe any white micaceous mineral in the field. In many cases a sericite overprint on high-grade mineralized zones could be interpreted as muscovite, a mineral stable with chlorite-sericite or sericitic/phyllic alteration. However, sericite may in fact be illite, which is indicative of a lower-temperature alteration overprint, such as recognized at Red Chris. This occurred at Bingham, whereby early studies by Moore and Nash (1974) and Moore (1978) report sericitic (muscovite) alteration superimposed upon the biotite (potassic) altered zone. However a study by Parry et al. (2002) identified both phyllic and intermediate argillic alteration assemblages of illite, smectite and kaolinite to represent the previously reported 'sericitic' zone. At Bingham, intermediate argillic alteration is superimposed on the potassic zone, including the quartz monzonite porphyry in the center of the deposit, and extends into the surrounding monzonite. Illite and kaolinite at Bingham decrease in abundance with depth (Parry et al., 2002), a feature also recognized at Red Chris. Similar alteration assemblages, possibly reflecting intermediate argillic alteration have been reported at Schaft Creek and Galore Creek but are under-described and not fully investigated.

At Schaft Creek, the sericite-chlorite alteration zone is noted to be transitional between potassic and propylitic alteration in the Main zone and parts of the Paramount zone (Scott et al., 2008). There, chlorite and sericite compose the sericitic/phyllic alteration type whereby intense chloritization of pyroxene phenocrysts and groundmass and lesser sericitization of plagioclase forms in the mafic volcanic country rocks (Scott et al., 2008). In more felsic rocks, sericitization of feldspar and groundmass dominates over chlorite alteration. Only local pyrite is observed within zones of sericite-chlorite alteration (Scott et al., 2008). Further investigation into the nature of the sericite was not undertaken, and it is not known if the mineralogy represents illite or muscovite. Due to the abundance of chlorite and the surrounding (as opposed to overprinting) nature of the sericite-chlorite alteration at Schaft Creek, it is likely that this alteration type correlates with the transitional chlorite-sericite alteration type recognized and described at Red Chris and not intermediate argillic alteration.

At the Central zone of Galore Creek, 3 mineralized centers (South Gold Lens, North Gold Lens and Central Replacement zone) locally report the presence of sericite-anhydrite-carbonate (SAC) alteration (Micko, 2010). SAC alteration is characterized by pale green sericite that replaces plagioclase phenocrysts and small, mm-sized veinlets of calcite-anhydrite cross-cutting

the host-rock (Micko, 2010). It is possible that sericite at Galore Creek of SAC alteration is composed of illite however no such study has been undertaken. The overprinting nature, pale green colour and lack of chlorite suggest that SAC alteration at Galore Creek is similar to intermediate argillic (illite) alteration at Red Chris. As the eastern Central Replacement zone represents the shallowest levels of the Galore Creek porphyry system (Micko, 2010) it is likely that illite represents sericite in SAC alteration. This provides additional evidence that intermediate argillic (illite ± kaolinite) alteration represents the upper parts of a porphyry system.

5.1.2 **Veins and High-grade Mineralization**

Much of the copper and gold is associated with copper-iron sulphides within various stages of veins. The veins and contained copper-iron sulphides provide additional information regarding the nature and evolution of the hydrothermal system at Red Chris.

- Seventeen different vein-types have been described, ordered, and divided into 5 major groups that represent a sequence from high to low temperature. Early Veins (E1-3), Sulphide Veins (S1-6), Anhydrite-Gypsum Veins (AG1-3), Pyrite Veins (P1-2), and Late Carbonate/Chlorite Veins (LC1-3). Four of the major groups are representative of A, B, or D veins, as classified by Gustafson and Hunt (1975) at the El Salvador porphyry deposit, Chile. Each of the major groups of veins have been interpreted to be associated with different alteration events:
  - Early Veins (E1-3) = A-Veins: quartz ± chalcopyrite ± molybdenite ± pyrite ± purple anhydrite ± magnetite: associated with onset of K-silicate alteration.
    - Anhydrite-Gypsum Veins (AG1-3) = peach-white anhydrite ± gypsum ± chlorite ± chalcopyrite: possible resurgence of K-silicate alteration.
  - Sulphide Veins (S1-6) = B-Veins: quartz, chalcopyrite ± bornite ± magnetite ± hematite ±pyrite ± covellite: associated with K-silicate alteration to chlorite-sericite alteration.
  - Pyrite Veins (P1-2) = D-Veins: pyrite ± quartz ± tourmaline: associated with sericitic/phyllic alteration.
  - Late Carbonate/Chlorite Veins (LC1-3) = Late stage veins: ankerite-dolomite ± calcite ± siderite ± chlorite: as infill of earlier veins and breccia cement, associated with carbonate alteration.

- Magmatic fluid exsolved from the porphyry stocks was CO_2-rich, accounting for the abundance of carbonate veins and weak yet pervasive carbonate alteration sourced from this fluid. B- and D-Veins of Gustafson and Hunt (1975) note the presence of anhydrite, which is not recognized in the B (Sulphide) Veins and D (Pyrite) Veins at Red Chris, however minor carbonate is noted. This discrepancy could be related to the original magmatic fluid being CO_2-rich, with lesser SO_4, accounting for minor anhydrite present in the system (Early Veins only) and only weakly negative $\delta^{34}S$ values. Another possibility is that anhydrite originally formed in the Sulphide Veins and Pyrite Veins, however was later replaced by carbonate.

- Copper and gold are associated with bornite, chalcopyrite and lesser pyrite (gold-only). The copper-iron sulphides display a zonation pattern common at porphyry deposits. Bornite + chalcopyrite occur in a narrow, yet vertically extensive core. A shell of chalcopyrite > pyrite surrounds the core and grades outward to a pyrite > chalcopyrite halo. Additionally, minor molybdenite flanks the copper-gold core as a weak halo at depth.

- High grade Cu-Au mineralized zones are associated with high quartz-vein density. Much of the copper-iron sulphides are hosted in banded quartz veins (Sulphide Veins S1-3; B-Veins) and to a lesser extent Early Veins (E3; A-Veins). A relationship between quartz vein density and highest Cu-Au grade is also recognized at Ridgeway (Wilson et al., 2003). However this is not the case at other porphyry deposits such as Butte. At the deepest drilled regions in the core of the Pittsmont Dome a stockwork of early, barren quartz (± Mo) veins exists, beneath the high grade Mo zone and Main Stage veins that contain the bulk of copper mineralization (Rusk et al., 2008).

- Two high-grade and vertically extensive zones (uppermost ~60 m in drillholes RC07-335 and RC09-354, and ~150 m in drillhole RC09-350) at Red Chris are composed of > 60 volume % and commonly up to 80 volume % quartz stockwork veins. The high-density quartz vein zones give rise to a 'stacked' geometry to the system. Each of the two noted high-grade zones has different textures and mineralogy, representing different fluid events. The cause and location of these high-grade quartz stockwork zones is not conclusive, however a comparison could be made with the Max Mo porphyry system in

southeastern British Columbia. Within the MAX system silicified zones of high quartz vein density within the high-grade zone are thought to reflect channeling of fluid flow in the narrow apical zones of the granodiorite dykes (Lawley et al., 2010). Similar to the MAX deposit, the high-grade, high quartz vein density zones at Red Chris could represent structurally focused copper- and gold-bearing fluids at the apices of separate porphyritic intrusions.

- Evidence from weakly negative δ^{34}S values (-0.9 to -1.9 ‰) indicates a high temperature weakly oxidized, sulphate-bearing magmatic fluid that produced sulphide ± sulphate minerals at the onset of K-silicate alteration. The oxidation state changed within the magmatic fluid as inorganic reduction of sulphate to sulphide was triggered by the oxidation of ferrous iron in the wall rock (hornblende) to ferric iron (magnetite). As the high-temperature alteration progressed, the proportion of sulphate to sulphide changed, thus affecting fractionation of ^{34}S and produced increasingly enriched δ^{34}S values within sulphide minerals. The most positive δ^{34}S$_{sulphide}$ values (+0.9 to +1.9 ‰) occur near surface, within the pyrite-dominant halo along the flanks of the high-grade core of the East zone.

- Evidence from sulphide-sulphide geothermometry provides temperatures of formation of different veins and sulphide assemblages, and is consistent with fluid inclusion studies from the Bingham and Butte porphyry deposits. At Red Chris, Early Veins (E2) formed at high temperatures near 596 °C prior to significant copper-iron sulphide deposition. This temperature is consistent with Bingham whereby fluids from a barren yet highly veined and potassically altered deep core of the system were trapped mostly at temperatures > 500 °C (Landtwing et al., 2010). Addtionally, at Red Chris much of the sulphide (copper-gold) mineralization was deposited in Sulphide Veins (S3) and sulphur geothermometry suggests this deposition occurred at temperatures near 380 °C. This is also consistent with Bingham, whereby fluid inclusions indicate that bornite, chalcopyrite and native gold were precipitated between 430 to 350 °C (Landtwing et al., 2010). Further, fluid inclusion studies at Butte indicate that ore mineral precipitation exctracts ~85 % of Cu and Au from the hydrothermal fluid, associated with K-silicate alteration at temperatures between 400 to 305 °C (Ulrich et al., 2001). The 380 °C temperature of Sulphide Vein formation at Red Chris is within the range of temperatures obtained from

fluid inclusions studies at Bingham and Butte for the stage of significant copper-gold deposition.

5.2   Implications for Exploration

Another major objective of this study was to indicate how knowledge generated in this study could aid in exploration within a high grade zone at Red Chris, across the Red Chris camp, and for porphyry deposits in general. Many of these suggestions are already established tools for the exploration of porphyry deposits.

An approach to exploring for a porphyry deposit would be to seek out evidence indicative of a nearby high-temperature core of a magmatic hydrothermal system. Evidence for these 'hot-spots' that are associated with copper-iron-sulphide mineralization includes discovery of remnants of K-silicate alteration. Within the realm of all porphyry deposits, exploration efforts are suggested.

- Intermediate argillic (illite-kaolinite) alteration characterizes the upper portions of Red Chris and correct field-identification of these minerals could be utilized in exploration targeting. In this study, intermediate argillic alteration destroyed much of the sericitic/phyllic zone and overprinted high-temperature K-silicate and chlorite-sericite alteration zones to depth. Exploration on the basis of high-temperature alteration mineralogy could be ineffective is such situations. Recognized in the field, illite and kaolinite could be considered to form in shallow portions of a porphyry deposit some distance above mineralization, however in this study illite and kaolinite are present right in the mineralized porphyry containing high-grade copper-iron-sulphide minerals. The use of a field-portable shortwave infrared spectrometer such as the TerraSpec could be used in identifying low temperature clay alteration minerals, however great care must be taken when interpreting results.

- The presence of kaolinite (intermediate argillic alteration) in shallow levels at Red Chris indicates that the Red Chris porphyry system could have transitioned to advanced argillic alteration in even shallower parts of the system. In higher-level and less eroded portions of the Red Chris porphyry system, it would be expected that advanced argillic alteration minerals such as diaspore, pyrophyllite and alunite would form. Exploration efforts could

174

include identification and mapping the distribution of advanced argillic alteration minerals.

Additionally, at the scale of the Red Chris camp, evidence for high-temperature alteration associated with copper-iron-sulphide mineralization to aid in exploration efforts are suggested.

- Quartz veins host nearly all of the copper-iron-sulphide mineralization at Red Chris and the presence of quartz veins with granular quartz could indicate a nearby high-temperature, magmatic hydrothermal system. Quartz veins are resistant to alteration and weathering effects and granular quartz within the veins is indicative of a high-temperature system. Additionally, the density of quartz veins at Red Chris is directly related to high-grade mineralization. An increase in quartz vein density could indicate closer proximity to the core of the system. Further, the presence of quartz veins could provide useful in geophysical studies, as abundant quartz veins would exhibit a resistivity-low on an induced polarization (IP) survey. Any connectivity of sulphide grains within the quartz veins could obscure such a signal.

- Carbonate alteration has been recognized as late-stage alteration products in several porphyry deposits of northern Stikinia. Carbon and oxygen isotopes on carbonate veins and alteration at Red Chris indicate a magmatic source of the carbonate with some degree of mixing with a meteoric fluid. Analysis of carbon and oxygen isotopes on carbonate could be used to indicate the presence of a nearby magmatic hydrothermal system. The use of the LGR desktop isotope analyser provides an inexpensive, relatively quick laboratory method for the analysis of carbon and oxygen isotopes on carbonate minerals.

- Irregular crystal boundaries of altered mafic mineral sites. Primary hornblende phenocrysts will alter to secondary biotite during addition of potassium (K-silicate alteration). Secondary biotite, also known as 'shreddy' biotite replaces a hornblende phenocryst with small aggregates of biotite and locally retains the original crystal shape of the hornblende. Subsequent chlorite alteration of the secondary biotite aggregates does not retain sharp crystal boundaries of the primary hornblende. Late-stage clay alteration of chlorite will result in phenocrysts with irregular to 'fuzzy' crystal boundaries. However, primary hornblende phenocrysts that do not experience K-silicate alteration (to

175

secondary biotite and chlorite) but experience late-stage clay alteration will retain sharp, primary crystal boundary shapes. The presence of irregular crystal boundaries is indicative of K-silicate alteration and possibly nearby high-grade mineralization.

- Magnetite is an alteration mineral introduced with high-temperature K-silicate alteration and copper-iron-sulphide mineralization. Magnetite commonly replaces mafic phenocrysts such as hornblende, forming as small sub-rounded grains. Late-stage, low temperature intermediate argillic alteration alters magnetite to hematite. The presence of hematite with cores of magnetite within clay altered mafic mineral sites is indicative of a nearby high-temperature, magmatic hydrothermal system and possible copper-iron-sulphide mineralization.

- Zonation in sulphur isotopes ($\delta^{34}S$) is a feature that has been recognized in the East zone at Red Chris as well as in other alkalic porphyry deposits in British Columbia such as Mount Polley, Galore Creek, Mt. Milligan, Afton and Lorraine (Dyell and Tosdal, 2005, Jago et al., In Press). In this study, the deep core of the system exhibits weakly negative $\delta^{34}S_{sulphide}$ values that grade upward and outward to weakly positive $\delta^{34}S$ values in the pyrite halo. The vertical and lateral zonation at Red Chris has implications for the utilization of sulphur isotopes in exploration in the area. Areas where positive $\delta^{34}S_{sulphide}$ values trend towards lower, and negative values could indicate the present of copper-iron-sulphide minerals.

Further, exploration implications within a high grade zone, such as the East zone at Red Chris are suggested.

- Quartz vein density. Copper-iron-sulphide mineralization is hosted in quartz veins and stockworks and grade increases directly with quartz vein density. An increase in quartz vein density could signify nearby high-grade zones.

- The presence of gypsum veins. High temperature anhydrite is recognized within Early Veins (A-veins) at Red Chris and in A-, B- and D-veins at El Salvador (Gustafson and Hunt, 1975). An influx if meteoric fluid will trigger the hydration of anhydrite, and alter it to gypsum. The recognition of gypsum veins in shallow levels of a porphyry system

176

could indicate previous of formation of anhydrite in a high-temperature magmatic environment and possibly nearby deposition of copper-iron-sulphide minerals.

- The presence of molybdenite. At Red Chris molybdenite does not occur in the high-grade (bornite, chalcopyrite) core of the deposit but as a deep, minor yet definable, peripheral halo. The presence of molybdenite could indicate that high-grade, copper-iron-sulphide core is in close proximity.

- The presence of A-veins. The wavy, discontinuous nature of A-veins indicates a high-temperature system where the rock is relatively ductile. A high-temperature, magmatic system that forms A-veins likely deposited copper-iron-sulphide minerals nearby.

5.3   Suggestions for Future Work

It is recommended that future work could be carried out on the Red Chris porphyry system in order to further the observations and conclusions of this study. Major areas of work could be undertaken pertaining to:

- Age of mineralization. To date, the Red Stock has been dated by U-Pb methods on zircon as 203.8 ± 1.3 Ma (Friedman and Ash, 1997). This sample was taken from a portion of the Red Stock that could have been emplaced well before subsequent porphyry stocks and associated copper-iron-sulphide minerals. Re-Os dating on molybdenite could be analyzed to better constrain the timing of mineralization relative to the U-Pb (zircon) age date of the host intrusion. Additionally, U-Pb analysis of zircon could be undertaken from different phases of the Red Stock that could be temporally related to copper-iron-sulphide deposition.

- Different porphyritic intrusive events. Differentiation between intrusive phases at Red Chris is obscured by pervasive intermediate argillic alteration, specifically in the shallow levels of the system. Possible intrusive contacts are commonly faulted and rehealed by carbonate cement and information regarding cross-cutting relationships is lost. The differentiation of intrusive phases can be used to understand the evolution of the porphyry system, especially in relation to changes within a magma chamber and related hydrothermal fluids with time. Multiple intrusive phases will cause overprinting of

177

alteration events upon older porphyritic phases. Additionally, younger intrusive events may experience different alteration histories than older phases. Recognizing different intrusive phases also has implications for mining and production.

- Cathodoluminescence (CL) microscopy on quartz veins. In hand sample and thin section quartz veins appear fairly uniform however multiple generations of quartz veins may cathodoluminesce differently. At Bingham, quartz associated with the dominant ore hosting quartz-sulphide veinlets is only visible by CL microscopy (Redmond and Einaudi, 2010). The quartz in the quartz-sulphide veinlets are dark-luminescing compared to brightly luminescing quartz of older quartz veinlets. A similar study could be undertaken at Red Chris to identify if there is any difference in quartz luminescence between different stages of quartz and quartz-sulphide veins.

- Fluid inclusion studies. Temperatures of formation were estimated for many of the isotopic interpretations in this study. Geothermometry of sulphur isotopes provided a base for copper-iron-sulphide deposition however certain sulphide species and pairs make for more accurate geothermometers. Fluid inclusion studies on quartz veins could help constrain temperature of formation, salinity and pressure conditions of the high-temperature copper-iron-sulphide-bearing magmatic fluids. Additionally, fluid inclusion studies could be undertaken on carbonate veins to better constrain parameters of carbonate formation within the system and the relationship to alteration and copper-iron-sulphide deposition.

- Recognition of late stage alteration in porphyry systems. At Red Chris the late-stage, low-temperature intermediate argillic alteration is a direct overprint on high-grade mineralization and high-temperature alteration zones. The recognition of low-temperature clay (illite-kaolinite) alteration could be difficult in the field without adequate methods of mineral identification. Intermediate argillic alteration could overprint high-grade, high-temperature zones to varying degrees in other porphyry systems however misidentified as 'sericite' and thus interpreted as sericitic/phyllic alteration. Proper use of short-wave infrared spectrometers, such as the TerraSpec could be used as a tool to aid in the identification of low-temperature clay minerals. Ultimately, such identification of low-

temperature clay minerals could affect the interpretation of specific alteration zones and the spatial relation to copper-iron-sulphide minerals.

- Carbonate alteration and mineralogy. Carbonate veins and alteration are widespread in the shallow levels of the Red Chris porphyry and commonly occurs as vein infill of copper-iron-sulphide-bearing quartz veins. Different species of carbonate have been recognized including dominantly ankerite-dolomite, minor calcite and lesser siderite. A study could be undertaken to determine the different carbonate species with relation to alteration, mineralization and the sequence of vein events. Further, carbon and oxygen isotope analysis of the different mineral species could better constrain the fluid sources of the different carbonate mineral species.

References

Andrews, G.D.M., and Russell, J.K., 2007, Mineral exploration potential beneath the Chilcotin Group (NTS 092O, P; 093A, B, C, F, G, J, K), south-central British Columbia: preliminary insights from volcanic facies analysis: Geological Fieldwork 2006, BC Ministry of Energy, Mines and Petroleum Resources, Paper 2007-1, p. 229-238.

Anderson, R.G., 1993, A Mesozoic stratigraphic and plutonic framework for northwestern Stikinia (Iskut River area), northwestern British Columbia, in Dunne, G., and McDougall, K., eds., Mesozoic paleogeography of the western United States, II: Los Angeles, CA: Society of Economic Paleontologists and Mineralogists, Pacific Section, p. 477-494.

Ash, C.H., Fraser, T.M., Blanchflower, J.D. and Thurston, B.G., 1995, Tatogga Lake project, northwestern British Columbia (104H/11, 12): Geological Fieldwork 1994, BC Ministry of Forests, Mines and Lands, Paper 1995-1, p. 343–358.

Ash, C.H., Stinson, P.K., MacDonald, R.W.J., and Nelson, K.J. 1996, Geology of the Todagin Plateau (104H/12NW): B.C. Ministry of Employment and Investment, Open File Map 1996-4, scale 1:20 000.

Ash, C.H., MacDonald, R.W.J., Stinson, P.K., Fraser, T.M., Read, P.B., Psutka, J.F., Nelson, K.J., Arden, K.M., Friedman, R.M., and Lefebure, D.V, 1997a, Geology and mineral occurrences of the Tatogga Lake area (104H/12NW, 13SW & 104G/9NE, 16SE): B.C. Ministry of Energy and Mines, Open File Map 1997-3, scale 1:50 000.

Ash, C., MacDonald, R., Friedman, R.M., 1997b, Stratigraphy of the Tatogga Lake Area, Northwestern British Columbia: Geological Fieldwork 1996, British Columbia Ministry of Employment and Investment, Geological Survey Branch, Paper 1997-1, p. 283-290.

Ault, W.V., and Jensen, M.L., 1963, Summary of sulfur isotope standards *in* Biogeochemistry of sulfur isotopes, M.L. Jensen ed., National Science Foundation, Symposium Proceedings, Yale University.

Baertschi, P., 1976, Absolute 18O content of standard mean ocean water: Earth and Planetary Science Letters, v. 3, p. 341-344.

Baker, T., Ash, C.H. and Thompson J.F.H., 1997, Geological setting and characteristics of the Red Chris copper-gold deposit, northwestern British Columbia: Exploration and Mining Geology, v. 6, no. 4, p. 297–316.

Barr, D.A., Fox, P.E., Northcote, K.E, and Preto, V.A., 1976, The alkaline suite porphyry deposits – A summary: Canadian Institute of Mining, Metallurgy and Petroleum Special Volume 15, p. 359-367.

Bath, A.B., Cooke, D.R., Friedman, R.M., Faure, K., Kamenetsky, V.S., Tosdal, R.M., and Berry, R.F., In Press, Mineralization, U-Pb geochronology and stable isotope geochemistry of the Lower Main zone of the Lorraine deposit, north-central British Columbia: a replacement-style alkalic Cu-Au porphyry: Economic Geology.

Beane, R.E., and Titley, S.R., 1981, Porphyry copper deposits: Part II. Hydrothermal alteration and mineralization: Economic Geology 75th Anniversary Volume, p. 235-269.

Beatty, T.W., Orchards, M.J., and Mustard, P.S., 2006, Geology and tectonic history of the Quesnel terrane in the area of Kamloops, British Columbia *in* Colpron, M. And Nelson, J.L., eds., Paleozoic Evolution and Metallogeny of Pericratonic Terranes at the Ancient Pacific Margin of North America, Canadian and Alaskan Cordillera: Geological Association of Canada, Special Paper 45, p. 483-504.

Blanchflower, J.D., 1995, 1995 exploration report on the Red Chris property: unpublished report prepared for American Bullion Minerals Ltd., 93p.

Brown, D.A, Gunning, M.H. and Greig, C.J., 1996, The Stikine Project: Geology of western Telegraph Creek map area, northwestern British Columbia (NTS 104/G5, 6, 11W, 12 and 13): British Columbia Ministry of Employment and Investment-Energy and Minerals Division, Bulletin 95, 175 p.

Burnham, C.L., 1979, Magmas and hydrothermal fluids *in* Geochemistry of hydrothermal ore deposits, 2nd ed., New York, John Wiley and Sons, p. 71-136.

Campbell, A.R., and Larson, P.B., 2005, Introduction to stable isotope applications in hydrothermal systems: Reviews in Economic Geology, v. 10, p. 173-193.

Canadian Gold Hunter Corporation, 2008, Measured and indicated resource at Main and North Donnelly zone increased by 25 percent: Canadian Gold Hunter Corporation, press release, October 7, 2008.

Chamberlain, C.M., Jackson, M., Jago, C.P., Pass, H.E., Simpson, K.A., Cooke, D.R., and Tosdal, R.M., 2007, Toward an integrated model for alkalic porphyry copper deposits in British Columbia (NTS 093A, N; 104G): Geological Fieldwork 2006, Paper 2007-1, p. 259-274.

Church, B.N., 1975, Geology of the Sustut area *in* Geology, exploration and mining in British Columbia 1974: British Columbia Department of Mines and Petroleum resources, p. 305-309.

Cohen, J.F., 2011, Mineralogy and geochemistry of hydrothermal alteration at the Ann-Mason porphyry copper deposit, Nevada: Comparison of large-scale ore exploration techniques to mineral chemistry: Unpublished M.Sc. thesis, Corvallis, Oregon, Oregon State University, 577p.

Collins, J., Colquhoun, W., Giroux, G.H., Nilsson, J.W. and Tenney, D., 2004, Technical report on the Red Chris copper-gold project, Liard Mining Division: unpublished company report, Red Chris Development Company Ltd.

Coney, P.J., Jones, D.L., Monger, J.W.H., 1980, Cordilleran suspect terranes: Nature, v. 288, p. 329-333.

Cooke, D.R., Wilson, A.J. , House, M.J. , Wolfe, R.C. , Walshe, J.L. , Lickfold, V. and Crawford, A.J., 2007, Alkalic porphyry Au - Cu and associated mineral deposits of the Ordovician to Early Silurian Macquarie Arc, New South Wales: Australian Journal of Earth Sciences, v. 54, no. 2, p. 445-463.

Cooper, M.F.J., 1978, Geology of the Rose property porphyry copper occurrence northwestern British Columbia: M.Sc. thesis, Kingston, Ontario, Queen's University, 230p.

Copper Fox Metals Incorporated, 2011, Measured and indicated resources estimate exceeds one billion tonnes at Schaft Creek deposit, Copper Fox Metals Incorporated company press release, July 11, 2011.

Craig, H., 1957, Isotopic standards for carbon and oxygen and correction factors for mass-spectrometric analysis of carbon dioxide: Geochimica et Cosmochimica Acta, v. 12, p. 133-149.

Craig, H., 1961, Isotopic variations in meteoric waters: Science, v. 133, no.3465, p. 1702-1703.

Dawson, K.M., Panteleyev, A., Sutherland Brown, A. and Woodsworth, G.J, 1991, Regional Metallogeny: Chapter 19 of Geology of the Canadian Orogen in Canada, H. Gabrielse and C.J. Yorath (ed.), Geological Survey of Canada, Geology of Canada, no. 4, p. 709-768 (also Geological Society of America, The Geology of North America, v. G-2).

Dilles, J.H., and Einaudi, M.T., 1992, Wall-rock alteration and hydrothermal flow paths about the Ann-Mason porphyry copper deposit, Nevada – A 6-km vertical reconstruction: Economic Geology, v. 87, p. 1963-2001.

Dilles, J.H., Einaudi, M.T., Proffett, J., and Barton, M.D., 2000, Overview of the Yerington porphyry copper district: magmatic to nonmagmatic sources of hydrothermal fluids: their flow paths and alteration effecs on rocks and Cu-Mo-Fe-Au ores: Society of Economic Geologists Guidebook Series, v. 32, p. 55-66.

Dostal, J., Gale, V., and Church, B.N., 1999, Upper Triassic Takla Group volcanic rocks, Stikine terrane, north-central British Columbia: geochemistry, petrogenesis and tectonic implications: Canadian Journal of Earth Sciences, v. 36, p. 1483-1494.

Dyell, C. L. and Tosdal, R. M., 2005, Alkalic Cu-Au deposits of British Columbia: Sulfur isotope zonation as a guide to mineral exploration: Geological Fieldwork 2004, British Columbia Geological Survey, Paper 2005-1, p. 191-208.

Eberl, D.D., and Velde, B., 1989, Beyond the Kubler index: Clay Minerals, v.24, no. 4, p. 571-577.

Edwards, B.R., and Russell, J.K., 2000, Distribution, nature and origin of Neogene-Quaternary magmatism in the northern Cordilleran volcanic province, Canada: Geological Society of America Bulletin, v. 112, no. 8, p. 1280-1295.

Einaudi, M.T., 1997, Mapping altered and mineralized rocks: An introduction to the Anaconda method: Stanford, CA, Stanford University.

Enns, S.G., Thompson, J.F.H., Stanley, C.R., and Yarrow, E.W., 1995, The Galore Creek porphyry copper-gold deposits, northwestern British Columbia: Porphyry Deposits of the Northwestern Cordillera of North America, T.G. Schroeter (ed.), Canadian Institute of Mining, Metallurgy and Petroleum Special Volume 46, p. 630-644.

Evenchick, C.A. and Thorkelson, D.J., 1993, Geology of the Spatsizi River, British Columbia (104H): Geological Survey of Canada, Open File Map 2719, scale 1:250 000.

Evenchick, C.A. and Thorkelson, D.J., 2005, Geology of the Spatsizi River map area, north-central British Columbia: Geological Survey of Canada, Bulletin 577, 276p.

Ferreira, L., 2009, 2008 diamond drilling report on the Red Chris project located in northwest British Columbia, Liard Mining District: unpublished company report, Red Chris Development Company Ltd.

Friedman, R.M. and Ash, C.H., 1997, U-Pb age on intrusions related to porphyry Cu-Au mineralization in the Tatogga Lake area, northwestern British Columbia (104H/12NW, 104G/9NE): Geological Fieldwork 1996, B.C. Ministry of Forests, Mines and Lands, Paper 1997-1, p. 291–298.

Gabrielse, H. and Tipper, H.W., 1984, Bedrock Geology of Spatsizi map area (104H); Geological Survey of Canada, Open File Map 1005, scale 1:250 000.

Gabrielse, H., Monger, J.W.H., Wheeler, J.O. and Yorath, C.J., 1991a, Tectonic Framework Part A. Morphogeological belts, tectonic assemblages and terranes: Chapter 2 of Geology of the Canadian Orogen in Canada, H. Gabrielse and C.J. Yorath (ed.), Geological Survey of Canada, Geology of Canada, no. 4, p. 15-28 (also Geological Society of America, The Geology of North America, v. G-2).

Gabrielse, H., Monger, J.W.H., Tempelman-Kluit, D.J. and Woodsworth, G.J., 1991b, Structural Styles Part C. Intermontane Belt: Chapter 17 of Geology of the Canadian Orogen in Canada, H. Gabrielse and C.J. Yorath (ed.), Geological Survey of Canada, Geology of Canada, no. 4, p. 571-675 (also Geological Society of America, The Geology of North America, v. G-2).

Giggenbach, W.F., 1992, Isotopic shifts in waters from geothermal and volcanic systems along convergent plate boundaries and their origin: Earth and Planetary Science Letters, v. 113, p. 495-510.

Gill, R., Kulla, G., Wortman, G., Melnyk, J., and Rogers, D., 2011, Galore Creek Project, British Columbia, NI 43-101 Technical Report on Pre-Feasibility Study, NovaGold Resources Inc., September 12, 2011.

Gillstrom, G. and Robertson, S., 2010, Red Chris deposit technical report: 2010 exploration, drilling and mineral resource update: unpublished company report, Imperial Metals Corporation.

Gillstrom, G., Anand, R., and Robertson, S., 2012, 2012 Technical report on the Red Chris Cu-Au project: unpublished company report, Imperial Metals Corporation.

Giroux, G.H., Rodger, R., Blanchflower, J.D., 2002, Report on the Red Chris Copper-Gold Project: private report prepared for American Reserve Energy Corporation.

Giroux, G.H. and Bellamy, J., 2004, Update report on the Red Chris copper-gold project: unpublished company report, bcMetals Corporation.

Green, G.M., 1992, Detailed sedimentology of the Bowser Lake Group, northern Bowser Basin, north-central British Columbia: M.Sc. thesis, Ottawa, Ontario, Carleton University, 197p.

Gruen, G., Heinrich, C.A., and Schroeder, K., 2010, The Bingham Canyon porphyry Cu-Mo-Au Deposit. II. Vein geometry and ore shell formation by pressure-driven rock extension: Economic Geology, v. 105, p. 69-90.

Gustafson, L.B., and Hunt, J.P., 1975, The porphyry copper deposit at El Salvador, Chile: Economic Geology, v. 70, no. 5, p. 857-912.

Hagemann, R., Nief, G., and Roth, E., 1970, Absolute isotopic scale for deuterium analysis of natural waters; Absolute D/H ratio for SMOW: Tellus, v. 22, p. 712-715.

Harland, W.B., Armstrong, R.L., Cox, A.V., Craig, L.E., Smith, A.G., and Smith, D.G., 1990, A Geologic Time Scale, 1989: Cambridge University Press, Cambridge, United Kingdom, 279p.

Harris, A.C., Golding, S.D, and White, N.C., 2005, Bajo de la Alumbrera copper-gold deposit: Stable isotope evidence for a porphyry-related hydrothermal system dominated by magmatic aqueous fluids: Economic Geology, v. 100, p. 863-886.

Hedenquist, J.D., Arribas, A., Jr., and Reynolds T.J., 1998, Evolution of an intrusion-centered hydrothermal system: Far Southeast-Lepanto porphyry and epithermal Cu-Au deposits, Philippines: Economic Geology, v. 93, no. 4, p.373-404.

Hedenquist, J.W, and Richards, J.P., 2005, The influence of geochemical techniques on the development of genetic models for porphyry copper deposits: Reviews in Economic Geology, v. 10, p. 235-256.

Hemley, J.J., and Jones, W.R., 1964, Chemical aspects of hydrothermal alteration with emphasis on hydrogen metasomatism: Economic Geology, v. 59, p. 538-569.

Hickson, C.J., and Souther, J.G., 1984, Late Cenozoic volcanic rocks of the Clearwater – Wells Gray area, British Columbia: Canadian Journal of Earth Science, v. 21, p. 267-277.

Hoefs, J., 1997, Stable Isotope Geochemistry: Berlin, Springer-Verlag, 201p.

Holbek, P.M., 1988, Geology and mineralization of the Stikine assemblage, Mess Creek area, northwestern British Columbia, M.Sc. thesis, Vancouver, British Columbia, The University of British Columbia, 184p.

Holliday, J.R., and Cooke, D.R., 2007, Advances in geologic models and exploration methods for copper ± gold porphyry deposits, *in* Milkereit, B., ed., Proceedings of Exploration 07: Fifth Decennial International Conference on Mineral Exploration: Toronto, Prospectors and Developers Association of Canada, p. 791-809.

Hollister, V.F., 1978, Geology of the porphyry copper deposits of the Western Hemisphere: New York, Society of Mining Engineers AIME, 219p.

Hunt, G.R., and Ashley, R.P., 1979, Spectra of altered rocks in the visible and near infrared: Economic Geology, v. 74, p. 1613-1629.

Imperial Metals Corporation, 2007, Over one kilometre grading 1.01% copper and 1.26 g/t gold intercepted at Imperial's Red Chris property: Imperial Metals Corporation, press release, October 16, 2007.

Imperial Metals Corporation, 2010, Imperial report results of the Red Chris feasibility study update: Imperial Metals Corporation, press release, November 16, 2010.

Imperial Metals Corporation, 2012, Red Chris Mineral Resource Tonnage Increased by 103%: Imperial Metals Corporation, press release, February 2, 2012.

Jago, C.P., 2008, Metal- and alteration-zoning, and hydrothermal flow paths at the moderately-tilted, silica saturated, Mt. Milligan Cu-Au alkali porphyry deposit: Unpublished M.Sc. thesis, Vancouver, British Columbia, University of British Columbia, 210p.

Jago, C.P., Tosdal, R.M., Cooke, D.R. and Harris, A.C., In Press, Vertical and lateral variation in mineralogy and chemistry in the Early Jurassic Mt. Milligan alkali porphyry Au-Cu deposit, British Columbia, Canada: Economic Geology.

Kerr, F.A., 1948, Lower Stikine and western Iskut river areas, British Columbia: Geological Survey of Canada, memoir 246, 95p.

Khashgerel, B., Rye, R.O., Kavalieris, I., and Hayashi, K., 2009, The sericite to advanced argillic transition: Stable isotope and mineralogical characteristics from the Hugo Dummett porphyry Cu-Au deposit, Oyu Tolgoi district, Mongolia: Economic Geology, v. 104, p. 1087-1110.

Kruse, F.A, and Hauff, P.L., 1991, Identification of illite polytype zoning in disseminated gold deposits using reflectance spectroscopy and X-ray diffraction – potential for mapping with imaging spectrometers: IEEE Transactions on Geoscience and Remote Sensing, v. 29, no. 1, p. 101-104.

Landtwing, M.R., Furrer, C., Redmond, P.B., Pettke, T., Guillong, M., and Heinrich, C.A., 2010, The Bingham Canyon porphyry Cu-Mo-Au deposit, III. Zoned copper-gold core deposition by magmatic vapor expansion: Economic Geology, v. 105, p. 91-118.

Lang, J.R., Stanley, C.R., and Thompson, J.F.H., 1994, Porphyry copper deposits related to alkalic igneous rocks in the Triassic-Jurassic arc terranes of British Columbia; in

Bootprints Along the Cordillera, J.G. Bolm and F.W. Pierce (Editors): Arizona Geological Society Digest Volume 20, p. 219-236.

Lang, J.R., Stanley, C.R., Thompson, J.F., and Dunne, K.P.E., 1995a, Na-K-Ca magmatic-hydrothermal alteration on alkalic porphyry Cu-Au deposits, British Columbia: Mineralogical Association of Canada Short Course Volume 23, p. 339-366.

Lang, J.R., Lueck, B., Mortensen, J.K., Russell, J.K., Stanley, C.R. and Thompson, J.F.H., 1995b, Triassic-Jurassic silica-undersaturated and silica-saturated alkalic intrusions in the Cordillera of British Columbia: Implications for arc magmatism: Geology, v. 23, no. 5, p. 451-454.

Lawley, C.J.M., Richards, J.P., Anderson, R.G., Creaser, R.A., and Heaman, L.M., 2010, Geochronology and geochemistry of the MAX porphyry Mo deposit and its relationship to Pb-Zn-Ag mineralization, Kootenay Arc, southeastern British Columbia, Canada: Economic Geology, v. 105, p. 1113-1142.

Logan, J.M. and Koyanagi, V.M, 1989, Geology and mineral deposits of the Galore Creek area, northwestern British Columbia (104G/3, 4): Geological Fieldwork, 1988, British Columbia Ministry of Energy, Mines and Petroleum Resources, Paper 1989-1, p. 269-283.

Logan, J.M., Koyanagi, V.M. and Rhys, D., 1989, Geology and mineral occurrences of the Galore Creek area, NTS 104G/03 and 04, British Columbia Ministry of Energy, Mines and Petroleum Resources, Open File 1989-8 (2 sheets).

Logan, J.M., Drobe, J.R., and McClelland, W.C., 2000, Geology of the Forest Kerr-Mess Creek area, northwestern British Columbia (NTS, 104B/10, 15 & 104G/2 and 7W): British Columbia Ministry of Energy and Mines, Bulletin 104, 164p.

Lowell, J.D., Guilbert, J.M., 1970, Lateral and Vertical Alteration-Mineralization Zoning in Porphyry Ore Deposits: Economic Geology, v. 65, no. 4, p. 373-408.

Lueck, B.A., Russell, J.K., Silica-undersaturated, zoned, alkaline intrusions within the British Columbia Cordillera: Geologic Fieldwork 1993, B.C. Ministry of Energy, Mines and Petroleum Resources, Paper 1994-1, p. 311-315.

MacIntyre, D.G., Villeneuve, M.E., and Schiarizza, P., 2001, Timing and tectonic setting of Stikine terrane magamtism, Babine-Takla lakes area, central British Columbia: Canadian Journal of Earth Sciences, v. 38, p. 579-601.

MacNamara, J., and Thode, H.G., 1950, Comparison of the isotopic constitution of terrestrial and meteoritic sulphur, Physics Reviews, v. 78, p. 307-308.

McMillan, W.J., Thompson, J.F., Hart, C.J.R., and Johnson, S.T., 1995, Regional geological and tectonic setting of porphyry deposits in British Columbia and Yukon Territory: Porphyry Deposits of the Northwestern Cordillera of North America, T.G. Schroeter (ed.), Canadian Institute of Mining, Metallurgy and Petroleum Special Volume 46, p. 40–57.

Massey, N.W.D., MacIntyre, D.G., Desjardins, P.J., and Cooney, R.T., 2005, Digital geology map of British Columbia, whole province, B.C. Ministry of Energy and Mines, Geofile 2005-1.

Mehner, D., 2005, Diamond Drilling, Wacker Drilling, IP, Resistivity & Ground Magnetic Geophysical Surveys, Silt, Soil & Rock Geochemical Sampling,Trenching and Prospecting On the Kinaskan Lake property, GJ project, 2004, Liard Mining Division, British Columbia, Canada: unpublished company report, Canadian Gold Hunter Coproration, 72p.

Mehner, D.T., Giroux, G.H., Peatfield, G.R., 2007, Technical report on the GJ copper-gold porphyry project, Liard Mining Division, British Columbia, Canada: unpublished company report, Canadian Gold Hunter Corporation, 134p.

Meunier, A., and Velde, B., 2004, Illite: Berlin, Springer, 286p.

Meyer, C., and Hemley, J.J., 1967, Geochemistry of hydrothermal ore deposits, New York, Holt, Reinhart and Winston, 670p.

Micko, J., 2010, The geology and genesis of the Central Zone alkalic copper-gold porphyry deposit, Galore Creek district, northwestern British Columbia, Canada: Unpublished PhD thesis, Vancouver, British Columbia, University of British Columbia, 359p.

Micko, J., Tosdal, R.M, Bissig, T., Chamberlain, C.M., and Simpson, K.A., In Press, Hydrothermal alteration and mineralization of the Galore Creek alkalic Cu-Au porphyry deposit, northwestern British Columbia, Canada: Economic Geology.

Monger, J.W.H., and Ross, C.A., 1971, Distribution of fusilinaceans in the western Canadian Cordillera: Canadian Journal of Earth Sciences, v. 8, p.259-278.

Monger, J.W.H., Wheeler, J.O., Tipper, H.W., Gabrielse, H., Harms, T., Struik, L.C., Campbell, R.B., Dodds, C.J., Gehrels, G.E. and O'Brien, J., 1991, Upper Devonian to Middle Jurassic Assemblages Part B. Cordilleran Terranes: Chapter 8 of Geology of the Canadian Orogen in Canada, H. Gabrielse and C.J. Yorath (ed.), Geological Survey of Canada, Geology of Canada, no. 4, p. 281-327 (also Geological Society of America, The Geology of North America, v. G-2).

Monger, J. and Price, R., 2002, The Candadian Cordillera: Geology and Tectonic Evolution: Canadian Society of Exploration Geophysicists Recorder, v. 27, no. 2, p. 17-36.

Moore, W.J., and Nash, J.T., Alteration and fluid inclusion studies of the porphyry copper ore body at Bingham, Utah: Economic Geology, v. 69, p. 631-645.

Moore, W.J., 1978, Chemical characteristics of hydrothermal alteration at Bingham, Utah: Economic Geology, v. 73, p. 1260-1269.

Moore, D.M., and Reynolds, R.C., Jr., 1997, X-Ray Diffraction and the identification of clay minerals: New York, Oxford University Press, 378p.

Mortensen, J.K, Ghosh, D.K., Ferri, F., 1995, U-Pb geochronology of intrusive rocks associated with copper-gold porphyry deposits in the Canadian Cordillera: Porphyry Deposits of the Northwestern Cordillera of North America, T.G. Schroeter (ed.), Canadian Institute of Mining, Metallurgy and Petroleum Special Volume 46, p. 142-158..

Mortimer, N., 1987, The Nicola Group: Late Triassic and Early Jurassic subduction related volcanism in British Columbia: Canadian Journal of Earth Sciences, v. 24, p. 2521-2536.

Mortimer, N., Van Der Heyden, P., Armstrong, R.L., and Harakal, J., 1990, U-Pb and K-Ar dates related to the timing of magmatism and deformation in the Cache Creek terrane and Quesnellia, southern British Columbia: Canadian Journal of Earth Sciences, v. 27, p. 117-123.

Nelson, J. and Mihalynuk, M., 1993, Cache Creek ocean: closure or enclosure?: Geology, v. 21, p. 173-176.

Nelson, J., and Colpron, M., 2007, Tectonics and metallogeny of the British Columbia, Yukon and Alaska n Cordillera, 1.8 Ga to the present, *in* Goodfellow, W.D., ed., Mineral Deposits of Canada: A Synthesis of Major Deposit-Types, District Metallogeny, the Evolution of Geological Provinces, and Exploration Methods: Geological Association of Canada, Mineral Deposits Division, Special Publication No. 5, p. 755-791.

Newell, J.M. and Peatfield, G.R., 1995, The Red-Chris porphyry copper-gold deposit, northwestern British Columbia: Porphyry Deposits of the Northwestern Cordillera of North America, T.G. Schroeter (ed.), Canadian Institute of Mining, Metallurgy and Petroleum Special Volume 46, p. 674–688.

Nixon, G.T., and Peatfield, G.R., 2003, Geological setting of the Lorraine Cu-Au porphyry deposit, Duckling Creek Syenite Complex, north-central British Columbia: B.C. Ministry of Energy and Mines, Open File 2003-4, 24p.

Norris, J.R., Hart, C.J.R., Tosdal, R.M. and Rees, C. (2010): Preliminary study of the magmatic evolution, mineralization and alteration of the Red Chris copper-gold porphyry deposit, northwestern British Columbia (NTS 104H/12W); *in* Geoscience BC Summary of Activities 2009, Geoscience BC, Report 2010-1, p. 77–86.

Norris, J.R., Hart, C.J.R., Tosdal, R.M. and Rees, C. (2011): Magmatic evolution, mineralization and alteration of the Red Chris copper-gold porphyry deposit, northwestern British Columbia (NTS 104H/12W); *in* Geoscience BC Summary of Activities 2010, Geoscience BC, Report 2011-1, p. 33–44.

Ohmoto, H., 1972, Systematics of sulfur and carbon isotopes in hydrothermal ore deposits: Economic Geology, v. 67, p. 551-578.

Ohmoto, H. and Rye, R.O., 1979, Isotopes of Carbon and Sulfur *in* Geochemistry of hydrothermal ore deposits, 2nd ed., New York, John Wiley and Sons, p. 509-567.

Ohmoto, H., and Lasaga, A.C., 1982, Kinetics of reactions between aqueous sulfates and sulfides in hydrothermal systems: Geochimica et Cosmochimica Acta, v. 46, p. 1727-1745.

Ohmoto, H. and Goldhaber, M.B., 1997, Sulfur and Carbon Isotopes *in* Geochemistry of hydrothermal ore deposits, 3rd ed., New York, John Wiley and Sons, p. 517-611.

Parry, W.T., Jasumback, M., and Wilson, P.N., 2002, Clay mineralogy of phyllic and intermediate argillic alteration at Bingham, Utah: Economic Geology, v. 97. P. 221-239.

Pass, H.E., Cooke, D.R., Davidson, G., Maas, R., Dipple, G., Rees, C., Ferreira, L., Taylor, C., and Dyell, C.L., In Press, Isotope geochemistry of the Northeast zone, Mount Polley alkalic Cu-Ag-Au porphyry deposit, British Columbia: A case for carbonate assimilation, Economic Geology.

Read, P.B., 1984, Geology Klastine River (104G/16E), Ealue Lake (104H/13W), Cake Hill (104I/4W), and Stikiine Canyon (104J/1E), British Columbia: Geological Survey of Canada, Open File Map 1080, scale 1:50 000.

Read, P.B. and Psutka, J.F., 1990, Geology of Ealue Lake east-half (104H/13E) and Cullivan Creek (104H/14) map areas, British Columbia: Geological Survery of Canada, Open File Map 2241, scale 1:50 000.

Redmond, P.B., Einaudi, M.T., 2010, The Bingham Canyon porphyry Cu-Mo-Au deposit. I. Sequence of intrusions, vein formation, and sulphide deposition: Economic Geology, v. 105, p. 43-68.

Reyes, A.G., 1990, Petrology of Philippine geothermal systems and the application of alteration mineralogy to their assessment: Journal of Volcanology and Geothermal Research, v. 43, p. 279-309.

Rhys, D.A, 1995, The Red Bluff gold-copper porphyry and associated precious and base metal veins, northwestern British Columbia: Porphyry Deposits of the Northwestern Cordillera of North America, T.G. Schroeter (ed.), Canadian Institute of Mining, Metallurgy and Petroleum Special Volume 46, p. 838–850.

Riddell, J., 2011, Lithostratigrpahic and tectonic framework of Jurassic and Cretaceous Intermontane sedimentary basins of south-central British Columbia: Canadian Journal of Earth Sciences, vol. 48, p.870-896.

Rye, R.O., Bethke, P.M. and Wasserman, M.D., 1992, The stable isotope geochemistry of acid sulfate alteration: Economic Geology, v. 87, p. 225-262.

Rusk, B.G., Reed, M.H., and Dilles, J.H., 2008, Fluid inclusion evidence for magmatic-hydrothermal fluid evolution in the porphyry copper-molybdenum deposit at Butte, Montana: Economic Geology, v. 103, p. 307-334.

Rye, R.O., The evolution of magmatic fluids in the epithermal environment: The stable isotope perspective: Economic Geology, v. 88, p. 733-753.

Savin, S.M., and Epstein, S., 1970, The oxygen and hydrogen isotope geochemistry of clay minerals: Geochimica et Cosmochimica Acta, v. 34, p. 25-42.

Schink, E.A., 1977, Geology of the Red Chris porphyry copper deposit, northwestern British Columbia: Unpublished M.Sc. thesis, Kingston, Ontario, Queens University, 211p.

Schwab, D.L., Petsel, S., Otto, B.R., Morris, S.K., Workman, E.E., and Tosdal, R.M., 2008, Overview of the Late Triassic Gaore Creek copper-gold porphyry system, northwestern British Columbia, Canada: Arizona Geological Society Digest 22, p. 471-484.

Scott, J.E., Richards, J.P, Heaman, L.M., Creaser, R.A., and Salazar, G.S., 2008, The Schaft Creek porphyry Cu-Mo-(Au) deposit, northwestern British Columbia: Exploration and Mining Geology, Canadian Institute of Mining, Metallurgy and Petroleum, v.17, no. 3-4, p. 163-196.

Seedorff, E., Dilles, J.H., Proffett, J.M., Jr., Einaudi, M., Zurcher, L., Stavast, W.J.A., Johnson, D.A., and Barton,M., 2005, Porphyry Deposits: Characteristics and Origin of Hypogene Features: Economic Geology 100th Anniversary Volume, p. 251-298.

Sharp, Z.D., 1990, Laser-based microanalytical method for the in situ determination of oxygen isotope ratios of silicates and oxides: Geochimica et Cosmochimica Acta, v. 54, p. 1353-1357.

Sheppard, S.M.F., Nielsen, R.L, and Taylor, H.P. Jr., 1969, Oxygen and hydrogen isotope ratios of clay minerals from porphyry copper deposits: Economic Geology, v. 64, p. 755-777.

Sheppard, S.M.F., Nielsen, R.L, and Taylor, H.P. Jr., 1971, Hydrogen and oxygen isotope rations in minerals from porphyry copper deposits: Economic Geology, v. 66, p. 515-542.

Sheppard, S.M.F., and Gilg, H.A., 1996, Stable isotope geochemistry of clay minerals: Clay Minerals, v. 31, p. 1-24.

Sillitoe, R.H., and Gappe, I.M., Jr., 1984, Philippine porphyry copper deposits: Geologic setting and characteristics: Bangkok, Thailand, United Nations ESCAP, CCOP Technical Publication 14, 89p.

Sillitoe, R.H., 2000, Gold-rich porphyry deposits: Descriptive and genetic models and their role in exploration and discovery: Reviews in Economic Geology, v. 13, p. 315-345.

Sillitoe, R.H., 2010, Porphyry Copper Systems: Economic Geology, v. 105, no.1, p. 3-41.

Sinclair, W.D., 2007, Porphyry deposits: Mineral Deposits of Canada: A synthesis of major deposit-types, district metallogeny, the evolution of geological provinces, and exploration methods, W.D. Goodfellow (ed.), Geological Association of Canada, Mineral Deposits Division, Special Publication No. 5, p. 223-243.

Skinner, B. J., 1979, The many origins of hydrothermal mineral deposits *in* Geochemistry of hydrothermal ore deposits, 2nd ed., New York, John Wiley and Sons, p. 1-21.

Souther, J.G., 1972, Telegraph Creek map-area, British Columbia: Geological Survey of Canada, Paper 71-44, 38p.

Souther, J.G., 1991, Volcanic regimes: Chapter 14 of Geology of the Canadian Orogen in Canada, H. Gabrielse and C.J. Yorath (ed.), Geological Survey of Canada, Geology of Canada, no. 4, p. 457-490 (also Geological Society of America, The Geology of North America, v. G-2).

Souther, J.G., 1992, The Late Cenozoic Mount Edziza Volcanic Complex, British Columbia: Geological Survey of Canada, Memoir 420, 329p.

Southerland Brown, A., 1976, Morphology and classification: Canadian Institute of Mining, Metallurgy and Petroleum Special Volume 15, p. 44-51.

Srodon, J., and Eberl, D.D., 1984, Illite, *in* Bailey, S.W., ed., Micas, v.13 in Reviews in Mineralogy, Mineralogical Society of America, Washington, D.C., p. 495-544.

Stanley, C.R., Holbek, P.M., Huyck, H.L.O., Lang, J.R., Preto, V.A.G., Blower, S.J., and Bottaro, J.C., 1995, Geology of the Copper Mountain alkali copper-gold porphyry deposits, Princeton, British Columbia: Porphyry Deposits of the Northwestern Cordillera of North America, T.G. Schroeter (ed.), Canadian Institute of Mining, Metallurgy and Petroleum Special Volume 46, p. 537-564.

Suzuoki, T., and Epstein, S., 1976, Hydrogen isotope fractionation between OH-bearing minerals and water: Geochimica et Cosmochimica Acta, v. 40, p. 1229-1240.

Taylor, B.E., 1987, Stable isotope geochemistry of ore-forming fluids *in* Stable Isotope Geochemistry of Low Temperature Fluids (ed. T. K. Kyser): Mineralogical Association of Canada short course handbook, no. 13, p. 337-445.

Taylor, H.P. Jr., 1974, The application of oxygen and hydrogen isotope studies to problems of hydrothermal alteration and ore deposition: Economic Geology, v. 69, p. 843-883.

Taylor, B.E., 1992, Degassing of H_2O from rhyolitic magma during eruption and shallow intrusion, and the isotopic composition of magmatic water in hydrothermal systems: Geological Survey of Japan Report, v. 279, p. 190–194.

Taylor, H.P. Jr., 1997, Oxygen and hydrogen isotope relationships in hydrothermal mineral deposits *in* Geochemistry of hydrothermal ore deposits, 3rd ed., New York, John Wiley and Sons, New York, John Wiley and Sons Inc., p. 229-302.

Thompson, A.J.B., Hauff, P.L., and Robitaille, A.J., 1999, Alteration mapping in exploration - application of short-wave infrared (SWIR) spectroscopy: SEG Newsletter, Society of Economic Geologists, no. 39, p. 15-27.

Thomson, R.C., Smith, P.L., Tipper, H.W., 1986, Lower to Middle Jurassic (Pliensbachian to Bajocian) stratigraphy of the northern Spatsizi area, north-central British Columbia, Canadian Journal of Earth Sciences, v. 23, p. 1963-1973.

Thorkelson, D.J., Mortensen, J.K., Marsden, H., and Taylor, R.P., 1995, Age and tectonic setting of Early Jurassic episodic volcanism along the northeastern margin of the Hazelton Trough, northern British Columbia *in* Jurassic Magmatism and Tectonics of the North

American Cordillera (eds. D.M. Miller and C. Busby): Geological Society of America, Special Paper 299, p. 83-94.

Tipper, H.W., and Richards, T.A., 1976, Jurassic stratigraphy and history of north-central British Columbia: Geological Survey of Canada, Bulletin 270, 73p.

Tooker, E.W., 1963, Altered wall rocks in the central part of the Front Range mineral belt, Gilpin and Clear Creek counties, Colorado: U.S. Geological Survey Professional Paper 439, 102p.

Ulrich, T., Gunther, D., and Heinrich, C.A, 2001, The evolution of a porphyry Cu-Au deposit, based on LA-ICP-MS analysis of fluid inclusions: Bajo de la Alumbrera, Argentina: Economic Geology, v. 96, p. 1743-1774.

Veizer, J., Ala, D., Azmy, K., Bruckschen, P., Buhl, D., Bruhn, F., Carden, G., Diener, A., Ebneth, S., and Godderis, Y., 1999, 87Sr/86Sr, [delta] 13C and [delta] 18O evolution of Phanerozoic seawater: Chemical Geology, v. 161, p. 59-88.

White, W.M., Sinclair, A.J., Harakal, J.E., Dawson, K.M, 1970, Potassium-argon ages of Topley Intrusions near Endako, British Columbia: Canadian Journal of Earth Sciences, v. 7, p. 1172-1178.

Wilson, A.J., Cooke, D.R., and, Harper, B.J., 2003, The Ridgeway gold-copper deposit: A high-grade alkalic porphyry deposit in the Lachlan Fold Belt, New South Wales, Australia: Economic Geology, v. 98, p. 1637-1666.

Wilson, A.J., Cooke, D.R., Harper, B.J., and Dyell, C.L., 2007, Sulfur isotopic zonation in the Cadia district, southeastern Australia: exploration significance and implications for the genesis of alkali porphyry gold-copper deposits: Mineralium Deposita, v. 42, p. 465-487.

Wolfe, R.C., and Cooke, D.R., 2011, Geology of the Didipio Region and genesis of the Dinkidi alkalic porphyry Cu-Au deposit and related pegmatites, Northern Luzon, Philippines: Economic Geology, v. 106, p. 1279-1315.

Woodsworth, G.J., Anderson, R.G. and Armstrong, R.L., 1991, Plutonic Regimes: Chapter 15 of Geology of the Canadian Orogen in Canada, H. Gabrielse and C.J. Yorath (ed.), Geological Survey of Canada, Geology of Canada, no. 4, p. 493-531 (also Geological Society of America, The Geology of North America, v. G-2).

Yorath, G.J., 1991, Upper Jurassic to Paleogene Assemblages: Chapter 9 of Geology of the Canadian Orogen in Canada, H. Gabrielse and C.J. Yorath (ed.), Geological Survey of Canada, Geology of Canada, no. 4, p. 329-371 (also Geological Society of America, The Geology of North America, v. G-2).

Zheng, Y., 1993, Calculation of oxygen isotope fractionation in hydroxyl-bearing silicates: Earth and Planetary Science Letters, v. 120, p. 247-263.

Zheng, Y., 1999, Oxygen isotope fractionation in carbonate and sulfate minerals: Geochemical Journal, v. 33, p. 109-126.

Zhou, T., and Dobos, S.K., 1994, Stable isotope geochemistry of kaolinite from the 'white section', Black Ridge, Clermont, Central Queensland: Implications for the age and origin of the 'white section': Clays and Clay Minerals, v. 42, no.3, p. 269-275.

List of Electronic Appendices

Appendix A1: Drill Core Logs (pdf)

Appendix A2: Sample List and Descriptions (pdf)

Appendix A3: Using XRD and TerraSpec for Differentiation of Illite and Muscovite (pdf)

Appendix A4: Clay Separation Procedure (pdf)